




Inhibition of dopamine receptor D1 signaling promotes human bile duct cancer progression via WNT signaling

Akitada Yogo^{1,2}  | Toshihiko Masui²  | Shigeo Takaishi^{1,3}  | Kenji Masuo^{1,3} | Ru Chen^{1,3} | Yosuke Kasai² | Kazuyuki Nagai² | Takayuki Anazawa² | Sadanori Watanabe^{1,4} | Satoko Sakamoto⁵ | Akira Watanabe⁵ | Ryosaku Inagaki^{1,4} | Masahiro M. Nakagawa^{1,6} | Seishi Ogawa^{1,6} | Hiroshi Seno^{1,3} | Shinji Uemoto^{2,7} | Etsuro Hatano²

¹DSK Project, Medical Innovation Center, Graduate School of Medicine, Kyoto University, Kyoto, Japan

²Division of Hepato-Biliary-Pancreatic Surgery and Transplantation, Department of Surgery, Graduate School of Medicine, Kyoto University, Kyoto, Japan

³Department of Gastroenterology and Hepatology, Graduate School of Medicine, Kyoto University, Kyoto, Japan

⁴Cancer Research Unit, Sumitomo Pharma Co., Ltd, Osaka, Japan

⁵Medical Innovation Center, Kyoto University Graduate School of Medicine, Kyoto, Japan

⁶Department of Pathology and Tumor Biology, Kyoto University, Kyoto, Japan

⁷Shiga University of Medical Science, Shiga, Japan

Correspondence

Toshihiko Masui, Division of Hepato-Biliary-Pancreatic Surgery and Transplantation, Department of Surgery, Graduate School of Medicine, Kyoto University, 54, Shogoin-Kawaharacho, Sakyo-ku, Kyoto 606-8507, Japan.
Email: tmasui@kuhp.kyoto-u.ac.jp

Shigeo Takaishi, Department of Gastroenterology and Hepatology, Graduate School of Medicine, Kyoto University, 54, Shogoin-Kawaharacho, Sakyo-ku, Kyoto 606-8507, Japan.
Email: takaishi.shigeo.7w@kyoto-u.jp

Funding information

Ministry of Education, Culture, Sports, Science and Technology, Grant/Award Number: KAKENHI (17K09460) and KAKENHI (21K08732); Sumitomo Pharma Co., Ltd

Abstract

Bile duct cancer (BDC) frequently invades the nerve fibers, making complete surgical resection difficult. A single tumor mass contains cells of variable malignancy and cell-differentiation states, with cancer stem cells (CSCs) considered responsible for poor clinical outcomes. This study aimed to investigate the contribution of autotransformed dopamine to CSC-related properties in BDC. Sphere formation assays using 13 commercially available BDC cell lines demonstrated that blocking dopamine receptor D1 (DRD1) signaling promoted CSC-related anchorage-independent growth. Additionally, we newly established four new BDC patient-derived organoids (PDOs) and found that blocking DRD1 increased resistance to chemotherapy and enabled xenotransplantation in vivo. Single-cell analysis revealed that the BDC PDO cells varied in their cell-differentiation states and responses to dopamine signaling. Further, DRD1 inhibition increased WNT7B expression in cells with bile duct-like phenotype, and it induced proliferation of other cell types expressing Wnt receptors and stem cell-like signatures. Reagents that inhibited Wnt function canceled the effect of DRD1 inhibition and reduced cell proliferation in BDC PDOs. In summary, in BDCs, DRD1

Abbreviations: BDC, bile duct cancer; CSCs, cancer stem cells; DRD1, dopamine receptor D1; PDOs, patient-derived organoids; qRT-PCR, quantitative real-time polymerase chain reaction; scRNA-seq, single-cell RNA-sequence; P/S, penicillin-streptomycin mixed solution; bFGF, recombinant human fibroblast growth factor-basic; EGF, human epidermal growth factor; KD, knockdown; TCGA, The Cancer Genome Atlas; KEGG, Kyoto Encyclopedia of Genes and Genomes.

Toshihiko Masui and Shigeo Takaishi jointly supervised this study.

This is an open access article under the terms of the [Creative Commons Attribution-NonCommercial-NoDerivs](https://creativecommons.org/licenses/by-nc-nd/4.0/) License, which permits use and distribution in any medium, provided the original work is properly cited, the use is non-commercial and no modifications or adaptations are made.

© 2022 The Authors. *Cancer Science* published by John Wiley & Sons Australia, Ltd on behalf of Japanese Cancer Association.

is a crucial protein involved in autonomous CSC proliferation through the regulation of endogenous WNT7B. As such, inhibition of the DRD1 feedback signaling may be a potential treatment strategy for BDC.

KEYWORDS

bile duct cancer, cancer stem cells, dopamine D1 receptors, organoids, single-cell analysis

1 | INTRODUCTION

Bile duct cancer (BDC) has a low 5-year survival rate of only 7%–20% and a high postoperative recurrence rate of approximately 60%.¹ Further, over 75% of symptomatic cases are ineligible for complete resection.² A single cancer tumor comprises numerous cells with different degrees of malignancy,³ with cancer stem cells (CSCs) considered the “root of recurrence and metastasis.” Consequently, CSCs have been set as critical therapeutic targets, particularly in hematopoietic malignancies or solid tumors, such as breast, brain, and colon cancers.⁴ Since the 2010s, a phenomenon called CSC plasticity has been highlighted. Non-CSCs can convert their phenotype into CSCs in limited conditions, and the surrounding environment is called the CSC niche.^{5,6,7} Thus, CSC niche-targeting therapy is gaining significant attention.⁸ However, in BDCs, although biomarkers for cancer stem-like properties have been reported,^{9,10} the mechanisms by which the niche regulates CSC plasticity remain to be elucidated.¹¹

Anatomically, the nerve fibers run parallel to the bile ducts, and the high rate of neural invasion (56.0%–88.0%) is a critical factor for the poor prognosis of BDCs.^{12–14} As such, BDCs are sometimes referred to as “neurotropic cancers.”¹⁵ Further, recent studies show that both the malignant behavior of BDC and normal bile duct development are affected by neurotransmitters.^{13,15–17} Notably, BDC cells synthesize dopamine by themselves under epigenetic regulation.^{16,18} In acute myeloid leukemia, breast cancer, or non-small lung carcinoma, dopamine signaling contributes to CSC homeostasis.^{19–21} However, the contribution of dopamine signaling to BDC CSC has not been elucidated thus far.

Patient-derived organoids (PDOs) are a novel cell resource cultured in 3D gels *in vitro*, retaining features of the original tumor *in vivo* containing CSCs and non-CSCs.^{22,23} Therefore, PDOs are advantageous for examining tumor heterogeneity with *in vitro* interventional experiments. This study aimed to elucidate the contribution of autotransmitted dopamine to CSC-related properties using four BDC PDOs.

2 | MATERIALS AND METHODS

2.1 | Cell culture

Commercially available cells were obtained from RIKEN, the Japanese Collection of Research Bioresources Cell Bank, or the American Type Culture Collection. The short tandem repeat analysis for cell line authentication and mycoplasma non-contamination

test had been performed by each cell bank before shipment. Details about Cat#, RRID, and culture conditions are given in Table S1.

2.2 | Sphere culture conditions and sphere formation assay

For sphere culture, cells were dissociated with TrypLE Express enzyme (Invitrogen), filtered through a 35- μ m cell strainer (Corning), and seeded in ultralow attachment six-well plates (Corning; 10,000 cells per well) with serum-free DMEM/Ham's F-12 (Nacalai Tesque). DMEM was supplemented with 1 \times B27 Supplement (Thermo Fisher Scientific), 10 ng/mL recombinant human fibroblast growth factor-basic (Thermo Fisher Scientific), 20 ng/mL recombinant human epidermal growth factor (EGF; Thermo Fisher Scientific), and 1% penicillin/streptomycin mixed solution (P/S; Nacalai Tesque). Spheres were passaged after 5–7 days. After two passages, cells were used for sphere formation assays or mRNA extraction. In sphere formation assays, dissociated and filtered cells were cultured in ultra-low attachment 24-well plates (Corning; 2000 cells per well) with a medium containing each reagent (DMSO and/or D1 inhibitor (SKF-83566, Abcam) and/or porcupine inhibitor (LGK974, Cayman Chemical Company)). On day 2, half the amount of medium with reagent was added. Spheres were imaged using the microscope IX73 (Olympus). On day 5 or 6, spheres larger than 75 μ m in diameter were counted using Cell3Imager CC5000 (SCREEN Holdings).

2.3 | Patient-derived organoid culture

Patient-derived organoids were established from fresh surgical specimens obtained from patients who underwent surgical resection at Kyoto University Hospital. Primary tumor tissue samples were processed as previously described with slight modifications.^{24–28} The cell aggregates were embedded in Matrigel (Corning) and covered by a conditioned medium composed of 50% L-WRN (ATCC Cat# CRL-3276, RRID: CVCL_DA06; containing Wnt3A, R-spondin 3, and Noggin), advanced DMEM/F12 (Invitrogen), 5% FBS (Cytiva), 2 mmol/L L-Alanyl-L-Glutamine (Wako), 1% P/S, 2.5 μ g/mL plasmocin prophylactic (Invitrogen), 10 μ M Y-27632 (Wako), 1 \times B27 Supplement, 100 ng/mL basic FGF, and 20 ng/mL EGF, denoted as “niche-enriched.” The medium containing advanced DMEM/F12, 5% FBS, 2 mmol/L L-Alanyl-L-Glutamine, and 1% P/S was called “niche deficient.” Used PDOs were passaged fewer than 35 times.

2.4 | Organoid formation assay

Patient-derived organoids were dissociated into single cells using TrypLE Express Enzyme, filtered through a 35- μ m cell strainer, and cultured in 48-well plates (250 cells per 5 μ L Matrigel per well, with 2 μ L Matrigel embedded a priori so that PDOs did not spread to the bottom) with the medium changed twice weekly. Images of PDOs were recorded using microscope IX73. On days 10–15, PDOs greater than 75 μ m in diameter were counted using Cell3Imager CC5000 with a multiplanar scanning option.

2.5 | RT-PCR

Total RNA extraction, single-strand complementary DNA synthesis, and qRT-PCR were performed in triplicate as previously described.²⁷ The relative quantification of each target, normalized to an endogenous control (GAPDH), was performed using the comparative Ct method. Table S2 lists the primer sequences. Further details are given in the [Supplementary Methods](#).

2.6 | ShRNA-mediated human DRD1 gene knockdown by lentiviral transduction

ShRNA-mediated knockdown (KD) was performed as described previously.²⁷ The two predesigned *DRD1*-targeting shRNA (A:TRCN0000356937, 5'- ccgTTATGCGCTTTAATGCTGATTctcgagaatcagcattaaggcataattttg-3, B:TRCN0000230254, 5'- ccgGTATCAGTCATATTGGACTATGctcgagcatagtcacaatgactgatattttg-3) were used. At 48–72h after viral infection, the cells were treated with a medium containing puromycin (Invitrogen) at 1–5 μ g/mL for 2 weeks to eliminate the non-infected cells. Further details are provided in the [Supplementary Methods](#).

2.7 | Xenograft assay

NOD/SCID mice were purchased from the Charles River Laboratories Japan. Cultured BDC cells including spheres were dissociated with TrypLE Express enzyme, centrifuged, and resuspended in iced PBS. PDO cells were dissociated with TrypLE Express enzyme, centrifuged, and resuspended in an iced "niche-deficient" medium at a concentration of 10⁵ or 10⁶ in 50 μ L. For subcutaneous transplantation, cells were injected into the flanks of 8–12-week-old NOD/SCID mice (PDO cell suspension was mixed with Matrigel [50% vol/vol]). The tumor constructions were examined by peeling off the skin. For spleen injection,²⁹ the NOD/SCID mice were anesthetized using isoflurane, and a 1.5-cm left-sided transverse laparotomy was performed to open the abdominal cavity. Cells were injected into the spleen using a 27-gauge needle. Tumor cells were allowed to circulate for 10 min, and the spleen was resected. For peri-sciatic nerve xenograft,³⁰ NOD/SCID mice were anesthetized, and a 1.5-cm

incision exposed their sciatic nerves. The cell mixture with Matrigel (50% vol/vol) was injected at the space of the branch of the tibial and sural nerves.

2.8 | Chemoresistance assay

Patient-derived organoids were dissociated and cultured in V-bottom 96-well plates (nerbe plus; 2000 cells in 4 μ L of Matrigel per well, covered by a "niche-enriched" medium). After 3 days, the medium was changed into a "niche-enriched" or "niche-deficient" medium (medium change, twice weekly). On days 7–10, PDOs were treated with gemcitabine hydrochloride (Tokyo Chemical Industry), cisplatin (Wako), or 5-fluorouracil (Nacalai Tesque). Subsequently, after 3 days, the medium was changed to 100 μ L of "niche-deficient" medium with 10 μ L of CCK-8 (Dojindo Labs). After incubation for 2 h, each medium was transferred to a new 96-well plate, and the optical absorbance at a wavelength of 450 nm was measured using the plate reader Infinite F50 (TECAN).

2.9 | scRNA-seq

Dissociated PDO cells in Matrigel were plated on a Matrigel-precoated six-well plate (10,000 cells per well) and cultured in a niche-enriched medium with DMSO or D1 inhibitor (SKF-83566 4 μ M) with the medium changed twice weekly. After 14 days, the cells were dissociated, and scRNA-seq was conducted using the 10X Genomics Chromium Single Cell 3' Gene Expression kit. Further details, including sequencing and bioinformatics, are given in [Supplementary Methods](#).

2.10 | Statistical analysis

Values were presented as the mean \pm standard error of the mean when data distribution was assumed to be normal (not formally tested); otherwise, a box plot was used. Student's *t*-test (two-tailed unpaired or paired), the Wilcoxon rank-sum test, or Tukey's test was used to compare groups as appropriate. All statistical analyses were performed using R (v.3.6.2) with R package multcomp (v.1.4–17). The *p*-values were as follows: *****p* < 0.0001, ****p* < 0.001, ***p* < 0.01, **p* < 0.05, and n.s. > 0.05.

3 | RESULTS

3.1 | Blocking of DRD1 increases bile duct cancer sphere formation

To find cell lines that followed the CSC plasticity model, sphere formation assays were applied to 13 commercially available BDC cell lines (Figure 1A and Figure S1A). In general, most monolayer-cultured

cells are non-CSC-like, and sphere culture can enrich CSC-like cells as spherical aggregates called spheres, with non-CSC-like cells suspended as single cells.^{22,31,32} The cell lines were divided into the following two groups according to the types of sphere formation: (1) a convertible type that formed spheres only in sphere culture (NOZ, KKKU213, TYGBK1, TYBDC1, HuCCA1, HuCCT1, and TKF1) and (2) an unconvertible type that formed no or few small spheres (KKU055, KKKU100, OCUG1, G415) or formed aggregates in either condition (OZ, TYGBK8; Figure 1A and Figure S1B). It was inferred that the convertible type lines were more likely to retain CSC plasticity than the unconvertible type.

Expressions of pluripotency-associated genes (i.e., *NANOG*, *SOX2*, and *POU5F1/OCT4*) and the recently reported slow-cycling CSC marker *PROX1*³³ were confirmed to be elevated in the convertible type (Figure S2A). In addition, “convertible type” sphere cells had higher tumorigenic potential than monolayer-cultured cells in vivo (Figure S2B). Then, the dopamine autotransformation capacity of BDC was confirmed by mRNA expression of dopamine synthesis genes (*TH* and *DDC*) and quantification of dopamine levels by enzyme-linked immunosorbent assay (ELISA; Figure S3). The expression of *TH*, the rate-limiting enzyme for dopamine synthesis, was higher in the convertible type than in the unconvertible type. These data suggested that these convertible-type BDC cell lines (NOZ, KKKU213, TYGBK1, TYBDC1, HuCCA1, HuCCT1, and TKF1)

followed the CSC plasticity model with higher dopamine autotransformation capacity.

Additionally, to explore the functions of dopamine receptors in CSCs, we evaluated the expressions of genes of five dopamine receptor subtypes (D1-like: *DRD1* and *DRD5*; D2-like: *DRD2*, *DRD3*, and *DRD4*) in conditions of the sphere and monolayer culture. The results showed that *DRD1* was the most upregulated in convertible-type spheres (Figure 1B). A selective D1 receptor inhibitor (SKF-83566) was applied to the sphere formation assay of three convertible-type lines that had the highest sphere-forming ability (TYGBK1, NOZ, and TKF1; Figure S1A). The D1 inhibitor increased the number of spheres (Figure 1C,D). The involvement of *DRD1* was confirmed using *DRD1*-KD (Figure 1E and Figure S2C). In summary, these results suggested that blocking of D1 signaling enhanced the CSC niche of BDC.

3.2 | Blocking of *DRD1* signaling augments patient-derived organoids initiation in vitro

To validate the above results with more clinically relevant resources, four BDC PDOs were newly established from fresh surgical specimens (Sph18-08, Sph18-16, Sph18-22, and Sph18-29; Table 1). Each PDO had genetic variants characteristic of BDCs

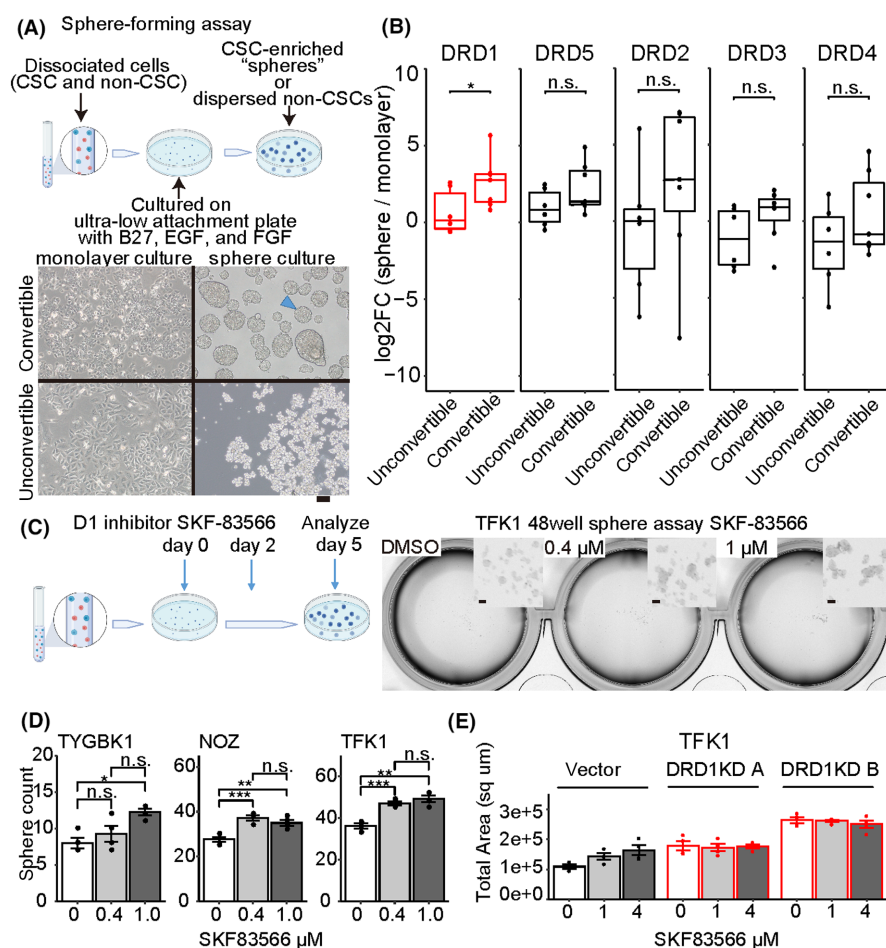


FIGURE 1 Sphere formation assay depicting increased spheres with *DRD1* inhibition. (A) Schematic picture of sphere formation assay, enriching cancer stem cells (CSCs) (blue dots) out of a mixture of CSC (blue dots) and non-CSC cells (red dots) (top). Examples of a convertible line (TYGBK1), an unconvertible line (KKU-100) (down), and a typical “sphere” (arrowhead). Scale bar, 100 μm. (B) Change in mRNA expression of dopamine receptors from monolayer culture to sphere culture quantified via qRT-PCR. Each value is calculated as the median of the triplicate. Comparison using Wilcoxon rank-sum test. *DRD1*: median log₂Foldchange (FC) of 2.8 in convertible and of 0.14 in “unconvertible,” $p = 0.035$. (C) Schematic picture of sphere formation assay (left). Examples of microscopic images of spheres (right). Scale bar, 100 μm. (D) Sphere formation assay with D1 inhibitor (SKF-83566 0.4 μM, 1 μM or DMSO) using TYGBK1, NOZ, and TKF1. Tukey’s test is used. $n = 4$. (E) Sphere formation assay with D1 inhibitor (SKF-83566 1 μM, 4 μM or DMSO) using vector-induced or *DRD1*-knockdown (KD) TKF1s $n = 4$

(Figure S4 and Table S3). The main mutations had a variant allele frequency of 50% or 100% (heterozygous or homozygous mutation), suggesting PDOs contained only tumor cells. The dopamine autosynthesis capacity in these PDOs was confirmed by qRT-PCR and ELISA (Figure S3).

Organoid formation assays were performed to evaluate the organoid-initiating cell frequency, and D1 inhibition or KD of *DRD1* increased the size and number of PDO initiations (Figure 2 and Figures S5A-D). Additionally, after long-term incubation over 2 weeks with D1 inhibition, the PDOs developed into unique warty shapes, whereas the control PDOs remained spherical in shape (Figure 2A). These results suggested that *DRD1* inhibition enhanced

reconstruction and growth of PDOs through the high tumor-initiating ability of CSC-like cells in PDOs.

3.3 | Single-cell RNA-sequence analysis revealed cancer stem cell-like and dopamine-responsive cells in patient-derived organoids

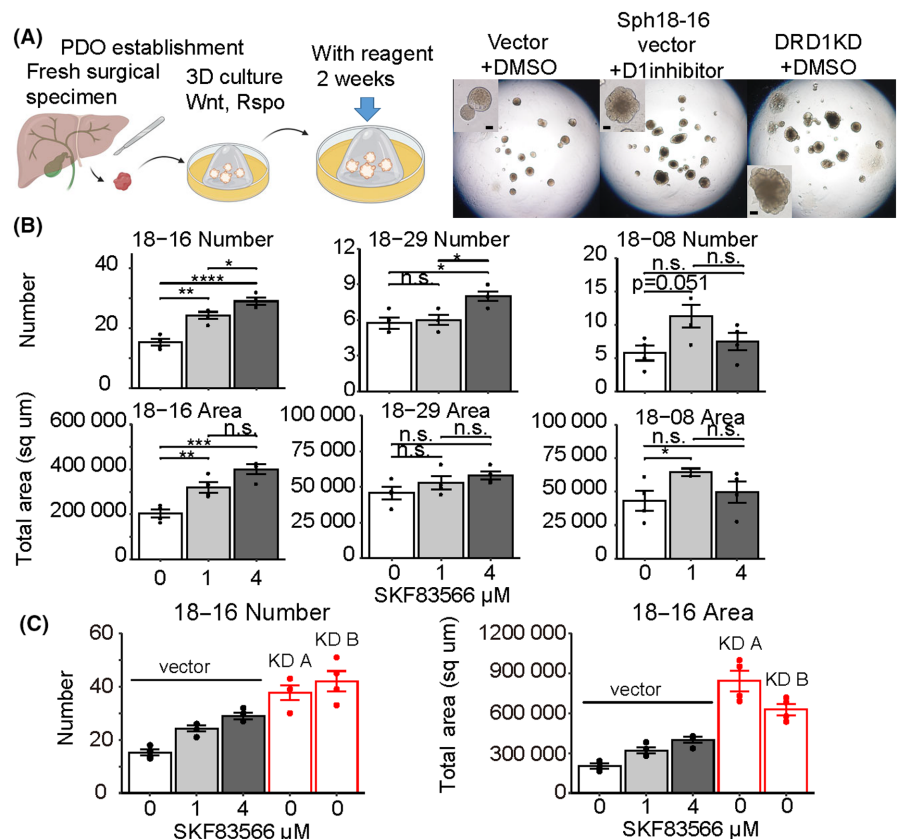
To detect how CSCs were enhanced in D1-inhibited PDOs, scRNA-seq with and without D1 inhibitor was conducted (Figure 3A). Several cell clusters with various cell cycle states were observed. Given the expressional bias in proliferating cells,³⁴ five cell clusters

TABLE 1 Clinical information of the established BDC PDOs

Number	Age	Sex	Tumor location	Histology	TNM staging by AJCC/UICC (8th)	Clinical IHC results
sph18-08	69	Male	Distal	well	T3N1M0	p53+ > 95%, IMP3+ 50%
sph18-16	76	Female	Gallbladder	mod	T2aN1M0	None
sph18-22	79	Female	Intrahepatic	mod	T1aN0M0	Focally p53+ < 5% claudin4+, IMP3+
sph18-29	73	Female	Distal	mod	T3N1M0	None

Abbreviations: AJCC, American Joint Committee on Cancer; BDC, bile duct cancer; IHC, Immunohistochemistry; mod, moderately differentiated tubular adenocarcinoma; PDO, patient-derived organoid; well, well-differentiated tubular adenocarcinoma; UICC, International Union Against Cancer.

FIGURE 2 Distinct patient-derived cancer organoid (PDO) formation with D1 inhibitor or *DRD1* KD. (A) Schematic picture of PDO establishment and organoid formation assay (left). Examples of microscopic images of PDOs cultured for 17 days (right). Scale bar, 100 μ m. (B) Organoid formation assay with D1 inhibitor (SKF-83566 1 μ M, 4 μ M, or DMSO) using Sph18-08, 16, 29. Tukey's test is used. $n = 4$. (C) Organoid formation assay with D1 inhibitor using vector-induced or *DRD1*-KD Sph18-16 $n = 4$



were further analyzed, most of which were cells in the G0/1 phase (Figure 3A right and Figure S6A-C). Three kinds of cells were found: (1) B1 and B2 with bile duct-like signatures, (2) H with hepatocyte-like signatures, and (3) INT1 and INT2 with intermediate signatures of the two.³⁵⁻³⁷ INT1, INT2, and H also expressed genes showing duodenal-stem-like signatures (Figure 3B).³⁸ In addition, B1 and B2 cells exhibited lower expression of genes related to gemcitabine, fluorouracil, doxorubicin, and docetaxel resistance, supporting that these cells were less CSC-like than were INT1, INT2, and H (Figure S7A).

Analysis of cell type-specific surface markers showed that *TROP2* (*TACSTD2*), a cell surface glycoprotein, was more highly expressed in B1 and B2 cells than in INT1 and INT2 cells, while its expression was the lowest in H cells (Figure 3C,D and Table S4). Additionally, FACS-sorted *TROP2*^{high} cells exhibited decreased organoid-initiating cell frequency and less plasticity to be *TROP2*^{low} (Figure S7B-D). This was consistent with a previous report that CD24+/CD44+ cells (INT cells, Figure 4D) had CSC-like potency in extrahepatic cholangiocarcinomas.¹⁰ Both results suggested that PDOs contained different

cell types represented by B, INT, and H clusters, among which INT and H cells revealed stem-like features.

Additionally, B1 and B2 cells exhibited higher expression of genes related to dopamine responsiveness of “adenyl-cyclase-activating” or “adenyl-cyclase-inhibiting” (Figure 3C,D). Varying protein expression levels of KRT19 (bile duct marker), PROX1 (hepatocyte marker), and DRD1 in a PDO were confirmed via immunohistochemistry (Figure S8A). In the original surgical specimen of Sph18-16, DRD1 expression overlapped with TROP2 in epithelial-like cells (Figure S8B). In addition, dopamine production among cells appeared to vary according to the expression of MAOB, a gene responsible for dopamine metabolism (Figure 3C,D, Figure S8C). This heterogeneity of dopamine responsiveness was also confirmed in another PDO, Sph18-29 (Figure S9A-D). Further, the expression of TROP2, the B cluster marker, was correlated to the gene signature associated with the dopamine D1 receptor in The Cancer Genome Atlas (TCGA) cholangiocarcinoma cohort (Figure S9E). These results indicated that TROP2-marked B cluster cells could be more dopamine-reactive than INT or H cells.

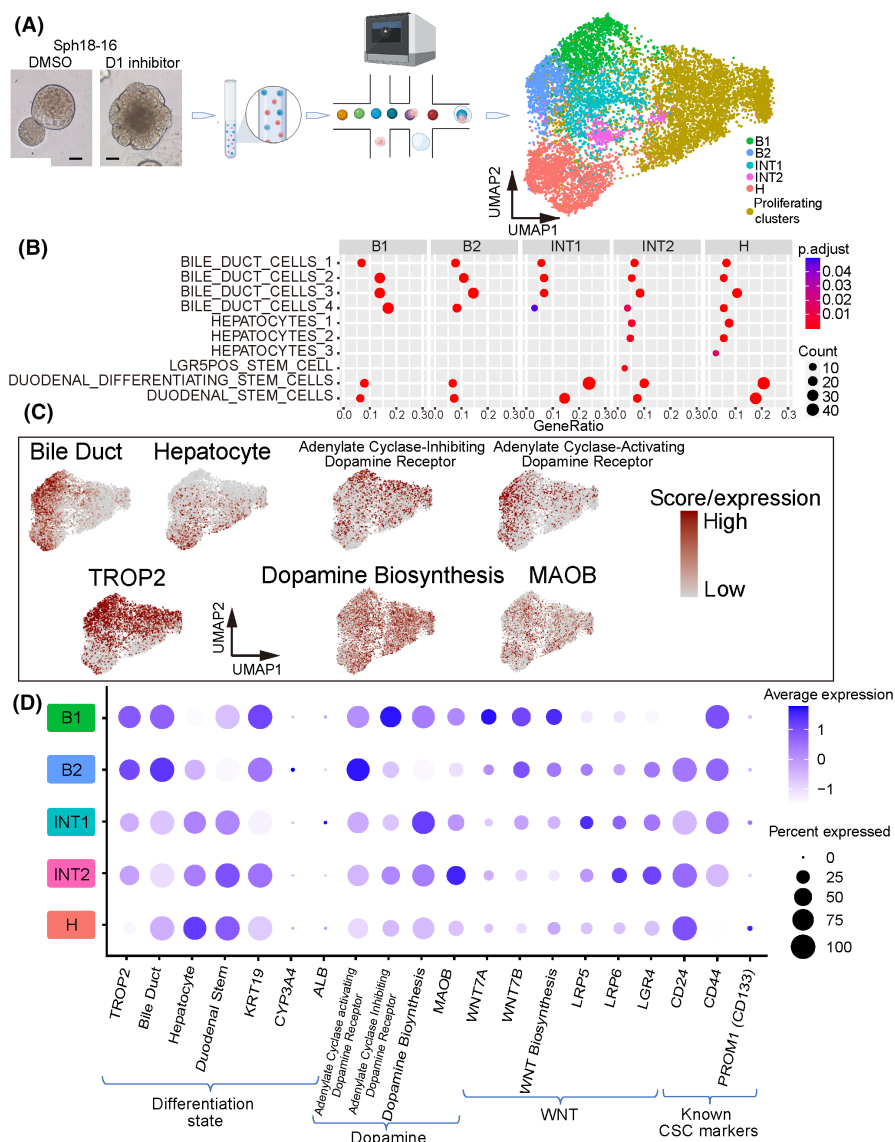


FIGURE 3 ScRNA-seq of PDO Sph18-16. (A) Schema of scRNA-seq (left) and clusters shown in Uniform Manifold Approximation and Projection (UMAP) (right). (B) Dot plot of enrichment analysis for each cluster. Gene sets related to hepato-biliary development or stem cells derived from MSigDB:C8 are listed. The color of the dots represents the adjusted *p*-value, and the diameter represents the count of enriched genes. Results of adjusted *p* < 0.05 are shown. (C) Feature plots of each gene signature score and expression of *TROP2* and *MAOB*. (D) Expressions of genes or gene signature scores of the five clusters. Table S6 shows the details of the gene sets

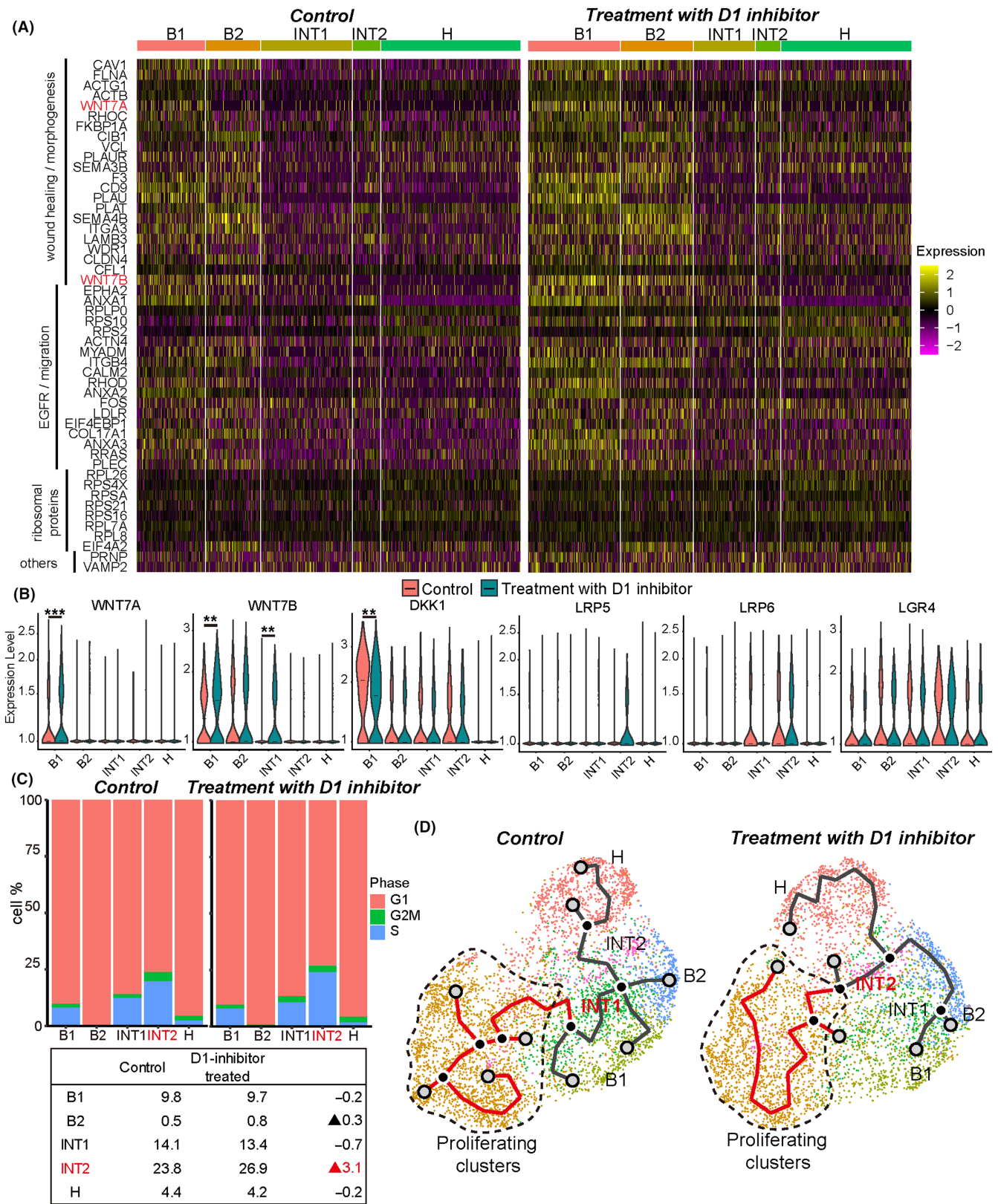


FIGURE 4 ScRNA-seq analysis comparing control (DMSO) and D1 inhibitor (SKF-83566 4 μ M) treatment. (A) Heatmap visualization of the 50 most frequently appearing upregulated genes in D1 inhibitor-treated Sph18-16 sample by enrichment analysis using all GOBP terms. The details are provided in Table S5. (B) Violin plots depicting the expression of genes compared with control (red) and D1 inhibitor-treated sample (teal). Bar indicates the median value. Adjusted *p*-value for B1 of WNT7A, 0.00058; B1 of WNT7B, 0.0029; INT1 of WNT7B, 0.0013; B1 of DKK1, 0.0018. (C) Proliferating cells of each cluster in control or D1 inhibitor-treated sample (top). Listed percentages of cells in S and G2/M phases of each cluster (down). (D) Trajectories showing INT1 as the center in DMSO and INT2 in D1 inhibitor treatment

3.4 | WNT7B is produced by B subtypes and enhanced by D1 inhibition

To explore the cause of CSC enhancement by D1 inhibition, we performed enrichment analysis and compared control and D1 inhibitor-treated samples with all gene sets of GO-term BP. Three significant pathways with high enrichment of highly expressed genes in D1 inhibitor-treated cells were identified: EGFR signaling, ribosomal proteins, and wound healing or morphogenesis (Figure 4A and Table S5). EGFR signaling is reported to be associated with cholangiocarcinoma plasticity, and its upregulation is concordant to enhancement of CSCs.¹ In addition, increased ribosomal protein might be interpreted as enhancement of cell proliferation. The current study focused on upregulated WNT7A/7B in wound healing-related genes because WNT7A/B could be the cause of increased proliferation or CSC-like potential.^{26,39,40}

Further, the expression of WNT7A/7B was higher in B cells, whereas expressions of the receptor or coreceptor genes of Wnt (*LRP5*, *LRP6*, and *LGR4*) were higher in INTs, the suspected CSC subtyped cells (Figure 3D). D1 inhibitor treatment increased WNT7A/7B expression in B1 and INT1 cells and decreased the expression of *DKK1*, a negative regulator of Wnt signaling. In contrast, the expressions of *LRP5*, *LRP6*, and *LGR4* showed no significant changes (Figure 4B). The increased expression of WNT7B in TROP2-positive cells was confirmed by confocal immunofluorescent image (Figure S10A). Additionally, D1 inhibitor treatment-induced increase in gene expression related to Wnt signaling was most evident in INT2 cells (Figure S10B). Wnt signaling is related to the self-renewal of CSCs,⁴¹ and D1 inhibition-induced increase in their proliferating population was most pronounced in INT2 cells (Figure 4C). Thus, it is supposed that increased WNT7A/7B by D1 inhibition in B cells promoted INT cell proliferation.

Trajectory analyses identified that INT cells were centered and branched into B, H, and proliferating clusters (Figure 4D), suggesting a cellular hierarchy with INT cells at the top. D1 inhibitor treatment shifted the center from INT1 to INT2, which also supported the above deduction that D1 inhibition promoted INT2 proliferation. Heterogeneous WNT7B expression in original surgical specimens was confirmed in Sph18-16 and 18-29 (Figure S10C). However, PDO Sph18-29 did not express WNT7A (Figure S9C). Further, in the TCGA datasets, the WNT7A expression level was not higher in BDCs than that in normal tissue (Figure S10D). In contrast, WNT7B expression was the highest in the Wnt gene family (Figure S10D). Hence, we assumed that WNT7B is the main possible CSC niche factor involved in D1 inhibition.

3.5 | Effect of D1 inhibitor depends on Wnt aut signaling

To elucidate the contribution of Wnt overexpression under DRD1-regulated control in BDC cell proliferation, Wnt signaling

was blocked via the porcupine inhibitor LGK974. Porcupine is an endoplasmic reticulum transmembrane protein essential for the processing and correct localization of Wnt proteins, and this was initially confirmed in PC12 rat neuronal cells.^{42,43} In sphere assays of TYGBK1, NOZ, and TFK1, LGK974 canceled the increase of sphere formation by D1 inhibition (Figure 5A). Similar results with LGK974 were confirmed in three PDOs: Sph18-08, Sph18-16, and Sph18-29 (Figure 5B and Figure S11A). To identify the mechanism of increased WNT7B by D1 inhibition, a Kyoto Encyclopedia of Genes and Genomes (KEGG) pathway map analysis was performed in B1 cells (Figure S11B).

The results showed increased c-FOS expression downstream of dopamine receptors. C-FOS is known to be increased by ERK.⁴⁴ In studies of osteosarcoma, in which D1 inhibitors or DRD1-KD increased its proliferation, a D1 inhibitor increased ERK1/2 activity,⁴⁵ and FOS directly controlled the expression of endogenous WNT7B.⁴⁶ Similarly, increased c-FOS expression downstream of ERK was confirmed in B1 cells in the current study (Figure S11C). In the TCGA dataset, the gene signature of DRD1 was correlated to that of ERK and so was that of ERK and FOS, or FOS and WNT7B (Figure S11D). Further, higher expression of WNT7B was a poor prognostic factor in BDC (Figure S11E). These results suggested that increased WNT7B by D1 inhibition was mediated by ERK-FOS signaling.

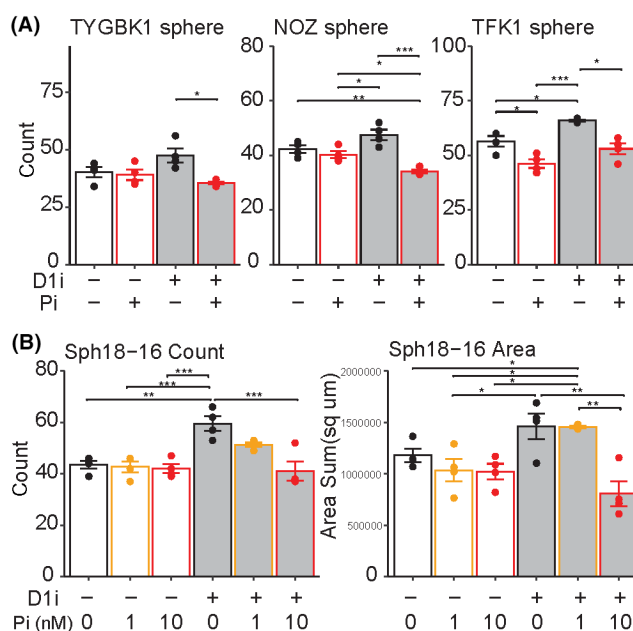


FIGURE 5 Aut signaling of Wnt as downstream of D1 inhibition. (A) Sphere formation assay with D1 inhibitor (SKF-83566 0.4 μ M for NOZ and TFK1, 1 μ M for TYGBK1, or DMSO) and porcupine inhibitor (LGK974 1 nM for NOZ and TFK1, 10 nM for TYGBK1 or DMSO). Tukey's test is used, $n = 4$. D1i, D1 inhibitor; Pi, porcupine inhibitor. (B) Organoid formation assay of Sph18-16 with D1 inhibitor (SKF-83566 4 μ M or DMSO) and porcupine inhibitor (LGK974 1 nM, 10 nM or DMSO). Tukey's test is used, $n = 4$. Results of Sph18-08 and 29 are shown in Figure S11A.

FIGURE 6 D1 inhibition enhancing cancer stem cell (CSC)-related capacities in the absence of exogenous niches. (A) Peri-sciatic nerve xenograft, subcutaneous xenograft, and splenic injection assay of Sph18-29. Vector or two independent DRD1-targeting shRNA is transduced to Sph18-29. Table of the result (right). (B) Gross images of xenografted tumor in the peri-sciatic nerve (left). Control patient-derived cancer organoid (PDO tumor forming only along the nerves (arrowhead). Scale bar, 5 mm. The tumor size vertical to the nerve (mm) is measured (right). Wilcoxon rank-sum test is used. (C) Macroscopic and HE-stained histological images of a subcutaneously xenografted tumor and lung metastasis of DRD1-KD sph18-29. Scale bar, 5 mm in macroscopic images and 100 μ m in histological images. (D) CCK8 proliferation assay of Sph18-16, 29 with 5FU in the niche-enriched or niche-deficient medium, $n = 4$. The result of cisplatin and gemcitabine is shown in Figure S12C. Two-tailed unpaired Student's *t*-test is used at each concentration

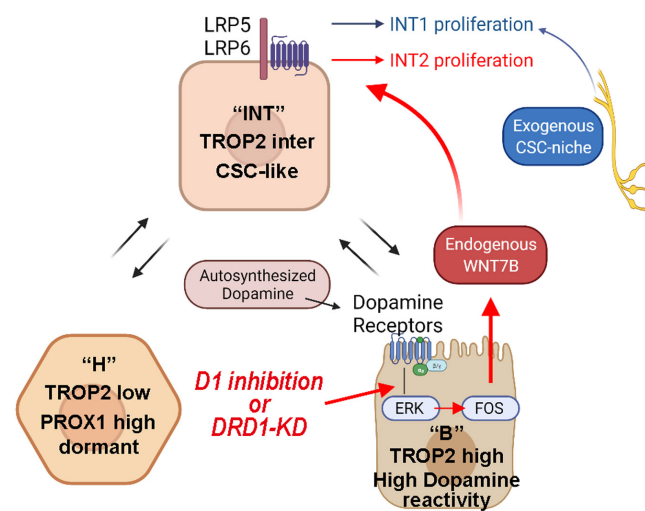
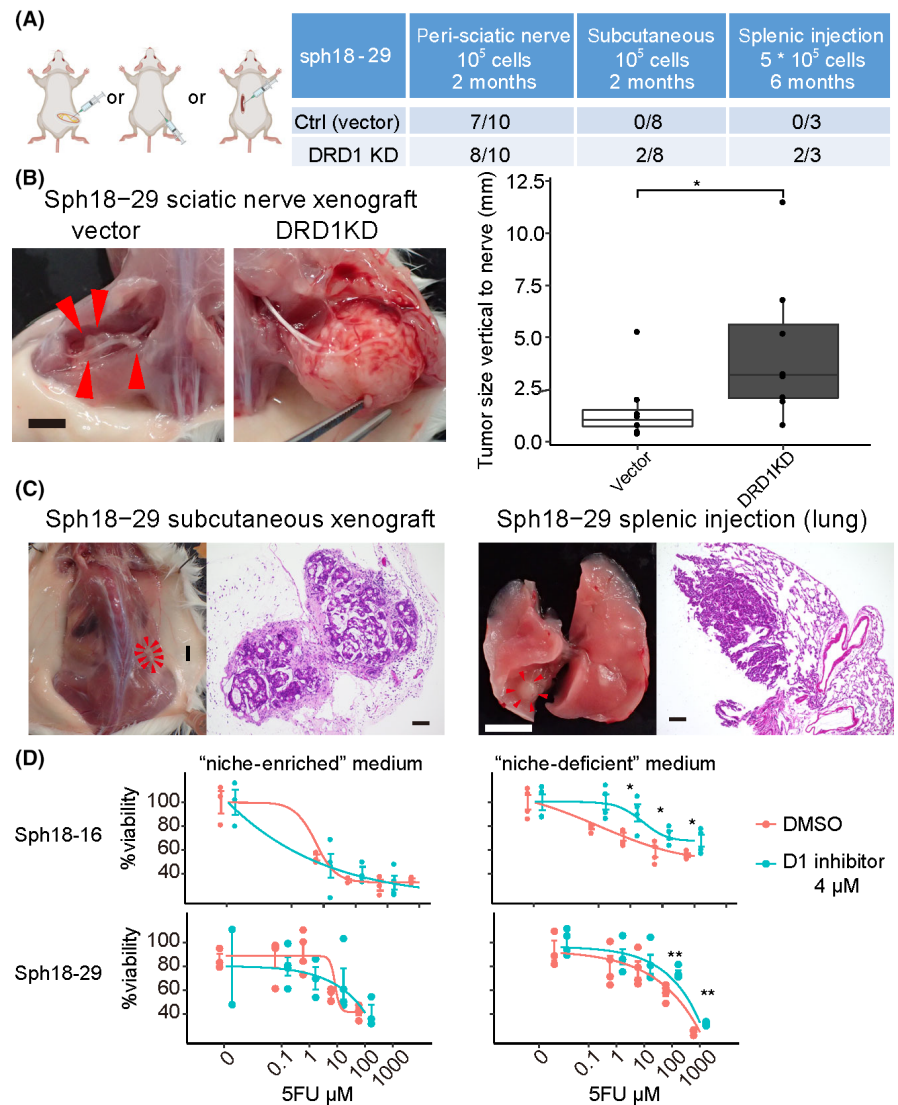


FIGURE 7 Schematic illustrations depicting variations of B, INT, H clusters, and WNT7B as endogenous cancer stem cell (CSC) niche downstream of DRD1-ERK-FOS

3.6 | Effect of D1 inhibition is pronounced in the absence of the exogenous cancer stem cell niches

Thus far, we have found that the autotransmitted dopamine of BDCs affected their endogenous Wnt signaling. Lastly, the effects of D1 inhibition were examined in different microenvironments. Given that BDCs are neurotropic cancers, comparative xenotransplantation assays with DRD1-KD PDOs were performed in three different sites in the NOD-SCID mouse: peri-sciatic nerve, subcutaneous, and spleen (Figure 6A). In peri-sciatic nerve xenografts, the efficacy of tumor initiation was similar between the vector and DRD1-KD PDOs (7/10 and 8/10; Figure 6A and Figure S12A). However, the size of the masses was larger in DRD1-KD PDOs (Figure 6B). Additionally, most of the vector PDO (6/7) formed masses only along the nerves (Figure 6B arrowhead), whereas DRD1-KD PDOs could grow away from the nerves (5/8). Tumor initiation of subcutaneous and splenic injected cells was lower than that of peri-sciatic-nerve transplanted cells, but only DRD1-KD PDO cells formed subcutaneous mass or

lung metastasis (Figure 6A,C). Similar findings were confirmed with another PDO (Figure S12B). These results suggested that the neural-related niche could also enhance CSCs and that the effect of D1 inhibition was more pronounced in their absence.

Given that the organoid culture medium contained neural stem cell-related niche factors such as B-27 supplement⁴⁷ or *Wnt3a*,⁴⁸ we next examined chemoresistant proliferation, another CSC-related property, with PDOs precultured with D1 inhibitor in niche-enriched and niche-deficient media. In the niche-enriched medium, there was no difference in chemoresistance between the D1 inhibition and control groups; however, in the “niche-deficient” medium, chemoresistance was enhanced by D1 inhibition in two PDOs with three cytotoxic reagents (5FU, cisplatin, and gemcitabine; Figure 6D and Figure S12C). Therefore, neural-related niche factors and D1 inhibition might partially overlap in enhancing CSC-related properties, and this is consistent with our result that D1 inhibition increased CSC proliferation via Wnt signaling (Figure 7).

4 | DISCUSSION

The genetic landscape of BDC is comparatively broad, and the common nongenetic mechanism causing therapeutic resistance has not been elucidated.¹ The current study, using single-cell analysis of clinical human materials, describes a spectrum of cell-differentiation states from bile duct-like to hepatocyte-like differentiation, including intermediate clusters such as CSCs. The findings are consistent with a previous report indicating similarity between differentiating lineages of tumor and normal tissue development.³ A previous study with scRNA-seq of normal liver tissue showed that TROP2 expression was negatively correlated with hepatocyte fate.³⁷ In our analysis, TROP2^{high} was inferred as a bile duct-like cell marker and TROP2^{inter} or TROP2^{low} as markers for suspected CSC-like cells. PROX1 is a stable hepatocyte marker,⁴⁹ and our scRNA-seq confirmed its expression in the hepatocyte-like cluster (Table S4E), although “hepatocyte-like” was a relative signature with low expression of the developed hepatocyte markers CYP3A4 and ALB (Figure 3D). Another report described PROX1 as a marker for dormant CSC.³³ Consistently, the current study found that hepatocyte-like clusters with the signature of duodenal stem genes (Figure 3B,D) had less proliferative fractions (Figure 4C). Conclusively, TROP2 and PROX1 are potential markers for analyzing BDC heterogeneity.

Using sphere/organoid formation assays focusing on autotransduced dopamine, the current study identified DRD1 signaling as a potential regulator of CSCs. Additionally, scRNA-seq analysis showed that D1 inhibition increased WNT7B expression in bile duct-like cells, resulting in the proliferation of CSC-like INT2 cells. This is in contrast with the self-inhibition of SP cell expansion by SFRP4, secreted from non-SP cells in B-cell lymphoma.⁵⁰ Thus, BDCs might monitor autotransduced dopamine by DRD1, with its low signaling leading to the autonomous proliferation of CSCs via increased endogenous WNT7B levels.

For the detailed molecular mechanism, we developed a cascade of DRD1-ERK-FOS-WNT7B based on KEGG pathway map analysis and previous reports⁴⁴⁻⁴⁶ and confirmed its clinical relevance in the TCGA dataset (Figures S9E and S11D,E). The scRNA-seq analysis did not detect mRNA expression of *DRD1* in many populations, although DRD1 protein expression was confirmed in Western blotting or immunohistochemistry (Figures S5B,D, S8A,B, and S9D). This result may be attributed to the technical limitation of detecting low or continuously expressed protein mRNA at a single-cell level.⁵¹ Thus, gene signature analysis was used to evaluate DRD1 signaling activity. In the BDC cohort of TCGA, higher expression of *WNT7B* was a poor prognostic factor (Figure S11E), and there were expressional correlations among *WNT7B*, *FOS*, ERK signaling and DRD1-related genes (Figure S11D). This suggested the clinical relevance of DRD1-ERK-FOS-WNT7B cascade in the entire BDC cohort.

However, BDCs are heterogeneous in their genetic backgrounds, and their individual reactivities to dopamine or WNT7B may vary. In the current study, 2 of the 13 commercially available BDC cell lines, TYGBK8 and OZ, form sphere-like aggregates even in 2D culture condition with a high expressional level of CSC-related genes (Figure S13A). The number of spheres was also increased in TYGBK8 under low-dose D1 inhibitor treatment but not in OZ (Figure S13B). This might imply that the CSC capacity of OZ did not depend on dopamine signaling and high malignancy of OZ, which was originally obtained from the ascitic effusion, was suspected.⁵² Sph18-29 had CTNNB1 exon 3 mutation (Figure S4), which is reported to be associated with activation of the Wnt/ β -catenin pathway.⁵³ Nevertheless, porcupine inhibitor suppressed organoid formation of Sph18-29 cells. We suspect that WNT7B also activated the noncanonical WNT pathway, as is reported in pancreatic progenitor cells⁵⁴ or prostate cancer.⁵⁵ Therefore, the contributions of D1 signaling or WNT7B could depend on the cell line characteristics.

This study has some limitations. It focused primarily on tumor cells and not on nontumor cells such as fibroblasts, immune cells, or neural cells. As for the neural-related niche, we showed its possible functional overlap with tumoral Wnt self-signaling (Figure 6). Moreover, in the genes upregulated by D1 inhibition (Figure 4A), there were other intercellular signaling genes, including the semaphorin gene family (*SEMA3B*, *SEMA4B*). The semaphorin gene family was initially identified as a neural developmental factor and recently emerged as a regulator of malignancy through cross-talk with tumor microenvironments.⁵⁶ The neural-related niche and cross-talks causing neurotropism of PDOs (Figure 6 and Figure S12B,C) require further analysis.

In conclusion, although more than 150 clinical trials targeting CSC are currently ongoing,⁸ most responses have been modest, especially in solid tumors. This implies that targeting only CSCs might trigger feedback signaling to enhance CSCs. The current study supports that the D1 self-signaling of BDCs might be a vital regulator of autonomous CSC growth via ERK-FOS and WNT7B. Thus, inhibition of this feedback signaling may lead to novel combination therapies with conventional chemotherapy.

AUTHOR CONTRIBUTIONS

Conceptualization, AY, TM, and ST; Methodology, AY, ST, KM, RC, SS, AW, RI, and MMN; Investigation, AY, ST, KM, RC, YK, KN, TA, SW, SS, AW, RI, and MMN; Validation, KM, RC, SS, AW, RI, and MMN; Software, AY, SS, AW, RI, and MMN; Data curation, AY and ST; Formal analysis, AY, SS, AW, RI, and MMN; Visualization, AY and AW; Resources, AY and ST; Funding acquisition, TM and ST; Project administration, TM, ST, SO, HS, SU, and EH; Supervision, TM and ST; Writing—original draft, AY; Writing—review & editing, TM, ST, and SW.

ACKNOWLEDGMENTS

We thank S. Yokoyama, previously from the Medical Innovation Center DSK Project, for mice breeding and technical support; H. Umehara, T Kodo, and M Takamura for project management; M. Nishikawa from the Kyoto Institute of Nutrition & Pathology for immunohistochemistry staining; MARUZEN-YUSHODO. (<https://kw.maruzen.co.jp/kousei-honyaku/>); and Editage (<https://www.editage.com/>) for the English language editing. Figures 1A,C, 2A, and 3A (middle), Figure 6A (left), and Figure 7 were created with a licensed version of BioRender.com (to AY, 2022) by adaption of BioRender templates, retrieved from <https://app.biorender.com/biorender-templates>.

FUNDING INFORMATION

TM received funding from Grants-in-Aid KAKENHI (21 K08732), and ST received funding from Grants-in-Aid KAKENHI (17 K09460), both research programs from the Ministry of Education, Culture, Sports, Science, and Technology. In addition, TM and ST received research funding from Sumitomo Pharma.

CONFLICT OF INTEREST

TM and ST received partial support from Sumitomo Pharma. SW and RI are employees of Sumitomo Pharma. SO and HS are editorial board members of *Cancer Science*. The other authors declare no competing financial interests in this study.

ETHICS STATEMENTS

Approval of the research protocol by an Institutional Review Board: The research protocol was approved by the ethical committee of Kyoto University Hospital (approval number: R1281). PDOs were established from fresh surgical specimens obtained from patients who underwent surgical resection at Kyoto University Hospital. All experiments were conducted according to the Declaration of Helsinki and the guidelines and regulations of the committee.

Informed Consent. For PDO establishment, informed consent in writing was obtained from each patient.

Registry and the Registration No. of the study/trial. N/A.

Animal Studies. All procedures for animal experiments were conducted in compliance with the ARRIVE guidelines and the Institutional Animal Welfare Guidelines of Kyoto University.

ORCID

Akitada Yogo  <https://orcid.org/0000-0002-7434-6974>

Toshihiko Masui  <https://orcid.org/0000-0002-4001-4824>

Shigeo Takaishi  <https://orcid.org/0000-0003-2236-6081>

REFERENCES

- Banales JM, Marin JGG, Lamarca A, et al. Cholangiocarcinoma 2020: the next horizon in mechanisms and management. *Nat Rev Gastroenterol Hepatol*. 2020;17(9):557-588. doi:10.1038/s41575-020-0310-z
- Van VJLA, Gaspersz MP, Coelen RJS, et al. The prognostic value of portal vein and hepatic artery involvement in patients with perihilar cholangiocarcinoma. *Int Hepato-Pancreato-Biliary Assoc*. 2018;20(1):83-92. doi:10.1016/j.hpb.2017.08.025
- Lee HO, Hong Y, Etlioglu HE, et al. Lineage-dependent gene expression programs influence the immune landscape of colorectal cancer. *Nat Genet*. 2020;52(6):594-603. doi:10.1038/s41588-020-0636-z
- Clevers H. The cancer stem cell: premises, promises and challenges. *Nat Med*. 2011;17(3):313-319. doi:10.1038/nm.2304
- Battle E, Clevers H. Cancer stem cells revisited. *Nat Med*. 2017;23(10):1124-1134. doi:10.1038/nm.4409
- Chaffer CL, Brueckmann I, Scheel C, et al. Normal and neoplastic nonstem cells can spontaneously convert to a stem-like state. *Proc Natl Acad Sci USA*. 2011;108(19):7950-7955. doi:10.1073/pnas.1102454108
- Shimokawa M, Ohta Y, Nishikori S, et al. Visualization and targeting of LGR5 + human colon cancer stem cells. *Nature*. 2017;545(7653):187-192. doi:10.1038/nature22081
- Yang L, Shi P, Zhao G, et al. Targeting cancer stem cell pathways for cancer therapy. *Signal Transduct Target Ther*. 2020;5(1):8. doi:10.1038/s41392-020-0110-5
- Shi C, Tian R, Wang M, et al. CD44+CD133+ population exhibits cancer stem cell-like characteristics in human gallbladder carcinoma. *Cancer Biol Ther*. 2010;10(11):1182-1190. doi:10.4161/cbt.10.11.13664
- Wang M, Xiao J, Shen M, et al. Isolation and characterization of tumorigenic extrahepatic cholangiocarcinoma cells with stem cell-like properties. *Int J Cancer*. 2011;128(1):72-81. doi:10.1002/ijc.25317
- Mayr C, Ocker M, Ritter M, Pichler M, Neureiter D, Kiesslich T. Biliary tract cancer stem cells - translational options and challenges. *World J Gastroenterol*. 2017;23(14):2470-2482. doi:10.3748/wjg.v23.i14.2470
- Chen S, Zhang B, Zhou B, Zhu C, Sun L, Feng Y. Perineural invasion of cancer : a complex crosstalk between cells and molecules in the perineural niche. *Am J Cancer Res*. 2019;9(1):1-21.
- Amit M, Na'Ara S, Gil Z. Mechanisms of cancer dissemination along nerves. *Nat Rev Cancer*. 2016;16(6):399-408. doi:10.1038/nrc.2016.38
- Kawamata H, Yamashita K, Nakamura K. Perineural invasion and preoperative serum CA19-9 as predictors of survival in biliary tract cancer. *Anticancer Res*. 2013;33(2):583-594.
- Tan X, Sivakumar S, Bednarsch J, et al. Nerve fibers in the tumor microenvironment in neurotropic cancer—pancreatic cancer and cholangiocarcinoma. *Oncogene*. 2021;40(5):899-908. doi:10.1038/s41388-020-01578-4
- Coufal M, Invernizzi P, Gaudio E, et al. Increased local dopamine secretion has growth-promoting effects in cholangiocarcinoma. *Int J Cancer*. 2010;126(9):2112-2122. doi:10.1002/ijc.24909
- Hall C, Sato K, Wu N, et al. Regulators of Cholangiocyte proliferation. *Gene Expr*. 2017;17(2):155-171. doi:10.3727/105221616X692568

18. Huang L, Frampton G, Rao A, et al. Monoamine oxidase a expression is suppressed in human cholangiocarcinoma via coordinated epigenetic and IL-6-driven events. *Lab Invest.* 2012;92(10):1451-1460. doi:10.1038/labinvest.2012.110
19. Sachlos E, Risueño RM, Laronde S, et al. Identification of drugs including a dopamine receptor antagonist that selectively target cancer stem cells. *Cell.* 2012;149(6):1284-1297. doi:10.1016/j.cell.2012.03.049
20. Yang L, Yao Y, Yong L, et al. Dopamine D1 receptor agonists inhibit lung metastasis of breast cancer reducing cancer stemness. *Eur J Pharmacol.* 2019;859:172499. doi:10.1016/j.ejphar.2019.172499
21. Hao F, Wang S, Zhu X, et al. Pharmacokinetic-pharmacodynamic modeling of the anti-tumor effect of sunitinib combined with dopamine in the human non-small cell lung cancer xenograft. *Pharm Res.* 2017;34(2):408-418. doi:10.1007/s11095-016-2071-5
22. Zhao H, Yan C, Hu Y, et al. Sphere-forming assay vs. organoid culture: determining long-term stemness and the chemoresistant capacity of primary colorectal cancer cells. *Int J Oncol.* 2019;54(3):893-904. doi:10.3892/ijo.2019.4683
23. Marsee A, Roos FJM, Verstegen MMA, et al. Building consensus on definition and nomenclature of hepatic, pancreatic, and biliary organoids. *Cell Stem Cell.* 2021;28(5):816-832. doi:10.1016/j.stem.2021.04.005
24. Miyoshi H, Stappenbeck TS. In vitro expansion and genetic modification of gastrointestinal stem cells in spheroid culture. *Nat Protoc.* 2013;8(12):2471-2482. doi:10.1038/nprot.2013.153
25. Boj SF, Il HC, Baker LA, et al. Organoid models of human and mouse ductal pancreatic cancer. *Cell.* 2015;160(1-2):324-338. doi:10.1016/j.cell.2014.12.021
26. Seino T, Kawasaki S, Shimokawa M, et al. Human pancreatic tumor organoids reveal loss of stem cell niche factor dependence during disease progression. *Cell Stem Cell.* 2018;22(3):454-467.e6. doi:10.1016/j.stem.2017.12.009
27. Masuo K, Chen R, Yogo A, et al. SNAIL2 contributes to tumorigenicity and chemotherapy resistance in pancreatic cancer by regulating IGFBP2. *Cancer Sci.* 2021;112(12):4987-4999. doi:10.1111/cas.15162
28. Watanabe S, Yogo A, Otsubo T, et al. Establishment of patient-derived organoids and a characterization-based drug discovery platform for treatment of pancreatic cancer. *BMC Cancer.* 2022;22(1):489. doi:10.1186/s12885-022-09619-9
29. Partecke IL, Kaeding A, Sendler M, et al. In vivo imaging of pancreatic tumours and liver metastases using 7 tesla MRI in a murine orthotopic pancreatic cancer model and a liver metastases model. *BMC Cancer.* 2011;11:40. doi:10.1186/1471-2407-11-40
30. Gil Z, Rein A, Brader P, et al. Nerve-sparing therapy with oncolytic herpes virus for cancers with neural invasion. *Clin Cancer Res.* 2007;13(21):6479-6485. doi:10.1158/1078-0432.CCR-07-1639
31. Reynolds B, Weiss S. Generation of neurons and astrocytes from isolated cells of the adult mammalian central nervous system. *Science.* 1992;255(5052):1707-1710. doi:10.1126/science.1553558
32. Pastrana E, Silva-Vargas V, Doetsch F. Eyes wide open: a critical review of sphere-formation as an assay for stem cells. *Cell Stem Cell.* 2011;8(5):486-498. doi:10.1016/j.stem.2011.04.007
33. Shiokawa D, Sakai H, Ohata H, et al. Slow-cycling cancer stem cells regulate progression and chemoresistance in colon cancer. *Cancer Res.* 2020;80(20):4451-4464. doi:10.1158/0008-5472.CAN-20-0378
34. Okamoto T, duVerle D, Yaginuma K, et al. Comparative analysis of patient-matched PDOs revealed a reduction in OLFM4-associated clusters in metastatic lesions in colorectal cancer. *Stem Cell Rep.* 2021;16(4):954-967. doi:10.1016/j.stemcr.2021.02.012
35. Liberzon A, Subramanian A, Pinchback R, Thorvaldsdóttir H, Tamayo P, Mesirov JP. Molecular signatures database (MSigDB) 3.0. *Bioinformatics.* 2011;27(12):1739-1740. doi:10.1093/bioinformatics/btr260
36. Aizarani N, Saviano A, Sagar ML, et al. A human liver cell atlas reveals heterogeneity and epithelial progenitors. *Nature.* 2019;572(7768):199-204. doi:10.1038/s41586-019-1373-2
37. Busslinger GA, Weusten BLA, Bogte A, Begthel H, Brosens LAA, Clevers H. Human gastrointestinal epithelia of the esophagus, stomach, and duodenum resolved at single-cell resolution. *Cell Rep.* 2021;34(10):108819. doi:10.1016/j.celrep.2021.108819
38. Gao S, Yan L, Wang R, et al. Tracing the temporal-spatial transcriptome landscapes of the human fetal digestive tract using single-cell RNA-sequencing. *Nat Cell Biol.* 2018;20(6):721-734. doi:10.1038/s41556-018-0105-4
39. Boulter L, Guest RV, Kendall TJ, et al. WNT signaling drives cholangiocarcinoma growth and can be pharmacologically inhibited. *J Clin Invest.* 2015;125(3):1269-1285. doi:10.1172/JCI76452
40. Arensman MD, Kovochich AN, Kulikauskas RM, et al. WNT7B mediates autocrine WNT/ β -catenin signaling and anchorage-independent growth in pancreatic adenocarcinoma. *Oncogene.* 2014;33(7):899-908. doi:10.1038/onc.2013.23
41. Zhan T, Rindtorff N, Boutros M. Wnt signaling in cancer. *Oncogene.* 2017;36(11):1461-1473. doi:10.1038/onc.2016.304
42. Kadowaki T, Wilder E, Klingensmith J, Zachary K, Perrimon N. The segment polarity gene porcupine encodes a putative multitransmembrane protein involved in wingless processing. *Genes Dev.* 1996;10(24):3116-3128. doi:10.1101/gad.10.24.3116
43. Caricasole A, Ferraro T, Rimland JM, Terstappen GC. Molecular cloning and initial characterization of the MG61/PORC gene, the human homologue of the drosophila segment polarity gene porcupine. *Gene.* 2002;288(1-2):147-157. doi:10.1016/s0378-1119(02)00467-5
44. Monje P, Hernández-Losa J, Lyons RJ, Castellone MD, Gutkind JS. Regulation of the transcriptional activity of c-Fos by ERK. A novel role for the prolyl isomerase PIN1. *J Biol Chem.* 2005;280(42):35081-35084. doi:10.1074/jbc.C500353200
45. Gao J, Zhang C, Gao F, Li H. The effect and mechanism of dopamine D1 receptors on the proliferation of osteosarcoma cells. *Mol Cell Biochem.* 2017;430(1-2):31-36. doi:10.1007/s11010-017-2951-y
46. Matsuoka K, Bakiri L, Wolff LI, et al. Wnt signaling and Lox12 promote aggressive osteosarcoma. *Cell Res.* 2020;30(10):885-901. doi:10.1038/s41422-020-0370-1
47. Brewer GJ, Torricelli JR, Evege EK, Price PJ. Optimized survival of hippocampal neurons in B27-supplemented neurobasal, a new serum-free medium combination. *J Neurosci Res.* 1993;35(5):567-576. doi:10.1002/jnr.490350513
48. Ikeya M, Lee SMK, Johnson JE, Mc Mahon AP, Takada S. Wnt signalling required for expansion of neural crest and CNS progenitors. *Nature.* 1997;389(6654):966-970. doi:10.1038/40146
49. Dudas J, Elmaouhoub A, Mansuroglu T, et al. Prospero-related homeobox 1 (Prox1) is a stable hepatocyte marker during liver development, injury and regeneration, and is absent from "oval cells". *Histochem Cell Biol.* 2006;126(5):549-562. doi:10.1007/s00418-006-0191-4
50. Koch R, Demant M, Aung T, et al. Populational equilibrium through exosome-mediated Wnt signaling in tumor progression of diffuse large B-cell lymphoma. *Blood.* 2014;123(14):2189-2198. doi:10.1182/blood-2013-08-523886
51. Mair F, Erickson JR, Voillet V, et al. A targeted multi-omic analysis approach measures protein expression and low-abundance

- transcripts on the single-cell level. *Cell Rep.* 2020;31(1):107499. doi:10.1016/j.celrep.2020.03.063
52. Homma S, Nagamori S, Fujise K, et al. Human bile duct carcinoma cell line producing abundant mucin in vitro. *Gastroenterol Jpn.* 1987;22(4):474-479. doi:10.1007/BF02773816
 53. Gao C, Wang Y, Broaddus R, Sun L, Xue F, Zhang W. Exon 3 mutations of CTNNB1 drive tumorigenesis: a review. *Oncotarget.* 2017;9(4):5492-5508. doi:10.18632/oncotarget.23695
 54. Kimura A, Toyoda T, Iwasaki M, Hiram R, Osafune K. Combined omics approaches reveal the roles of non-canonical WNT7B signaling and YY1 in the proliferation of human pancreatic progenitor cells. *Cell Chem Biol.* 2020;27(12):1561-1572.e7. doi:10.1016/j.chembiol.2020.08.018
 55. Zheng D, Decker KF, Zhou T, et al. Role of WNT7B-induced non-canonical pathway in advanced prostate cancer. *Mol Cancer Res.* 2013;11(5):482-493. doi:10.1158/1541-7786.MCR-12-0520
 56. Mastrantonio R, You H, Tamagnone L. Semaphorins as emerging clinical biomarkers and therapeutic targets in cancer. *Theranostics.* 2021;11(7):3262-3277. doi:10.7150/thno.54023

SUPPORTING INFORMATION

Additional supporting information can be found online in the Supporting Information section at the end of this article.

How to cite this article: Yogo A, Masui T, Takaishi S, et al. Inhibition of dopamine receptor D1 signaling promotes human bile duct cancer progression via WNT signaling. *Cancer Sci.* 2022;00:1-13. doi:10.1111/cas.15676

Original Article

Inhibition of Dopamine Receptor D1 Signaling Promotes Human Bile Duct Cancer

Progression via WNT signaling

Akitada Yogo^{1,2}, Toshihiko Masui^{2*}, Shigeo Takaishi^{1,3*}, Kenji Masuo^{1,3}, Ru Chen^{1,3}, Yosuke Kasai², Kazuyuki Nagai², Takayuki Anazawa², Sadanori Watanabe^{1,4}, Satoko Sakamoto⁵, Akira Watanabe⁵, Ryosaku Inagaki^{1,4}, Masahiro M. Nakagawa^{1,6}, Seishi Ogawa^{1,6}, Hiroshi Seno^{1,3}, Shinji Uemoto^{2,7}, Etsuro Hatano²

¹DSK Project, Medical Innovation Center, Graduate School of Medicine, Kyoto University, Kyoto, Japan

²Division of Hepato-Biliary-Pancreatic Surgery and Transplantation, Department of Surgery, Graduate School of Medicine, Kyoto University, Kyoto, Japan

³Department of Gastroenterology and Hepatology, Graduate School of Medicine, Kyoto University, Kyoto, Japan

⁴Cancer Research Unit, Sumitomo Pharma Co., Ltd. Osaka, Japan

⁵Medical Innovation Center, Kyoto University Graduate School of Medicine, Kyoto, Japan

⁶Department of Pathology and Tumor Biology, Kyoto University, Kyoto, Japan

⁷Shiga University of Medical Science, Shiga, Japan

*These authors jointly supervised this study.

Corresponding authors:

*Toshihiko Masui, M.D., Ph.D.

Division of Hepato-Biliary-Pancreatic Surgery and Transplantation, Department of Surgery,
Graduate School of Medicine, Kyoto University, 54, Shogoin-Kawaharacho, Sakyo-ku, Kyoto,
606-8507, Japan

E-mail: tmasui@kuhp.kyoto-u.ac.jp

Tel: +81-75-751-3242

Fax: +81-75-751-4263

*Shigeo Takaishi, M.D., Ph.D.

Department of Gastroenterology and Hepatology, Graduate
School of Medicine, Kyoto University, 54, Shogoin-Kawaharacho, Sakyo-ku, Kyoto, 606-8507,
Japan

E-mail: takaishi.shigeo.7w@kyoto-u.jp

Tel: +81-75-751-4319

Fax: +81-75-751-4303

Keywords: Bile Duct Cancer, Cancer Stem Cells, Dopamine D1 Receptors, Organoids, Single-
Cell Analysis

Word count: 5,807 words (abstract: 197 words)

Number of Figures: 7 figures

Number of Tables: 1 table

Number of Supporting Information: 1 material and method, 13 figures, and 7 tables

Abstract

Bile duct cancer (BDC) frequently invades the nerve fibers, making complete surgical resection difficult. A single tumor mass contains cells of variable malignancy and cell-differentiation states, with cancer stem cells (CSCs) considered responsible for poor clinical outcomes. This study aimed to investigate the contribution of auto-synthesized dopamine to CSC-related properties in BDC. Sphere formation assays using 13 commercially available BDC cell lines demonstrated that blocking dopamine receptor D1 (DRD1) signaling promoted CSC-related anchorage-independent growth. Additionally, we newly established four new BDC patient-derived organoids (PDOs) and found that blocking DRD1 increased resistance to chemotherapy and enabled xenotransplantation *in vivo*. Single-cell analysis revealed that the BDC PDO cells varied in their cell-differentiation states and responses to dopamine signaling. Further, DRD1 inhibition increased WNT7B expression in cells with bile duct-like phenotype, and it induced proliferation of other cell types expressing Wnt receptors and stem cell-like signatures. Reagents that inhibited Wnt function canceled the effect of DRD1 inhibition and reduced cell proliferation in BDC PDOs. In summary, in BDCs, DRD1 is a crucial protein involved in autonomous CSC proliferation through the regulation of endogenous WNT7B. As such, inhibition of the DRD1 feedback signaling may be a potential treatment strategy in BDC.

Abbreviations

BDC, bile duct cancer

CSCs, cancer stem cells

DRD1, dopamine receptor D1

PDOs, patient-derived organoids

qRT-PCR, quantitative real-time polymerase chain reaction

scRNA-seq, single-cell RNA-sequencing

P/S, penicillin-streptomycin mixed solution

bFGF, recombinant human fibroblast growth factor-basic

EGF, human epidermal growth factor

KD, knockdown

TCGA, The Cancer Genome Atlas

KEGG, Kyoto Encyclopedia of Genes and Genomes

Introduction

Bile duct cancer (BDC) has a low 5-year survival rate of only 7%–20% and has a high postoperative recurrence rate of approximately 60%.¹ Further, over 75% of symptomatic cases are ineligible for complete resection.² A single cancer tumor comprises numerous cells with different degrees of malignancy,³ with cancer stem cells (CSCs) considered as the “root of recurrence and metastasis.” Consequently, CSCs have been set as critical therapeutic targets, particularly in hematopoietic malignancies or solid tumors such as breast, brain, and colon cancers.⁴ Recently, a phenomenon called CSC plasticity has been highlighted. Non-CSCs can convert their phenotype into CSCs in limited conditions, and the surrounding environment is called the CSC niche.^{5,6,7} Thus, CSC niche-targeting therapy is gaining significant attention.⁸ However, in BDCs, although biomarkers for cancer stem-like properties have been reported,^{9,10} the mechanisms by which the niche regulates CSC plasticity remain to be elucidated.¹¹

Anatomically, the nerve fibers run parallel to the bile ducts, and the high rate of neural invasion (56.0%–88.0%) is a critical factor for the poor prognosis of BDCs.^{12,13,14} As such, BDCs are sometimes referred to as “neurotropic cancers.”¹⁵ Furthermore, recent studies show that both the malignant behavior of BDC and normal bile duct development are affected by neurotransmitters.^{13,15,16,17} Notably, BDC cells synthesize dopamine by themselves under epigenetic regulation.^{16,18} In acute myeloid leukemia, breast cancer, or non-small lung carcinoma, dopamine signaling contributes to CSC homeostasis.^{19,20,21} However, the

contribution of dopamine signaling to BDC CSC has not been elucidated thus far.

Patient-derived organoids (PDOs) are a novel cell resource cultured in 3D gels *in vitro*, retaining features of the original tumor *in vivo* containing CSCs and non-CSCs.^{22,23} Therefore, PDOs are advantageous for examining tumor heterogeneity with *in vitro* interventional experiments. This study aimed to elucidate the contribution of auto-synthesized dopamine to CSC-related properties, using four BDC PDOs.

Materials and Methods

Cell culture

Commercially available cells were obtained from RIKEN (Ibaraki, Japan), Japanese Collection of Research Bioresources Cell Bank (Osaka, Japan), or American Type Culture Collection (Manassas, VA, USA). The short tandem repeat analysis for cell line authentication and Mycoplasma non-contamination test had been performed by each cell bank before shipment. Details about Cat#, RRID, and culture conditions are given in Table S1.

Sphere culture conditions and sphere formation assay

For sphere culture, cells were dissociated with TrypLE Express enzyme (Invitrogen, Carlsbad, CA), filtered through a 35- μ m cell strainer (Corning, Cambridge, MA, USA), and seeded in ultralow attachment 6-well plates (Corning) (10,000 cells per well) with serum-free Dulbecco's Modified Eagle Medium (DMEM)/Ham's F-12 (Nacalai Tesque, Kyoto, Japan). DMEM was

supplemented with 1× B27 Supplement (Thermo Fisher Scientific, Waltham, MA, USA), 10 ng/ml recombinant human fibroblast growth factor-basic (Thermo Fisher Scientific), 20 ng/ml recombinant human epidermal growth factor (EGF; Thermo Fisher Scientific), and 1% penicillin/streptomycin mixed solution (P/S; Nacalai Tesque). Spheres were passaged after 5–7 d. Cells after two passages were used for sphere formation assays or mRNA extraction. In sphere formation assays, dissociated and filtered cells were cultured in ultra-low attachment 24-well plates (Corning) (2,000 cells per well) with a medium containing each reagent (DMSO and/or D1 inhibitor (SKF-83566, Abcam, Cambridge, UK) and/or Porcupine inhibitor (LGK974, Cayman Chemical Company, Ann Arbor, MI, USA)). On day 2, half the amount of medium with reagent was added. Spheres were imaged using the microscope IX73 (Olympus, Tokyo, Japan). On day 5 or 6, spheres larger than 75 μm in diameter were counted using Cell3Imager CC5000 (SCREEN Holdings, Kyoto, Japan).

PDO culture

PDOs were established from fresh surgical specimens obtained from patients who underwent surgical resection at Kyoto University Hospital. Primary tumor tissue samples were processed as previously described with slight modifications.^{24,25,26,27,28} The cell aggregates were embedded in Matrigel (Corning) and covered by a conditioned medium composed of 50% L-WRN (ATCC Cat# CRL-3276, RRID: CVCL_DA06; containing Wnt3A, R-spondin 3, and Noggin), advanced DMEM/F12 (Invitrogen), 5% FBS (Cytiva, Marlborough, MA, USA), 2

mmol/l L-Alanyl-L-Glutamine (Wako, Tokyo, Japan), 1% P/S, 2.5 μ g/ml plasmocin prophylactic (Invitrogen), 10 μ M Y-27632 (Wako), 1 \times B27 Supplement, 100 ng/ml basic FGF, and 20 ng/ml EGF, denoted as “niche-enriched.” The medium containing advanced DMEM/F12, 5% FBS, 2 mmol/l L-Alanyl-L-Glutamine, and 1% P/S was called “niche deficient.” Used PDOs were passaged less than 35 times.

Organoid formation assay

PDOs were dissociated into single cells using TrypLE Express Enzyme, filtered through a 35- μ m cell strainer, and cultured in 48-well plates (250 cells per 5 μ l Matrigel per well, with 2 μ l Matrigel embedded *a priori* so that PDOs did not spread to the bottom) with the medium changed twice weekly. Images of PDOs were recorded using microscope IX73. On days 10–15, PDOs greater than 75 μ m in diameter were counted using Cell3Imager CC5000 with a multiplanar scanning option.

RT-PCR

Total RNA extraction, single-strand complementary DNA synthesis, and quantitative real-time polymerase chain reaction (qRT-PCR) were performed in triplicate as previously described.²⁷

The relative quantification of each target, normalized to an endogenous control (GAPDH), was performed using the comparative Ct method. Table S2 lists the primer sequences. Further details are also given in Supplementary Methods.

ShRNA-mediated human DRD1 gene knockdown by lentiviral transduction

ShRNA-mediated knockdown (KD) was performed as described previously.²⁷ The two predesigned *DRDI*-targeting shRNA (A:TRCN0000356937, 5-ccggTTATGCCTTTAATGCTGATTTctcgagaaatcagcattaaaggcataatTTTTg-3, B:TRCN0000230254, 5-ccggTATCAGTCATATTGGACTATGctcgagcatagccaatatgactgatTTTTg-3) was used. At 48–72 h after viral infection, the cells were treated with a medium containing puromycin (Invitrogen) at 1–5 $\mu\text{g/ml}$ for 2 weeks to eliminate the non-infected cells. Further details are given in Supplementary Methods.

Xenograft assay

NOD/SCID mice were purchased from the Charles River Laboratories Japan (Yokohama, Japan). Cultured BDC cells including spheres were dissociated with TrypLE Express enzyme, centrifuged, and resuspended in iced PBS. PDO cells were dissociated with TrypLE Express enzyme, centrifuged, and resuspended in an iced “niche-deficient” medium at a concentration of 10^5 or 10^6 in 50 μl . For subcutaneous transplantation, cells were injected into the flanks of 8–12-week-old NOD/SCID mice (PDO cell suspension was mixed with Matrigel (50% vol/vol)). The tumor constructions were examined by peeling off the skin. For spleen injection,²⁹ the NOD/SCID mice were anesthetized using isoflurane, and a 1.5 cm left-sided transverse laparotomy was performed to open the abdominal cavity. Cells were injected into the spleen using a 27-gauge needle. Tumor cells were allowed to circulate for 10 min, and the

spleen was resected. For peri-sciatic nerve xenograft,³⁰ NOD/SCID mice were anesthetized, and a 1.5-cm incision exposed their sciatic nerves. The cell mixture with Matrigel (50% vol/vol) was injected at the space of the branch of the tibial and sural nerves.

Chemoresistance assay

PDOs were dissociated and cultured in V-bottom 96-well plates (nerbe plus GmbH & Co. KG, Winsen, German) (2000 cells in 4 μ l of Matrigel per well, covered by a “niche-enriched” medium). After 3 d, the medium was changed into a “niche-enriched” or “niche-deficient” medium (medium change, twice weekly). On days 7–10, PDOs were treated with gemcitabine hydrochloride (Tokyo Chemical Industry, Tokyo, Japan), cisplatin (Wako), or 5-fluorouracil (Nacalai Tesque). Subsequently, after 3 d, the medium was changed with 100 μ l of “niche-deficient” medium with 10 μ l of CCK-8 (Dojindo Labs, Kumamoto, Japan). After incubation for 2 h, each medium was transferred to a new 96-well plate, and the optical absorbance at a wavelength of 450 nm was measured using the plate reader Infinite F50 (TECAN, Zürich, Switzerland).

scRNA-seq

Dissociated PDO cells in Matrigel were plated on a Matrigel-precoated 6-well plate (10,000 cells per well) and cultured in a niche-enriched medium with DMSO or D1 inhibitor (SKF-83566 4 μ M) with the medium changed twice weekly. After 14 d, the cells were dissociated, and scRNA-seq was conducted using the 10X Genomics Chromium Single Cell 3' Gene

Expression kit. Further details, including sequencing and bioinformatics, are given in Supplementary Methods.

Statistical analysis

Values were presented as the mean \pm standard error of mean when data distribution was assumed to be normal (not formally tested); otherwise, boxplot was used. Student's *t*-test (two-tailed unpaired or paired), Wilcoxon rank-sum test, or Tukey's test was used to compare groups as appropriate. All statistical analyses were performed using R (v.3.6.2) with R package multcomp (v.1.4-17). The *p*-values were as follows: **** $p < 0.0001$, *** $p < 0.001$, ** $p < 0.01$, * $p < 0.05$, and n.s. > 0.05 .

Results

Blocking of DRD1 increases BDC sphere formation

To find cell lines that followed the CSC plasticity model, sphere formation assays were applied to 13 commercially available BDC cell lines (Figure 1A and S1A). In general, the majority of monolayer-cultured cells are non-CSC-like, and sphere culture can enrich CSC-like cells as spherical aggregates called spheres, with non-CSC-like cells suspended as single cells.^{22,31} The cell lines were divided into the following two groups according to the types of sphere formation: (1) convertible type that formed spheres only in sphere culture (NOZ, KCU213, TYGBK1, TYBDC1, HuCCA1, HuCCT1, and TKF1) and (2) unconvertible type that formed

no or few small spheres (KKU055, KKU100, OCU1, G415) or formed aggregates in either condition (OZ, TYGBK8) (Figure 1A and S1B). It was inferred that the convertible type lines were more likely to retain CSC plasticity than were the unconvertible type.

Expressions of pluripotency-associated genes (i.e., *NANOG*, *SOX2*, *POU5F1/OCT4*) and of the recently reported slow-cycling CSC marker *PROX1*³³ were confirmed to be elevated in the convertible type (Figure S2A). In addition, “convertible type” sphere cells had higher tumorigenic potential than did monolayer-cultured cells *in vivo* (Figure S2B). Then, the dopamine autosynthesis capacity of BDC was confirmed by mRNA expression of dopamine synthesis genes (*TH* and *DDC*) and quantification of dopamine levels by enzyme-linked immunosorbent assay (ELISA) (Figure S3). The expression of *TH*, the rate-limiting enzyme for dopamine synthesis, was higher in the convertible type than in the unconvertible type. These data suggested that these convertible-type BDC cell lines (NOZ, KKU213, TYGBK1, TYBDC1, HuCCA1, HuCCT1, and TKF1) followed the CSC plasticity model with higher dopamine autosynthesis capacity.

Additionally, to explore the functions of dopamine receptors in CSCs, we evaluated the expressions of genes of five dopamine receptor subtypes (D1-like: *DRD1* and *DRD5*; D2-like: *DRD2*, *DRD3*, and *DRD4*) in conditions of the sphere and monolayer culture. The results showed that *DRD1* was the most upregulated in convertible-type spheres (Figure 1B). A selective D1 receptor inhibitor (SKF-83566) was applied to sphere formation assay of three

convertible-type lines that had the highest sphere-forming ability (TYGBK1, NOZ, and TFK1) (Figure S1A). The D1 inhibitor increased the number of spheres (Figure 1CD). The involvement of DRD1 was confirmed using *DRD1*-KD (Figure 1E and S2C). In summary, these results suggested that blocking of D1 signaling enhanced the CSC niche of BDC.

Blocking of DRD1 signaling augments PDO initiation *in vitro*

To validate the above results with more clinically relevant resources, four BDC PDOs were newly established from fresh surgical specimens (Sph18-08, Sph18-16, Sph18-22, and Sph18-29) (Table 1). Each PDO had genetic variants characteristic of BDCs (Figure S4 and Table S3). The main mutations had a variant allele frequency of 50% or 100% (hetero- or homozygous mutation), suggesting PDOs contained only tumor cells. The dopamine autosynthesis capacity in these PDOs was confirmed by qRT-PCR and ELISA (Figure S3).

Organoid formation assays were performed to evaluate the organoid-initiating cell frequency, and D1 inhibition or KD of *DRD1* increased the size and number of PDO initiations (Figure 2 and S45ABC). Additionally, after long-term incubation over 2 weeks with D1 inhibition, the PDOs developed into unique warty shapes, whereas the control PDOs remained spherical in shape (Figure 2A). These implicated that DRD1 inhibition enhanced reconstruction and growth of PDOs apparently through the high tumor-initiating ability of CSC-like cells in PDOs.

Single-cell RNA-sequence analysis revealed CSC-like and dopamine-responsive cells in PDO

To detect how CSCs were enhanced in D1-inhibited PDOs, scRNA-seq with and without D1 inhibitor was conducted (Figure 3A). Several cell clusters with various cell cycle states were observed. Given the expressional bias in proliferating cells,³⁴ five cell clusters were further analyzed, most of which were cells in the G0/1 phase (Figure 3A right and S6ABC). Three kinds of cells were found: (1) B1 and B2 with bile duct-like signatures, (2) H with hepatocyte-like signatures, and (3) INT1 and INT2 with intermediate signatures of the two.^{35,36,37} INT1, INT2, and H also expressed genes showing duodenal-stem-like signatures (Figure 3B).³⁸ In addition, B1 and B2 cells exhibited lower expression of genes related to gemcitabine, fluorouracil, doxorubicin, and docetaxel resistance, supporting that these cells were less CSC-like than were INT1, INT2, and H (Figure S7A).

Analysis of cell type-specific surface markers showed that *TROP2* (*TACSTD2*), a cell surface glycoprotein, was more highly expressed in B1 and B2 cells than in INT1 and INT2 cells, while its expression was the lowest in H cells (Figure 3CD and Table S4). Additionally, FACS-sorted *TROP2*^{high} cells exhibited decreased organoid-initiating cell frequency and less plasticity to be *TROP2*^{low} (Figure S7BCD). This was consistent with a previous report that CD24⁺/CD44⁺ cells (INT cells, Figure 4D) had CSC-like potency in extrahepatic cholangiocarcinomas.¹⁰ Both results suggested that PDOs contained different cell types represented by B, INT, and H clusters, among which INT and H cells revealed stem-like features.

Additionally, B1 and B2 cells exhibited higher expression of genes related to dopamine

responsiveness of “adenyl-cyclase-activating” or “adenyl-cyclase-inhibiting” (Figure 3CD). Varying protein expression levels of KRT19 (bile duct marker), PROX1 (hepatocyte marker), and DRD1 in a PDO was confirmed via immunohistochemistry (Figure S8A). In the original surgical specimen of Sph18-16, DRD1 expression overlapped with TROP2 in epithelial-like cells (Figure S8B). In addition, dopamine production among cells appeared to vary according to the expression of MAOB, a gene responsible for dopamine metabolism (Figure 3CD, Figure S8C). This heterogeneity of dopamine responsiveness was also confirmed in another PDO, Sph18-29 (Figure S9ABCD). Furthermore, the expression of TROP2, the B cluster marker, was correlated to the gene signature associated with the dopamine D1 receptor in The Cancer Genome Atlas (TCGA) cholangiocarcinoma cohort (Figure S9E). These results indicated that TROP2-marked B cluster cells could be more dopamine-reactive than could be INT or H cells.

WNT7B is produced by B subtypes and enhanced by D1 inhibition

To explore the cause of CSC enhancement by D1 inhibition, we performed enrichment analysis and compared control and D1 inhibitor-treated samples with all gene sets of GO-term BP. Three significant pathways with high enrichment of highly expressed genes in D1 inhibitor-treated cells were identified: EGFR signaling, ribosomal proteins, and wound healing or morphogenesis (Figure 4A and Table S5). EGFR signaling is reported to be associated with cholangiocarcinoma plasticity, and its upregulation is concordant to enhancement of CSCs.¹ In addition, increased ribosomal protein might be interpreted as enhancement of cell proliferation.

Meanwhile, the current study focused on upregulated *WNT7A/7B* in wound healing-related genes because *WNT7A/B* could be the cause of increased proliferation or CSC-like potential.^{26,39,40}

Furthermore, the expression of *WNT7A/7B* was higher in B cells, whereas expressions of the receptor or coreceptor genes of Wnt (*LRP5*, *LRP6*, and *LGR4*) were higher in INTs, the suspected CSC subtyped cells (Figure 3D). D1 inhibitor treatment increased *WNT7A/7B* expression in B1 and INT1 cells and decreased the expression of *DKK1*, a negative regulator of Wnt signaling. In contrast, the expressions of *LRP5*, *LRP6*, and *LGR4* showed no significant changes (Figure 4B). The increased expression of *WNT7B* in TROP2-positive cells was confirmed by confocal immunofluorescent image (Figure S10A). Additionally, D1 inhibitor treatment-induced increase in gene expression related to Wnt signaling was most evident in INT2 cells (Figure S10B). Wnt signaling is related to the self-renewal of CSCs,⁴¹ and D1 inhibition-induced increase in their proliferating population was most pronounced in INT2 cells (Figure 4C). Thus, it is supposed that increased *WNT7A/7B* by D1 inhibition in B cells promoted INT cell proliferation.

Trajectory analyses identified that INT cells were centered and branched into B, H, and proliferating clusters (Figure 4D), suggesting a cellular hierarchy with INT cells at the top. D1 inhibitor treatment shifted the center from INT1 to INT2, which also supported the above deduction that D1 inhibition promoted INT2 proliferation. Heterogeneous *WNT7B* expression

in original surgical specimens was confirmed in Sph18-16 and 18-29 (Figure S10C). However, PDO Sph18-29 did not express WNT7A (Figure S9C). Further, in the TCGA datasets, WNT7A expression level was not higher in BDCs than that in normal tissue (Figure S10D). In contrast, WNT7B expression was the highest in the Wnt gene family (Figure S10D). Hence, we assumed that WNT7B is the main possible CSC niche factor involved in D1 inhibition.

Effect of D1 inhibitor depends on Wnt aut signaling

To elucidate the contribution of Wnt overexpression under DRD1-regulated control in BDC cell proliferation, Wnt signaling was blocked via the porcupine inhibitor LGK974. Porcupine is an endoplasmic reticulum transmembrane protein essential for the processing and correct localization of Wnt proteins, and this initially confirmed in PC12 rat neuronal cells.^{42,43} In sphere assays of TYGBK1, NOZ, and TFK1, LGK974 canceled the increase of sphere formation by D1 inhibition (Figure 5A). Similar results with LGK974 were confirmed in three PDOs: Sph18-08, Sph18-16, and Sph18-29 (Figure 5B and S11A). To identify the mechanism of increased WNT7B by D1 inhibition, a Kyoto Encyclopedia of Genes and Genomes (KEGG) pathway map analysis was performed in B1 cells (Figure S11B)

The results showed increased c-FOS expression downstream of dopamine receptors. C-FOS is known to be increased by ERK.⁴⁴ In studies of osteosarcoma, in which D1 inhibitors or DRD1-KD increased its proliferation, a D1 inhibitor increased ERK1/2 activity,⁴⁵ and FOS directly controlled the expression of endogenous WNT7B.⁴⁶ Similarly, increased c-FOS expression

downstream of ERK was confirmed in B1 cells in the current study (Figure S11C). In the TCGA dataset, the gene signature of DRD1 was correlated to that of ERK and so did that of ERK and *FOS*, or *FOS* and *WNT7B* (Figure S11D). Further, higher expression of *WNT7B* was a poor prognostic factor in BDC (Figure S11E). These results suggested that increased WNT7B by D1 inhibition was mediated by ERK-FOS signaling.

Effect of D1 inhibition is pronounced in the absence of the exogenous CSC niches

Thus far, we have found that the auto-synthesized dopamine of BDCs affected their endogenous Wnt signaling. Lastly, the effects of D1 inhibition was examined in different microenvironments. Given that BDCs are neurotropic cancers, comparative xenotransplantation assays with *DRDI*-KD PDOs was performed in three different sites in the NOD-SCID mouse: peri-sciatic nerve, subcutaneous, and spleen (Figure 6A). In peri-sciatic nerve xenografts, the efficacy of tumor initiation was similar between the vector and *DRDI*-KD PDOs (7/10 and 8/10) (Figure 6A and S12A). However, the size of the masses was larger in *DRDI*-KD PDOs (Figure 6B). Additionally, most of the vector PDO (6/7) formed masses only along the nerves (Figure 6B arrowhead), whereas *DRDI*-KD PDOs could grow away from the nerves (5/8). Tumor initiation of subcutaneous and splenic injected cells was fewer than that of peri-sciatic-nerve transplanted cells, but only *DRDI*-KD PDO cells formed subcutaneous mass or lung metastasis (Figure 6AC). Similar findings were also confirmed with another PDO (Figure S12B). These results suggested that the neural-related niche could also

enhance CSCs and that the effect of D1 inhibition was more pronounced in their absence.

Given that the organoid culture medium contained neural stem cell-related niche factors such as B-27 supplement⁴⁷ or *Wnt3a*,⁴⁸ we next examined chemoresistant proliferation, another CSC-related property, with PDOs precultured with D1 inhibitor in niche-enriched and niche-deficient media. In the niche-enriched medium, there was no difference in chemoresistance between the D1 inhibition and control groups; however, in the “niche-deficient” medium, chemoresistance was enhanced by D1 inhibition in two PDOs with three cytotoxic reagents (5FU, cisplatin, and gemcitabine) (Figure 6D and S12C). Therefore, neural-related niche factors and D1 inhibition might partially overlap in enhancing CSC-related properties, and this is consistent with our result that D1 inhibition increased CSC proliferation via Wnt signaling (Figure 7).

Discussion

The genetic landscape of BDC is comparatively broad, and the common nongenetic mechanism causing therapeutic resistance has not been elucidated.¹ The current study, using single-cell analysis of clinical human materials, describes a spectrum of cell-differentiation states from bile duct-like to hepatocyte-like differentiation, including intermediate clusters such as CSCs. The findings are consistent with a previous report indicating similarity between differentiating lineages of tumor and normal tissue development.³ A previous study with scRNA-seq of normal

liver tissue showed that TROP2 expression was negatively correlated with hepatocyte fate.³⁷ In our analysis, TROP2^{high} was inferred as a bile duct-like cell marker and TROP2^{inter} or TROP2^{low} as markers for suspected CSC-like cells. PROX1 is a stable hepatocyte marker,⁴⁹ and our scRNA-seq confirmed its expression in the hepatocyte-like cluster (Table S4E), although “hepatocyte-like” was a relative signature with low expression of the developed hepatocyte markers *CYP3A4* and *ALB* (Figure 3D). Another report described PROX1 as a marker for dormant CSC.³³ Consistently, the current study found that hepatocyte-like clusters with the signature of duodenal stem genes (Figure 3BD) had less proliferative fractions (Figure 4C). Conclusively, TROP2 and PROX1 are potential markers for analyzing BDC heterogeneity. Using sphere/organoid formation assays focusing on auto-synthesized dopamine, the current study identified DRD1 signaling as a potential regulator of CSCs. Additionally, ScRNA-seq analysis showed that D1 inhibition increased WNT7B expression in bile duct-like cells, resulting in the proliferation of CSC-like INT2 cells. This is in contrast with the self-inhibition of SP cell expansion by SFRP4, secreted from non-SP cells in B-cell lymphoma.⁵⁰ Thus, BDCs might monitor auto-synthesized dopamine by DRD1, with its low signaling leading to the autonomous proliferation of CSCs via increased endogenous WNT7B levels.

For the detailed molecular mechanism, we developed a cascade of DRD1-ERK-FOS-WNT7B based on KEGG pathway map analysis and previous reports^{44,45,46} and confirmed its clinical relevance in the TCGA dataset (Figure S9E and S11DE). The scRNA-seq analysis did not

detect mRNA expression of *DRD1* in many populations, although DRD1 protein expression was confirmed in Western blotting or immunohistochemistry (Figure S5BD, S8AB, and S9D). This result may be attributed to the technical limitation of detecting low or continuously expressed protein mRNA at a single-cell level.⁵¹ Thus, gene signature analysis was used to evaluate DRD1 signaling activity. In the BDC cohort of TCGA, higher expression of *WNT7B* was a poor prognostic factor (Figure S11E), and there were expressional correlations among *WNT7B*, *FOS*, ERK signaling, and DRD1-related genes (Figure S11D). This suggested the clinical relevance of DRD1-ERK-FOS-WNT7B cascade in the entire BDC cohort.

However, BDCs are heterogenous in their genetic backgrounds, and their individual reactivities to dopamine or WNT7B may vary. In the current study, 2 of the 13 commercially available BDC cell lines, TYGBK8 and OZ, form sphere-like aggregates even in 2D culture condition with high expressional level of CSC-related genes (Figure S13A). The number of spheres was also increased in TYGBK8 under low-dose D1 inhibitor treatment, but not in OZ (Figure S13B). This might imply that the CSC capacity of OZ did not depend on dopamine signaling, and high malignancy of OZ, which was originally obtained from the ascitic effusion, was suspected.⁵² Sph18-29 had CTNNB1 exon 3 mutation (Figure S4), which is reported to be associated with activation of the Wnt/ β -catenin pathway.⁵³ Nevertheless, porcupine inhibitor suppressed organoid formation of Sph18-29 cells. We suspect that WNT7B also activated the noncanonical WNT pathway, as is reported in pancreatic progenitor cells⁵⁴ or prostate cancer.⁵⁵ Therefore,

the contributions of D1 signaling or WNT7B could depend on the cell line characteristics.

This study has some limitations. It focused primarily on tumor cells and not on nontumor cells such as fibroblasts, immune cells, or neural cells. As for the neural-related niche, we showed its possible functional overlap with tumoral Wnt self-signaling (Figure 6). Moreover, in the genes upregulated by D1 inhibition (Figure 4A), there were other intercellular signaling genes including the semaphorin gene family (*SEMA3B*, *SEMA4B*). The semaphorin gene family was initially identified as a neural developmental factor and recently emerged as a regulator of malignancy through cross-talk with tumor microenvironments.⁵⁶ The neural-related niche and cross-talks causing neurotropism of PDOs (Figure 6 and S12BC) require further analysis.

In conclusion, although more than 150 clinical trials targeting CSC are currently ongoing,⁸ most responses have been modest, especially in solid tumors. This implies that targeting only CSCs might trigger feedback signaling to enhance CSCs. The current study supports that the D1 self-signaling of BDCs might be a vital regulator of autonomous CSC growth via ERK-FOS and WNT7B. Thus, inhibition of this feedback signaling may lead to novel combination therapies with conventional chemotherapy.

Acknowledgments

We thank S. Yokoyama, previously from Medical Innovation Center DSK Project, for mice breeding and technical support; H. Umehara, T Kodo, and M Takamura for project management; M. Nishikawa from the Kyoto Institute of Nutrition & Pathology Inc. for immunohistochemistry staining; MARUZEN-YUSHODO Co., Ltd. (<https://kw.maruzen.co.jp/kousei-honyaku/>); and Editage (<https://www.editage.com/>) for the English language editing. Figure 1AC, Figure 2A, Figure 3A (middle), Figure 6A (left), and Figure 7 were created with a licensed version of BioRender.com (to AY, 2022), by adaption of BioRender templates, retrieved from <https://app.biorender.com/biorender-templates>.

Disclosure:

Funding Information

TM received funding from Grants-in-Aid KAKENHI (21K08732), and ST received funding from Grants-in-Aid KAKENHI (17K09460), both research programs from the Ministry of Education, Culture, Sports, Science, and Technology. In addition, TM and ST received research funding from Sumitomo Pharma Co., Ltd.

Conflict of interest

TM and ST received partial supports from Sumitomo Pharma Co., Ltd.. SW and RI are employees of Sumitomo Pharma Co., Ltd.. SO and HS are editorial board members of Cancer

Science. The other authors declare no competing financial interests in this study.

Ethics Statement

The research protocol was approved by the ethical committee of Kyoto University Hospital (approval number: R1281). PDOs were established from fresh surgical specimens obtained from patients who underwent surgical resection at Kyoto University Hospital. All experiments were conducted according to the Declaration of Helsinki and the guidelines and regulations of the Committee.

- Informed Consent. For PDO establishment, informed consent in writing was obtained from each patient.

- Registry and the Registration No. of the study/trial. N/A.

- Animal Studies. All procedures for animal experiments were conducted in compliance with the ARRIVE guidelines and the Institutional Animal Welfare Guidelines of Kyoto University.

Author Contributions

Conceptualization, AY, TM, and ST; Methodology, AY, ST, KM, RC, SS, AW, RI, and MMN; Investigation, AY, ST, KM, RC, YK, KN, TA, SW, SS, AW, RI, and MMN; Validation, KM, RC, SS, AW, RI, and MMN; Software, AY, SS, AW, RI, and MMN; Data curation, AY and ST; Formal analysis, AY, SS, AW, RI, and MMN; Visualization, AY and AW; Resources, AY and ST; Funding acquisition, TM and ST; Project administration, TM, ST, SO, HS, SU, and EH; Supervision, TM and ST; Writing—original draft, AY; Writing—review & editing, TM, ST,

and SW.

References:

1. Banales JM, Marin JJG, Lamarca A, Rodrigues PM, Khan SA, Roberts LR, et al. Cholangiocarcinoma 2020: the next horizon in mechanisms and management. *Nat Rev Gastroenterol Hepatol* 2020;17(9):557-588.
doi: 10.1038/s41575-020-0310-z.
2. Vugt JLA Van, Gaspersz MP, Coelen RJS, Vugts J, Labeur TA, Jonge J De, et al. The prognostic value of portal vein and hepatic artery involvement in patients with perihilar cholangiocarcinoma. *Int Hepato-Pancreato-Biliary Assoc* 2018;20(1):83-92.
doi: 10.1016/j.hpb.2017.08.025.
3. Lee HO, Hong Y, Etlioglu HE, Cho YB, Pomella V, Van den Bosch B, et al. Lineage-dependent gene expression programs influence the immune landscape of colorectal cancer. *Nat Genet* 2020;52(6):594-603.
doi: 10.1038/s41588-020-0636-z.
4. Clevers H. The cancer stem cell: premises, promises and challenges. *Nat Med*. 2011;17(3):313-9.
doi: 10.1038/nm.2304.
5. Batlle E, Clevers H. Cancer stem cells revisited. *Nat Med* 2017;23(10):1124-1134.
doi: 10.1038/nm.4409.
6. Chaffer CL, Brueckmann I, Scheel C, Kaestli AJ, Wiggins PA, Rodrigues LO, et al.

Normal and neoplastic nonstem cells can spontaneously convert to a stem-like state. *Proc Natl Acad Sci U S A* 2011;108(19):7950-5.

doi: 10.1073/pnas.1102454108.

7. Shimokawa M, Ohta Y, Nishikori S, Matano M, Takano A, Fujii M, et al. Visualization and targeting of LGR5 + human colon cancer stem cells. *Nature* 2017;545(7653):187-192.

doi: 10.1038/nature22081.

8. Yang L, Shi P, Zhao G, Xu J, Peng W, Zhang J, et al. Targeting cancer stem cell pathways for cancer therapy. *Signal Transduct Target Ther.* 2020;5(1):8.

doi: 10.1038/s41392-020-0110-5.

9. Shi C, Tian R, Wang M, Wang X, Jiang J, Zhang Z, et al. CD44+CD133+ population exhibits cancer stem cell-like characteristics in human gallbladder carcinoma. *Cancer Biol Ther* 2010;10(11):1182-90.

doi: 10.4161/cbt.10.11.13664.

10. Wang M, Xiao J, Shen M, Yahong Y, Tian R, Zhu F, et al. Isolation and characterization of tumorigenic extrahepatic cholangiocarcinoma cells with stem cell-like properties. *Int J Cancer* 2011;128(1):72-81.

doi: 10.1002/ijc.25317.

11. Mayr C, Ocker M, Ritter M, Pichler M, Neureiter D, Kiesslich T. Biliary tract cancer stem cells - Translational options and challenges. *World J Gastroenterol* 2017;23(14):2470-

2482.

doi: 10.3748/wjg.v23.i14.2470.

12. Chen S, Zhang B, Zhou B, Zhu C, Sun L, Feng Y. Perineural invasion of cancer : a complex crosstalk between cells and molecules in the perineural niche. *Am J Cancer Res* 2019;9(1):1-21.

13. Amit M, Na'Ara S, Gil Z. Mechanisms of cancer dissemination along nerves. *Nat Rev Cancer* 2016;16(6):399-408.

doi: 10.1038/nrc.2016.38.

14. Kawamata H, Yamashita K, Nakamura K. Perineural Invasion and Preoperative Serum CA19-9 as Predictors of Survival in Biliary Tract Cancer. *Anticancer Res.* 2013;33(2):583-94.

15. Tan X, Sivakumar S, Bednarsch J, Wiltberger G, Kather JN, Niehues J, et al. Nerve fibers in the tumor microenvironment in neurotropic cancer—pancreatic cancer and cholangiocarcinoma. *Oncogene* 2021;40(5):899-908.

doi: 10.1038/s41388-020-01578-4.

16. Coufal M, Invernizzi P, Gaudio E, Bernuzzi F, Frampton GA, Onori P, et al. Increased local dopamine secretion has growth-promoting effects in cholangiocarcinoma. *Int J Cancer* 2010;126(9):2112-22.

doi: 10.1002/ijc.24909.

17. Hall C, Sato K, Wu N, Zhou T, Kyritsi K, Meng F, et al. Regulators of Cholangiocyte

Proliferation. *Gene Expr.* 2017;17(2):155-171.

doi: 10.3727/105221616X692568.

18. Huang L, Frampton G, Rao A, Zhang KS, Chen W, Lai JM, et al. Monoamine oxidase A expression is suppressed in human cholangiocarcinoma via coordinated epigenetic and IL-6-driven events. *Lab Invest* 2012;92(10):1451-60.

doi: 10.1038/labinvest.2012.110.

19. Sachlos E, Risueño RM, Laronde S, Shapovalova Z, Lee JH, Russell J, et al. Identification of drugs including a dopamine receptor antagonist that selectively target cancer stem cells. *Cell* 2012;149(6):1284-97.

doi: 10.1016/j.cell.2012.03.049.

20. Yang L, Yao Y, Yong L, Feng Y, Su H, Yao Q, et al. Dopamine D1 receptor agonists inhibit lung metastasis of breast cancer reducing cancer stemness. *Eur J Pharmacol* 2019;859:172499.

doi: 10.1016/j.ejphar.2019.172499.

21. Hao F, Wang S, Zhu X, Xue J, Li J, Wang L, et al. Pharmacokinetic-Pharmacodynamic Modeling of the Anti-Tumor Effect of Sunitinib Combined with Dopamine in the Human Non-Small Cell Lung Cancer Xenograft. *Pharm Res* 2017;34(2):408-418.

doi: 10.1007/s11095-016-2071-5.

22. Zhao H, Yan C, Hu Y, Mu L, Huang K, Li Q, et al. Sphere-forming assay vs. Organoid

culture: Determining long-term stemness and the chemoresistant capacity of primary colorectal cancer cells. *Int J Oncol* 2019;54(3):893-904.

doi: 10.3892/ijo.2019.4683.

23. Marsee A, Roos FJM, Verstegen MMA, Consortium HPBO, Gehart H, de Koning E, et al. Building consensus on definition and nomenclature of hepatic, pancreatic, and biliary organoids. *Cell Stem Cell* 2021;28(5):816-832.

doi: 10.1016/j.stem.2021.04.005.

24. Miyoshi H, Stappenbeck TS. In vitro expansion and genetic modification of gastrointestinal stem cells in spheroid culture. *Nat Protoc* 2013;8(12):2471-82.

doi: 10.1038/nprot.2013.153.

25. Boj SF, Hwang C Il, Baker LA, Chio IIC, Engle DD, Corbo V, et al. Organoid models of human and mouse ductal pancreatic cancer. *Cell* 2015;160(1-2):324-38.

doi: 10.1016/j.cell.2014.12.021.

26. Seino T, Kawasaki S, Shimokawa M, Tamagawa H, Toshimitsu K, Fujii M, et al. Human Pancreatic Tumor Organoids Reveal Loss of Stem Cell Niche Factor Dependence during Disease Progression. *Cell Stem Cell* 2018;22(3):454-467.e6.

doi: 10.1016/j.stem.2017.12.009.

27. Masuo K, Chen R, Yogo A, Sugiyama A, Fukuda A, Masui T, et al. SNAIL2 contributes to tumorigenicity and chemotherapy resistance in pancreatic cancer by regulating

IGFBP2. *Cancer Sci* 2021;112(12):4987-4999.

doi: 10.1111/cas.15162.

28. Watanabe S, Yogo A, Otsubo T, Umehara H, Oishi J, Kodo T, et al. Establishment of patient-derived organoids and a characterization-based drug discovery platform for treatment of pancreatic cancer. *BMC Cancer*. 2022;22(1):489.

doi: 10.1186/s12885-022-09619-9.

29. Partecke IL, Kaeding A, Sendler M, Albers N, Kühn JP, Speerforck S, et al. In vivo imaging of pancreatic tumours and liver metastases using 7 Tesla MRI in a murine orthotopic pancreatic cancer model and a liver metastases model. *BMC Cancer* 2011;11:40.

doi: 10.1186/1471-2407-11-40.

30. Gil Z, Rein A, Brader P, Li S, Shah JP, Fong Y, et al. Nerve-sparing therapy with oncolytic herpes virus for cancers with neural invasion. *Clin Cancer Res* 2007;13(21):6479-85.

doi: 10.1158/1078-0432.CCR-07-1639.

31. Reynolds B, Weiss S. Generation of neurons and astrocytes from isolated cells of the adult mammalian central nervous system. *Science*. 1992;255(5052):1707-10.

doi: 10.1126/science.1553558.

32. Pastrana E, Silva-Vargas V, Doetsch F. Eyes wide open: A critical review of sphere-formation as an assay for stem cells. *Cell Stem Cell* 2011;8(5):486-98.

doi: 10.1016/j.stem.2011.04.007.

33. Shiokawa D, Sakai H, Ohata H, Miyazaki T, Kanda Y, Sekine S, et al. Slow-Cycling Cancer Stem Cells Regulate Progression and Chemoresistance in Colon Cancer. *Cancer Res* 2020;80(20):4451-4464.
doi: 10.1158/0008-5472.CAN-20-0378.
34. Okamoto T, duVerle D, Yaginuma K, Natsume Y, Yamanaka H, Kusama D, et al. Comparative Analysis of Patient-Matched PDOs Revealed a Reduction in OLFM4-Associated Clusters in Metastatic Lesions in Colorectal Cancer. *Stem Cell Reports* 2021;16(4):954-967.
doi: 10.1016/j.stemcr.2021.02.012.
35. Liberzon A, Subramanian A, Pinchback R, Thorvaldsdóttir H, Tamayo P, Mesirov JP. Molecular signatures database (MSigDB) 3.0. *Bioinformatics* 2011;27(12):1739-40.
doi: 10.1093/bioinformatics/btr260.
36. Aizarani N, Saviano A, Sagar, Mailly L, Durand S, Herman JS, et al. A human liver cell atlas reveals heterogeneity and epithelial progenitors. *Nature* 2019;572(7768):199-204.
doi: 10.1038/s41586-019-1373-2.
37. Busslinger GA, Weusten BLA, Bogte A, Begthel H, Brosens LAA, Clevers H. Human gastrointestinal epithelia of the esophagus, stomach, and duodenum resolved at single-cell resolution. *Cell Rep* 2021;34(10):108819.
doi: 10.1016/j.celrep.2021.108819.
38. Gao S, Yan L, Wang R, Li J, Yong J, Zhou X, et al. Tracing the temporal-spatial

transcriptome landscapes of the human fetal digestive tract using single-cell RNA-sequencing.

Nat Cell Biol 2018;20(6):721-734.

doi: 10.1038/s41556-018-0105-4.

39. Boulter L, Guest R V., Kendall TJ, Wilson DH, Wojtacha D, Robson AJ, et al. WNT signaling drives cholangiocarcinoma growth and can be pharmacologically inhibited. J Clin Invest 2015;125(3):1269-85.

doi: 10.1172/JCI76452.

40. Arensman MD, Kovoichich AN, Kulikauskas RM, Lay AR, Yang P, Li X, Donahue T, et al. WNT7B mediates autocrine Wnt/ β -catenin signaling and anchorage-independent growth in pancreatic adenocarcinoma. Oncogene 2014;33(7):899-908.

doi: 10.1038/onc.2013.23.

41. Zhan T, Rindtorff N, Boutros M. Wnt signaling in cancer. Oncogene 2017;36(11):1461-1473.

doi: 10.1038/onc.2016.304.

42. Kadowaki T, Wilder E, Klingensmith J, Zachary K, Perrimon N. The segment polarity gene porcupine encodes a putative multitransmembrane protein involved in Wingless processing. Genes Dev 1996;10(24):3116-28.

doi: 10.1101/gad.10.24.3116.

43. Caricasole A, Ferraro T, Rimland JM, Terstappen GC. Molecular cloning and initial

characterization of the MG61/PORC gene, the human homologue of the *Drosophila* segment polarity gene Porcupine. *Gene* 2002;288(1-2):147-57.

doi: 10.1016/s0378-1119(02)00467-5.

44. Monje P, Hernández-Losa J, Lyons RJ, Castellone MD, Gutkind JS. Regulation of the transcriptional activity of c-Fos by ERK. A novel role for the prolyl isomerase PIN1. *J Biol Chem*. 2005;280(42):35081-4.

doi: 10.1074/jbc.C500353200.

45. Gao J, Zhang C, Gao F, Li H. The effect and mechanism of dopamine D1 receptors on the proliferation of osteosarcoma cells. *Mol Cell Biochem*. 2017;430(1-2):31-36.

doi: 10.1007/s11010-017-2951-y.

46. Matsuoka K, Bakiri L, Wolff LI, Linder M, Mikels-Vigdal A, Patiño-García A, et al. Wnt signaling and Lox12 promote aggressive osteosarcoma. *Cell Res* 2020;30(10):885-901.

doi: 10.1038/s41422-020-0370-1.

47. Brewer GJ, Torricelli JR, Evege EK, Price PJ. Optimized survival of hippocampal neurons in B27-supplemented Neurobasal, a new serum-free medium combination. *J Neurosci Res* 1993;35(5):567-76.

doi: 10.1002/jnr.490350513.

48. Ikeya M, Lee SMK, Johnson JE, Mc Mahon AP, Takada S. Wnt signalling required for expansion of neural crest and CNS progenitors. *Nature* 1997;389(6654):966-70.

doi: 10.1038/40146.

49. Dudas J, Elmaouhoub A, Mansuroglu T, Batusic D, Tron K, Saile B, et al. Prospero-related homeobox 1 (Prox1) is a stable hepatocyte marker during liver development, injury and regeneration, and is absent from "oval cells". *Histochem Cell Biol* 2006;126(5):549-62.

doi: 10.1007/s00418-006-0191-4.

50. Koch R, Demant M, Aung T, Diering N, Cicholas A, Chapuy B, et al. Populational equilibrium through exosome-mediated Wnt signaling in tumor progression of diffuse large B-cell lymphoma. *Blood* 2014;123(14):2189-98.

doi: 10.1182/blood-2013-08-523886.

51. Mair F, Erickson JR, Voillet V, Simoni Y, Bi T, Tyznik AJ, et al. A Targeted Multi-omic Analysis Approach Measures Protein Expression and Low-Abundance Transcripts on the Single-Cell level. *Cell Rep* 2020;31(1):107499.

doi: 10.1016/j.celrep.2020.03.063.

52. Homma S, Nagamori S, Fujise K, Yamazaki K, Hasumura S, Sujino H, et al. Human bile duct carcinoma cell line producing abundant mucin in vitro. *Gastroenterol Jpn.* 1987;22(4):474-9.

doi: 10.1007/BF02773816.

53. Gao C, Wang Y, Broaddus R, Sun L, Xue F, Zhang W. Exon 3 mutations of CTNNB1 drive tumorigenesis: a review. *Oncotarget.* 2017;9(4):5492-5508.

doi: 10.18632/oncotarget.23695.

54. Kimura A, Toyoda T, Iwasaki M, Hiramata R, Osafune K. Combined Omics Approaches Reveal the Roles of Non-canonical WNT7B Signaling and YY1 in the Proliferation of Human Pancreatic Progenitor Cells. *Cell Chem Biol.* 2020;27(12):1561-1572.e7.

doi: 10.1016/j.chembiol.2020.08.018.

55. Zheng D, Decker KF, Zhou T, Chen J, Qi Z, Jacobs K, et al. Role of WNT7B-induced noncanonical pathway in advanced prostate cancer. *Mol Cancer Res.* 2013;11(5):482-93.

doi: 10.1158/1541-7786.MCR-12-0520.

56. Mastrantonio R, You H, Tamagnone L. Semaphorins as emerging clinical biomarkers and therapeutic targets in cancer. *Theranostics* 2021;11(7):3262-3277.

doi: 10.7150/thno.54023.

Figure Legends

Figure 1. Sphere formation assay depicting increased spheres with DRD1 inhibition. (A)

Schematic picture of sphere formation assay, enriching CSC cells (blue dots) out of mixture of CSC (blue dots) and non-CSC cells (red dots) (top). Examples of a convertible line (TYGBK1), an unconvertible line (KKU-100) (down), and a typical “sphere” (arrowhead). Scale bar, 100 μm . (B) Change in mRNA expression of dopamine receptors from monolayer culture to sphere culture quantified via qRT-PCR. Each value is calculated as the median of triplicate. Comparison using Wilcoxon rank-sum test. DRD1: median \log_2 Foldchange (FC) of 2.8 in convertible and of 0.14 in “unconvertible,” $p = 0.035$. (C) Schematic picture of sphere formation assay (left). Examples of microscopic images of spheres (right). Scale bar, 100 μm . (D) Sphere formation assay with D1 inhibitor (SKF-83566 0.4 μM , 1 μM or DMSO) using TYGBK1, NOZ, and TFK1. Tukey’s test is used. $n = 4$. (E) Sphere formation assay with D1 inhibitor (SKF-83566 1 μM , 4 μM or DMSO) using vector-induced or *DRD1*-knockdown (KD) TFK1s. $n = 4$.

Figure 2. Distinct patient-derived cancer organoid (PDO) formation with D1 inhibitor or DRD1 KD. (A)

Schematic picture of PDO establishment and organoid formation assay (left). Examples of microscopic images of PDOs cultured for 17 d (right). Scale bar, 100 μm . (B) Organoid formation assay with D1 inhibitor (SKF-83566 1 μM , 4 μM , or DMSO) using Sph18-08, 16, 29. Tukey’s test is used. $n = 4$. (C) Organoid formation assay with D1 inhibitor using

vector-induced or *DRDI*-KD Sph18-16. n = 4.

Figure 3. ScRNA-seq of PDO Sph18-16. (A) Schema of scRNA-seq (left) and clusters shown in Uniform Manifold Approximation and Projection (UMAP) (right). (B) Dot plot of enrichment analysis for each cluster. Gene sets related to hepato-biliary development or stem cells derived from MSigDB:C8 are listed. The color of the dots represents the adjusted p -value, and the diameter represents the count of enriched genes. Results of adjusted $p < 0.05$ are shown. (C) Feature plots of each gene signature score and expression of *TROP2* and *MAOB*. (D) Expressions of genes or gene signature scores of the five clusters. Table S6 shows the details of the gene sets.

Figure 4. ScRNA-seq analysis comparing control (DMSO) and D1 inhibitor (SKF-83566 4 μ M) treatment. (A) Heatmap visualization of the 50 most frequently appearing upregulated genes in D1 inhibitor-treated Sph18-16 sample by enrichment analysis using all GOBP terms. The details are given in Table S5. (B) Violin plots depicting the expression of genes compared with control (red) and D1 inhibitor-treated sample (green). Bar indicates the median value. Adjusted p -value for B1 of WNT7A, 0.00058; B1 of WNT7B, 0.0029; INT1 of WNT7B, 0.0013; B1 of DKK1, 0.0018. (C) Proliferating cells of each cluster in control or D1 inhibitor-treated sample (top). Listed percentages of cells in S and G2/M phases of each cluster (down). (D) Trajectories showing INT1 as the center in DMSO and INT2 in D1 inhibitor treatment.

Figure 5. Autosignaling of Wnt as downstream of D1 inhibition. (A) Sphere formation assay

with D1 inhibitor (SKF-83566 0.4 μ M for NOZ and TFK1, 1 μ M for TYGBK1, or DMSO) and porcupine inhibitor (LGK974 1 nM for NOZ and TFK1, 10 nM for TYGBK1 or DMSO). Tukey's test is used. n = 4. D1i, D1 inhibitor; Pi, Porcupine inhibitor. (B) Organoid formation assay of Sph18-16 with D1 inhibitor (SKF-83566 4 μ M or DMSO) and porcupine inhibitor (LGK974 1 nM, 10 nM or DMSO). Tukey's test is used. n = 4. Results of Sph18-08 and 29 are shown in Figure S11A.

Figure 6. D1 inhibition enhancing CSC-related capacities in the absence of exogenous niches. (A) Peri-sciatic nerve xenograft, subcutaneous xenograft, and splenic injection assay of Sph18-29. Vector or two independent DRD1-targeting shRNA is transduced to Sph18-29. Table of the result (right). (B) Gross images of xenografted tumor in the peri-sciatic nerve (left). Control PDO tumor forming only along the nerves (arrowhead). Scale bar, 5 mm. The tumor size vertical to the nerve (mm) is measured (right). Wilcoxon rank-sum test is used. (C) Macroscopic and HE-stained histological images of a subcutaneously xenografted tumor and lung metastasis of *DRDI*-KD sph18-29. Scale bar, 5 mm in macroscopic images and 100 μ m in histological images. (D) CCK8 proliferation assay of Sph18-16, 29 with 5FU in the niche-enriched or niche-deficient medium. n = 4. The result of cisplatin and gemcitabine is shown in Figure S12C. Two-tailed unpaired Student's *t*-test is used at each concentration.

Figure 7. Schematic illustrations depicting variations of B, INT, H clusters, and WNT7B as endogenous CSC niche downstream of DRD1-ERK-FOS.

List of Supporting Information:**Document S1: Supplementary material and method****Document S2: Supporting Figures****Document S3: Supporting Tables****Figure S1: Characterization of 13 cell lines****Figure S2: CSC-like characteristics of sphere cells****Figure S3: Dopamine secretion of the cell lines and patient-derived cancer organoids (PDOs)****Figure S4: Genetic mutational hotspot analysis of organoid lines****Figure S5: DRD1 expression of PDOs****Figure S6: Proliferating cells in Sph18-16****Figure S7: CSC-like cells in Sph18-16****Figure S8: Dopamine reactive cells in Sph18-16****Figure S9: Validation of results of sph18-16****Figure S10: Analysis of WNT expression****Figure S11: WNT7B and FOS as downstream of DRD1 signal****Figure S12: Xenotransplantation and chemoresistant assays of PDOs****Figure S13: Exceptional sphere formation of OZ and TYGBK8**

Table S1: List of the cell lines

Table S2: PCR primers

Table S3: Hotspot mutation of patient-derived organoids

Table S4: List of conserved markers in single-cell RNA sequence analysis of Sph18-16

Table S5: Enriched gene sets for highly expressed genes in D1 inhibitor-treated cells

Table S6: Details of used gene sets

Table S7: List of the antibodies

Table 1. Clinical information of the established BDC PDOs

Number	Age	Sex	Tumor location	Histology	TNM staging by	
					AJCC/UICC (8th)	Clinical IHC results
sph18-08	69	Male	distal	well	T3N1M0	p53+ > 95%, IMP3+ 50%
sph18-16	76	Female	gallbladder	mod	T2aN1M0	none
sph18-22	79	Female	intrahepatic	mod	T1aN0M0	focally p53 + < 5% claudin4+, IMP3+
sph18-29	73	Female	distal	mod	T3N1M0	none

BDC, bile duct cancer; PDO, patient-derived organoid; well, well differentiated tubular adenocarcinoma; mod, moderately differentiated tubular adenocarcinoma; AJCC, American Joint Committee on Cancer; UICC, International Union Against Cancer; IHC, Immunohistochemistry

Fig1

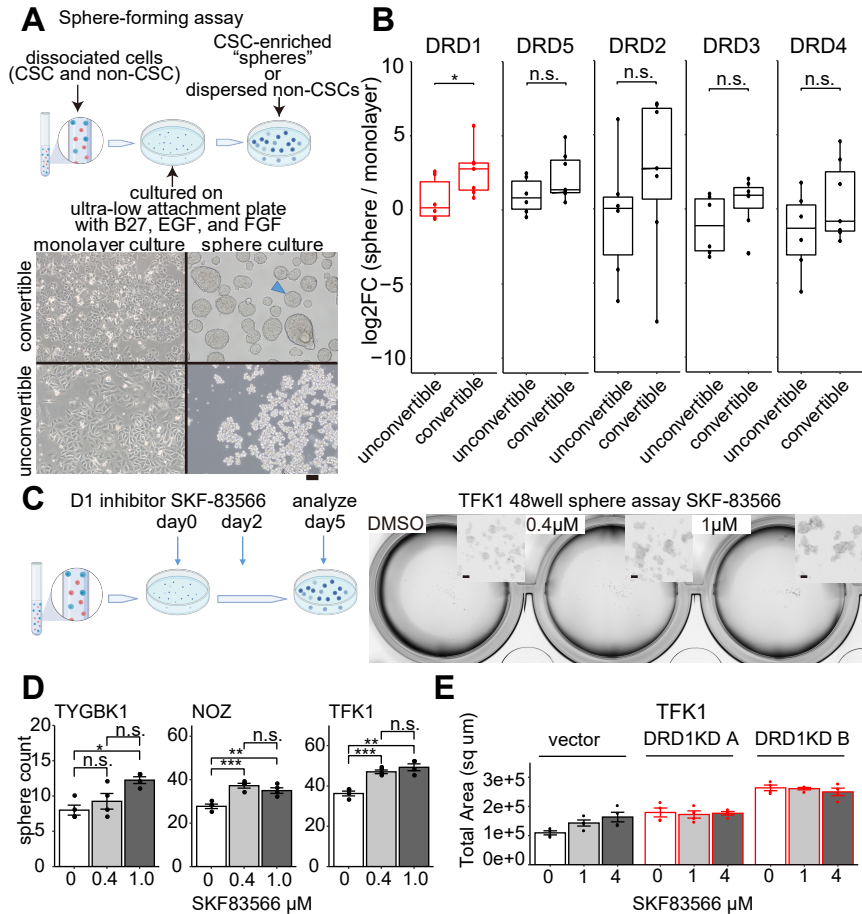


Fig2

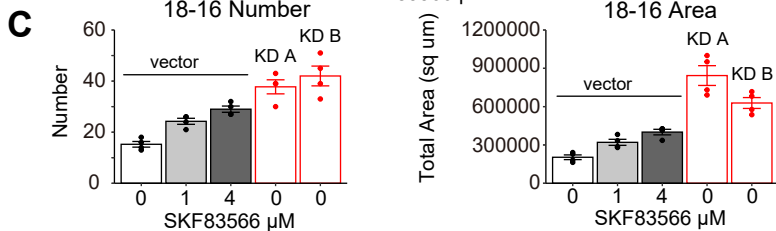
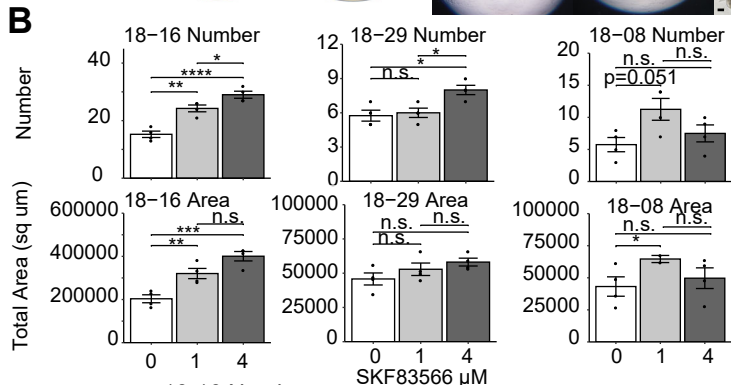
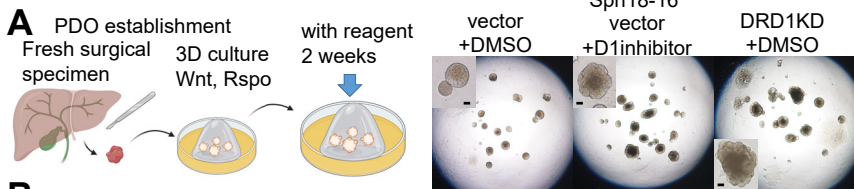


Fig3

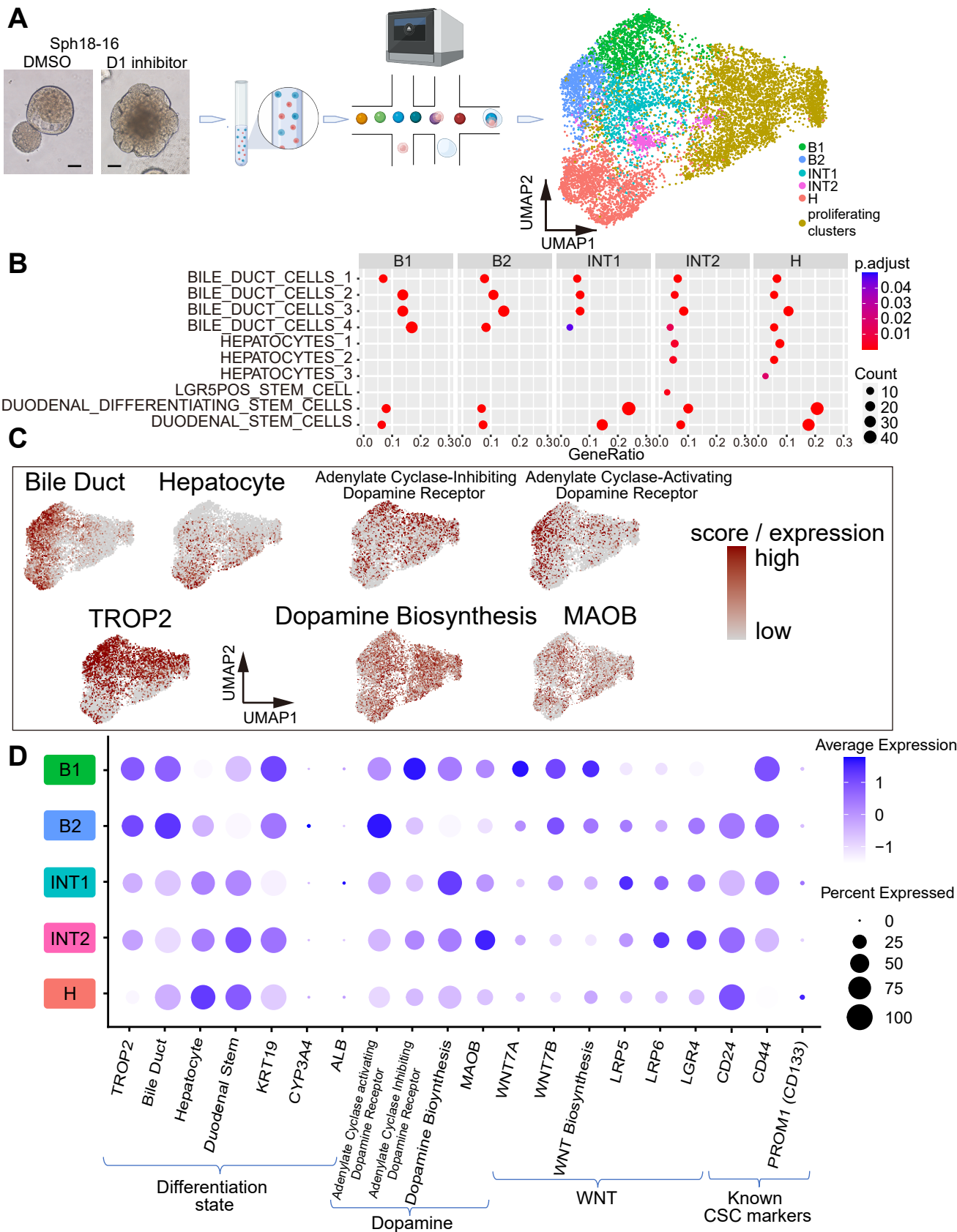


Fig4

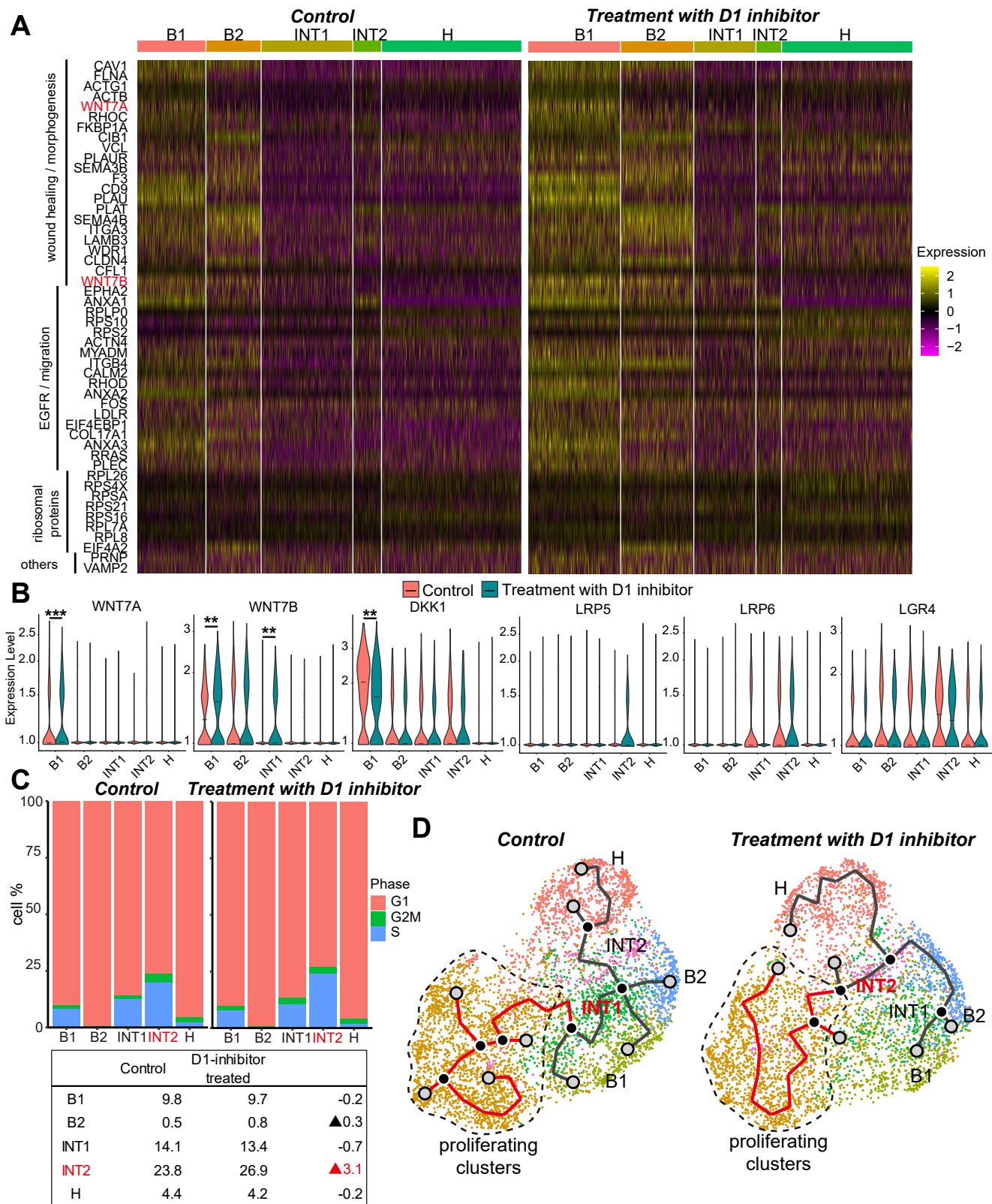


Fig5

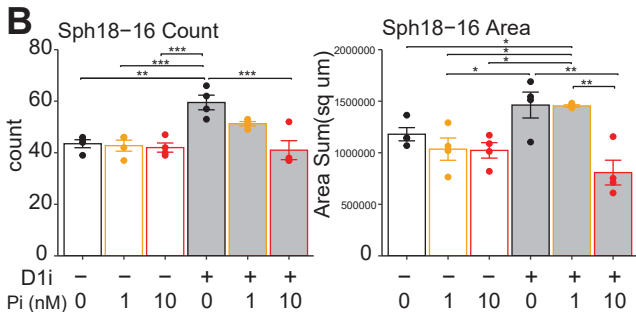
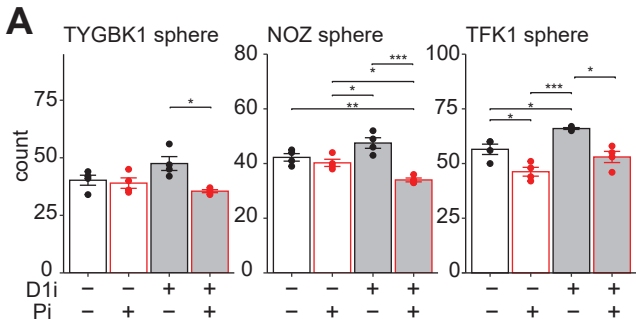


Fig6

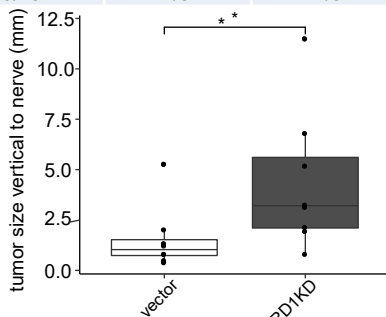
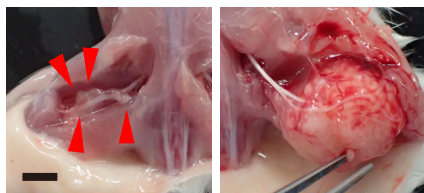
A



sph18-29	peri-sciatic nerve 10 ⁵ cells 2 months	subcutaneous 10 ⁵ cells 2 months	splenic injection 5 * 10 ⁵ cells 6 months
Ctrl (vector)	7/10	0/8	0/3
DRD1 KD	8/10	2/8	2/3

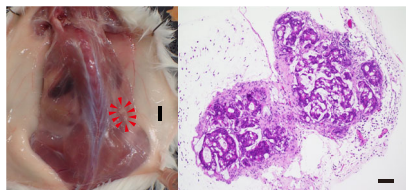
B

Sph18-29 sciatic nerve xenograft
vector DRD1KD

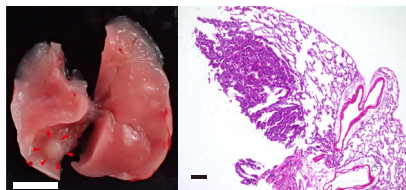


C

Sph18-29 subcutaneous xenograft



Sph18-29 splenic injection (lung)



D

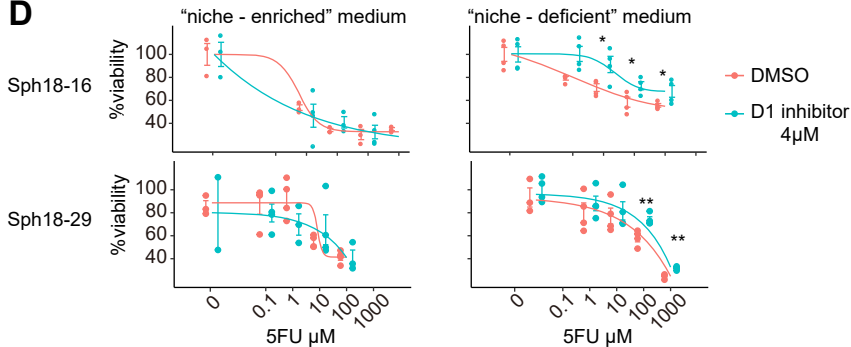
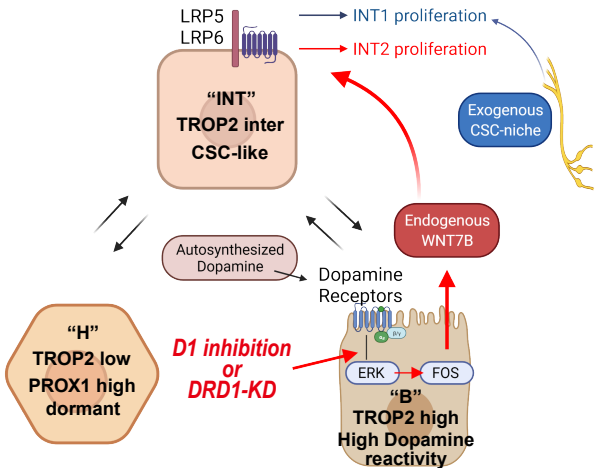


Fig7



Supporting Material and Methods

Genetic mutational hotspot analysis of organoid lines

Organoids were dissociated, and DNA was isolated using the QIAamp DNA Mini Kit (Qiagen, Hilden, Germany). Genetic mutations of PDOs were determined by next-generation sequencing analysis using the Ion AmpliSeq 50-gene Cancer Hotspot Panel v2 with additional genes (Thermo Fisher Scientific; sequencing, mapping alignment, and annotation were outsourced to Takara Bio, Kusatsu, Japan). The panel included mutation hotspots for the following cancer-related genes: *ABL1*, *AKT1*, *ALK*, *APC*, *ATM*, *BRAF*, *CDH1*, *CDKN2A*, *CSF1R*, *CTNNB1*, *EGFR*, *ERBB2*, *ERBB4*, *EZH2*, *FBXW7*, *FGFR1*, *FGFR2*, *FGFR3*, *FLT3*, *GNAI1*, *GNAS*, *GNAQ*, *GNF1A*, *HRAS*, *JAK2*, *JAK3*, *IDH1*, *IDH2*, *KDR/VEGFR2*, *KIT*, *KRAS*, *MET*, *MLH1*, *MPL*, *NOTCH1*, *NPM1*, *NRAS*, *PDGFRA*, *PIK3CA*, *PTEN*, *PTPN11*, *RBI*, *RET*, *SMAD4*, *SMARCB1*, *SMO*, *SRC*, *STK11*, *TP53*, *VH*, *ARID1A*, *ARID2*, *ATRX*, *BAP1*, *DAXX*, *MEN1*, *RNF43*, and *TGFBR2*. Additionally, to preserve the quality of mutation detection, mutation candidates with homopolymer regions with lengths of ≥ 5 base pairs and those with sequencing coverage of ≤ 250 base pairs were excluded from the analysis. Further details are given in Table S3ABCD.

Short-hairpin RNA-mediated human DRD1 gene knockdown by lentiviral transduction

DRD1 knockdown in the bile duct cancer cell lines and PDO was performed by infection with a lentiviral particle that expressed human DRD1-targeting short-hairpin RNA (shRNA). The

lentivirus vector plasmid encoding human DRD1-targeting shRNA (Sigma-Aldrich) was cotransfected together with packaging plasmids consisting of pMDLg/pRRE (RRID:Addgene_12251), pRSV-Rev (RRID:Addgene_12253), and pMD2.G (RRID:Addgene_12259) (Addgene, Watertown, MA, USA) into 293T cells using Lipofectamine 3000 (Invitrogen). After 48 h, the supernatant was collected and used as a lentiviral particle without enrichment. The two predesigned DRD1-targeting shRNAs (A: 5-ccggTTATGCCTTTAATGCTGATTTctcgagaaatcagcattaaaggcataatTTTTg-3, B: 5-ccggTATCAGTCATATTGGACTATGctcgagcatagtccaatatgactgatatTTTTg-3) were used. Then, 48–72 h after viral infection, the cells were treated with medium containing puromycin (INVIVOGEN, San Diego, CA, USA) at 1–5 µg/ml for 2 weeks to remove noninfected cells.

Immunohistochemical staining

In vivo specimens were isolated and fixed in 4% paraformaldehyde (Nacalai Tesque) overnight for histological analyses. *In vitro* PDOs were isolated from Matrigel using an ice-cold cell recovery solution (Corning, Cambridge, MA, USA), embedded in iPGell (Genostaff, Tokyo, Japan), and fixed in 4% paraformaldehyde overnight. The samples were paraffin embedded and sliced into 5-µm-thick sections. Sections were then deparaffinized, rehydrated, and stained with hematoxylin and eosin. For immunohistochemical analyses, sections were deparaffinized, rehydrated, and placed in 3% (v/v) H₂O₂–methanol (Nacalai Tesque) for 15 min at 25°C.

Sections were then immersed in blocking solution (Dako-Cytomation, Kyoto, Japan) for 15

min and incubated with the primary antibodies listed below at 4°C overnight. Antigen–antibody complexes were detected with a secondary antibody (Nichirei, Tokyo, Japan) and visualized using 3,30-diaminobenzidine (0.5 mg/ml in Tris-buffered saline). The primary antibodies and dilution ratios were as follows: Anti-Dopamine Receptor D1 antibody (1:600, Abcam, Cambridge, UK, Cat# ab20066, RRID:AB_445306), Anti-WNT7B antibody (1:500, Sigma, St Louis, MO, USA, Cat# SAB2108321), Anti-PROX1 antibody (1:500, Abcam, Cat# ab199359, RRID:AB_2868427), and Anti-Cytokeratin 19 (1:6400, ProteinTech Group, Chicago, IL, USA, Cat# 10712-1-AP, RRID:AB_2133325). The antibodies used are listed in Table S7.

Immunofluorescence staining

Formalin-fixed, paraffin-embedded samples were sliced into 5- μ m sections, deparaffinized, rehydrated, and blocked with Block Ace (KAC Co., Ltd., Kyoto, Japan) for 60 min at room temperature. Slides were incubated with Anti-Dopamine Receptor D1 antibody (1:600, Abcam, Cambridge, UK, Cat# ab20066, RRID:AB_445306), Anti-TROP2 antibody (1:200, BioLegend, San Diego, CA, USA, Cat# 363802, RRID:AB_2564376), Anti-TH antibody (1:100, Merck Millipore, Darmstadt, Germany, Cat# MAB318, RRID:AB_2313764), and Anti-MAOB antibody (1:100, Proteintech Cat# 12602-1-AP, RRID:AB_2137273) at 4°C overnight.

Then, they were incubated with Alexa Fluor 488-conjugated anti-rabbit IgG antibody (1:400; Abcam Cat# ab150081, RRID:AB_2734747) and Alexa Fluor 594-conjugated anti-mouse IgG antibody (1:400; Abcam Cat# ab150120, RRID:AB_2631447) for 60 mins at room temperature.

For confocal imaging of PDO, clearing and slide preparation were performed following a previous report.¹ Fluorescence images were obtained using a fluorescence microscope BZ9000 (Keyence, Osaka, Japan). Three-dimensional confocal images were integrated by full-focus function. WNT7B-positive areas were identified using ImageJ.

Western blot

Samples were extracted using ice-cold RIPA buffer (Nacalai Tesque) and separated using sodium dodecyl sulfate-polyacrylamide gel electrophoresis in 10%–20% acrylamide gel (Wako). Proteins were transferred onto polyvinylidene fluoride membranes (Merck Millipore, Darmstadt, Germany) and blocked using 5% skim milk (Wako). Proteins were incubated with the primary antibodies at 4°C overnight. The primary antibodies used in this study were as follows: Anti-Dopamine Receptor D1 antibody Anti-Dopamine Receptor D1 antibody (1:1000, Abcam, Cat# ab20066, RRID: AB_445306) and anti-beta Actin (1:50000, Abcam) and then incubated with Horseradish peroxidase (HRP)-conjugated antimouse or antirabbit secondary antibodies (Jackson ImmunoResearch Labs, West Grove, PA, USA) for 60 min at room temperature. Immunoreactive protein bands were identified with a chemiluminescent HRP substrate (Merck Millipore). Chemiluminescence signals were analyzed using ImageQuant LAS 4000 (Cytiva, Logan, UT, USA). The antibodies used are listed in Table S7.

Flow cytometry

PDOs were dissociated with TrypLE Express enzyme into single cells and then filtered through

a 35- μ m cell strainer. The incubation buffer was prepared as 1 \times PBS, 2% FBS, and 10 μ M Y-27632 (Tocris Bioscience). In addition, single-cell suspensions were washed with cooled incubation buffer and resuspended in incubation buffer on ice for 30 min for antibody blocking. Next, cell pellets were centrifuged, resuspended, and incubated for 30 min on ice with a 100-fold dilution of the following antibodies: PE antihuman TACSTD2 (TROP2) (Cat# 363804, RRID: AB_2572022, BioLegend, San Diego, CA, USA). Next, samples were passed through a 35- μ m cell strainer and suspended in 500 μ l incubation with 1 \times PBS + 2% FBS and 10 μ M Y-27632 to reach a final concentration of 10^6 cells per 100 μ l. Flow cytometry was carried out using BD FACS AriaII or BD FACSVerse flow cytometer (Becton, Dickinson and Co., Franklin Lakes, NJ, USA). Cell debris was excluded by forward scatter pulse width and side scatters pulse width. Dead cells were excluded by DAPI labeling (BioLegend). Data were analyzed using FlowJo version 10.8.0 software (Tree Star, Ashland, OR, USA). The antibodies used are listed in Table S7.

ELISA

The culture supernatant was collected, and dopamine preservatives were added (1 mM EDTA, 4 mM Na₂S₂O₅, 10 mM HCl) and stored at -80° C until assay. The samples were assayed using a commercially available dopamine ELISA kit (ImmuSmol SAS, Bordeaux, France).

scRNA-seq

For sample preparation, PDOs were dissociated and plated in a Matrigel-precoated well of a 6-

well plate (10,000 cells per well). The PDOs were then cultured in a niche-enriched medium with DMSO or D1 inhibitor (SKF 83566 (Abcam), 4 μ M) with the medium changed twice weekly. After 14 d of culture, PDOs were dissociated with TrypLE Express enzyme into single cells, filtered through a 35- μ m cell strainer, and resuspended in 0.04% bovine serum albumin (Nacalai Tesque)/PBS. Single-cell suspensions (Cell Stock Concentration 700 cells/ μ l) were added onto Chromium Controller (10X Genomics, Pleasanton, CA, USA) to generate single-cell gel beads in an emulsion, with approximately 7,000 target cells recovered for each sample. scRNA-seq libraries were prepared using the following Single-Cell 3' Reagent Kits v3.1: Single Cell 3' GEM, Library & Gel Bead Kit v3.1, Chip G Single Cell Kit, and i7 Multiplex Kit (catalog nos. PN-1000121, PN-1000120, PN-120262, 10X Genomics).

The quality of the amplified library was assessed using Agilent 2200 TapeStation (Agilent Technologies, Inc.) with High Sensitivity D5000 ScreenTape (Catalogue number 5067-5592, Agilent Technologies, Inc., Santa Clara, CA, USA). Pooled libraries were run on Illumina HiSeq 2500 (San Diego, CA, USA) with the following parameters: Read 1: 28 cycles, i7 index: 8 cycles; Read 2: 91 s for Sph18-16, and HiSeq 4000 using settings of 2 \times 150 paired-end reads for Sph18-29 and one full lane per sample, for approximately > 90% sequencing saturation. We used the Cell Ranger v.3.1.0 pipeline from 10X Genomics to process raw sequencing reads. Briefly, raw sequencing reads were demultiplexed, aligned to the human genome (hg38), and filtered for quality using default parameters. UMI counts for each gene per cell were

consequently calculated.

Filtered gene–barcode matrices were then analyzed using the Seurat v.3.2.1 R package². Seurat objects were generated with CreateSeuratObject. Sph18-16 with DMSO cells and Sph18-16 with D1 inhibitor cells were merged to create a single gene–barcode matrix. Cells were further filtered based on the distribution of genes (nFeature) and percent mitochondrial genes (percent.mito) per cell across the dataset: $nFeature_RNA > 200$ & $nFeature_RNA < 6000$ & $percent.mt < 15$. Data were normalized for sequencing depth, multiplied by a scaling factor of 10000, and log-transformed using the default parameters of NormalizeData. The top 2000 variable genes within each dataset were selected on the basis of a variance stabilizing transformation (FindVariableFeatures, selection. method = ‘vst’) and used in the downstream principal component analysis (PCA).

The principal components (PCs) identified with RunPCA and PCs included in the downstream analysis were empirically determined by visualization of PCs in an ElbowPlot. Normalized data were scaled using the ScaleData function. Cell clusters were identified by constructing a shared nearest neighbor graph (FindNeighbors) and a modularity optimization-based clustering algorithm (FindClusters) using the PCs determined by PCA (dims = 1:20). Clustering was performed at resolutions of 0.7. Cells and clustering were visualized using Uniform Manifold Approximation and Projection (UMAP) dimensional reduction (RunUMAP). Several outlying clusters were removed from further analysis. Clusters with low nFeature_RNA, low

nFeature_RNA, and low percent.mt (cluster 7, 9) were identified using violin plot, and clusters in the S and G2/M phase (clusters 1, 4, 5, and 8) of the cell cycle were found via cell cycle analysis with CellCycleScoring.

Original gene lists for the enrichment analysis were gained with FindMarkers with the parameter “only.pos = FALSE, logfc.threshold = 0, min.pct = 0.” Input data were gained via filter function with the parameter “avg_logFC > 0” and then via slice_min function with a parameter of “order_by=p_val_adj (or p_val), n = 200.” Enrichment analysis was performed via enricher function in clusterProfiler R package (v.3.14.3)³ with the parameter “pvalueCutoff = 0.05, pAdjustMethod = "BH", minGSSize = 10, maxGSSize = 500, qvalueCutoff = 0.2.” Gene sets were downloaded from MSigDB (v7.2 and 7.4) and EnrichmentMap (Human_GO_AllPathways_no_GO_ica_January_01_2022_symbol.gmt). Gene signature scores were calculated using the AddModuleScore function in Seurat. Conserved cell type markers for each cluster among the samples were identified with FindConservedMarkers using default parameters (Table S4ABCDE). Trajectory graphs were constructed using monocle3 R package (v.1.0.0).^{4,5,6}

Data Availability

The datasets analyzed during the current study are available from the corresponding author upon request.

References

1. Dekkers JF, Alieva M, Wellens LM, Ariese HCR, Jamieson PR, Vonk AM, et al. High-resolution 3D imaging of fixed and cleared organoids. *Nat Protoc.* 2019 Jun;14(6):1756-1771.
2. Stewart A, Lowe A, Smales L, Bajer A, Bradley J, Dwuznik D, et al. Parasitic nematodes of the genus *Syphacia* Seurat, 1916 infecting Muridae in the British Isles, and the peculiar case of *Syphacia frederici*. *Parasitology.* 2018 Mar;145(3):269-280.
3. Yu G, Wang LG, Han Y, He QY. clusterProfiler: an R package for comparing biological themes among gene clusters. *OMICS* 2012;16:284–7.
4. Trapnell C, Cacchiarelli D, Grimsby J, Pokharel P, Li S, Morse M, et al. The dynamics and regulators of cell fate decisions are revealed by pseudotemporal ordering of single cells. *Nat Biotechnol.* 2014 Apr;32(4):381-386.
5. Qiu X, Hill A, Packer J, Lin D, Ma YA, Trapnell C. Single-cell mRNA quantification and differential analysis with Census. *Nat Methods.* 2017 Mar;14(3):309-315.
6. Qiu X, Mao Q, Tang Y, Wang L, Chawla R, Pliner HA, et al. Reversed graph embedding resolves complex single-cell trajectories. *Nat Methods.* 2017 Oct;14(10):979-982.

A

Name	cell type / origin	sampling location	sphere type
OZ	pap. and por. bile duct	ascites	2-2
NOZ	mod. gallbladder	ascites	1
KKU-055	por.	biliary tract	2-1
KKU-213	pap. and non-pap.	biliary tract	1
KKU-100	por.	biliary tract	2-1
TYGBK-1	pap.	gallbladder	1
TYBDC-1	bile duct	liver metastasis	1
TYGBK-8	mod.	pancreatic biliary	2-2
HuCCA1	Cholangiocarcinoma	intrahepatic bile duct	1
OCUG-1	gallbladder	peritoneal effusion	2-1
HuCCT1	mod. intrahepatic bile duct	ascites	1
TFK1	pap.	common bile duct	1
G415	gallbladder	gallbladder	2-1

	shape	number	size (μm), largest	size (μm), median
OZ	smooth	547.0	170.1	39.1
NOZ	warty	158.0	352.2	106.2
KKU055	no	-	-	-
KKU213	smooth	28.0	122.2	31.6
KKU100	very small, few	-	-	-
TYGBK1	smooth	567.0	214.2	84.6
TYBDC1	warty	201.0	159.7	42.6
TYGBK8	warty	375.2	495.1	80.1
HuCCA1	smooth	181.0	79.5	35.2
OCUG1	very small, few	-	-	-
HuCCT1	smooth	169.0	81.1	34.3
TFK1	smooth	346.3	125.3	49.9
G415	no	-	-	-

B

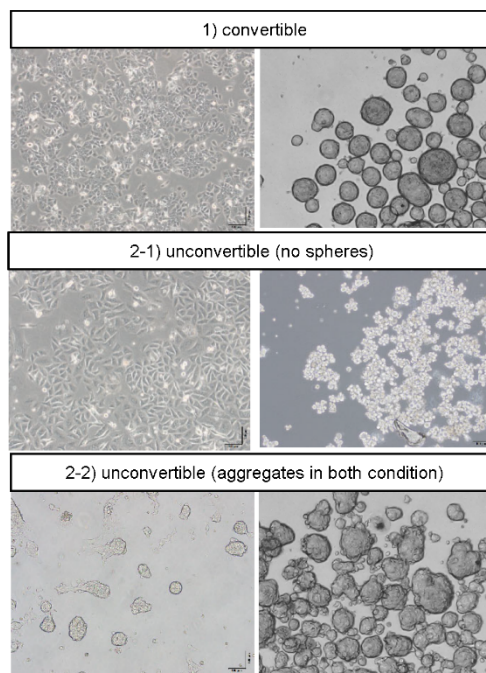


Figure S1. Characterization of 13 cell lines. (A) Information on 13 commercially available bile duct cancer cell lines (top) and their sphere formation performed in a 6-well plate (bottom). Values are the mean of triplicate. pap., papillary; por., poorly differentiated; and mod., moderately differentiated. (B) Typical examples of three types of phenotypical changes: (1) TYGBK-1; (2-1) KKU-100; (2-2) TYGBK8. Scale bar, 100 μm.

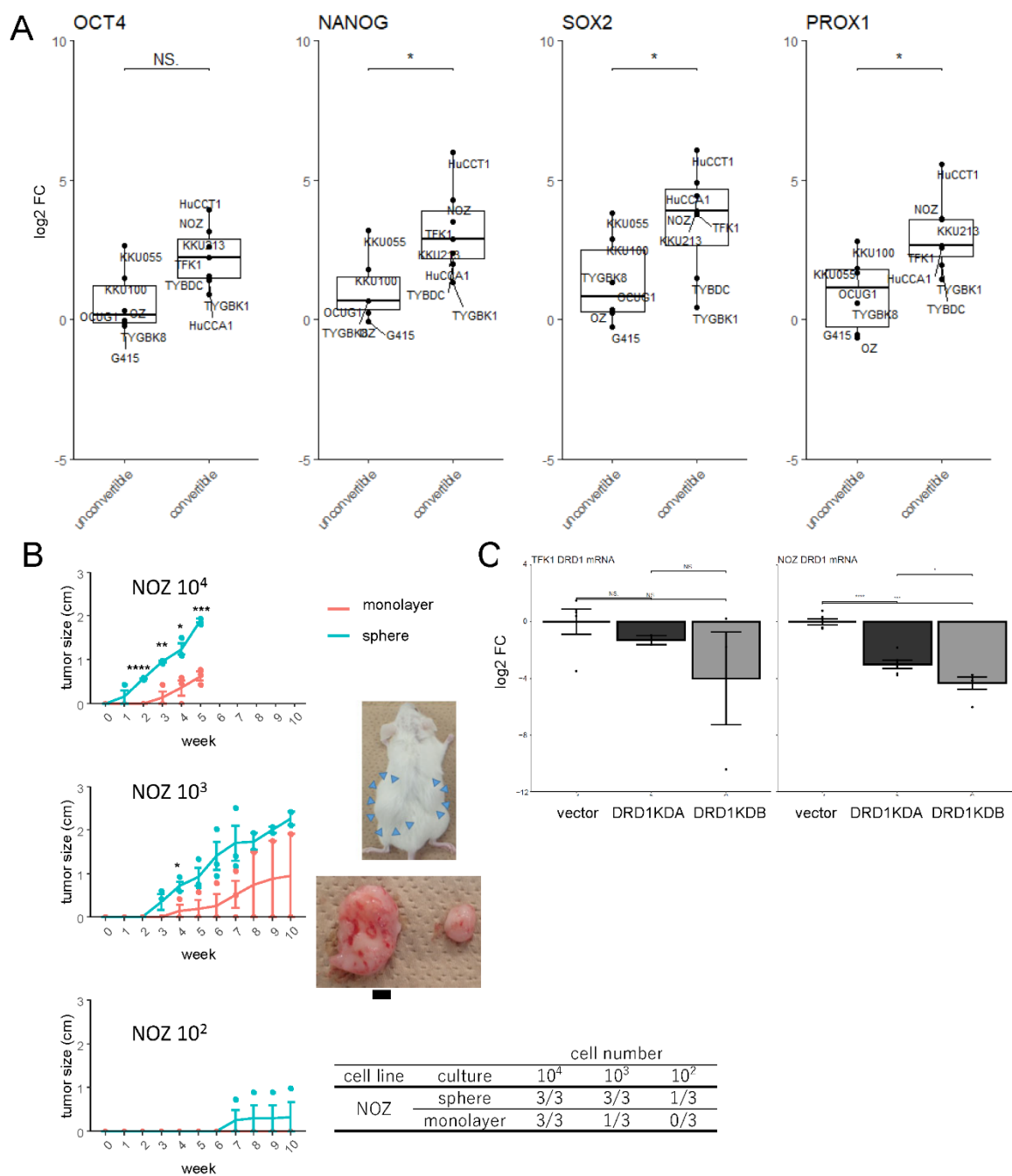


Figure S2. CSC-like characteristics of sphere cells. (A) Dependence of mRNA expression of cancer stem cell (CSC)-related genes on monolayer culture to sphere culture quantified via qRT-PCR. Each value is calculated as the median of triplicate. *NANOG* (median log₂ fold change 2.9 in “convertible” and 0.68 in “unconvertible,” $p = 0.022$), *SOX2* (3.9 and 0.84, $p = 0.035$), *POU5F1/OCT4* (2.2 and 0.16, $p = 0.051$), and *PROX1* (2.6 and 1.1, $p = 0.035$). FC,

fold change. (B) Subcutaneous transplantation of NOZ cells cultured in sphere or monolayer condition into NOD-SCID mice (10^4 , 10^3 , and 10^2 cells, $n = 3$). Tumor growth curves after transplantation (left) (mean + SE). Macroscopic images of formed tumor (right). Left of the mouse, tumor of sphere cells 10^4 ; right of the mouse, tumor of monolayer cells 10^4 . Scale bar, 5 mm. Number of tumor-forming mice per total transplanted mice at 10 weeks after transplantation (bottom). (C) Efficacy of *DRD1*-knockdown (KD) shown by relative mRNA of *DRD1*. FC, fold change.

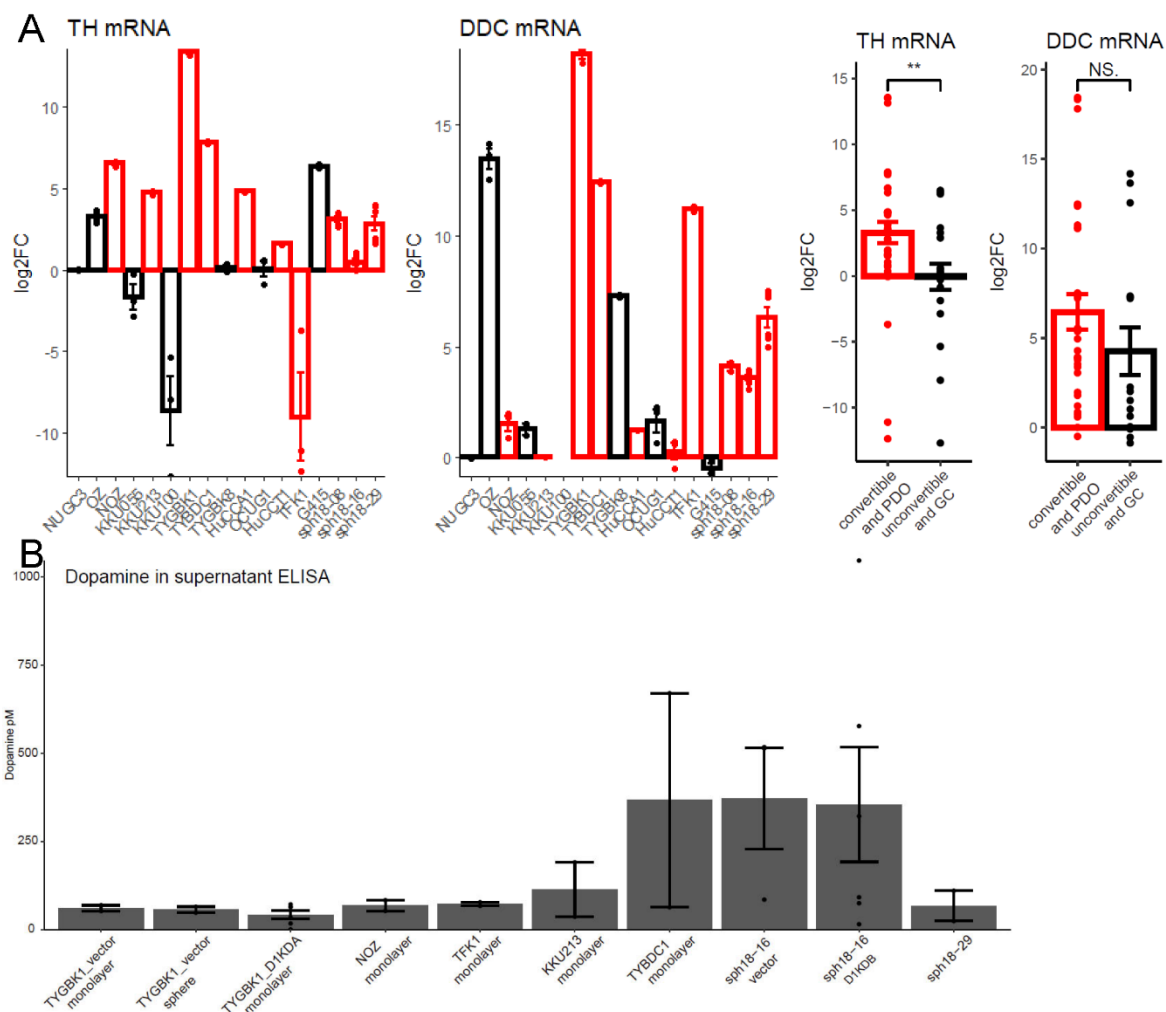


Figure S3. Dopamine secretion of the cell lines and patient-derived cancer organoids

(PDOs). (A) Relative mRNA expression of dopamine-synthesizing genes (*TH*, *DDC*)

standardized to gastric cancer cell line NUGC3. Red, convertible cell lines or PDOs. FC, fold

change; GC, gastric cancer. (B) ELISA-quantified dopamine concentration in the supernatant

of culture medium. n = 2–6.

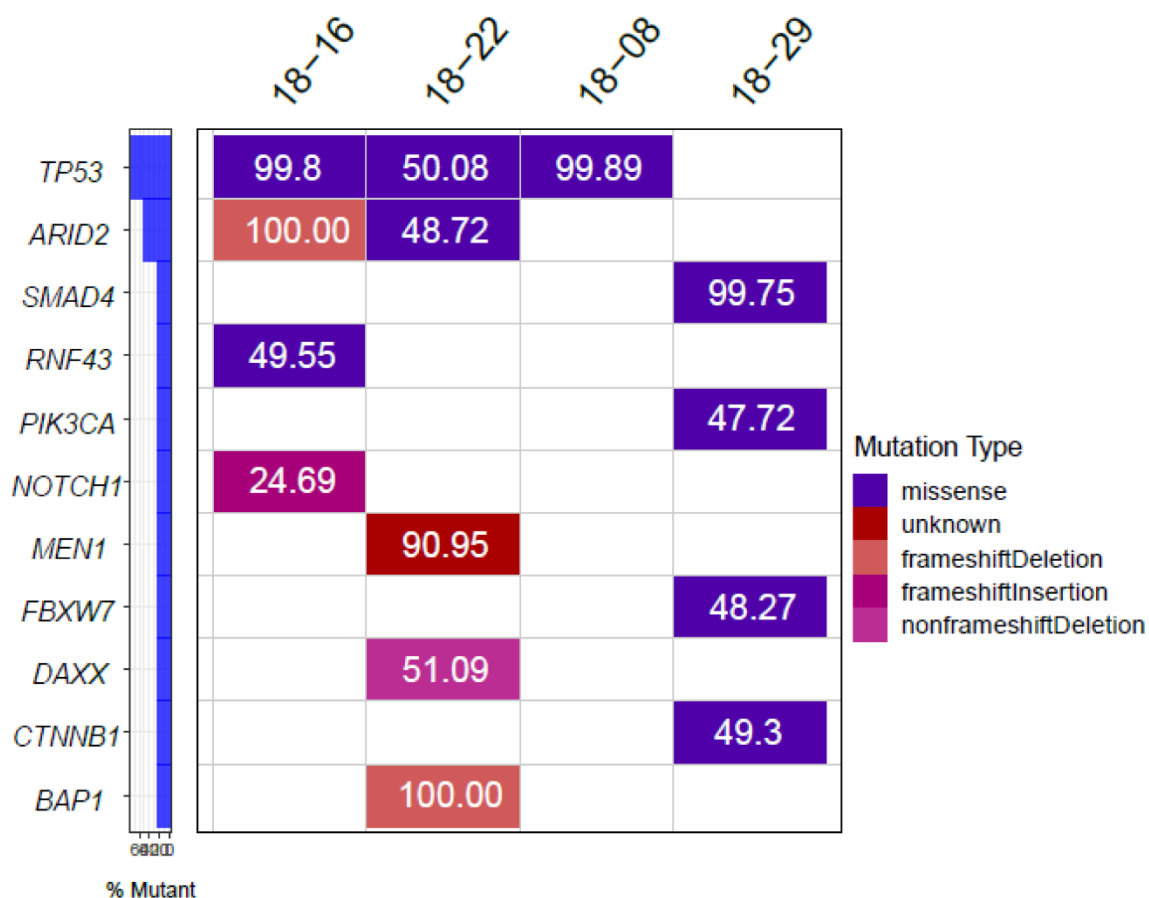


Figure S4. Genetic mutational hotspot analysis of organoid lines. Information of confirmed mutations in PDO lines. Mutations confirmed by the ClinVar and COSMIC databases are shown. Numbers indicate the percentage frequency of the mutation. Further details are shown in Table S3ABCD.

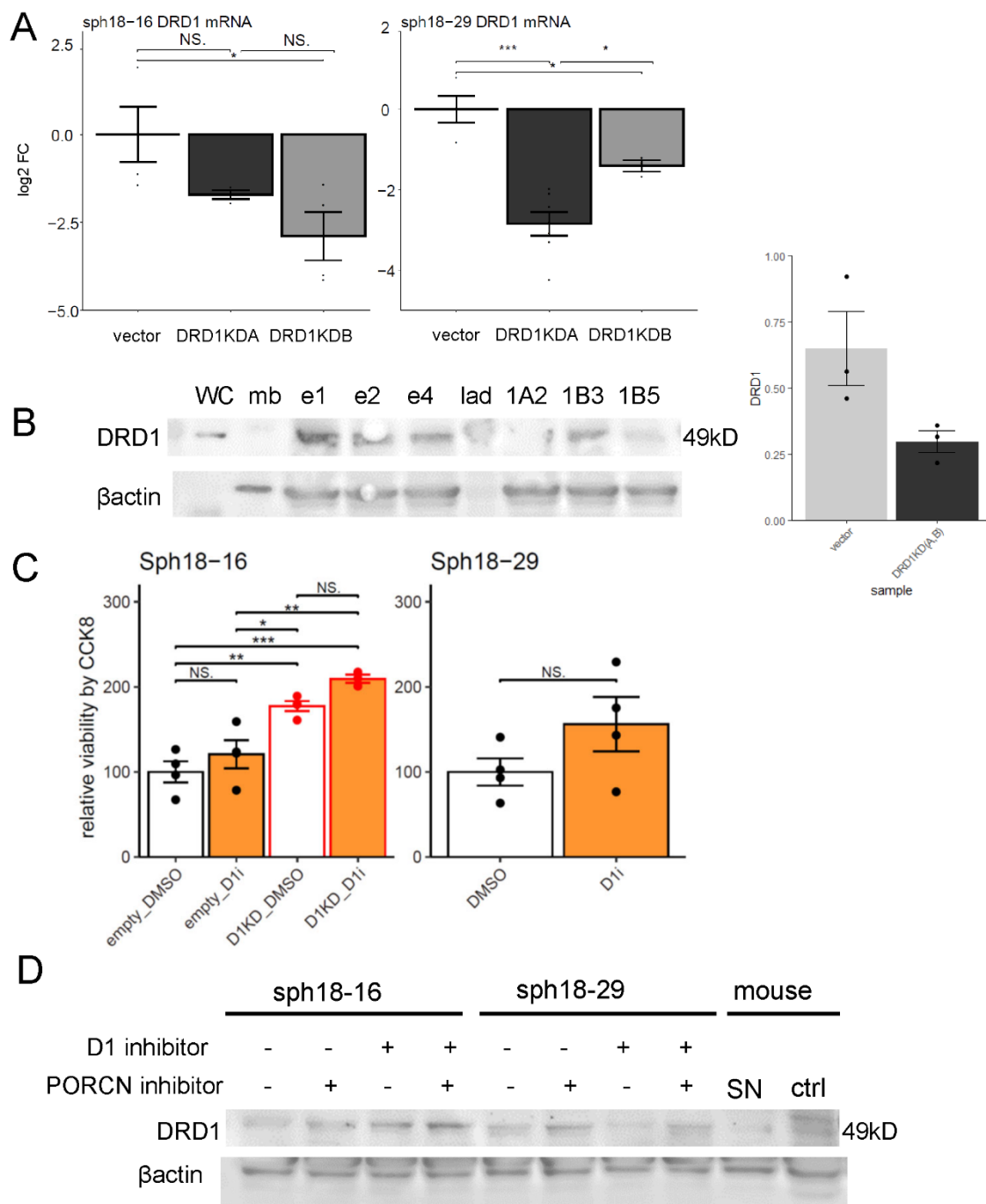


Figure S5. DRD1 expression of PDOs. (A) Efficacy of *DRD1*-KD shown by relative mRNA of *DRD1*. FC, fold change. (B) Western blot stain of DRD1 in comparison with that of vector (e1, e2, and e4) and DRD1 KD (1A2, 1B3, and 1B5) sph18-16 (top). Overall, 30 μg total protein is loaded. Quantitative comparisons are standardized by beta-actin. lad, ladder; WC, WesternC Standards; mb, the brain of NOD/SCID mouse as control (down). (C) Cell viability

of PDO with D1 inhibitor (SKF-83566 4 μ M) or D1KD measured by CCK8 assay. n = 4. (D)

Western blot stain of DRD1 in comparison with that of sph18-16 and 29 using D1 inhibitor (SKF-83566 4 μ M or DMSO) and/or porcupine inhibitor (LGK974 10nM or DMSO). Overall, 20 μ g total protein is loaded. mouse_SN, sciatic nerve of NOD/SCID mouse; mouse_ctrl, the brain of NOD/SCID mouse.

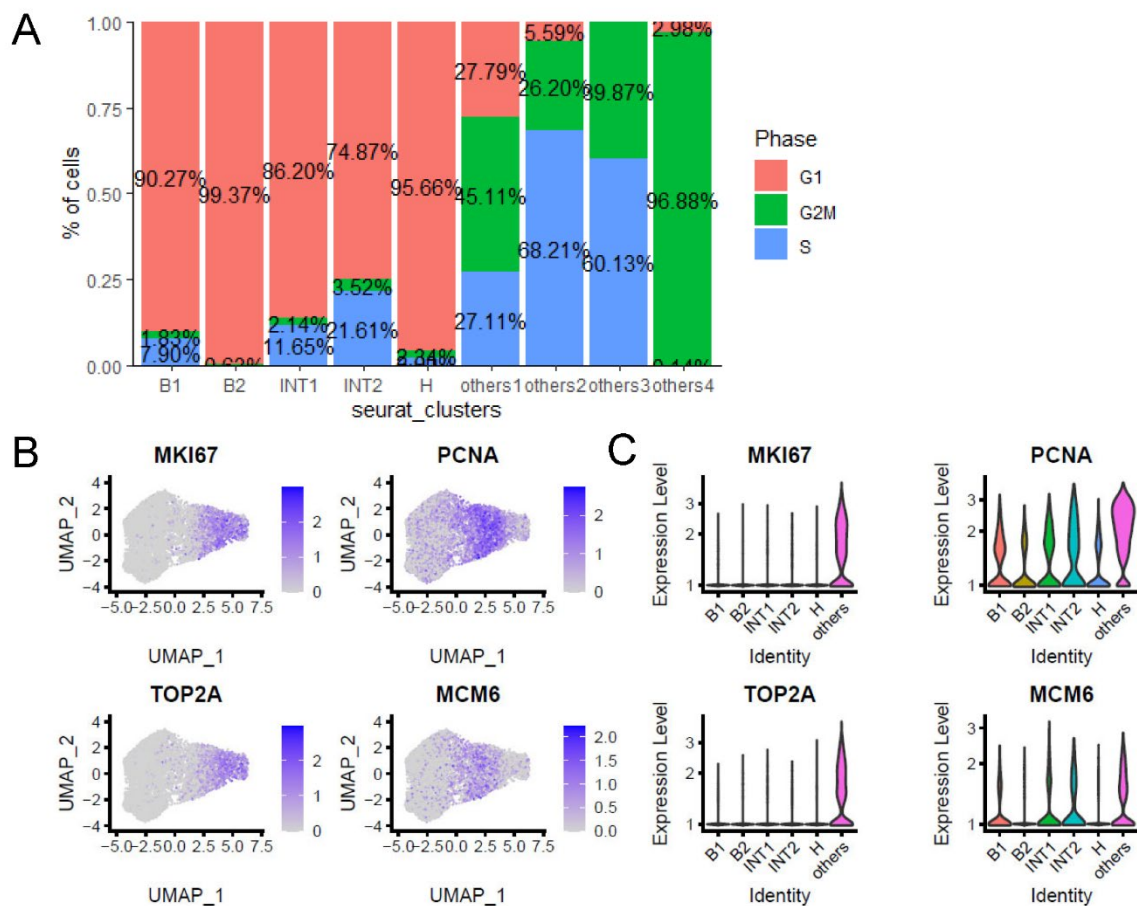


Figure S6. Proliferating cells in Sph18-16. (A) Percentage of proliferating cells in each cluster of Sph18-16. (B) Feature plots of cell cycle-related genes. (C) Violin plots of cell cycle-related genes.

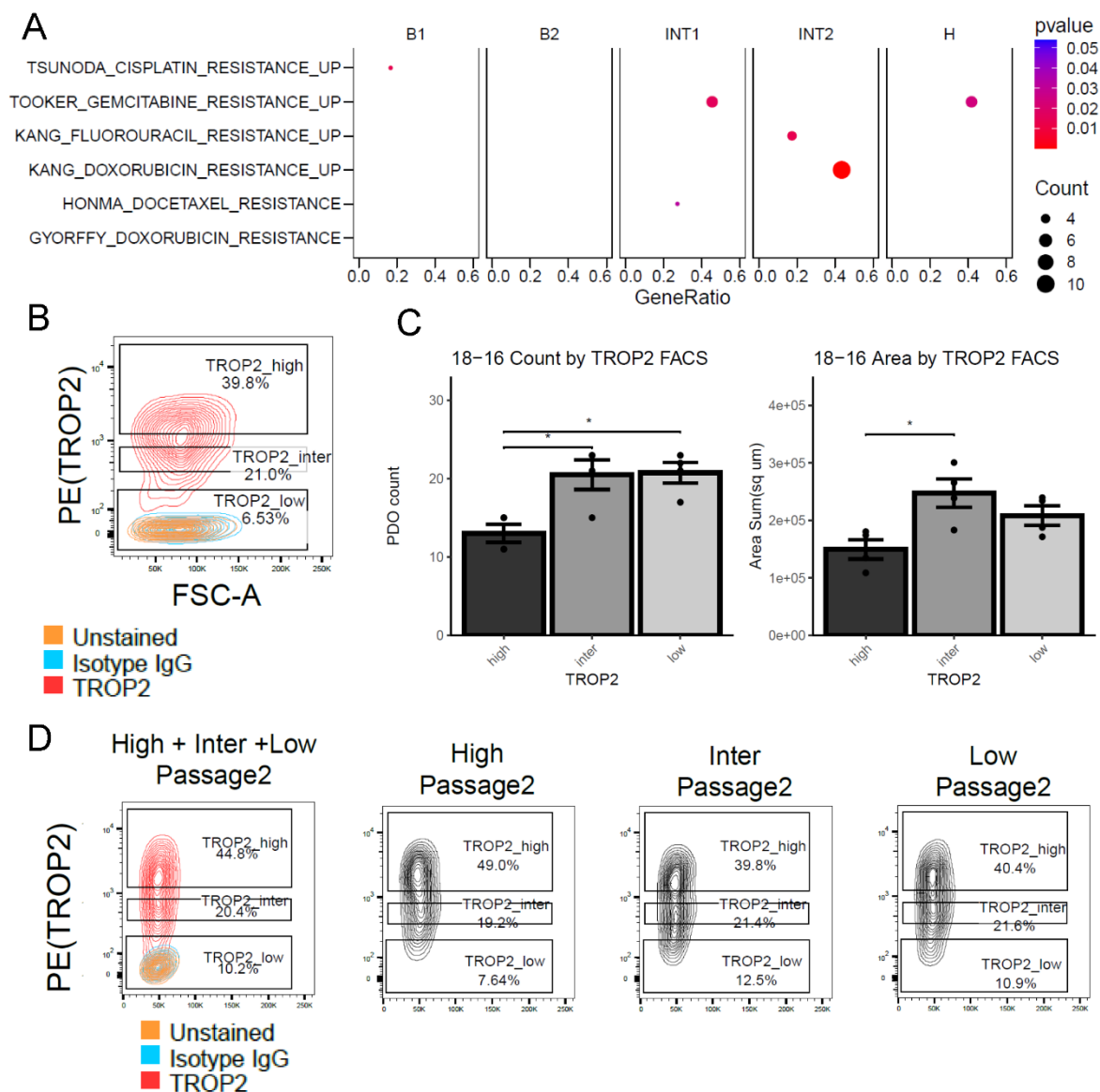


Figure S7. CSC-like cells in Sph18-16. (A) Dot plot of enrichment analysis using gene sets related to chemotherapy resistance. Results of $p < 0.05$ are shown. (B) Flow cytometry-based sorting by TROP2. (C) Organoid formation assay of Sph18-16 in comparison with TROP2^{high}, TROP2^{inter}, and TROP2^{low} cluster. Tukey's test is used. $n = 4$. (D) Each sorted cell type (TROP2-high, -inter, and -low) or mixed cells (equal number of TROP2-high, -inter, and -low cells) are cultured in enriched medium, and cell type fraction is assessed at passage 2.

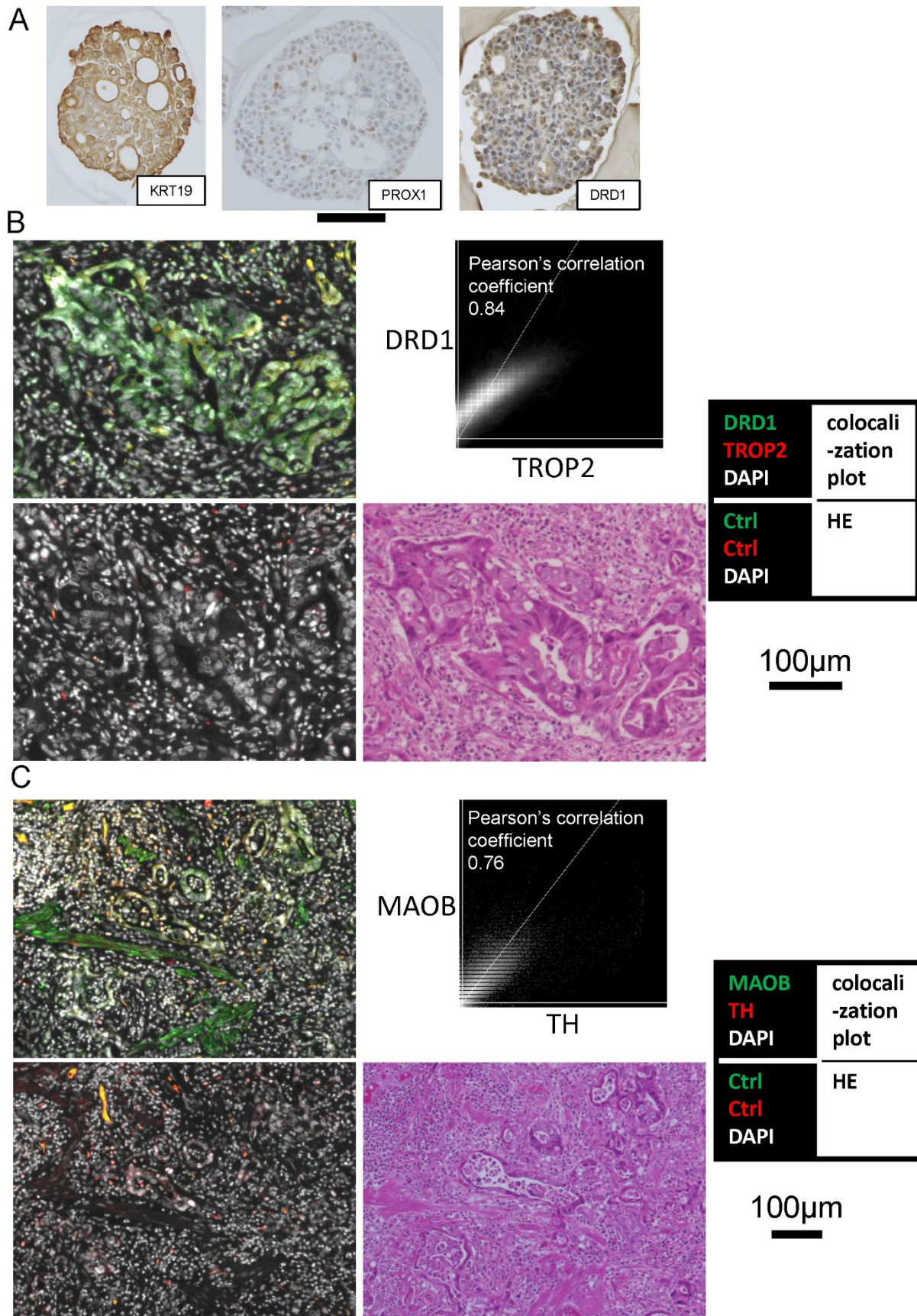


Figure S8. Dopamine-reactive cells in Sph18-16. (A) Immunohistochemical analysis of

Sph18-16 (left: KRT19, middle: PROX1, right: DRD1). Scale bar, 100 μm . (B)(C)

Pleomorphic tumor cells shown by immunofluorescent and HE histological imaging of the original surgical specimen of Sph18-16. Scale bar, 100 μm . Pearson's correlation coefficient in tumor cells is calculated using ImageJ.

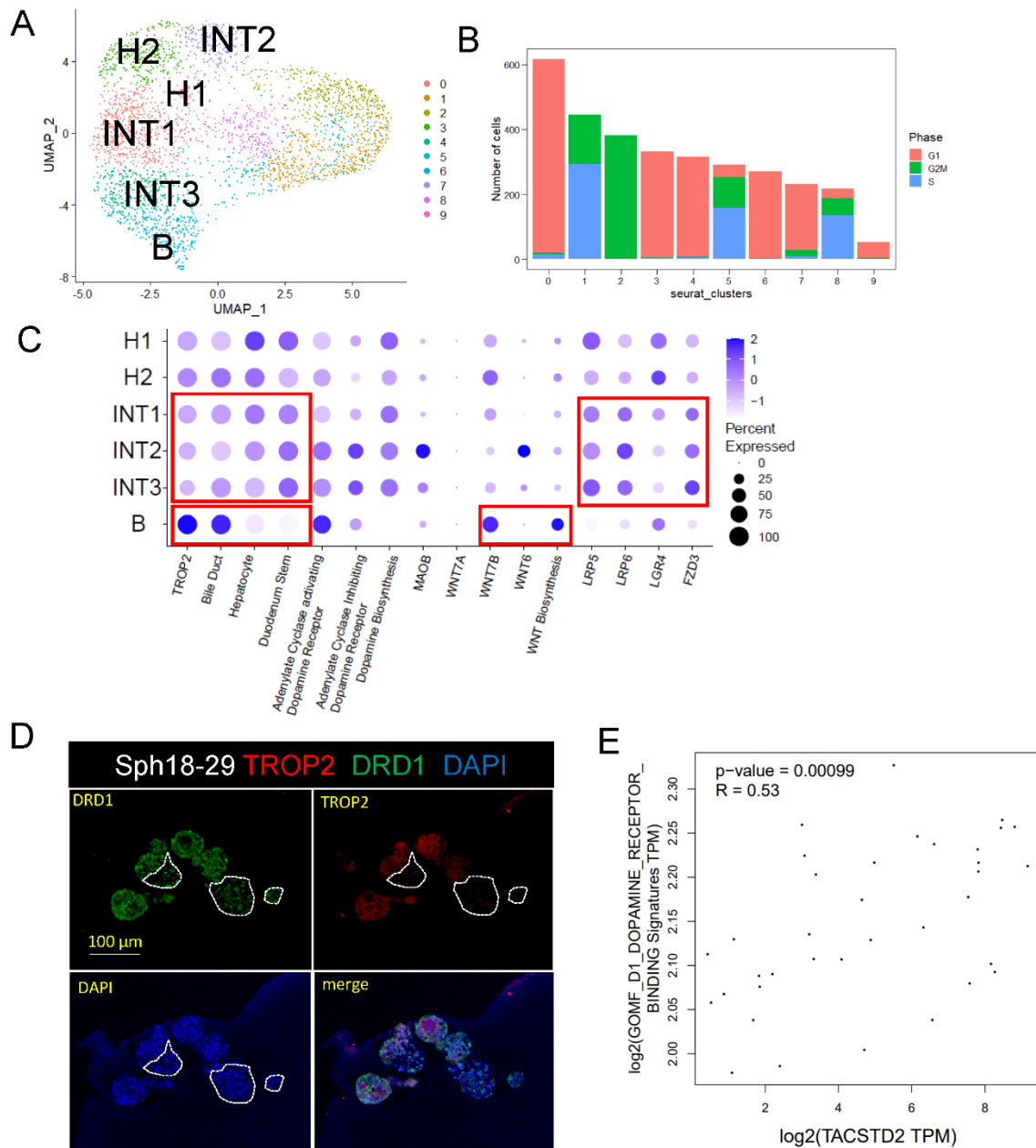


Figure S9. Validation of results of Sph18-16. (A) Uniform Manifold Approximation and Projection (UMAP) gained by scRNA-seq analysis of Sph18-29. (B) Cell cycle analysis of each cluster of Sph18-29. (C) Expressions of genes or gene signature scores of the cells in quiescent clusters (B, H1, H2, INT1, INT2, and INT3) of Sph18-29. (D) Immunofluorescent staining of Sph18-29 (green: DRD1, red: TROP2, blue: DAPI, marked area: low-stained cells). Scale bar, 100 μ m. (E) Expressional correlational plot between TROP2 (TACSTD2) and gene

signature of “GOMF_D1_DOPAMINE_RECEPTOR_BINDING” in TCGA CHOL (cholangiocarcinoma) cohort. Obtained from GEPIA2 (Tang Z, et al. *Nucleic Acids Res.* 2019;47:W556-W560). Spearman’s correlation coefficient.

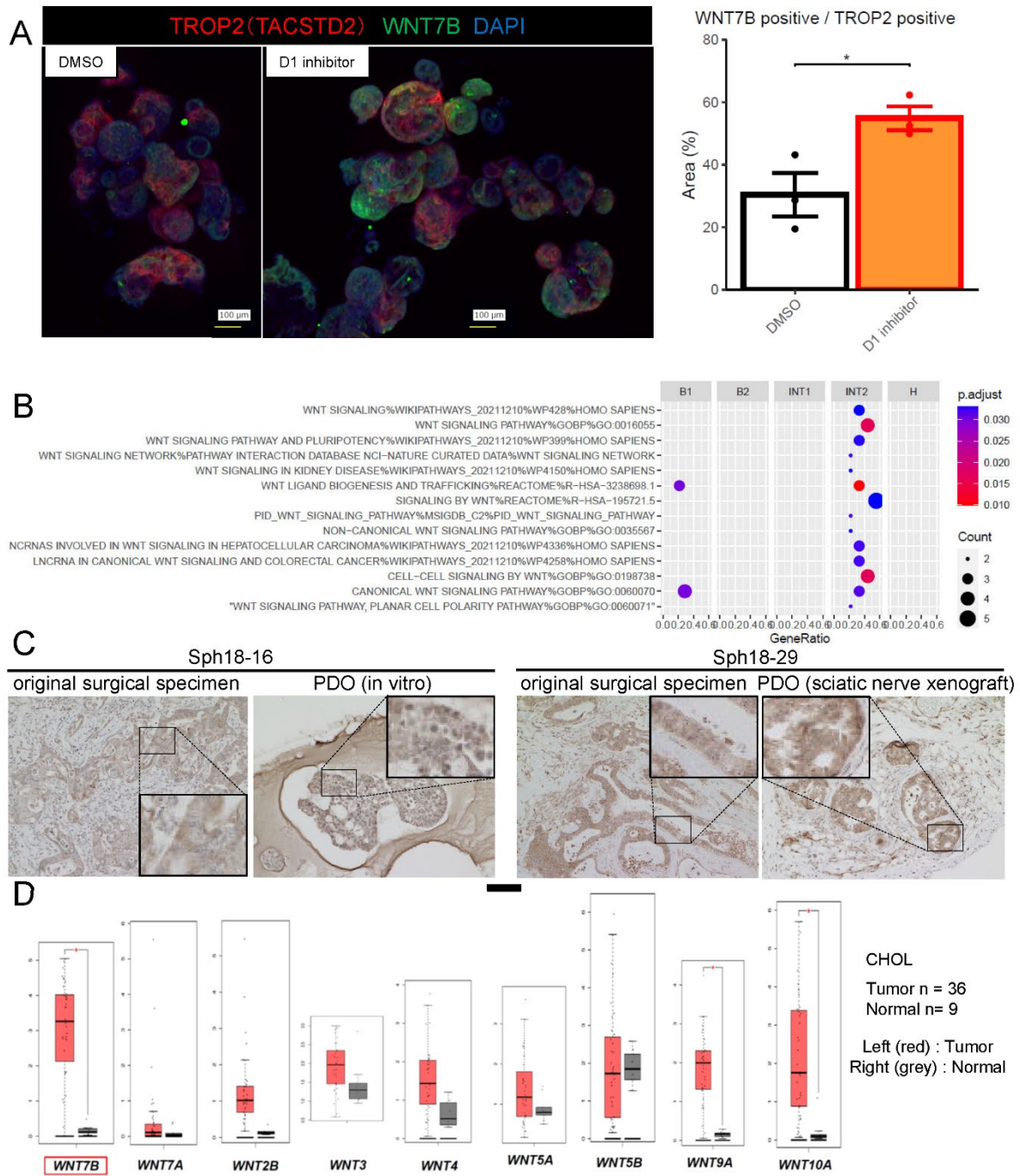


Figure S10. Analysis of WNT expression. (A) Left: 3D confocal image of immunofluorescent staining of Sph18-16 (green: WNT7B, red: TROP2, blue: DAPI). Scale bar, 100 μ m. Right: quantification of WNT7B-positive area in TROP2-positive area with DMSO or D1 inhibitor (SKF-83566 4 μ M). n=3. (B) Dot plot of enrichment analysis with upregulated genes in D1 inhibitor-treated PDO in each cluster, using gene sets related to WNT signaling without

negative terms. (C) Heterogeneous WNT7B expression is confirmed by IHC analysis and comparison with original surgical specimens and PDOs. Scale bar, 100 μ m. (D) The expressions of WNT7A/B and other WNT ligands such as WNT2B, WNT3, WNT4, WNT5A/B, WNT9A, and WNT10A in TCGA CHOL (cholangiocarcinoma) cohort in comparison with those in the tumor (red) and normal epithelium (grey). Obtained from GEPIA2 (Tang Z, et al. *Nucleic Acids Res.* 2019;47:W556-W560). The differential analysis is based on the “TCGA tumors vs TCGA normal + GTEx normal.” Differential analysis is performed using one-way ANOVA, with disease state (tumor or normal) as variable for calculating differential expression. The expression data are first $\log_2(\text{TPM}+1)$ transformed for differential analysis, and the $\log_2\text{FC}$ is defined as the median (tumor) – median (normal). Log Scale: $\log_2(\text{TPM} + 1)$ transformed expression data for plotting. $|\log_2\text{FC}|$ cutoff: 1. p-Value cutoff: 0.01. With respect to WNT1, WNT2, WNT3A, WNT6, WNT8A/B, WNT9B, WNT10B, WNT11, and WNT16, the data are not shown because their expression levels are less than 1.0 unit [$\log_2(\text{TPM}+1)$].

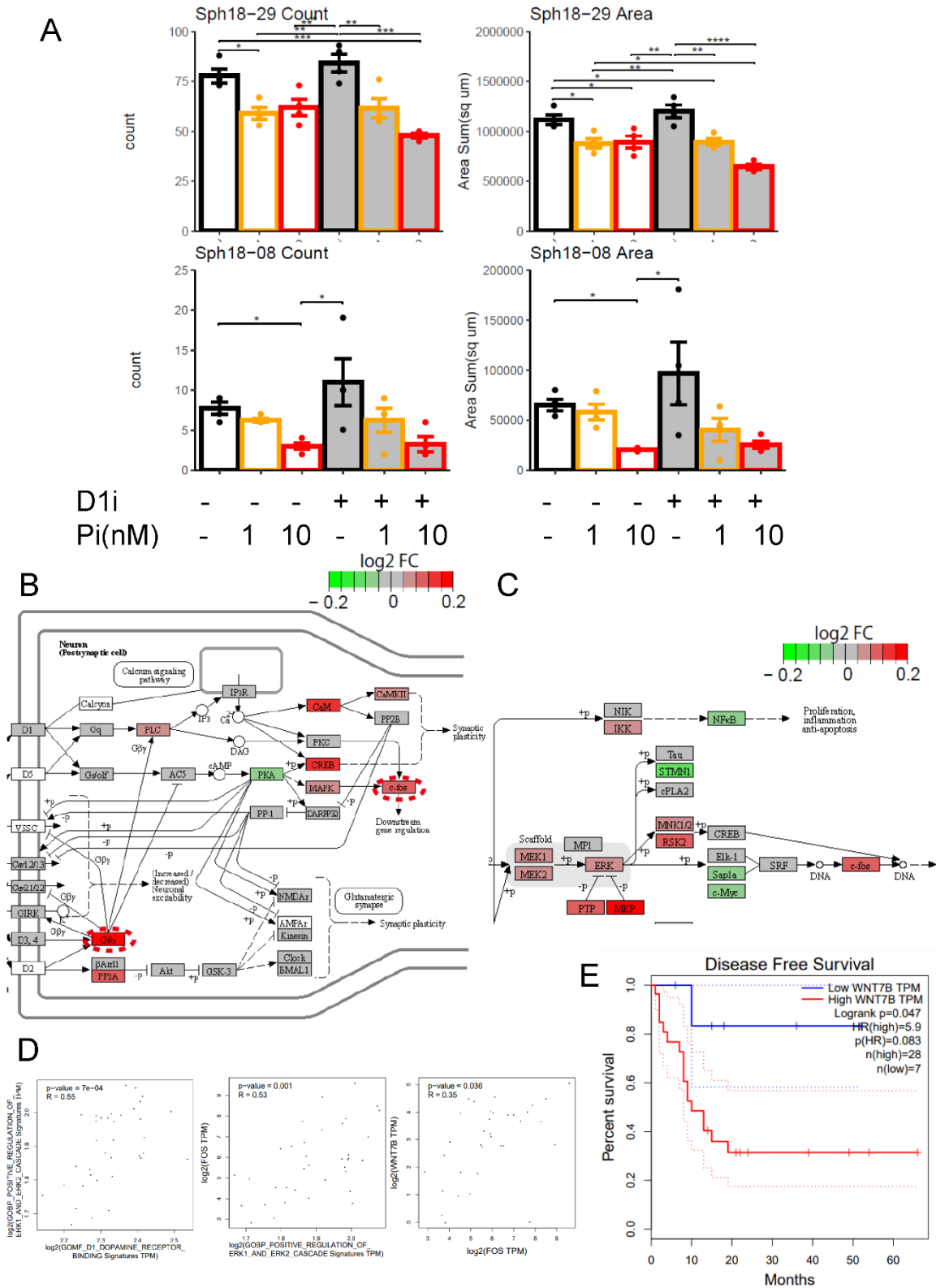


Figure S11. WNT7B and FOS as downstream of DRD1 signaling. (A) Organoid formation assay of Sph18-08, 29 with D1 inhibitor (SKF 83566 4 μ M or DMSO as control) and porcupine

inhibitor (LGK974 1 nM, 10nM, or DMSO as control). Tukey's test is used. n = 4. D1i, D1 inhibitor; Pi, Porcupine inhibitor. (B,C) KEGG pathway map obtained using scRNA-seq compared with that of D1 inhibitor sample and control at B1 cluster. FC, fold change. Rendered by Pathview (Luo W, et al. *Bioinformatics* 2013;29:1830–1). B: Hsa04728 dopaminergic synapse. C: Hsa04010 MAPK signaling pathway. (D) Expressional correlational plot in TCGA CHOL (cholangiocarcinoma) cohort. Obtained from GEPIA2 (Tang Z, et al. *Nucleic Acids Res.* 2019;47:W556-W560). Spearman's correlation coefficient. (E) Comparison of Kaplan–Meier disease-free survival plot between the expressional cutoff-high 20% and cutoff-low 20% in TCGA CHOL cohort. Obtained from GEPIA2 (Tang Z, et al. *Nucleic Acids Res.* 2019;47:W556-W560).

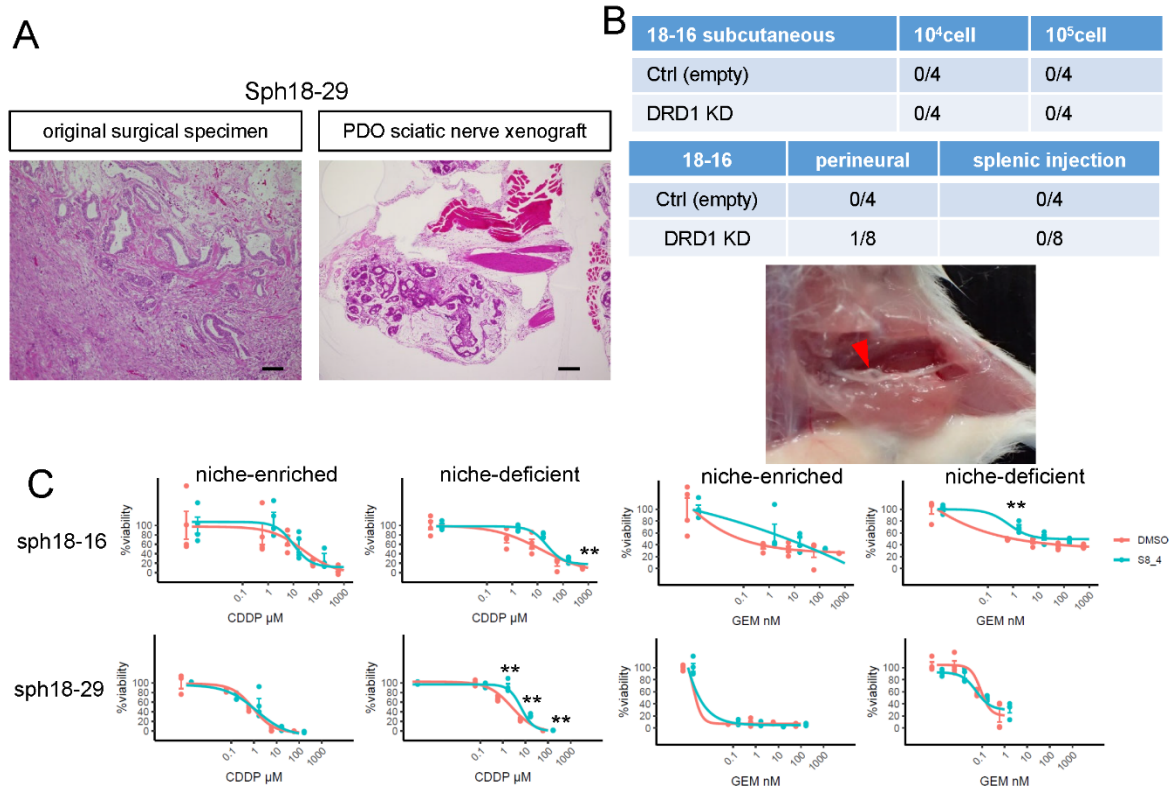


Figure S12. Xenotransplantation and chemoresistant assays of PDOs. (A) HE-stained histological images of peri-sciatic nerve xenografted tumor of Sph18-29 in comparison with those of the original surgical specimen. (B) Xenograft of Sph18-16. Only peri-sciatic nerve xenografted *DRD1*-KD Sph18-16 formed tumor (arrowhead). (C) CCK8 proliferation assay of Sph18-16, 29 responding to cisplatin (CDDP) and gemcitabine (GEM) in the niche-enriched or niche-deficient medium. $n = 4$. Two-tailed unpaired Student's t-test is used at each concentration.

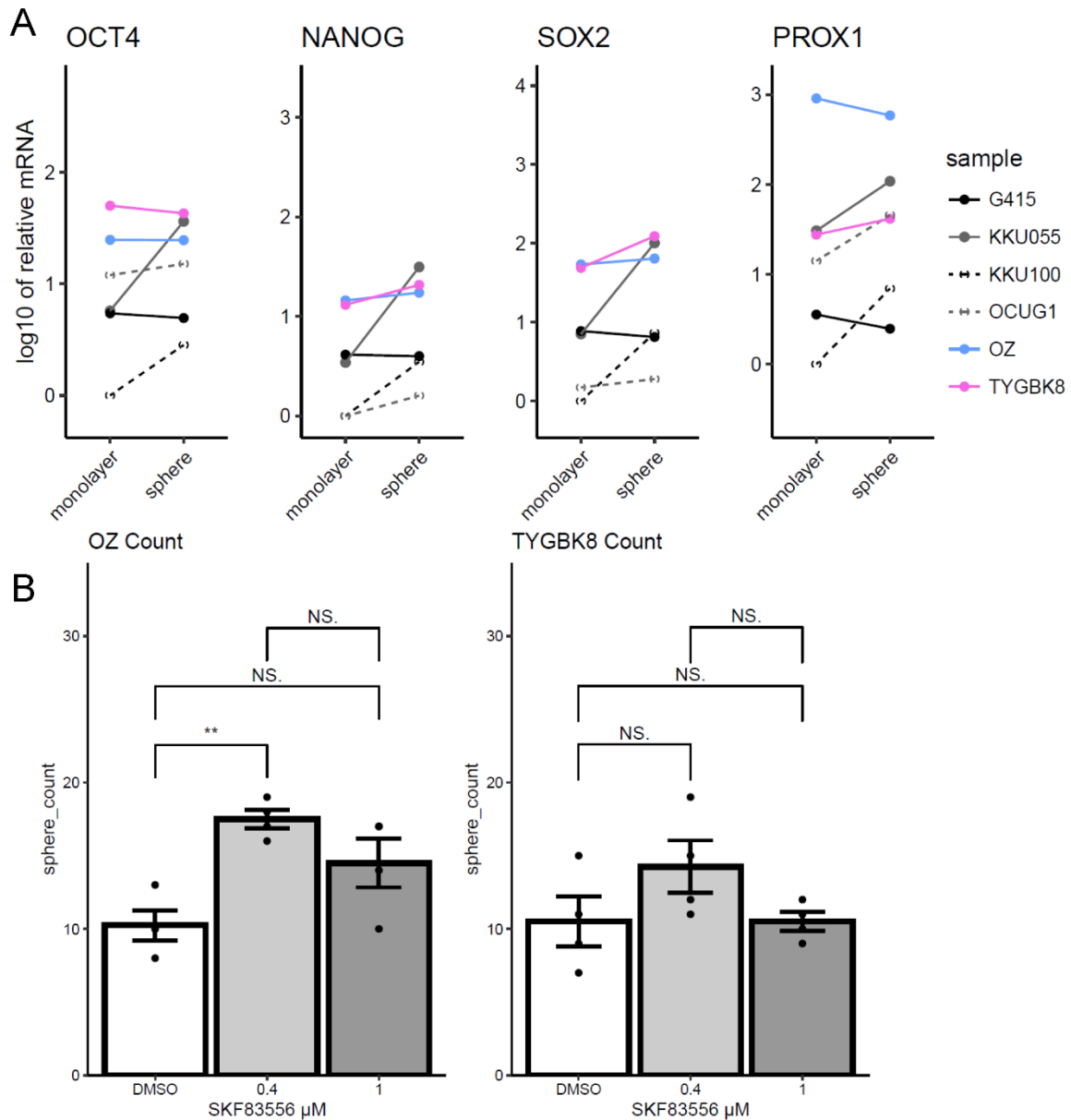


Table S1. List of the cell lines.

Name	Compan	Cat#	RRID	Culture medium
OZ (1)	JCRB	JCRB1032	CVCL_3118	DMEM, 10% FBS, 1% P/S
NOZ (2)	JCRB	JCRB1033	CVCL_3079	DMEM, 10% FBS, 1% P/S
KKU-055	JCRB	JCRB1551	CVCL_M258	DMEM, 10% FBS, 1% P/S
KKU-213	JCRB	JCRB1557	CVCL_M261	DMEM, 10% FBS, 1% P/S
KKU-100	JCRB	JCRB1568	CVCL_3996	DMEM, 10% FBS, 1% P/S
TYGBK-1	JCRB	JCRB1499	CVCL_J034	DMEM/Ham's F-12, 5% FBS, 1% P/S
TYBDC-1	JCRB	JCRB1501	CVCL_4W80	DMEM/Ham's F-12, 5% FBS, 3% P/S
TYGBK-8	JCRB	JCRB1590	CVCL_4W81	DMEM/Ham's F-12, 5% FBS, 2% P/S
HuCCA-1	JCRB	JCRB1657	CVCL_M255	Ham's F-12, 10% FBS, 1% P/S
OCUG-1	JCRB	JCRB0191	CVCL_3083	DMEM, 10% FBS, 1% P/S
HuCCT1	JCRB	JCRB0425	CVCL_0324	RPMI-1640, 10% FBS, 1% P/S
TFK1	RIKEN	RCB2537	CVCL_2214	RPMI-1640, 10% FBS, 1% P/S
G415	RIKEN	RCB2640	CVCL_8198	RPMI-1640, 10% FBS, 1% P/S
NUGC3	JCRB	JCRB0822	CVCL_1612	DMEM, 10% FBS, 1% P/S
293T	ATCC	CRL-3216	CVCL_0063	DMEM, 10% FBS, 1% P/S

All cell lines were maintained at 37°C, 5% CO₂, and 95% humidified air.

JCRB, Japanese Collection of Research Bioresources Cell Bank; ATCC, American Type Culture Collection

DMEM (Nacalai Tesque, Kyoto, Japan); FBS: fetal bovine serum (Cytiva, Marlborough, MA, USA); P/S, penicillin–streptomycin mixed solution (Nacalai Tesque); DMEM/Ham's F-12 (Nacalai Tesque); Ham's F-12 (Nacalai Tesque), RPMI-1640 (Nacalai Tesque)

1. Homma S, Nagamori S, Fujise S, Yamazaki K, Hasumura S, Sujino H et al, Human bile duct carcinoma cell line producing abundant mucin in vitro. *Gastroenterol Jpn* 1987; 22(4):474-9. PMID:2889643

2. Hasumura S, Nagamori S, Fujise K, Homma S, Sujino H, T Matsuura T et al, [Combination therapy of hyperthermia and other methods in liver and bile tract cancers - evaluation of these methods using cancer cell lines in vitro] *Gan To Kagaku Ryoho* 1989;16:1905-12. PMID:2543327

Table S2. PCR Primers.

	Forward primer (5' to 3')	Reverse primer (5' to 3')
DRD1	TTGGGTGGGCTAATTCATCCTT	CGGCCCCATTGTTATTGATACT
DRD2	AAAACCCGGACCTCCCTCAAGA	ACAGGCGGGATGTTGCAGTCAC
DRD3	TTCGGGAGAAGAAGGCAACC	ACTGTAAAGCTCTGGGGACACG
DRD4	TGCCGCTCTTCGTCTACTCC	GCTGATGGCGCACAGGTTGA
DRD5	GACGCCCTGGGAGGAGGACTTT	CGGTAGATGCGCGTGTAGGTCA
TH	CGTGCAGCCCTACCAAGACC	ACGTCGATGGCCAGCGTGTA
DDC	ACATATGGCTGCACGTTGATGC	CAATAGCCATTTGTGGGGATTA
POU5F1	TGCAGAAGTGGGTGGAGGAAGC	TTCGGGCACTGCAGGAACAAAT
NANOG	CCCAGCCTTTACTCTTCCTACCA	TTGGGTGCACCAGGTCTGAGT
SOX2	TACAGCATGTCCTACTCGCAG	GAGGAAGAGGTAACCACAGGG
PROX1	AAAGGACGGTAGGGACAGCAT	CCTTGGGGATTCATGGCACTAA
GAPDH	GACATCAAGAAGGTGGTGAAGC	GTCCACCACCTGTTGCTGTAG

Table S3. Hotspot mutation of patient-derived organoids. (A) Sph18-08.

Type	Genes	Location	% Frequency	Variant Effect	UCSC Common SNPs	ClinVar Coverage	Homopolymer Length
SNV	FLT3	FLT3:intronic:NM_004119.2	100.00	unknown	YES	0 1996	1
SNV	RNF43	RNF43:exonic:NM_017763.5	100.00	missense	YES	Benign 1994	1
SNV	TGFBR2	TGFBR2:intronic:NM_001024847.2	99.75	unknown	YES	Benign 1982	2
MNV	CSF1R,HMGXB3	CSF1R:utr_3:NM_005211.3, HMGXB3:downstream:NM_014983.2	99.09	unknown, unknown	YES	0 1978	1
SNV	STK11	STK11:intronic:NM_000455.4	99.95	unknown	YES	0 1932	1
SNV	TP53	TP53:exonic:NM_000546.5	99.89	missense		0 0 1884	1,1,1
SNV	RNF43	RNF43:exonic:NM_017763.5	64.33	missense	YES	0 1971	1
INDEL	KDR	KDR:intronic:NM_002253.2	60.78	unknown	YES	0 1994	2
SNV	ERBB4	ERBB4:intronic:NM_005235.2	52.50	unknown	YES	0 1998	1
SNV	KDR	KDR:exonic:NM_002253.2	52.21	missense	YES	not prov 1994	2
SNV	TGFBR2	TGFBR2:intronic:NM_001024847.2	48.92	unknown	YES	Benign 1995	1
SNV	ARID2	ARID2:intronic:NM_152641.3	47.17	unknown	YES	0 1993	1
SNV	ALK	ALK:intronic:NM_004304.4	33.50	unknown	YES	0 1994	3
SNV	MEN1	MEN1:intronic:NM_000244.3	31.28	unknown	YES	0 1995	1
SNV	RNF43	RNF43:exonic:NM_017763.5	31.35	missense	YES	Benign 1997	1
SNV	DAXX	DAXX:intronic:NM_001141970.1	46.52	unknown	YES	0 948	3
INDEL	ARID2	ARID2:intronic:NM_152641.3	1.99, 4.61	unknown	YES	0 1909	2,1,2
SNV	ATRX	ATRX:intronic:NM_000489.4	6.31	unknown		1965	1
SNV	ARID2	ARID2:intronic:NM_152641.3	7.00	unknown		0 0 1999	2
SNV	ARID1A	ARID1A:exonic:NM_006015.5	4.85	missense		0 0 1998	2
SNV	ATRX	ATRX:intronic:NM_000489.4	2.64	unknown		1895	2

Table S3. Hotspot mutation of patient-derived organoids. (B) Sph18-16.

Type	Genes	Location	% Frequency	Variant Effect	UCSC Common SNPs	ClinVar Coverage	Homopolymer Length
SNV	RNF43	RNF43:exonic:NM_017763.5	99.90	missense	YES	Benign 1988	1
SNV	KDR	KDR:intronic:NM_002253.2	2.55, 97.15	unknown, unknown	YES	0 1998	1,1
SNV	KDR	KDR:intronic:NM_002253.2	2.55,97.15	unknown, unknown	YES	0 1998	1,1
SNV	ERBB4	ERBB4:intronic:NM_005235.2	99.70	unknown	YES	0 1997	1
SNV	RNF43	RNF43:exonic:NM_017763.5	99.95	missense	YES	Benign 1996	1
SNV	FLT3	FLT3:intronic:NM_004119.2	99.60	unknown	YES	0 1998	1
SNV	ARID2	ARID2:intronic:NM_152641.3	99.90	unknown	YES	0 1966	1
SNV	TP53	TP53:exonic:NM_000546.5	99.8	missense		0 0 1993	1,1,1,1,1
INDEL	ARID2	ARID2:exonic:NM_152641.3	100.00	frameshiftDeletion		0 0 1409	3
SNV	STK11	STK11:intronic:NM_000455.4	65.25	unknown	YES	0 1971	1
SNV	RNF43	RNF43:exonic:NM_017763.5	49.55	missense		0 0 1992	1
MNV	CSF1R,HMGXB3	CSF1R:utr_3:NM_005211.3, HMGXB3:downstream:NM_014983.2	44.32	unknown, unknown	YES	0 1988	1
SNV	ATRX	ATRX:intronic:NM_000489.4	33.80	unknown	YES	2000	1
SNV	TGFBR2	TGFBR2:intronic:NM_001024847.2	33.08	unknown	YES	Benign 1995	2
SNV	ATRX	ATRX:exonic:NM_000489.4	31.06	missense	YES	Benign/1 1996	1
SNV	DAXX	DAXX:intronic:NM_001141970.1	98.87	unknown	YES	0 265	3
INDEL	NOTCH1	NOTCH1:exonic:NM_017617.4	24.69	frameshiftInsertion		0 0 1985	1
INDEL	ARID2	ARID2:intronic:NM_152641.3	2.25, 5.29	unknown		0 0 1380	4,1,3,1,1
SNV	ARID1A	ARID1A:exonic:NM_006015.5	5.46	missense		0 0 1996	2
INDEL	ARID2	ARID2:intronic:NM_152641.3	5.35	unknown	YES	0 1852	2,2
INDEL	ARID2	ARID2:intronic:NM_152641.3	4.62	unknown		0 0 1408	3,1
INDEL	ATM	ATM:intronic:NM_000051.3	3.42	unknown		0 0 1989	0
SNV	ATRX	ATRX:intronic:NM_000489.4	2.53	unknown		1973	2
SNV	ARID1A	ARID1A:exonic:NM_006015.5	2.51	missense		0 0 1994	1

Table S3. Hotspot mutation of patient-derived organoids. (C) Sph18-22.

Type	Genes	Location	% Frequency	Variant Effect	UCSC Common SNPs	ClinVar Coverage	Homopolymer Length
SNV	FLT3	FLT3:intronic:NM_004119.2	99.90	unknown	YES	0 1996	1
SNV	KDR	KDR:intronic:NM_002253.2	2.20,97.30	unknown, unknown	YES	0 2000	1,1
SNV	KDR	KDR:intronic:NM_002253.2	2.20, 97.30	unknown, unknown	YES	0 2000	1,1
INDEL	BAP1	BAP1:exonic:NM_004656.3	100.00	frameshiftDeletion		0 0 1959	1
SNV	MEN1	MEN1:intronic:NM_000244.3	1.07,89.08	unknown		0 0 1960	1,1,1
INDEL	KDR	KDR:intronic:NM_002253.2	59.82	unknown	YES	0 1991	2
SNV	ERBB4	ERBB4:intronic:NM_005235.2	50.98	unknown	YES	0 1997	1
SNV	KDR	KDR:exonic:NM_002253.2	50.55	missense	YES	not prov 1994	2
INDEL	DAXX	DAXX:exonic:NM_001141970.1	47.17, 3.92	nonframeshiftDeletion		0 0 1963	1,2
SNV	RNF43	RNF43:intronic:NM_017763.5	2.76, 46.36	unknown	YES	0 1991	1,1
SNV	KDR	KDR:intronic:NM_002253.2	48.82	unknown	YES	0 1999	2
SNV	ARID2	ARID2:exonic:NM_152641.3	48.72	missense		0 not prov 1995	1
SNV	RNF43	RNF43:exonic:NM_017763.5	47.92	missense	YES	Benign 1995	1
SNV	STK11	STK11:intronic:NM_000455.4	49.20	unknown	YES	0 1935	1
SNV	ARID2	ARID2:exonic:NM_152641.3	47.37	missense		0 0 1999	1
SNV	ARID2	ARID2:intronic:NM_152641.3	47.06	unknown	YES	0 1970	1
SNV	RNF43	RNF43:exonic:NM_017763.5	46.77	missense	YES	Benign 1997	1
SNV	ARID2	ARID2:intronic:NM_152641.3	46.30	unknown		0 0 2000	2
SNV	TP53	TP53:exonic:NM_000546.5	50.08	missense		0 Conflict 1999	1
SNV	DAXX	DAXX:intronic:NM_001141970.1	47.07	unknown	YES	0 1400	3
MNV	CSF1R,HMGXB3	CSF1R:utr_3:NM_005211.3, HMGXB3:downstream:NM_014983.2	26.23	unknown, unknown	YES	0 1994	1
SNV	MEN1	MEN1:intronic:NM_000244.3	25.29	unknown	YES	0 1997	1
INDEL	ARID2	ARID2:intronic:NM_152641.3	5.4	unknown	YES	0 1872	2,2
SNV	ARID1A	ARID1A:exonic:NM_006015.5	4.25	missense		0 0 1999	2

Table S3. Hotspot mutation of patient-derived organoids. (D) Sph18-29.

Type	Genes	Location	% Frequency	Variant Effect	UCSC Common SNPs	ClinVar Coverage	Homopolymer Length
SNV	TGFBR2	TGFBR2:intronic:NM_001024847.2	49.67	unknown	YES	Benign 1997	2
SNV	TGFBR2	TGFBR2:intronic:NM_001024847.2	49.65	unknown	YES	Benign 1994	1
SNV	CTNNB1	CTNNB1:exonic:NM_001904.3	49.3	missense		Pathogenic 2000	1,1,1
SNV	PIK3CA	PIK3CA:exonic:NM_006218.3	47.72	missense		Pathogenic 1953	1,1
SNV	KDR	KDR:intronic:NM_002253.3	46.43	unknown	YES	1975	1
SNV	FBXW7	FBXW7:exonic:NM_033632.3	48.27	missense		Likely pathogenic 1999	1,1,1,1
MNV	CSF1R,HMGXB3	CSF1R:utr_3:NM_005211.3, HMGXB3:downstream:NM_014983.2	99.60	unknown, unknown	YES	1978	1
SNV	DAXX	DAXX:intronic:NM_001141970.1	43.76	unknown	YES	1138	3
SNV	MEN1	MEN1:intronic:NM_000244.3	99.90	unknown	YES	1994	1
SNV	ARID2	ARID2:intronic:NM_152641.3	99.80	unknown	YES	1954	1
INDEL	ARID2	ARID2:intronic:NM_152641.3	5.93	unknown	YES	1888	2
SNV	FLT3	FLT3:intronic:NM_004119.2	51.38	unknown	YES	1997	1
SNV	RNF43	RNF43:intronic:NM_017763.5	100.00	unknown	YES	Benign 1995	1
SNV	SMAD4	SMAD4:exonic:NM_005359.5	99.75	missense		1993	3
SNV	ATRX	ATRX:intronic:NM_000489.5	4.95	unknown		1980	2
SNV	ATRX	ATRX:intronic:NM_000489.5	65.30	unknown	YES	2000	1
SNV	ATRX	ATRX:exonic:NM_000489.5	68.19	missense	YES	Benign 1996	1
SNV	ATRX	ATRX:intronic:NM_000489.5	64.40	unknown	YES	632	4

Table S4. List of “Conserved Markers” in single cell RNA sequence analysis of Sph18-16. (A) B1 cluster.

pct.1, The percentage of cells where the feature is detected in the B1 cluster.

pct.2 : The percentage of cells where the feature is detected in the other clusters.

D1, D1-inhibited sample; Ctrl, DMSO-used sample.

	D1_p_val	D1_avg logFC	D1_pct.1	D1_pct.2	D1_p_val_ adj	Ctrl_p_val	Ctrl_avg logFC	Ctrl_pct.1	Ctrl_pct.2	Ctrl_p_val_ adj
GABRP	5.54E-177	0.7654	0.994	0.842	1.86E-172	3.05E-184	0.8822	0.996	0.837	1.02E-179
ANXA2	2.01E-149	0.5579	1	0.962	6.76E-145	1.20E-141	0.5785	1	0.97	4.03E-137
LAMC2	9.09E-153	0.6235	0.811	0.356	3.05E-148	4.00E-139	0.6833	0.796	0.351	1.34E-134
CALB1	5.31E-163	0.8372	0.902	0.419	1.78E-158	1.17E-126	0.6731	0.878	0.408	3.94E-122
PMEPA1	1.33E-123	0.7943	0.956	0.717	4.48E-119	1.73E-180	1.0306	0.982	0.674	5.79E-176
KRT7	1.48E-142	0.6670	1	0.928	4.95E-138	1.26E-117	0.6696	0.996	0.932	4.23E-113
PLAU	8.09E-149	0.8763	0.805	0.36	2.71E-144	6.75E-117	0.8204	0.747	0.323	2.26E-112
OCIAD2	1.56E-139	0.6081	0.998	0.924	5.23E-135	8.57E-117	0.5731	0.998	0.936	2.88E-112
CD59	1.50E-121	0.5751	0.986	0.853	5.04E-117	4.43E-112	0.6004	0.993	0.84	1.49E-107
ANXA1	8.69E-137	0.6372	0.959	0.572	2.91E-132	1.08E-106	0.5815	0.935	0.555	3.62E-102
TMSB10	3.46E-92	0.3472	1	0.975	1.16E-87	4.74E-95	0.3783	1	0.983	1.59E-90
CXCL8	5.74E-92	0.5635	0.583	0.231	1.93E-87	6.12E-130	0.7411	0.729	0.28	2.05E-125
CD9	6.93E-92	0.4502	0.982	0.798	2.32E-87	1.86E-93	0.5304	0.976	0.768	6.25E-89
ITGB1	1.57E-100	0.4295	0.998	0.886	5.27E-96	2.55E-91	0.4706	0.991	0.883	8.56E-87
IL32	3.19E-89	0.5245	0.968	0.761	1.07E-84	1.07E-126	0.6848	0.987	0.776	3.60E-122
ITGB8	1.72E-89	0.2545	0.505	0.167	5.78E-85	4.30E-87	0.3445	0.536	0.19	1.44E-82
WWTR1	2.02E-90	0.3708	0.719	0.349	6.76E-86	2.02E-82	0.3978	0.729	0.369	6.77E-78
DKK1	2.29E-82	0.5152	0.707	0.361	7.69E-78	1.34E-106	0.7095	0.775	0.384	4.51E-102
CDH6	1.32E-85	0.2934	0.439	0.137	4.43E-81	1.06E-79	0.3149	0.431	0.134	3.54E-75
FTL	1.46E-78	-0.5713	0.997	0.943	4.88E-74	1.09E-88	-0.6668	0.998	0.958	3.65E-84
TACSTD2	3.42E-77	0.3844	0.811	0.467	1.15E-72	2.13E-80	0.4367	0.835	0.481	7.14E-76
DCBLD2	1.57E-76	0.4086	0.992	0.898	5.27E-72	6.49E-91	0.4854	0.993	0.887	2.18E-86
CCND1	1.57E-75	0.4330	0.989	0.866	5.27E-71	7.37E-86	0.5138	0.995	0.875	2.47E-81
SYNGR2	7.45E-74	0.3723	0.957	0.784	2.50E-69	2.33E-74	0.4116	0.947	0.776	7.82E-70
CAV1	2.26E-81	0.5021	0.988	0.809	7.58E-77	5.99E-69	0.4929	0.971	0.779	2.01E-64
NFE2L3	3.83E-68	0.2790	0.525	0.224	1.29E-63	4.41E-85	0.3658	0.636	0.277	1.48E-80
HMGA1	3.66E-94	0.4704	0.997	0.912	1.23E-89	4.68E-68	0.4494	0.993	0.915	1.57E-63
CFLAR	3.30E-91	0.4130	0.876	0.56	1.11E-86	1.07E-65	0.3872	0.822	0.54	3.60E-61
KRT6A	8.20E-100	0.6924	0.502	0.166	2.75E-95	3.18E-65	0.4079	0.378	0.121	1.07E-60
ETS1	2.95E-64	0.2763	0.472	0.193	9.89E-60	5.32E-77	0.2797	0.509	0.188	1.78E-72
STAP2	3.95E-64	0.3277	0.781	0.485	1.33E-59	9.65E-74	0.3920	0.804	0.486	3.24E-69
EDN1	1.00E-63	0.4051	0.531	0.238	3.36E-59	6.36E-93	0.5532	0.616	0.25	2.13E-88
CITED4	1.02E-63	0.2637	0.497	0.208	3.41E-59	7.13E-105	0.3911	0.598	0.214	2.39E-100
PLK2	1.95E-68	0.2888	0.729	0.405	6.55E-64	3.27E-62	0.3527	0.689	0.387	1.10E-57
F3	2.51E-95	0.7076	0.822	0.493	8.42E-91	2.48E-61	0.5324	0.74	0.435	8.33E-57
ITGA2	6.60E-61	0.3427	0.96	0.819	2.21E-56	4.27E-72	0.4647	0.973	0.803	1.43E-67
ARL6IP1	4.43E-60	-0.5885	0.837	0.855	1.49E-55	4.78E-61	-0.6331	0.802	0.86	1.60E-56
CAV2	4.83E-60	0.3389	0.963	0.793	1.62E-55	4.78E-61	0.3684	0.945	0.787	1.60E-56
AKAP12	2.03E-100	0.9467	0.649	0.28	6.82E-96	2.78E-57	0.7086	0.449	0.183	9.31E-53
ANXA3	6.32E-81	0.4246	0.862	0.554	2.12E-76	1.24E-56	0.3874	0.773	0.512	4.17E-52
MAP1B	1.74E-56	0.3530	0.515	0.236	5.83E-52	1.43E-126	0.6302	0.675	0.246	4.80E-122
FERMT1	1.56E-54	0.3491	0.929	0.727	5.24E-50	1.27E-71	0.4712	0.916	0.683	4.26E-67
EFHD2	1.25E-75	0.3984	0.936	0.74	4.20E-71	3.95E-54	0.3681	0.924	0.734	1.32E-49
MYL6	4.81E-104	0.4939	1	0.939	1.61E-99	8.95E-54	0.3546	1	0.95	3.00E-49
SAV1	2.42E-53	0.3575	0.853	0.626	8.12E-49	9.56E-55	0.3810	0.853	0.617	3.20E-50
LGALS4	9.02E-51	-0.5912	0.903	0.883	3.03E-46	5.97E-52	-0.6193	0.924	0.906	2.00E-47
FAM3C	1.48E-50	0.2930	0.98	0.833	4.95E-46	1.35E-71	0.4162	0.971	0.832	4.52E-67
TRIM29	3.56E-80	0.3451	0.664	0.319	1.20E-75	3.69E-49	0.3206	0.585	0.31	1.24E-44
IQGAP2	1.15E-50	-0.3976	0.212	0.512	3.85E-46	5.25E-49	-0.4311	0.256	0.566	1.76E-44
MET	3.71E-54	0.2933	0.877	0.643	1.24E-49	1.20E-47	0.2924	0.842	0.621	4.04E-43
VAMP8	8.21E-73	0.3842	0.985	0.876	2.75E-68	1.92E-47	0.3230	0.989	0.882	6.43E-43

CD63	2.22E-47	0.2823	1	0.924	7.45E-43	3.15E-66	0.3334	1	0.938	1.06E-61
ITGB4	1.95E-52	0.3290	0.977	0.846	6.53E-48	2.85E-47	0.3512	0.949	0.765	9.57E-43
SLC7A11	3.67E-47	0.2838	0.767	0.518	1.23E-42	2.61E-49	0.2755	0.771	0.501	8.76E-45
TNFRSF12A	3.73E-52	0.3179	0.988	0.848	1.25E-47	4.42E-47	0.3332	0.987	0.806	1.48E-42
TMSB4X	2.26E-46	0.2826	0.998	0.958	7.57E-42	1.68E-95	0.4418	1	0.974	5.63E-91
RRM2	5.54E-50	-0.7165	0.055	0.335	1.86E-45	9.13E-46	-0.7494	0.058	0.348	3.06E-41
FEZ2	1.72E-53	0.2541	0.799	0.528	5.76E-49	2.07E-45	0.2664	0.749	0.518	6.94E-41
TINAGL1	1.02E-51	0.2977	0.865	0.639	3.43E-47	6.30E-45	0.2990	0.813	0.563	2.11E-40
PPP1R14B	3.49E-66	0.3209	1	0.905	1.17E-61	1.73E-44	0.2839	0.996	0.91	5.82E-40
FLNA	6.35E-44	0.2815	0.813	0.558	2.13E-39	1.13E-45	0.2883	0.764	0.508	3.78E-41
SH3BGRL3	1.51E-43	0.2999	0.995	0.903	5.08E-39	1.19E-46	0.3522	0.993	0.91	3.99E-42
CXCL5	2.79E-43	0.5158	0.883	0.726	9.36E-39	7.15E-87	0.6711	0.96	0.778	2.40E-82
TSPAN1	1.47E-65	0.3939	0.837	0.55	4.92E-61	3.43E-43	0.3361	0.742	0.487	1.15E-38
KRT19	6.39E-79	0.3593	0.998	0.954	2.14E-74	3.79E-43	0.2917	0.996	0.954	1.27E-38
UCA1	9.51E-52	0.3529	0.995	0.881	3.19E-47	2.18E-42	0.3347	0.985	0.857	7.32E-38
PCLAF	3.97E-42	-0.6880	0.235	0.474	1.33E-37	4.52E-45	-0.7619	0.245	0.507	1.52E-40
PLAT	2.05E-50	0.3795	0.988	0.924	6.86E-46	5.84E-42	0.3917	0.989	0.905	1.96E-37
CYSTM1	4.51E-44	-0.4921	0.968	0.912	1.51E-39	6.22E-42	-0.5073	0.965	0.925	2.08E-37
GIPC1	8.66E-51	0.2915	0.865	0.671	2.90E-46	1.17E-41	0.2740	0.845	0.628	3.91E-37
COL17A1	3.56E-41	0.2642	0.891	0.672	1.19E-36	2.66E-44	0.2728	0.885	0.625	8.92E-40
TNIP1	7.40E-41	0.2705	0.664	0.426	2.48E-36	8.05E-47	0.3073	0.729	0.465	2.70E-42
HS3ST1	5.44E-50	0.3007	0.957	0.778	1.83E-45	6.57E-40	0.2936	0.935	0.787	2.20E-35
MKI67	1.07E-39	-0.4911	0.067	0.307	3.57E-35	4.01E-48	-0.5671	0.04	0.342	1.34E-43
CDK1	4.69E-39	-0.4241	0.067	0.303	1.57E-34	4.20E-41	-0.4597	0.058	0.329	1.41E-36
CAPG	7.76E-42	0.2905	0.83	0.607	2.60E-37	5.89E-39	0.2781	0.849	0.627	1.97E-34
MYBL2	3.22E-38	-0.3184	0.06	0.294	1.08E-33	1.01E-39	-0.3280	0.038	0.303	3.38E-35
TM4SF1	1.34E-37	0.3049	0.991	0.88	4.49E-33	5.31E-56	0.3939	0.987	0.876	1.78E-51
LINC02300	1.83E-42	0.3173	0.643	0.382	6.14E-38	2.53E-37	0.3106	0.622	0.37	8.49E-33
MDK	2.58E-36	-0.5142	0.79	0.815	8.66E-32	2.73E-36	-0.5438	0.782	0.841	9.14E-32
TOP2A	4.18E-36	-0.4023	0.061	0.286	1.40E-31	2.49E-38	-0.4943	0.073	0.333	8.35E-34
LRRC8A	8.64E-101	0.5154	0.83	0.505	2.90E-96	5.00E-36	0.2646	0.66	0.427	1.68E-31
NUSAP1	5.03E-36	-0.3666	0.071	0.299	1.69E-31	1.36E-36	-0.4060	0.069	0.321	4.57E-32
LCN2	1.12E-35	0.4210	0.969	0.868	3.76E-31	6.71E-68	0.6685	0.995	0.913	2.25E-63
BIRC5	1.30E-35	-0.4690	0.1	0.324	4.37E-31	6.54E-46	-0.5752	0.073	0.371	2.19E-41
BPIFB1	2.22E-35	-0.4451	0.206	0.467	7.44E-31	9.42E-41	-0.6063	0.202	0.49	3.16E-36
BZW2	1.77E-56	0.2908	0.922	0.703	5.94E-52	3.23E-35	0.2540	0.893	0.714	1.08E-30
SLC40A1	2.42E-49	-0.5494	0.319	0.586	8.13E-45	3.57E-35	-0.4685	0.362	0.606	1.20E-30
SFTA2	1.22E-47	0.2646	0.647	0.377	4.09E-43	6.76E-34	0.2674	0.627	0.397	2.27E-29
ISG20	5.14E-69	0.4461	0.972	0.799	1.72E-64	2.47E-33	0.2908	0.955	0.801	8.29E-29
CENPN	3.39E-33	-0.2941	0.155	0.376	1.14E-28	9.22E-35	-0.3153	0.145	0.399	3.09E-30
TYMS	4.24E-33	-0.4215	0.144	0.367	1.42E-28	6.65E-35	-0.4757	0.155	0.402	2.23E-30
RPA3	2.22E-35	-0.4631	0.824	0.805	7.45E-31	1.04E-32	-0.4690	0.827	0.827	3.50E-28
REG4	8.78E-32	-0.7364	0.061	0.266	2.94E-27	3.73E-32	-0.6865	0.044	0.271	1.25E-27
UBE2C	1.82E-31	-0.6464	0.115	0.318	6.09E-27	3.69E-39	-0.7184	0.078	0.341	1.24E-34
CDKN3	1.97E-31	-0.3703	0.146	0.357	6.62E-27	2.04E-32	-0.4638	0.149	0.382	6.84E-28
HMGB2	4.40E-31	-0.2573	0.071	0.277	1.47E-26	5.76E-39	-0.3119	0.049	0.313	1.93E-34
PHLDA2	3.02E-46	0.2886	0.988	0.885	1.01E-41	1.43E-30	0.2692	0.975	0.874	4.81E-26
RHOC	4.54E-61	0.3487	0.98	0.834	1.52E-56	2.25E-30	0.2503	0.958	0.829	7.53E-26
ASF1B	2.96E-30	-0.2612	0.092	0.299	9.94E-26	2.82E-31	-0.2598	0.073	0.304	9.47E-27
TK1	7.05E-34	-0.5693	0.298	0.498	2.36E-29	1.33E-29	-0.5880	0.304	0.494	4.48E-25
DHFR	2.46E-29	-0.4187	0.294	0.468	8.25E-25	4.76E-31	-0.4447	0.271	0.481	1.60E-26
MAD2L1	5.11E-29	-0.2888	0.16	0.361	1.71E-24	9.06E-33	-0.3422	0.147	0.389	3.04E-28
ZWINT	1.70E-28	-0.2880	0.19	0.391	5.69E-24	2.81E-32	-0.3255	0.162	0.399	9.43E-28
CENPF	2.18E-28	-0.2995	0.044	0.227	7.33E-24	3.44E-28	-0.3700	0.064	0.273	1.15E-23
FABP5	4.50E-28	-0.4118	0.577	0.677	1.51E-23	2.26E-31	-0.4174	0.56	0.711	7.59E-27
AGR2	5.97E-28	-0.3721	0.992	0.944	2.00E-23	1.17E-33	-0.4327	0.991	0.959	3.91E-29
OARD1	9.06E-28	-0.4612	0.713	0.761	3.04E-23	4.56E-34	-0.4815	0.724	0.788	1.53E-29
MACROD2	3.49E-34	-0.6299	0.207	0.434	1.17E-29	2.36E-27	-0.5144	0.255	0.476	7.90E-23
NEAT1	7.71E-31	-1.0827	0.824	0.878	2.59E-26	2.43E-27	-0.8715	0.825	0.882	8.14E-23
TIMP1	8.98E-27	0.2620	0.989	0.892	3.01E-22	4.45E-33	0.2528	0.993	0.904	1.49E-28
HMMR	2.60E-25	-0.3165	0.13	0.314	8.72E-21	7.48E-31	-0.4121	0.116	0.349	2.51E-26
LINC00326	5.48E-25	0.3009	0.334	0.17	1.84E-20	7.82E-64	0.5785	0.513	0.214	2.62E-59

SPRR3	3.48E-67	0.6005	0.822	0.536	1.17E-62	2.58E-24	0.3599	0.676	0.487	8.64E-20
SNRNP25	3.07E-24	-0.3103	0.413	0.549	1.03E-19	6.70E-34	-0.3654	0.336	0.557	2.25E-29
HIST1H1A	1.08E-24	-0.5230	0.106	0.279	3.62E-20	1.20E-23	-0.5911	0.111	0.298	4.03E-19
H2AFZ	1.42E-23	-0.4929	0.954	0.873	4.78E-19	9.82E-30	-0.5859	0.947	0.874	3.29E-25
CLSPN	3.53E-25	-0.2524	0.095	0.282	1.19E-20	2.19E-23	-0.2553	0.091	0.285	7.35E-19
TM4SF20	3.38E-23	-0.4817	0.026	0.177	1.13E-18	2.27E-29	-0.6991	0.022	0.225	7.62E-25
FXYD3	1.85E-31	-0.3954	0.905	0.882	6.20E-27	3.44E-23	-0.3875	0.933	0.895	1.16E-18
PTTG1	4.14E-25	-0.5300	0.236	0.418	1.39E-20	1.09E-22	-0.6618	0.289	0.457	3.66E-18
FAM111B	3.05E-22	-0.3761	0.141	0.314	1.02E-17	7.01E-23	-0.3910	0.125	0.318	2.35E-18
UBE2T	3.70E-22	-0.4086	0.382	0.5	1.24E-17	2.75E-25	-0.4297	0.347	0.503	9.22E-21
STMN1	1.32E-23	-0.5961	0.414	0.522	4.44E-19	4.98E-22	-0.6318	0.475	0.558	1.67E-17
CCL20	2.36E-21	0.3823	0.853	0.699	7.91E-17	8.32E-71	0.8723	0.913	0.714	2.79E-66
SNRPD1	2.45E-21	-0.2915	0.948	0.874	8.22E-17	2.99E-25	-0.3189	0.922	0.889	1.00E-20
CEACAM5	5.43E-21	-0.4327	0.262	0.453	1.82E-16	4.02E-21	-0.4954	0.191	0.387	1.35E-16
HELLS	8.68E-20	-0.3479	0.213	0.376	2.91E-15	1.35E-20	-0.3456	0.204	0.388	4.54E-16
TPX2	1.02E-19	-0.3453	0.178	0.327	3.42E-15	1.83E-28	-0.4043	0.14	0.357	6.12E-24
SCD	9.76E-19	-0.4029	0.822	0.846	3.27E-14	4.01E-22	-0.4693	0.795	0.837	1.34E-17
NUCKS1	4.08E-20	-0.2951	0.923	0.859	1.37E-15	1.26E-18	-0.2640	0.907	0.88	4.23E-14
SMC4	1.61E-18	-0.2758	0.27	0.421	5.39E-14	1.75E-24	-0.3433	0.264	0.458	5.85E-20
CKS2	1.46E-18	-0.4699	0.658	0.685	4.91E-14	3.43E-18	-0.5400	0.684	0.704	1.15E-13
CCNB2	4.32E-18	-0.2584	0.092	0.236	1.45E-13	1.42E-24	-0.3525	0.095	0.291	4.76E-20
HMGB1	6.67E-18	-0.2754	0.995	0.932	2.24E-13	5.36E-20	-0.3115	0.991	0.946	1.80E-15
CISD3	8.93E-18	-0.3562	0.768	0.753	2.99E-13	1.42E-20	-0.3840	0.742	0.764	4.75E-16
ATAD2	1.29E-21	-0.2769	0.129	0.298	4.33E-17	1.17E-17	-0.2768	0.155	0.316	3.94E-13
TMC5	7.68E-19	-0.5106	0.768	0.817	2.58E-14	1.29E-17	-0.4917	0.76	0.798	4.33E-13
PSMB3	4.77E-17	-0.3653	0.989	0.907	1.60E-12	1.47E-17	-0.3789	0.987	0.919	4.95E-13
FAM111A	8.47E-18	-0.3071	0.31	0.447	2.84E-13	5.75E-17	-0.2830	0.309	0.457	1.93E-12
GINS2	1.21E-20	-0.3093	0.233	0.393	4.04E-16	5.96E-17	-0.3049	0.255	0.408	2.00E-12
CXCL1	6.28E-17	0.3050	0.288	0.161	2.11E-12	4.74E-33	0.3361	0.429	0.213	1.59E-28
ANLN	8.39E-17	-0.2607	0.16	0.304	2.81E-12	1.29E-25	-0.3100	0.115	0.322	4.32E-21
CENPV	1.07E-16	-0.2560	0.77	0.755	3.59E-12	2.64E-20	-0.2752	0.691	0.746	8.84E-16
TFF1	2.29E-20	-0.5982	0.5	0.62	7.67E-16	2.65E-16	-0.5616	0.489	0.606	8.88E-12
CCNB1	9.38E-17	-0.3533	0.107	0.243	3.15E-12	3.59E-16	-0.4452	0.151	0.298	1.21E-11
BRCA1	4.97E-19	-0.2723	0.206	0.365	1.67E-14	5.67E-16	-0.2687	0.222	0.381	1.90E-11
S100P	1.51E-15	-0.3179	0.916	0.886	5.05E-11	7.24E-22	-0.4268	0.905	0.886	2.43E-17
HIST1H4C	9.58E-16	-0.6517	0.725	0.701	3.21E-11	1.75E-15	-0.7146	0.789	0.754	5.87E-11
MIEN1	1.87E-15	-0.3187	0.817	0.797	6.26E-11	5.87E-30	-0.4293	0.773	0.816	1.97E-25
SIVA1	3.94E-15	-0.2915	0.834	0.777	1.32E-10	5.83E-16	-0.3041	0.831	0.785	1.96E-11
HIST1H1C	2.13E-14	-0.3975	0.357	0.477	7.15E-10	2.37E-20	-0.5130	0.411	0.548	7.94E-16
PRSS1	2.30E-17	-0.4509	0.198	0.355	7.71E-13	2.76E-14	-0.3666	0.147	0.3	9.26E-10
HMGN2	2.90E-14	-0.3335	0.755	0.732	9.73E-10	3.52E-26	-0.4308	0.68	0.75	1.18E-21
H2AFX	1.33E-13	-0.2927	0.276	0.384	4.45E-09	5.44E-22	-0.3483	0.213	0.391	1.82E-17
RPL23	6.94E-20	-0.4639	1	0.98	2.33E-15	1.38E-13	-0.4248	0.998	0.98	4.61E-09
ONECUT2	2.31E-16	-0.4912	0.367	0.501	7.76E-12	2.83E-13	-0.4525	0.404	0.53	9.49E-09
H1FO	3.31E-13	-0.3058	0.748	0.754	1.11E-08	4.13E-16	-0.3418	0.682	0.733	1.39E-11
ADD3	6.49E-21	-0.3484	0.479	0.601	2.18E-16	4.98E-13	-0.2671	0.54	0.633	1.67E-08
GDF15	5.53E-13	-0.3430	0.163	0.29	1.86E-08	1.56E-18	-0.4661	0.127	0.301	5.23E-14
TMPO	1.06E-12	-0.2715	0.48	0.558	3.56E-08	9.79E-15	-0.2644	0.475	0.589	3.28E-10
H2AFV	3.30E-12	-0.2601	0.871	0.796	1.11E-07	2.10E-14	-0.2840	0.86	0.806	7.05E-10
CENPM	1.33E-21	-0.3205	0.334	0.478	4.47E-17	3.50E-12	-0.2637	0.378	0.48	1.17E-07
UBE2S	5.11E-12	-0.5230	0.495	0.526	1.71E-07	7.53E-18	-0.5657	0.456	0.536	2.53E-13
PCNA	9.43E-12	-0.3563	0.549	0.583	3.16E-07	2.94E-11	-0.4020	0.564	0.594	9.86E-07
GOLM1	4.57E-11	-0.2939	0.511	0.578	1.53E-06	8.99E-19	-0.3630	0.42	0.567	3.01E-14
DUOXA2	9.14E-12	-0.3078	0.052	0.147	3.06E-07	3.00E-10	-0.2665	0.044	0.137	1.00E-05
ONECUT1	4.05E-10	-0.4003	0.363	0.461	1.36E-05	2.30E-16	-0.3411	0.333	0.5	7.71E-12
ELF3	5.16E-10	-0.3337	0.902	0.891	1.73E-05	5.53E-15	-0.3443	0.862	0.877	1.85E-10
TMEM106C	8.92E-10	-0.2512	0.629	0.619	2.99E-05	5.97E-11	-0.2806	0.613	0.623	2.00E-06
DUT	1.82E-09	-0.3175	0.704	0.678	6.10E-05	1.98E-13	-0.3652	0.665	0.675	6.63E-09
SPINK1	6.62E-16	-0.4115	0.109	0.243	2.22E-11	1.12E-08	-0.3793	0.147	0.251	0.0003772
ZNF292	9.33E-13	-0.4279	0.443	0.557	3.13E-08	2.54E-07	-0.3322	0.48	0.57	0.0085028
MALAT1	4.98E-09	-1.4141	0.983	0.976	0.000167	2.55E-07	-1.0552	0.995	0.986	0.0085677
PRSS2	8.46E-06	-0.3059	0.25	0.326	0.28372	4.09E-05	-0.2601	0.204	0.285	1

NDRG1	0.0006275	-0.2634	0.345	0.39	1	0.0023176	-0.2570	0.3	0.349	1
XIST	1.88E-08	-1.0340	0.617	0.664	0.000629	0.0031615	-0.6157	0.625	0.667	1
TFF2	0.0197976	-0.2882	0.218	0.257	1	0.0119886	-0.3126	0.164	0.209	1
TUBA1B	0.2321045	-0.2542	0.986	0.878	1	0.0052305	-0.3515	0.98	0.873	1
MT1X	0.0145654	-0.3076	0.38	0.419	1	0.4200794	-0.3156	0.462	0.418	1
ANKRD36C	0.8146921	-0.5764	0.601	0.571	1	0.0344428	-0.3949	0.636	0.562	1

Table S4. List of “Conserved Markers” in single cell RNA sequence analysis of Sph18-16. (B) B2 cluster.

pct.1, The percentage of cells where the feature is detected in the B2 cluster.

pct.2 : The percentage of cells where the feature is detected in the other clusters.

D1, D1-inhibited sample; Ctrl, DMSO-used sample.

	D1_p_val	D1_avg logFC	D1_pct.1	D1_pct.2	D1_p_val_ adj	Ctrl_p_val	Ctrl_avg logFC	Ctrl_pct.1	Ctrl_pct.2	Ctrl_p_val_ adj
ERO1A	2.42E-142	0.90294	0.981	0.808	8.12E-138	4.72E-141	1.04657	0.977	0.804	1.58E-136
TGM2	2.56E-129	1.05999	0.951	0.714	8.57E-125	3.99E-136	1.15388	0.959	0.714	1.34E-131
NDRG1	2.94E-131	0.81829	0.77	0.342	9.86E-127	1.84E-126	0.82141	0.767	0.312	6.16E-122
PGK1	2.40E-124	0.6461	1	0.926	8.04E-120	5.29E-120	0.70008	1	0.932	1.77E-115
APOL1	8.56E-140	0.95429	0.961	0.642	2.87E-135	1.65E-119	0.93684	0.934	0.666	5.53E-115
LINC01559	2.03E-116	0.70669	0.969	0.771	6.82E-112	1.44E-104	0.73346	0.961	0.75	4.85E-100
C4orf3	1.54E-103	0.63626	0.949	0.787	5.15E-99	3.17E-107	0.71281	0.954	0.794	1.06E-102
CIB1	4.12E-99	0.50745	0.998	0.929	1.38E-94	6.10E-100	0.55959	0.998	0.944	2.04E-95
PDZK1IP1	2.33E-132	0.94142	0.889	0.509	7.82E-128	5.31E-99	0.83445	0.916	0.616	1.78E-94
EGLN3	2.35E-113	0.72723	0.85	0.472	7.89E-109	5.59E-99	0.76114	0.806	0.432	1.87E-94
BNIP3L	4.56E-96	0.59728	0.918	0.702	1.53E-91	3.32E-96	0.641	0.925	0.714	1.12E-91
ANGPTL4	9.65E-117	0.66585	0.462	0.108	3.24E-112	9.37E-91	0.56463	0.363	0.077	3.14E-86
MT1X	2.98E-114	1.13899	0.772	0.375	9.99E-110	1.00E-88	1.14696	0.747	0.397	3.37E-84
P4HA1	1.74E-103	0.68977	0.92	0.685	5.84E-99	1.17E-88	0.72188	0.888	0.659	3.94E-84
PLAT	3.37E-86	0.59789	0.994	0.925	1.13E-81	8.86E-81	0.70016	0.989	0.907	2.97E-76
SLC16A3	1.39E-94	0.56293	0.873	0.58	4.66E-90	2.24E-79	0.60094	0.822	0.541	7.52E-75
PTPRR	5.31E-107	0.61403	0.774	0.401	1.78E-102	7.68E-79	0.58227	0.692	0.366	2.58E-74
AL133453.1	3.04E-78	0.59681	0.758	0.478	1.02E-73	2.40E-79	0.63702	0.767	0.466	8.04E-75
TPT1	3.25E-89	0.32841	1	0.971	1.09E-84	1.86E-77	0.31343	1	0.979	6.25E-73
RANBP1	1.09E-75	-0.7242	0.749	0.859	3.66E-71	4.23E-78	-0.811	0.678	0.86	1.42E-73
H2AFZ	5.62E-83	-0.8926	0.821	0.891	1.89E-78	1.30E-75	-0.9524	0.779	0.889	4.34E-71
CALB1	2.37E-113	0.87762	0.854	0.439	7.94E-109	6.45E-75	0.8873	0.751	0.427	2.16E-70
TUBA1B	1.03E-73	-1.0272	0.867	0.894	3.44E-69	6.60E-73	-1.161	0.811	0.888	2.21E-68
RAN	1.51E-72	-0.4868	0.943	0.92	5.08E-68	1.10E-72	-0.5437	0.934	0.932	3.68E-68
NME1	3.91E-71	-0.6161	0.63	0.835	1.31E-66	1.91E-75	-0.7137	0.557	0.823	6.39E-71
STMN1	5.86E-70	-0.8531	0.144	0.549	1.96E-65	3.97E-72	-0.9678	0.137	0.583	1.33E-67
DHRS3	1.78E-107	0.64111	0.93	0.689	5.95E-103	9.06E-70	0.57964	0.881	0.703	3.04E-65
CA9	3.06E-69	0.5111	0.614	0.283	1.03E-64	2.29E-71	0.54085	0.6	0.261	7.69E-67
SNRPD1	2.12E-72	-0.586	0.825	0.89	7.11E-68	7.38E-69	-0.6113	0.788	0.9	2.48E-64
ID1	2.79E-77	0.67789	0.881	0.659	9.36E-73	5.19E-66	0.7146	0.822	0.603	1.74E-61
MCM7	9.13E-60	-0.5958	0.201	0.57	3.06E-55	5.74E-65	-0.6522	0.13	0.56	1.92E-60
UCA1	1.13E-86	0.67853	0.984	0.885	3.80E-82	1.36E-59	0.60892	0.963	0.861	4.55E-55
B2M	4.62E-63	0.53456	0.998	0.949	1.55E-58	2.65E-59	0.58253	0.998	0.962	8.90E-55
CEACAM6	1.49E-66	0.43785	0.994	0.938	4.98E-62	8.91E-59	0.46032	1	0.944	2.99E-54
PCLAF	3.92E-58	-0.7971	0.111	0.48	1.31E-53	8.49E-58	-0.8595	0.112	0.512	2.85E-53
GAPDH	1.10E-64	0.33426	1	0.966	3.70E-60	1.52E-57	0.34147	1	0.974	5.11E-53
TSPO	1.31E-58	0.35494	0.988	0.912	4.39E-54	1.80E-57	0.40448	0.991	0.921	6.04E-53
CTSD	4.82E-75	0.67906	0.887	0.732	1.62E-70	2.80E-57	0.63169	0.87	0.74	9.40E-53
UBE2S	2.35E-64	-0.7654	0.17	0.561	7.89E-60	3.58E-57	-0.7896	0.164	0.557	1.20E-52
DCTPP1	7.06E-57	-0.4764	0.347	0.693	2.37E-52	4.77E-57	-0.5213	0.342	0.711	1.60E-52
ITGB1	2.12E-56	0.37526	0.982	0.892	7.12E-52	8.18E-57	0.44904	0.973	0.886	2.74E-52
TMEM123	2.63E-56	0.40838	0.961	0.874	8.83E-52	5.63E-59	0.47197	0.95	0.893	1.89E-54
TMPRSS4	1.79E-64	0.44251	0.934	0.808	6.00E-60	5.08E-56	0.42079	0.945	0.817	1.70E-51
ORC6	2.19E-56	-0.49	0.043	0.405	7.34E-52	2.49E-55	-0.4797	0.025	0.417	8.34E-51
CCNI	2.73E-54	0.40304	0.961	0.887	9.16E-50	3.93E-54	0.42393	0.968	0.888	1.32E-49
APOL2	5.02E-56	0.54975	0.717	0.466	1.68E-51	8.20E-54	0.54023	0.719	0.469	2.75E-49
ITGB4	2.26E-54	0.42668	0.949	0.853	7.58E-50	8.22E-54	0.49958	0.902	0.772	2.76E-49
C15orf48	3.01E-62	0.81178	0.786	0.503	1.01E-57	2.21E-53	0.88905	0.763	0.519	7.42E-49
SLC44A4	1.53E-73	0.49618	0.717	0.416	5.14E-69	2.64E-53	0.45314	0.689	0.441	8.87E-49
SEMA4B	6.10E-66	0.45325	0.717	0.448	2.05E-61	4.28E-53	0.51484	0.651	0.412	1.43E-48
CKS2	7.56E-53	-0.6577	0.4	0.713	2.54E-48	1.52E-53	-0.791	0.4	0.725	5.10E-49

GPRC5A	1.89E-58	0.49477	0.963	0.868	6.33E-54	7.66E-53	0.54414	0.936	0.846	2.57E-48
DSG2	1.22E-52	0.44786	0.867	0.76	4.08E-48	6.03E-57	0.5043	0.87	0.734	2.02E-52
CAST	1.83E-58	0.37234	0.959	0.88	6.14E-54	1.40E-52	0.3976	0.952	0.897	4.70E-48
HSP90AA1	1.17E-51	-0.472	0.992	0.965	3.92E-47	3.51E-52	-0.5165	0.989	0.972	1.18E-47
MUC1	1.69E-61	0.53747	0.809	0.583	5.67E-57	1.26E-51	0.54632	0.783	0.598	4.22E-47
CYCS	1.65E-51	-0.4441	0.854	0.902	5.53E-47	1.11E-52	-0.4775	0.82	0.907	3.74E-48
UBE2T	1.82E-51	-0.5429	0.175	0.519	6.09E-47	2.98E-55	-0.5775	0.119	0.518	1.00E-50
GIN52	2.18E-51	-0.4657	0.064	0.407	7.32E-47	4.15E-52	-0.5039	0.043	0.422	1.39E-47
FAM3D	6.19E-69	0.51796	0.912	0.734	2.07E-64	2.23E-51	0.50039	0.881	0.712	7.49E-47
NPM1	2.43E-50	-0.3313	0.998	0.95	8.15E-46	5.82E-56	-0.3721	0.986	0.963	1.95E-51
APP	2.49E-50	0.41065	0.943	0.86	8.33E-46	2.40E-52	0.40076	0.95	0.869	8.04E-48
DHRS9	4.22E-50	0.43288	0.887	0.722	1.41E-45	2.58E-65	0.5894	0.893	0.669	8.66E-61
HNRNPA2B1	9.52E-50	-0.413	0.936	0.941	3.19E-45	3.41E-58	-0.4844	0.927	0.949	1.14E-53
ALDOC	4.45E-54	0.40043	0.596	0.328	1.49E-49	1.08E-49	0.46654	0.591	0.329	3.61E-45
FABP5	1.82E-55	-0.5594	0.363	0.698	6.10E-51	1.09E-49	-0.526	0.377	0.722	3.67E-45
TSPAN1	3.63E-52	0.42618	0.784	0.565	1.22E-47	1.12E-49	0.51175	0.726	0.493	3.77E-45
LDHB	2.34E-49	-0.4665	0.887	0.891	7.84E-45	4.38E-61	-0.5353	0.836	0.91	1.47E-56
RPA3	5.68E-49	-0.5895	0.676	0.822	1.91E-44	4.85E-56	-0.6653	0.66	0.84	1.63E-51
SAT1	1.13E-50	0.31134	0.996	0.949	3.80E-46	5.80E-49	0.40134	0.993	0.957	1.95E-44
SLCO4A1	9.54E-54	0.50054	0.739	0.53	3.20E-49	9.86E-49	0.49378	0.728	0.517	3.31E-44
TUBB	6.12E-54	-0.696	0.669	0.811	2.05E-49	1.09E-48	-0.7516	0.596	0.79	3.64E-44
RNF128	4.74E-48	0.37115	0.727	0.512	1.59E-43	3.90E-60	0.49421	0.763	0.517	1.31E-55
SNRNP25	1.64E-47	-0.4279	0.24	0.564	5.48E-43	4.50E-49	-0.4552	0.189	0.564	1.51E-44
ITGA3	3.46E-60	0.41814	0.809	0.599	1.16E-55	5.06E-47	0.41961	0.737	0.54	1.70E-42
HK2	2.86E-76	0.5154	0.635	0.322	9.60E-72	7.66E-47	0.45083	0.546	0.296	2.57E-42
CENPN	9.57E-49	-0.3591	0.051	0.381	3.21E-44	8.18E-47	-0.3889	0.048	0.401	2.74E-42
DHFR	1.09E-50	-0.5129	0.136	0.48	3.66E-46	8.19E-47	-0.5268	0.126	0.488	2.75E-42
MCM4	2.74E-52	-0.444	0.094	0.453	9.20E-48	1.30E-46	-0.4321	0.084	0.453	4.36E-42
MAD2L1	2.34E-46	-0.357	0.047	0.367	7.85E-42	4.86E-52	-0.4413	0.023	0.394	1.63E-47
PKM	8.30E-47	0.30991	0.998	0.948	2.78E-42	2.46E-46	0.32234	0.998	0.96	8.24E-42
FEN1	3.94E-47	-0.3935	0.101	0.437	1.32E-42	3.95E-46	-0.4032	0.066	0.424	1.32E-41
ENO1	4.29E-46	0.35598	1	0.944	1.44E-41	1.10E-50	0.36804	0.995	0.961	3.70E-46
ELF3	3.75E-58	0.34859	0.967	0.884	1.26E-53	4.48E-46	0.36827	0.97	0.868	1.50E-41
CENPM	1.26E-50	-0.4439	0.136	0.495	4.23E-46	6.41E-46	-0.4626	0.137	0.497	2.15E-41
LIFR	1.44E-45	0.3687	0.622	0.396	4.84E-41	1.65E-49	0.48928	0.584	0.329	5.54E-45
AGTR1	1.55E-49	0.26699	0.296	0.092	5.19E-45	1.60E-45	0.32679	0.279	0.083	5.37E-41
MUC5B	2.49E-70	0.73058	0.52	0.214	8.34E-66	2.53E-45	0.59156	0.461	0.204	8.50E-41
BIRC5	2.80E-45	-0.5224	0.023	0.325	9.39E-41	2.80E-49	-0.635	0.014	0.369	9.38E-45
C1QBP	2.93E-45	-0.4414	0.786	0.866	9.84E-41	6.07E-47	-0.4782	0.726	0.872	2.04E-42
SPRR3	3.02E-45	0.62826	0.784	0.549	1.01E-40	4.37E-56	0.82236	0.744	0.486	1.47E-51
HMGB1	3.04E-45	-0.4493	0.955	0.938	1.02E-40	2.82E-45	-0.5056	0.966	0.949	9.47E-41
SNRPB	5.99E-47	-0.4078	0.864	0.897	2.01E-42	3.60E-45	-0.4304	0.852	0.901	1.21E-40
QSOX1	6.48E-45	0.3857	0.77	0.6	2.17E-40	6.72E-50	0.4566	0.731	0.541	2.25E-45
DTYMK	7.14E-45	-0.4215	0.23	0.552	2.39E-40	2.74E-48	-0.4914	0.183	0.542	9.17E-44
MUC16	3.53E-67	0.35775	0.433	0.152	1.18E-62	1.53E-44	0.30011	0.336	0.119	5.13E-40
LDHA	8.78E-55	0.37012	1	0.93	2.94E-50	1.57E-44	0.36287	0.995	0.944	5.26E-40
CLDN4	1.50E-60	0.47789	0.967	0.866	5.02E-56	1.91E-44	0.478	0.943	0.869	6.40E-40
HNRNPAB	8.15E-56	-0.5355	0.587	0.802	2.73E-51	2.11E-44	-0.5077	0.566	0.804	7.08E-40
ASPH	6.48E-44	0.3159	0.975	0.911	2.17E-39	1.08E-47	0.41668	0.954	0.898	3.63E-43
ZWINT	1.85E-46	-0.3622	0.072	0.398	6.21E-42	1.03E-43	-0.3851	0.062	0.402	3.47E-39
PA2G4	1.16E-46	-0.4466	0.741	0.847	3.90E-42	1.26E-43	-0.4503	0.719	0.856	4.24E-39
HSPE1	5.72E-53	-0.4859	0.788	0.874	1.92E-48	1.72E-43	-0.4642	0.799	0.886	5.76E-39
APRT	3.90E-47	-0.3642	0.945	0.911	1.31E-42	2.87E-43	-0.3592	0.947	0.923	9.61E-39
PIIF	1.42E-46	-0.372	0.201	0.549	4.77E-42	2.87E-43	-0.3613	0.169	0.538	9.62E-39
CD2AP	3.01E-43	0.36168	0.838	0.7	1.01E-38	4.19E-47	0.42324	0.886	0.725	1.41E-42
CHCHD2	5.45E-50	-0.2776	0.996	0.941	1.83E-45	3.37E-43	-0.2909	0.998	0.953	1.13E-38
CENPH	2.70E-43	-0.322	0.096	0.417	9.06E-39	3.69E-43	-0.3383	0.075	0.425	1.24E-38
TUFM	3.93E-43	-0.397	0.725	0.851	1.32E-38	1.15E-47	-0.4436	0.648	0.854	3.84E-43
MKI67	4.20E-43	-0.519	0.016	0.305	1.41E-38	1.59E-44	-0.5721	0.009	0.338	5.34E-40
CCT2	2.08E-44	-0.4252	0.819	0.877	6.98E-40	5.04E-43	-0.4442	0.797	0.882	1.69E-38
HLA-C	6.23E-59	0.44232	0.981	0.9	2.09E-54	5.76E-43	0.39422	0.975	0.916	1.93E-38
FTH1	2.66E-56	0.32569	1	0.975	8.91E-52	1.88E-42	0.32673	1	0.979	6.30E-38

UBE2C	2.36E-42	-0.6872	0.031	0.321	7.91E-38	7.29E-43	-0.7645	0.018	0.341	2.45E-38
SDC1	2.53E-42	0.47264	0.877	0.782	8.48E-38	1.90E-50	0.58846	0.879	0.8	6.38E-46
CDKN3	4.76E-42	-0.4119	0.058	0.36	1.60E-37	1.01E-42	-0.5134	0.053	0.385	3.40E-38
TK1	6.05E-42	-0.6476	0.211	0.502	2.03E-37	4.29E-47	-0.7495	0.16	0.502	1.44E-42
HELLS	3.62E-46	-0.4495	0.062	0.388	1.21E-41	6.51E-42	-0.4487	0.059	0.396	2.18E-37
GCNT3	4.05E-45	0.39543	0.801	0.631	1.36E-40	3.60E-41	0.43704	0.792	0.619	1.21E-36
RRM2	1.13E-43	-0.7218	0.033	0.329	3.79E-39	3.68E-41	-0.7487	0.03	0.344	1.24E-36
CHEK1	2.28E-43	-0.3266	0.088	0.407	7.66E-39	5.60E-41	-0.3441	0.096	0.439	1.88E-36
CENPW	5.80E-41	-0.3528	0.09	0.389	1.95E-36	1.56E-48	-0.452	0.064	0.428	5.24E-44
DNMT1	2.36E-41	-0.3897	0.244	0.56	7.93E-37	6.91E-41	-0.4102	0.196	0.549	2.32E-36
TXNIP	5.32E-50	0.31436	0.984	0.906	1.78E-45	9.44E-41	0.34992	0.97	0.898	3.17E-36
CENPX	1.08E-40	-0.5783	0.735	0.831	3.63E-36	3.92E-47	-0.6644	0.648	0.834	1.31E-42
LPP	1.63E-40	0.33233	0.869	0.778	5.46E-36	1.32E-56	0.47487	0.904	0.787	4.43E-52
EIF4A2	1.20E-56	0.4517	0.92	0.839	4.02E-52	2.13E-40	0.45677	0.877	0.818	7.16E-36
CDK1	2.36E-40	-0.4405	0.023	0.301	7.91E-36	3.26E-41	-0.4848	0.016	0.327	1.09E-36
MRPS16	1.20E-39	-0.3256	0.871	0.896	4.02E-35	1.19E-40	-0.3846	0.795	0.896	4.00E-36
ODC1	4.05E-48	-0.5169	0.312	0.631	1.36E-43	1.73E-39	-0.4269	0.263	0.608	5.80E-35
PDCD5	2.36E-39	-0.3893	0.587	0.795	7.91E-35	1.19E-40	-0.4235	0.55	0.788	3.99E-36
FAM111B	4.35E-41	-0.474	0.033	0.32	1.46E-36	4.44E-39	-0.5063	0.021	0.322	1.49E-34
TSPAN3	1.28E-43	0.33256	0.957	0.872	4.29E-39	1.06E-38	0.34922	0.952	0.879	3.57E-34
TPX2	1.10E-38	-0.3998	0.053	0.337	3.69E-34	1.83E-41	-0.466	0.039	0.361	6.13E-37
PTTG1	1.42E-38	-0.6125	0.123	0.425	4.76E-34	3.87E-41	-0.7817	0.132	0.465	1.30E-36
SDCBP2	1.48E-38	0.37492	0.708	0.503	4.96E-34	4.59E-50	0.51121	0.703	0.446	1.54E-45
PERP	4.75E-39	0.28796	0.973	0.903	1.59E-34	4.50E-38	0.30288	0.979	0.92	1.51E-33
CENPK	1.25E-38	-0.2948	0.049	0.334	4.18E-34	4.76E-38	-0.2966	0.039	0.352	1.60E-33
MYBL2	3.29E-41	-0.3459	0.014	0.292	1.10E-36	5.05E-38	-0.3491	0.009	0.3	1.69E-33
PCNA	5.28E-38	-0.5594	0.331	0.606	1.77E-33	1.07E-40	-0.6271	0.308	0.613	3.59E-36
EIF5A	1.95E-38	-0.3751	0.844	0.88	6.53E-34	6.64E-38	-0.4167	0.719	0.869	2.23E-33
GGCT	7.56E-38	-0.396	0.47	0.712	2.53E-33	6.92E-43	-0.4512	0.432	0.733	2.32E-38
NDUFB10	9.10E-38	-0.3171	0.934	0.918	3.05E-33	5.71E-39	-0.3469	0.913	0.93	1.91E-34
PTMA	3.31E-43	-0.3234	0.996	0.952	1.11E-38	1.22E-37	-0.3091	0.995	0.965	4.08E-33
ASF1B	8.81E-40	-0.3072	0.023	0.3	2.95E-35	2.09E-37	-0.3143	0.014	0.304	7.00E-33
H2AFX	8.66E-39	-0.3863	0.101	0.4	2.90E-34	3.36E-37	-0.4211	0.087	0.397	1.13E-32
BMP2	4.10E-37	0.31811	0.38	0.176	1.37E-32	6.00E-48	0.4454	0.441	0.192	2.01E-43
MRPL12	1.16E-37	-0.3982	0.657	0.8	3.90E-33	5.77E-37	-0.3981	0.598	0.806	1.94E-32
PPP1CB	2.83E-43	0.33508	0.926	0.847	9.49E-39	6.48E-37	0.32918	0.936	0.877	2.17E-32
CAMK2N1	6.57E-37	0.36119	0.934	0.851	2.21E-32	2.76E-38	0.37531	0.902	0.847	9.25E-34
MPZL2	8.60E-37	0.3354	0.595	0.414	2.89E-32	4.90E-38	0.3893	0.614	0.433	1.64E-33
TUBA1C	1.38E-46	-0.5592	0.828	0.878	4.62E-42	1.28E-36	-0.5386	0.822	0.883	4.30E-32
KPNA2	1.41E-36	-0.499	0.218	0.512	4.73E-32	1.34E-44	-0.6275	0.169	0.52	4.51E-40
BRCA1	1.59E-36	-0.3468	0.09	0.373	5.32E-32	3.38E-42	-0.4087	0.057	0.39	1.13E-37
TOP2A	1.89E-37	-0.4207	0.021	0.283	6.35E-33	2.27E-36	-0.4897	0.037	0.331	7.60E-32
CLSPN	2.99E-38	-0.3064	0.018	0.285	1.00E-33	3.27E-36	-0.3223	0.007	0.287	1.10E-31
EEF1B2	4.21E-36	-0.2584	0.982	0.938	1.41E-31	3.46E-38	-0.2889	0.979	0.955	1.16E-33
MMEL1	2.78E-47	0.37968	0.468	0.226	9.31E-43	7.36E-36	0.39198	0.436	0.22	2.47E-31
ALCAM	1.51E-51	0.414	0.893	0.786	5.07E-47	1.07E-35	0.36977	0.877	0.81	3.59E-31
SLC14A1	1.35E-35	0.3633	0.756	0.582	4.54E-31	1.62E-36	0.50541	0.694	0.513	5.42E-32
PSMB3	1.58E-35	-0.4944	0.943	0.915	5.31E-31	1.07E-37	-0.5393	0.932	0.924	3.59E-33
CD24	6.84E-41	0.28779	0.998	0.947	2.29E-36	1.59E-35	0.29399	0.998	0.959	5.34E-31
PLOD2	1.65E-35	0.4476	0.47	0.267	5.54E-31	1.72E-48	0.56949	0.537	0.277	5.75E-44
DNAJC9	2.35E-54	-0.4887	0.253	0.613	7.88E-50	1.97E-35	-0.4243	0.295	0.598	6.62E-31
EBNA1BP2	2.33E-46	-0.401	0.327	0.659	7.80E-42	2.57E-35	-0.3628	0.333	0.645	8.61E-31
H2AFV	8.28E-42	-0.4667	0.669	0.821	2.78E-37	3.12E-35	-0.455	0.655	0.823	1.05E-30
TIMP2	3.62E-35	0.39707	0.813	0.725	1.21E-30	9.78E-43	0.48329	0.806	0.663	3.28E-38
TYMS	3.92E-35	-0.4544	0.097	0.365	1.32E-30	1.91E-38	-0.5063	0.087	0.402	6.41E-34
MIR210HG	2.49E-41	0.34547	0.649	0.427	8.35E-37	4.51E-35	0.39318	0.616	0.403	1.51E-30
CDH1	7.73E-37	0.32656	0.895	0.817	2.59E-32	4.86E-35	0.3507	0.87	0.813	1.63E-30
PRSS8	1.30E-34	0.43718	0.499	0.308	4.38E-30	2.36E-46	0.47756	0.521	0.281	7.91E-42
RFC2	1.59E-34	-0.2993	0.14	0.428	5.34E-30	1.58E-34	-0.3192	0.105	0.418	5.28E-30
ERH	1.81E-34	-0.3288	0.811	0.871	6.06E-30	1.22E-35	-0.355	0.783	0.882	4.08E-31
FAM3C	6.26E-49	0.40107	0.94	0.842	2.10E-44	2.02E-34	0.35018	0.925	0.839	6.78E-30
GPI	2.23E-37	0.37346	0.817	0.697	7.48E-33	3.50E-34	0.41588	0.804	0.696	1.17E-29

MRPS34	1.33E-34	-0.3377	0.823	0.873	4.47E-30	5.49E-34	-0.3486	0.783	0.89	1.84E-29
CDA	3.00E-35	0.36393	0.466	0.258	1.01E-30	6.08E-34	0.40664	0.45	0.238	2.04E-29
POLR3K	7.91E-34	-0.3136	0.214	0.506	2.65E-29	8.90E-35	-0.3126	0.169	0.487	2.98E-30
DKC1	8.62E-34	-0.3516	0.45	0.704	2.89E-29	2.17E-43	-0.43	0.345	0.69	7.26E-39
CAV1	3.96E-47	0.47683	0.943	0.819	1.33E-42	1.31E-33	0.44859	0.902	0.788	4.38E-29
NOP56	2.12E-33	-0.3788	0.466	0.727	7.12E-29	3.57E-34	-0.3905	0.422	0.727	1.20E-29
SERPINA1	1.37E-38	0.87418	0.526	0.301	4.61E-34	3.55E-33	0.91345	0.523	0.307	1.19E-28
FAM162A	3.87E-33	0.34228	0.86	0.778	1.30E-28	6.03E-53	0.48387	0.888	0.794	2.02E-48
CCT5	7.69E-37	-0.3828	0.71	0.828	2.58E-32	4.02E-33	-0.3781	0.646	0.829	1.35E-28
CDT1	9.11E-33	-0.2624	0.068	0.326	3.06E-28	3.17E-38	-0.2918	0.021	0.322	1.06E-33
ISG20	9.14E-39	0.41217	0.934	0.808	3.07E-34	1.35E-32	0.43635	0.881	0.81	4.51E-28
TMEM45B	1.81E-32	0.30568	0.899	0.815	6.07E-28	1.20E-42	0.39802	0.888	0.802	4.02E-38
TUBB4B	8.83E-38	-0.5835	0.899	0.89	2.96E-33	2.23E-32	-0.6463	0.852	0.879	7.49E-28
PGP	1.29E-47	-0.465	0.4	0.708	4.34E-43	2.24E-32	-0.3906	0.395	0.673	7.53E-28
KIF23	2.38E-32	-0.2523	0.006	0.231	7.98E-28	1.06E-33	-0.3052	0.005	0.268	3.55E-29
POLR2I	2.44E-32	-0.3252	0.487	0.73	8.17E-28	9.46E-37	-0.3674	0.434	0.74	3.17E-32
MRPS12	2.50E-32	-0.3202	0.487	0.735	8.38E-28	1.28E-33	-0.3536	0.441	0.726	4.30E-29
NUSAP1	3.51E-34	-0.3744	0.043	0.296	1.18E-29	2.52E-32	-0.3996	0.046	0.318	8.44E-28
CDC6	4.58E-35	-0.2561	0.043	0.306	1.54E-30	3.27E-32	-0.264	0.034	0.302	1.10E-27
PNRC1	2.43E-40	0.32375	0.809	0.655	8.16E-36	4.86E-32	0.32642	0.811	0.681	1.63E-27
SFPQ	7.06E-32	-0.3935	0.458	0.72	2.37E-27	3.03E-37	-0.4327	0.434	0.739	1.02E-32
GABRP	1.07E-37	0.31891	0.951	0.852	3.60E-33	1.41E-31	0.32584	0.945	0.844	4.72E-27
FAM129B	5.30E-33	0.34055	0.558	0.374	1.78E-28	1.44E-31	0.3309	0.546	0.351	4.84E-27
HLA-A	2.67E-38	0.43001	0.899	0.796	8.96E-34	1.51E-31	0.44385	0.89	0.809	5.08E-27
LYAR	7.07E-33	-0.3002	0.218	0.514	2.37E-28	1.94E-31	-0.2862	0.174	0.485	6.50E-27
TUBG1	4.86E-40	-0.345	0.166	0.483	1.63E-35	2.13E-31	-0.3152	0.153	0.458	7.14E-27
ATAD2	2.72E-34	-0.3363	0.045	0.302	9.14E-30	2.55E-31	-0.34	0.05	0.321	8.54E-27
RPS26	2.81E-31	-0.2918	0.942	0.918	9.44E-27	1.19E-33	-0.3161	0.936	0.925	3.98E-29
HMMR	4.27E-31	-0.3325	0.068	0.316	1.43E-26	2.20E-31	-0.4326	0.075	0.347	7.39E-27
TXN	3.19E-35	-0.2563	0.998	0.95	1.07E-30	7.56E-31	-0.2521	0.993	0.962	2.53E-26
SEC61G	3.25E-31	0.26666	0.994	0.919	1.09E-26	1.79E-30	0.28391	0.993	0.938	6.00E-26
PRKDC	2.11E-30	-0.4183	0.598	0.798	7.07E-26	5.85E-39	-0.487	0.541	0.794	1.96E-34
NDUFS6	2.88E-30	-0.3015	0.836	0.874	9.66E-26	2.48E-39	-0.3586	0.767	0.882	8.32E-35
CKS1B	3.26E-30	-0.3879	0.446	0.678	1.09E-25	3.44E-35	-0.4471	0.39	0.672	1.15E-30
HMGB2	3.60E-30	-0.2613	0.041	0.274	1.21E-25	4.44E-31	-0.3009	0.043	0.308	1.49E-26
C19orf48	3.93E-30	-0.2618	0.224	0.517	1.32E-25	1.16E-31	-0.2855	0.178	0.492	3.90E-27
INSIG2	4.16E-30	0.3029	0.637	0.489	1.40E-25	6.87E-40	0.41548	0.669	0.484	2.31E-35
FXSD3	3.79E-31	0.28259	0.963	0.876	1.27E-26	4.70E-30	0.34441	0.961	0.893	1.58E-25
CCNB2	4.88E-30	-0.3038	0.019	0.24	1.64E-25	5.08E-31	-0.3918	0.034	0.291	1.70E-26
PPIA	5.17E-30	-0.2802	0.996	0.949	1.73E-25	1.58E-37	-0.3187	0.995	0.959	5.30E-33
IGFBP6	6.24E-30	0.34581	0.951	0.838	2.09E-25	4.17E-32	0.48668	0.916	0.812	1.40E-27
CDK4	6.50E-30	-0.2821	0.275	0.559	2.18E-25	8.98E-34	-0.3089	0.24	0.575	3.01E-29
MRPL51	1.02E-29	-0.3208	0.784	0.853	3.41E-25	3.60E-35	-0.3655	0.737	0.866	1.21E-30
TM4SF4	1.07E-29	0.31487	0.967	0.883	3.59E-25	5.52E-31	0.37073	0.938	0.891	1.85E-26
SRM	8.11E-36	-0.3364	0.337	0.631	2.72E-31	1.12E-29	-0.3153	0.276	0.584	3.76E-25
ITGAE	1.06E-30	-0.2536	0.205	0.495	3.57E-26	1.24E-29	-0.2684	0.189	0.498	4.16E-25
ASS1	1.05E-53	0.58048	0.655	0.385	3.53E-49	1.28E-29	0.5868	0.587	0.408	4.31E-25
GPRC5C	8.95E-32	0.32349	0.671	0.511	3.00E-27	1.62E-29	0.34654	0.646	0.502	5.45E-25
SMC4	1.74E-29	-0.309	0.162	0.428	5.82E-25	4.03E-35	-0.3965	0.148	0.464	1.35E-30
LRP10	3.77E-33	0.28053	0.889	0.809	1.26E-28	3.49E-29	0.32844	0.856	0.798	1.17E-24
PHB	7.42E-30	-0.3003	0.838	0.882	2.49E-25	3.87E-29	-0.3185	0.811	0.882	1.30E-24
MCM6	7.10E-32	-0.255	0.088	0.35	2.38E-27	3.92E-29	-0.2736	0.08	0.351	1.32E-24
HNRNPM	5.33E-29	-0.33	0.481	0.735	1.79E-24	1.83E-32	-0.377	0.468	0.752	6.14E-28
S100P	6.31E-29	0.41099	0.955	0.883	2.12E-24	1.11E-30	0.42073	0.943	0.883	3.72E-26
SIVA1	7.51E-29	-0.3974	0.673	0.797	2.52E-24	1.37E-30	-0.4248	0.644	0.801	4.61E-26
CCT6A	8.94E-29	-0.3061	0.86	0.885	3.00E-24	6.34E-33	-0.3692	0.79	0.895	2.13E-28
LSM5	1.00E-28	-0.3051	0.836	0.874	3.37E-24	8.50E-31	-0.3368	0.808	0.882	2.85E-26
ANLN	4.99E-30	-0.3035	0.066	0.31	1.67E-25	1.83E-28	-0.3512	0.066	0.322	6.13E-24
ERBB3	5.23E-30	0.25062	0.68	0.515	1.75E-25	2.05E-28	0.25113	0.708	0.563	6.88E-24
RUVBL1	2.75E-33	-0.2898	0.261	0.569	9.21E-29	2.60E-28	-0.2774	0.26	0.56	8.71E-24
WDR45B	6.94E-39	0.33435	0.827	0.707	2.33E-34	3.10E-28	0.31608	0.769	0.679	1.04E-23
GCSH	2.20E-47	-0.396	0.302	0.636	7.36E-43	4.07E-28	-0.3398	0.372	0.634	1.36E-23

ATP5MC1	6.27E-28	-0.351	0.743	0.834	2.10E-23	3.18E-42	-0.4763	0.71	0.85	1.07E-37
NCL	7.39E-28	-0.3708	0.813	0.879	2.48E-23	8.83E-34	-0.4152	0.779	0.892	2.96E-29
HMG2	8.84E-28	-0.4239	0.567	0.754	2.96E-23	2.75E-28	-0.4448	0.562	0.758	9.22E-24
POLD2	3.34E-30	-0.3303	0.596	0.769	1.12E-25	1.08E-27	-0.3524	0.568	0.759	3.63E-23
C20orf27	1.31E-27	-0.2641	0.296	0.569	4.40E-23	1.47E-28	-0.2761	0.244	0.548	4.92E-24
COTL1	2.20E-33	-0.3198	0.333	0.629	7.37E-29	1.62E-27	-0.2897	0.29	0.584	5.43E-23
HIST1H1A	1.73E-27	-0.5336	0.062	0.279	5.80E-23	5.54E-28	-0.6109	0.055	0.298	1.86E-23
VAMP8	1.91E-28	0.28463	0.975	0.88	6.39E-24	2.97E-27	0.35694	0.947	0.887	9.95E-23
AL121761.2	3.40E-48	0.46082	0.749	0.569	1.14E-43	3.29E-27	0.34649	0.61	0.455	1.10E-22
PTBP3	2.93E-29	0.25966	0.885	0.809	9.82E-25	3.86E-27	0.28938	0.879	0.833	1.29E-22
FNDC3B	2.57E-34	0.26248	0.71	0.549	8.61E-30	4.26E-27	0.26668	0.703	0.565	1.43E-22
MRPL52	5.05E-27	-0.3114	0.717	0.836	1.69E-22	3.40E-35	-0.3847	0.694	0.848	1.14E-30
TNFSF10	5.15E-27	0.3352	0.442	0.258	1.73E-22	1.82E-31	0.44575	0.573	0.377	6.11E-27
ALYREF	1.44E-37	-0.4054	0.53	0.741	4.83E-33	6.18E-27	-0.3704	0.516	0.729	2.07E-22
CLSTN1	1.25E-32	0.30135	0.655	0.506	4.19E-28	7.08E-27	0.31852	0.637	0.499	2.38E-22
NUDT1	7.42E-27	-0.2716	0.312	0.583	2.49E-22	3.42E-35	-0.3387	0.251	0.577	1.15E-30
SLBP	4.77E-31	-0.3942	0.376	0.626	1.60E-26	1.53E-26	-0.3818	0.322	0.603	5.14E-22
WASF2	3.37E-30	0.28614	0.809	0.734	1.13E-25	1.67E-26	0.33098	0.781	0.71	5.59E-22
TACSTD2	3.90E-48	0.4745	0.71	0.488	1.31E-43	1.89E-26	0.44072	0.648	0.503	6.33E-22
CENPF	2.14E-26	-0.293	0.023	0.224	7.19E-22	6.51E-31	-0.3878	0.018	0.272	2.18E-26
PCBD1	2.98E-26	-0.2656	0.91	0.907	1.00E-21	8.63E-30	-0.3021	0.9	0.913	2.89E-25
ILF2	2.89E-33	-0.3207	0.38	0.657	9.68E-29	3.01E-26	-0.2902	0.374	0.661	1.01E-21
MCM3	2.71E-31	-0.2716	0.162	0.44	9.09E-27	3.14E-26	-0.2672	0.151	0.423	1.05E-21
SRSF7	1.01E-31	-0.3809	0.604	0.794	3.38E-27	6.75E-26	-0.3699	0.55	0.785	2.26E-21
SRSF3	7.88E-26	-0.3011	0.682	0.833	2.64E-21	2.45E-31	-0.3564	0.674	0.852	8.20E-27
CPM	8.58E-26	0.31889	0.489	0.314	2.88E-21	7.79E-36	0.43245	0.575	0.363	2.61E-31
LSM3	4.92E-30	-0.3456	0.647	0.802	1.65E-25	8.75E-26	-0.3196	0.646	0.808	2.93E-21
SAV1	6.50E-32	0.38908	0.76	0.643	2.18E-27	9.34E-26	0.39358	0.719	0.633	3.13E-21
TMEM59	1.19E-27	0.27567	0.869	0.799	3.98E-23	1.78E-25	0.3131	0.874	0.821	5.95E-21
SNRPE	2.89E-30	-0.319	0.62	0.799	9.69E-26	1.91E-25	-0.3112	0.619	0.812	6.39E-21
TMEM106C	1.96E-25	-0.3541	0.437	0.641	6.56E-21	8.29E-36	-0.4376	0.347	0.643	2.78E-31
PFN1	2.28E-25	-0.3115	0.984	0.92	7.63E-21	3.23E-32	-0.3923	0.952	0.932	1.08E-27
AGR2	7.64E-36	0.35325	1	0.945	2.56E-31	2.40E-25	0.31449	1	0.959	8.05E-21
CISD3	2.68E-25	-0.4301	0.637	0.768	8.98E-21	6.75E-33	-0.4813	0.555	0.778	2.26E-28
MAGOHB	2.52E-32	-0.2696	0.257	0.554	8.46E-28	2.97E-25	-0.2705	0.258	0.543	9.97E-21
AGRN	1.55E-32	0.28285	0.626	0.452	5.21E-28	3.33E-25	0.33012	0.568	0.421	1.12E-20
ACOT7	1.29E-29	-0.256	0.238	0.52	4.33E-25	3.39E-25	-0.2509	0.187	0.462	1.14E-20
NUDC	2.01E-34	-0.376	0.6	0.777	6.74E-30	4.23E-25	-0.3106	0.557	0.78	1.42E-20
PRSS1	4.42E-25	-0.5714	0.131	0.358	1.48E-20	3.96E-27	-0.6679	0.057	0.304	1.33E-22
ATP1B1	5.52E-41	0.34829	0.984	0.913	1.85E-36	4.53E-25	0.29459	0.989	0.935	1.52E-20
PSAT1	2.72E-37	-0.3666	0.129	0.429	9.11E-33	4.63E-25	-0.2721	0.144	0.407	1.55E-20
SSBP1	4.69E-25	-0.2683	0.881	0.895	1.57E-20	4.82E-26	-0.2936	0.888	0.914	1.62E-21
GSTO1	9.33E-25	-0.308	0.71	0.825	3.13E-20	1.93E-26	-0.3273	0.664	0.829	6.47E-22
NASP	1.81E-29	-0.3857	0.464	0.698	6.07E-25	9.72E-25	-0.3644	0.477	0.706	3.26E-20
CACYBP	2.72E-26	-0.2555	0.345	0.611	9.14E-22	2.49E-24	-0.3008	0.363	0.628	8.36E-20
CCNB1	2.53E-24	-0.3805	0.047	0.245	8.48E-20	2.80E-33	-0.5266	0.032	0.304	9.40E-29
SOX4	2.69E-24	0.26294	0.854	0.753	9.01E-20	6.31E-28	0.36187	0.868	0.769	2.12E-23
NAA10	2.79E-24	-0.2857	0.575	0.767	9.36E-20	1.89E-31	-0.3412	0.484	0.762	6.33E-27
TIMM13	2.96E-24	-0.2831	0.706	0.827	9.92E-20	3.54E-32	-0.3315	0.662	0.839	1.19E-27
ST3GAL4	2.62E-32	0.30665	0.388	0.199	8.80E-28	3.00E-24	0.2749	0.322	0.164	1.01E-19
TOMM40	4.53E-24	-0.2577	0.281	0.535	1.52E-19	1.56E-28	-0.2685	0.219	0.525	5.23E-24
CLDN3	1.27E-43	0.41989	0.723	0.54	4.27E-39	5.79E-24	0.36554	0.705	0.579	1.94E-19
PLS3	6.27E-24	0.27231	0.78	0.683	2.10E-19	1.05E-36	0.3987	0.785	0.667	3.54E-32
IARS	3.60E-31	-0.3299	0.281	0.577	1.21E-26	8.75E-24	-0.2761	0.272	0.561	2.93E-19
ST14	2.88E-39	0.35639	0.789	0.663	9.67E-35	1.05E-23	0.30916	0.742	0.654	3.53E-19
NDUFAF8	1.72E-23	-0.273	0.579	0.762	5.78E-19	4.86E-24	-0.3041	0.523	0.772	1.63E-19
NHP2	1.76E-23	-0.2746	0.733	0.831	5.92E-19	1.03E-36	-0.3745	0.646	0.83	3.45E-32
ENO2	3.43E-23	0.25678	0.398	0.233	1.15E-18	3.59E-23	0.29562	0.363	0.199	1.21E-18
CCT3	2.45E-36	-0.3712	0.7	0.84	8.22E-32	4.20E-23	-0.2925	0.646	0.839	1.41E-18
AHNAK	4.40E-23	0.26416	0.953	0.879	1.48E-18	1.47E-36	0.35198	0.952	0.854	4.93E-32
F3	8.24E-28	0.3896	0.7	0.517	2.76E-23	4.93E-23	0.5239	0.594	0.452	1.65E-18
HMG3	7.74E-23	-0.2597	0.261	0.505	2.60E-18	3.37E-25	-0.2876	0.242	0.525	1.13E-20

UBE2H	2.34E-30	0.27628	0.721	0.601	7.83E-26	9.36E-23	0.28966	0.674	0.586	3.14E-18
ITM2B	1.84E-22	0.26394	0.828	0.774	6.16E-18	4.51E-23	0.27915	0.872	0.821	1.51E-18
MTHFD2	1.46E-33	-0.4209	0.394	0.656	4.88E-29	2.07E-22	-0.3034	0.363	0.63	6.93E-18
BIK	2.14E-40	0.44084	0.842	0.708	7.17E-36	2.10E-22	0.34735	0.776	0.685	7.03E-18
SRSF2	2.00E-29	-0.3858	0.671	0.818	6.72E-25	2.39E-22	-0.3365	0.637	0.815	8.01E-18
PRSS2	9.26E-24	-0.9352	0.123	0.338	3.11E-19	2.72E-22	-0.8361	0.075	0.293	9.12E-18
BACE2	7.03E-27	0.27524	0.928	0.858	2.36E-22	2.86E-22	0.26157	0.916	0.868	9.59E-18
HSPD1	2.94E-22	-0.2896	0.906	0.905	9.87E-18	1.19E-36	-0.3694	0.872	0.92	3.98E-32
NDUFAB1	3.34E-22	-0.2569	0.809	0.869	1.12E-17	1.62E-22	-0.2809	0.779	0.883	5.44E-18
COMMD4	3.56E-22	-0.289	0.474	0.676	1.19E-17	8.44E-35	-0.3715	0.402	0.702	2.83E-30
CEMIP	1.49E-31	0.34624	0.657	0.501	4.98E-27	3.75E-22	0.38824	0.582	0.453	1.26E-17
CAPG	1.60E-29	0.33525	0.772	0.62	5.36E-25	4.19E-22	0.35111	0.728	0.641	1.40E-17
EFNA1	1.15E-25	0.34009	0.517	0.351	3.85E-21	4.44E-22	0.34453	0.505	0.357	1.49E-17
MUC5AC	9.34E-43	0.51258	0.359	0.144	3.13E-38	9.69E-22	0.44087	0.26	0.116	3.25E-17
WBP2	1.26E-21	0.27103	0.686	0.61	4.23E-17	9.88E-23	0.29165	0.674	0.578	3.31E-18
VPS13D	6.89E-25	0.26167	0.493	0.334	2.31E-20	1.27E-21	0.28856	0.477	0.325	4.26E-17
RBP1	1.36E-22	-0.5427	0.32	0.543	4.57E-18	1.99E-21	-0.4484	0.333	0.582	6.66E-17
DUT	1.54E-24	-0.4234	0.532	0.697	5.17E-20	2.17E-21	-0.4336	0.511	0.687	7.27E-17
CENPV	2.93E-23	-0.2993	0.606	0.774	9.84E-19	3.70E-21	-0.2925	0.578	0.754	1.24E-16
STOML2	6.90E-23	-0.2694	0.729	0.818	2.31E-18	6.60E-21	-0.2577	0.651	0.818	2.21E-16
HSD17B10	5.76E-27	-0.2928	0.493	0.725	1.93E-22	1.32E-20	-0.267	0.498	0.72	4.44E-16
SNRPD2	2.58E-20	-0.2586	0.813	0.877	8.65E-16	2.11E-26	-0.3063	0.797	0.893	7.07E-22
LSM4	2.80E-20	-0.2597	0.708	0.819	9.38E-16	2.26E-26	-0.3254	0.621	0.801	7.57E-22
PRR15	7.65E-31	0.32469	0.558	0.389	2.57E-26	3.11E-20	0.3116	0.527	0.405	1.04E-15
MRPL11	3.57E-20	-0.2528	0.731	0.825	1.20E-15	2.08E-26	-0.2963	0.658	0.831	6.97E-22
CHCHD10	3.82E-20	-0.2951	0.776	0.852	1.28E-15	3.23E-22	-0.3243	0.735	0.856	1.08E-17
FUT11	2.22E-27	0.26856	0.507	0.326	7.44E-23	5.90E-20	0.29232	0.425	0.276	1.98E-15
PSMC3	4.88E-23	-0.2583	0.444	0.659	1.64E-18	6.26E-20	-0.2585	0.425	0.662	2.10E-15
DEK	8.46E-20	-0.3138	0.725	0.819	2.84E-15	4.63E-21	-0.3236	0.728	0.834	1.55E-16
ARPC5L	4.30E-28	-0.2951	0.429	0.696	1.44E-23	8.81E-20	-0.2529	0.432	0.677	2.95E-15
ARFGAP3	2.14E-23	0.26146	0.616	0.49	7.17E-19	1.02E-19	0.27242	0.573	0.46	3.44E-15
METTTL26	1.60E-23	-0.2785	0.61	0.783	5.38E-19	1.27E-19	-0.2645	0.573	0.775	4.25E-15
LAPTM4A	7.88E-31	0.27451	0.887	0.826	2.64E-26	1.85E-19	0.26084	0.895	0.846	6.21E-15
TMPRSS2	7.53E-29	0.26702	0.454	0.27	2.52E-24	2.17E-19	0.30177	0.436	0.285	7.29E-15
ADK	6.73E-29	-0.3151	0.4	0.666	2.26E-24	2.56E-19	-0.2653	0.381	0.644	8.58E-15
BUB3	2.20E-24	-0.2976	0.435	0.663	7.37E-20	2.73E-19	-0.2628	0.427	0.664	9.15E-15
SFN	7.31E-30	-0.3318	0.366	0.631	2.45E-25	3.11E-19	-0.2716	0.361	0.601	1.04E-14
PRMT1	3.83E-21	-0.2644	0.647	0.787	1.28E-16	3.25E-19	-0.2534	0.591	0.777	1.09E-14
DCXR	6.76E-22	-0.299	0.745	0.831	2.27E-17	3.51E-19	-0.2672	0.68	0.816	1.18E-14
PAICS	2.21E-34	-0.3335	0.394	0.681	7.41E-30	5.22E-19	-0.2533	0.447	0.681	1.75E-14
RPL23	1.94E-21	-0.4337	0.994	0.981	6.50E-17	5.23E-19	-0.4372	0.998	0.98	1.76E-14
POLR2G	6.36E-19	-0.2539	0.579	0.753	2.13E-14	2.00E-27	-0.3148	0.521	0.761	6.69E-23
FGF19	2.37E-30	0.41181	0.947	0.883	7.96E-26	6.47E-19	0.43132	0.927	0.881	2.17E-14
PARP1	6.91E-19	-0.2659	0.495	0.689	2.32E-14	1.55E-22	-0.293	0.42	0.678	5.19E-18
CD109	3.18E-26	0.26915	0.606	0.464	1.07E-21	1.40E-18	0.25336	0.582	0.485	4.71E-14
CD99	5.26E-27	0.31104	0.721	0.6	1.76E-22	1.47E-18	0.27356	0.669	0.586	4.92E-14
SLC9A3R1	1.02E-25	0.26468	0.899	0.822	3.42E-21	2.04E-18	0.26028	0.833	0.813	6.83E-14
COL17A1	6.75E-18	0.25411	0.774	0.691	2.26E-13	1.72E-29	0.40703	0.763	0.64	5.77E-25
SUPT16H	1.68E-19	-0.2808	0.464	0.672	5.65E-15	9.90E-18	-0.2767	0.473	0.698	3.32E-13
SNRPG	6.05E-20	-0.2563	0.762	0.84	2.03E-15	1.05E-17	-0.2645	0.801	0.861	3.51E-13
TAPBP	1.02E-21	0.27768	0.655	0.54	3.42E-17	1.72E-17	0.28771	0.678	0.589	5.78E-13
COL6A1	7.17E-28	0.27283	0.48	0.301	2.41E-23	1.74E-17	0.27251	0.427	0.289	5.85E-13
S100A4	1.37E-34	0.39268	0.651	0.458	4.58E-30	2.39E-17	0.32253	0.573	0.459	8.00E-13
CCDC85B	3.62E-17	-0.2552	0.581	0.746	1.21E-12	2.02E-29	-0.3292	0.468	0.734	6.76E-25
TMPO	4.96E-17	-0.2827	0.374	0.567	1.66E-12	2.35E-17	-0.2871	0.37	0.595	7.87E-13
PSCA	3.71E-39	0.43413	0.3	0.108	1.24E-34	5.88E-17	0.38917	0.231	0.108	1.97E-12
HIST1H4C	2.51E-18	-0.6376	0.591	0.716	8.40E-14	2.04E-16	-0.7161	0.662	0.764	6.83E-12
CALD1	6.33E-17	-0.3773	0.727	0.826	2.12E-12	4.84E-16	-0.3134	0.721	0.845	1.62E-11
DDX46	4.95E-16	-0.3178	0.556	0.753	1.66E-11	5.36E-18	-0.3161	0.505	0.741	1.80E-13
ZKSCAN1	1.22E-25	0.27645	0.772	0.697	4.08E-21	5.60E-16	0.25062	0.731	0.699	1.88E-11
TMBIM1	8.20E-16	0.25824	0.61	0.54	2.75E-11	3.45E-19	0.33916	0.6	0.507	1.16E-14
TMCC1	4.10E-24	0.2639	0.515	0.37	1.38E-19	2.82E-15	0.25708	0.466	0.349	9.47E-11

IFITM3	5.15E-19	0.35313	0.567	0.438	1.73E-14	8.56E-15	0.33671	0.566	0.475	2.87E-10
SPP1	1.25E-14	0.52907	0.77	0.716	4.20E-10	6.26E-33	0.77777	0.868	0.803	2.10E-28
SEMA3B	4.37E-25	0.28781	0.548	0.39	1.46E-20	1.31E-14	0.27624	0.429	0.311	4.40E-10
CLDN2	1.50E-14	-0.3616	0.647	0.753	5.03E-10	5.36E-18	-0.374	0.639	0.798	1.80E-13
KRT13	8.62E-17	0.35277	0.172	0.071	2.89E-12	1.63E-14	0.26254	0.144	0.055	5.47E-10
FAM89B	4.43E-16	0.28004	0.499	0.403	1.49E-11	2.38E-14	0.25474	0.452	0.34	7.98E-10
RNASET2	2.66E-14	0.27867	0.657	0.577	8.91E-10	4.42E-16	0.37939	0.623	0.561	1.48E-11
FOSL2	4.08E-16	0.25007	0.452	0.33	1.37E-11	6.12E-14	0.2539	0.429	0.328	2.05E-09
SLC2A1	8.48E-19	0.27892	0.565	0.455	2.84E-14	1.23E-13	0.27885	0.495	0.398	4.13E-09
SLC3A2	7.33E-17	-0.3085	0.536	0.726	2.46E-12	7.15E-13	-0.2595	0.495	0.707	2.40E-08
REG4	2.28E-18	-0.5551	0.084	0.258	7.65E-14	8.99E-13	-0.4942	0.11	0.262	3.02E-08
IRF1	1.75E-17	0.27807	0.503	0.368	5.87E-13	1.02E-12	0.27646	0.489	0.399	3.43E-08
DNPH1	1.23E-12	-0.2695	0.789	0.829	4.13E-08	1.33E-18	-0.3206	0.751	0.849	4.47E-14
LGALS1	1.97E-22	0.35319	0.505	0.333	6.61E-18	1.65E-12	0.42115	0.495	0.393	5.53E-08
GLRX	6.81E-22	0.30164	0.591	0.454	2.29E-17	3.95E-12	0.26293	0.527	0.451	1.33E-07
TCN1	2.15E-35	0.61939	0.476	0.262	7.21E-31	4.08E-12	0.50164	0.457	0.344	1.37E-07
MRPS10	1.07E-12	-0.3409	0.694	0.79	3.60E-08	6.58E-12	-0.3574	0.658	0.794	2.21E-07
HIST1H1C	7.84E-12	-0.3507	0.31	0.478	2.63E-07	3.64E-21	-0.496	0.308	0.553	1.22E-16
TM4SF20	5.21E-15	-0.4463	0.039	0.171	1.75E-10	2.92E-11	-0.4794	0.082	0.216	9.79E-07
FA2H	6.89E-20	0.32686	0.493	0.368	2.31E-15	2.98E-11	0.26358	0.409	0.326	1.00E-06
TPM1	1.74E-24	-0.3823	0.951	0.955	5.85E-20	5.18E-11	-0.2626	0.97	0.96	1.74E-06
HLA-B	5.13E-20	0.37138	0.772	0.695	1.72E-15	6.88E-10	0.29678	0.751	0.73	2.31E-05
LINC02404	2.06E-10	-0.288	0.25	0.402	6.92E-06	6.28E-09	-0.2897	0.274	0.424	0.0002107
FUS	2.24E-14	-0.3509	0.608	0.78	7.51E-10	1.72E-08	-0.291	0.6	0.764	0.0005756
HNRNPH1	1.55E-05	-0.2749	0.692	0.786	0.518351	1.32E-09	-0.2773	0.696	0.812	4.41E-05
TFF3	8.11E-06	0.4623	0.168	0.109	0.271915	0.0015035	0.58994	0.16	0.117	1
NNMT	9.38E-12	0.37479	0.526	0.44	3.15E-07	0.0019961	0.25811	0.507	0.519	1
TFF2	3.56E-06	0.73493	0.312	0.246	0.119537	0.0374996	0.67121	0.226	0.203	1
TFF1	0.1185968	0.39635	0.573	0.609	1	0.3176377	0.76365	0.532	0.601	1
XIST	0.44526	-0.7988	0.635	0.661	1	0.0038458	-0.3035	0.683	0.662	1
CEACAM5	0.0458066	0.27108	0.349	0.438	1	0.8386167	0.43695	0.324	0.373	1

Table S4. List of “Conserved Markers” in single cell RNA sequence analysis of Sph18-16. (C)
INT1 cluster.

pct.1, The percentage of cells where the feature is detected in the INT1 cluster.

pct.2 : The percentage of cells where the feature is detected in the other clusters.

D1, D1-inhibited sample; Ctrl, DMSO-used sample.

	D1_p_val	D1_avg logFC	D1_pct.1	D1_pct.2	D1_p_val_ adj	Ctrl_p_val	Ctrl_avg logFC	Ctrl_pct.1	Ctrl_pct.2	Ctrl_p_val_ adj
LYZ	3.13E-72	0.5481	1	0.937	1.05E-67	3.68E-95	0.48555	0.997	0.956	1.23E-90
MT-ND3	9.88E-63	0.48947	0.993	0.931	3.31E-58	7.62E-84	0.4001	0.993	0.96	2.55E-79
LCN2	2.01E-61	0.78382	0.986	0.871	6.75E-57	6.38E-59	0.55682	0.989	0.911	2.14E-54
MT-ATP6	7.62E-57	0.51592	0.995	0.959	2.56E-52	1.74E-69	0.38572	0.999	0.974	5.83E-65
GPX2	1.60E-50	0.50504	0.972	0.841	5.38E-46	6.54E-67	0.43717	0.981	0.891	2.19E-62
MT-CO3	3.07E-50	0.43167	1	0.974	1.03E-45	1.40E-63	0.35954	0.999	0.985	4.70E-59
BACE2	2.37E-42	0.3248	0.947	0.857	7.95E-38	6.01E-46	0.27609	0.933	0.863	2.02E-41
MT-ND4	3.32E-42	0.35279	0.995	0.969	1.11E-37	7.89E-61	0.29102	0.999	0.981	2.65E-56
MT-CO1	4.07E-38	0.34185	1	0.982	1.37E-33	5.30E-53	0.28506	0.999	0.986	1.78E-48
MT-ND1	1.28E-35	0.34902	0.991	0.945	4.28E-31	1.92E-61	0.33344	0.993	0.965	6.45E-57
CLDN2	2.60E-35	0.51985	0.88	0.73	8.72E-31	7.99E-42	0.39616	0.913	0.769	2.68E-37
MT-ND5	3.91E-34	0.32211	0.993	0.946	1.31E-29	1.67E-62	0.31909	0.996	0.968	5.62E-58
VDAC2	5.68E-34	-0.3082	0.991	0.939	1.90E-29	1.77E-50	-0.313	0.974	0.945	5.94E-46
TST	9.74E-34	0.37564	0.677	0.479	3.27E-29	9.53E-41	0.317	0.674	0.511	3.19E-36
MT-CYB	5.17E-33	0.31685	0.998	0.966	1.74E-28	1.91E-48	0.29861	0.996	0.979	6.40E-44
RRM2	5.32E-33	-0.6878	0.051	0.322	1.78E-28	1.27E-64	-0.7725	0.05	0.359	4.25E-60
F3	1.87E-35	-0.6795	0.274	0.559	6.28E-31	3.84E-32	-0.45	0.266	0.489	1.29E-27
CDK1	1.04E-30	-0.4258	0.039	0.295	3.47E-26	1.64E-52	-0.4502	0.065	0.337	5.51E-48
S100A10	1.99E-30	-0.3181	0.988	0.947	6.67E-26	1.29E-36	-0.2714	0.996	0.951	4.32E-32
ACTB	5.53E-30	-0.2638	1	0.967	1.85E-25	1.67E-45	-0.2742	0.996	0.968	5.60E-41
UBE2C	8.66E-30	-0.6484	0.058	0.314	2.91E-25	7.32E-63	-0.7721	0.05	0.354	2.45E-58
SH3BGRL3	9.13E-30	-0.3851	0.956	0.911	3.06E-25	4.04E-38	-0.3825	0.943	0.914	1.36E-33
ANXA4	9.57E-30	0.32691	0.998	0.948	3.21E-25	3.34E-66	0.36158	0.999	0.952	1.12E-61
CTSD	5.16E-29	0.29972	0.887	0.735	1.73E-24	2.67E-32	0.27045	0.855	0.735	8.97E-28
MYBL2	1.53E-27	-0.3101	0.044	0.285	5.13E-23	7.54E-52	-0.3313	0.044	0.312	2.53E-47
CLDN10	1.76E-27	0.34391	0.521	0.315	5.90E-23	1.30E-30	0.31805	0.55	0.398	4.35E-26
NQO1	9.47E-27	0.3437	0.744	0.571	3.18E-22	2.03E-27	0.28063	0.742	0.624	6.81E-23
LGALS3BP	1.25E-26	0.27267	0.922	0.813	4.21E-22	1.88E-38	0.26835	0.918	0.828	6.31E-34
TUBA1B	2.34E-26	-0.6602	0.912	0.889	7.84E-22	2.41E-54	-0.7766	0.891	0.882	8.08E-50
CST3	1.46E-25	0.26972	0.991	0.913	4.90E-21	2.38E-32	0.25378	0.992	0.927	7.97E-28
C15orf48	2.41E-25	-0.902	0.325	0.55	8.07E-21	5.97E-41	-0.8384	0.33	0.565	2.00E-36
TUBB4B	2.53E-25	-0.5195	0.894	0.89	8.49E-21	4.25E-60	-0.674	0.829	0.884	1.43E-55
SOD1	5.93E-25	0.28641	0.982	0.899	1.99E-20	4.20E-36	0.28695	0.985	0.914	1.41E-31
MKI67	7.83E-25	-0.4553	0.069	0.296	2.63E-20	5.58E-55	-0.5358	0.064	0.349	1.87E-50
TESC	1.10E-24	0.30632	0.933	0.804	3.70E-20	3.06E-36	0.29745	0.936	0.829	1.03E-31
SLC12A2	2.43E-24	0.31207	0.965	0.883	8.15E-20	2.44E-31	0.28605	0.974	0.918	8.18E-27
TCN1	6.42E-24	0.45568	0.472	0.265	2.15E-19	6.87E-40	0.57475	0.543	0.325	2.30E-35
BIRC5	2.23E-23	-0.4267	0.092	0.314	7.48E-19	3.00E-50	-0.5352	0.105	0.377	1.01E-45
AGR2	3.79E-23	0.32954	0.998	0.946	1.27E-18	6.62E-52	0.39099	0.996	0.958	2.22E-47
ANLN	2.70E-22	-0.2914	0.085	0.304	9.06E-18	7.49E-48	-0.3761	0.074	0.335	2.51E-43
EGLN3	6.27E-22	-0.4353	0.297	0.529	2.10E-17	2.10E-25	-0.3971	0.285	0.483	7.03E-21
TNFRSF12A	3.05E-21	-0.3391	0.843	0.868	1.02E-16	1.50E-30	-0.3593	0.746	0.833	5.04E-26
SFN	3.45E-21	-0.3337	0.433	0.62	1.16E-16	1.27E-35	-0.3328	0.39	0.61	4.27E-31
NUSAP1	7.20E-21	-0.3331	0.081	0.288	2.42E-16	3.86E-52	-0.417	0.059	0.331	1.29E-47
UBE2T	8.62E-21	-0.4112	0.304	0.502	2.89E-16	6.04E-46	-0.4491	0.271	0.519	2.03E-41
ERO1A	9.92E-26	-0.6156	0.7	0.836	3.33E-21	9.82E-21	-0.5137	0.75	0.825	3.29E-16
TUBB	2.08E-20	-0.4697	0.763	0.8	6.98E-16	6.73E-65	-0.6779	0.666	0.792	2.26E-60
DHFR	5.05E-20	-0.3876	0.265	0.463	1.69E-15	4.76E-31	-0.3752	0.285	0.486	1.60E-26
TUBA1C	1.05E-19	-0.4097	0.887	0.872	3.51E-15	2.57E-45	-0.4792	0.859	0.881	8.63E-41
AC020656.1	1.44E-19	0.33625	0.806	0.682	4.82E-15	1.66E-30	0.29278	0.905	0.809	5.58E-26
SERPINB1	4.10E-19	-0.3441	0.952	0.907	1.38E-14	1.40E-23	-0.3213	0.932	0.906	4.69E-19

LINC00326	2.22E-31	0.51186	0.382	0.174	7.44E-27	4.78E-19	0.32269	0.357	0.225	1.60E-14
TOP2A	5.35E-19	-0.3422	0.081	0.274	1.79E-14	1.49E-43	-0.4564	0.089	0.34	5.01E-39
CAV1	2.46E-17	-0.4015	0.781	0.836	8.27E-13	1.67E-25	-0.3961	0.723	0.807	5.59E-21
PCLAF	3.08E-17	-0.5595	0.293	0.457	1.03E-12	2.75E-43	-0.6759	0.291	0.509	9.24E-39
H2AFX	4.42E-17	-0.3226	0.2	0.386	1.48E-12	1.42E-38	-0.3759	0.171	0.403	4.76E-34
DMBT1	6.79E-17	0.27596	0.191	0.077	2.28E-12	1.71E-18	0.32703	0.18	0.083	5.74E-14
HMMR	7.50E-17	-0.2721	0.12	0.307	2.51E-12	6.17E-46	-0.4314	0.1	0.359	2.07E-41
ZWINT	1.29E-16	-0.2559	0.196	0.382	4.32E-12	2.61E-38	-0.3024	0.168	0.406	8.75E-34
CKS1B	1.68E-16	-0.3103	0.507	0.668	5.62E-12	6.91E-26	-0.3256	0.535	0.667	2.32E-21
PLAT	2.84E-16	-0.3711	0.945	0.931	9.54E-12	1.11E-17	-0.3138	0.869	0.918	3.71E-13
CDKN3	4.21E-16	-0.306	0.164	0.346	1.41E-11	1.86E-50	-0.4719	0.117	0.394	6.23E-46
TPX2	7.38E-16	-0.3213	0.145	0.324	2.48E-11	9.47E-32	-0.38	0.156	0.363	3.17E-27
DUOX2	1.07E-15	-0.3297	0.028	0.174	3.60E-11	3.04E-21	-0.2679	0.031	0.163	1.02E-16
CENPF	1.23E-15	-0.2624	0.058	0.218	4.13E-11	2.35E-33	-0.3472	0.072	0.279	7.89E-29
DUOXA2	1.36E-15	-0.338	0.009	0.146	4.55E-11	9.56E-23	-0.3288	0.015	0.144	3.21E-18
TYMS	1.44E-15	-0.3604	0.177	0.354	4.81E-11	3.24E-40	-0.4481	0.172	0.408	1.09E-35
DUSP5	1.70E-15	-0.2529	0.23	0.436	5.69E-11	5.17E-29	-0.2821	0.175	0.392	1.74E-24
LY6E	1.81E-15	0.27517	0.7	0.617	6.07E-11	2.23E-24	0.25356	0.737	0.621	7.47E-20
MUC5B	2.27E-15	0.37139	0.385	0.232	7.61E-11	6.53E-45	0.57773	0.4	0.198	2.19E-40
UBE2S	3.90E-15	-0.5186	0.389	0.534	1.31E-10	7.60E-58	-0.7018	0.295	0.561	2.55E-53
ORC6	1.42E-14	-0.3025	0.205	0.384	4.77E-10	6.84E-32	-0.3066	0.196	0.415	2.30E-27
ATAD2	1.62E-14	-0.2562	0.12	0.291	5.44E-10	1.07E-28	-0.2823	0.124	0.326	3.60E-24
TK1	6.78E-14	-0.4464	0.334	0.486	2.27E-09	7.25E-40	-0.5804	0.285	0.503	2.43E-35
IL32	8.54E-14	-0.3504	0.689	0.796	2.86E-09	3.49E-33	-0.4644	0.696	0.809	1.17E-28
AKAP12	1.33E-13	-0.5645	0.175	0.341	4.45E-09	1.83E-16	-0.3013	0.091	0.223	6.15E-12
IGFBP6	1.79E-13	-0.417	0.82	0.852	6.01E-09	1.52E-20	-0.354	0.765	0.827	5.11E-16
AL133453.1	2.66E-13	-0.3553	0.341	0.521	8.91E-09	8.55E-18	-0.327	0.338	0.508	2.87E-13
CEACAM5	3.08E-13	-0.355	0.26	0.445	1.03E-08	4.21E-19	-0.303	0.214	0.391	1.41E-14
TM4SF20	6.69E-13	-0.4059	0.037	0.169	2.24E-08	1.90E-26	-0.6178	0.059	0.227	6.37E-22
STMN1	1.15E-12	-0.4786	0.394	0.519	3.86E-08	1.30E-32	-0.6196	0.416	0.569	4.36E-28
MT1X	1.20E-12	-0.6255	0.272	0.428	4.01E-08	4.42E-17	-0.6092	0.289	0.44	1.48E-12
HIST1H1A	3.51E-12	-0.4539	0.127	0.269	1.18E-07	5.04E-29	-0.5923	0.12	0.303	1.69E-24
PHLDA2	4.34E-12	-0.2519	0.924	0.896	1.46E-07	2.25E-19	-0.259	0.891	0.882	7.55E-15
FLNB	2.51E-13	-0.3831	0.735	0.825	8.43E-09	2.31E-11	-0.2815	0.674	0.759	7.75E-07
FAM111B	3.31E-11	-0.3346	0.164	0.304	1.11E-06	9.00E-23	-0.3627	0.151	0.321	3.02E-18
MACROD2	4.40E-11	-0.4536	0.267	0.418	1.48E-06	1.70E-20	-0.4491	0.297	0.477	5.71E-16
RPL23	7.21E-11	-0.3993	0.998	0.981	2.42E-06	2.20E-14	-0.3237	0.999	0.979	7.38E-10
CKS2	9.37E-11	-0.414	0.629	0.687	3.14E-06	8.25E-43	-0.6283	0.561	0.721	2.77E-38
DNAJC9	1.77E-10	-0.2629	0.472	0.587	5.93E-06	3.10E-20	-0.2658	0.446	0.594	1.04E-15
PLAU	3.37E-10	-0.4709	0.29	0.428	1.13E-05	7.45E-24	-0.4347	0.199	0.384	2.50E-19
HELLS	3.49E-10	-0.2923	0.224	0.368	1.17E-05	1.36E-23	-0.3172	0.207	0.394	4.55E-19
DUT	3.23E-09	-0.3206	0.638	0.685	0.000108	8.08E-17	-0.3528	0.614	0.682	2.71E-12
CCNB1	4.08E-09	-0.3207	0.12	0.235	0.000137	7.94E-32	-0.461	0.102	0.309	2.66E-27
NDRG1	3.60E-08	-0.3072	0.267	0.395	0.001207	5.43E-11	-0.2936	0.236	0.36	1.82E-06
BPIFB1	3.76E-08	0.28083	0.525	0.425	0.001263	2.96E-11	0.32831	0.539	0.453	9.94E-07
H2AFZ	1.14E-07	-0.347	0.94	0.878	0.003834	3.57E-31	-0.5111	0.9	0.878	1.20E-26
APOL1	3.56E-07	-0.3066	0.583	0.682	0.011931	4.29E-12	-0.3114	0.595	0.698	1.44E-07
SPINK1	6.92E-07	-0.2774	0.131	0.235	0.023209	1.73E-07	-0.2622	0.164	0.252	0.005789
PSCA	1.46E-06	0.26971	0.198	0.121	0.048979	3.69E-16	0.25941	0.202	0.105	1.24E-11
ANKRD36C	2.38E-05	-0.398	0.634	0.57	0.799789	5.75E-12	-0.2657	0.645	0.558	1.93E-07
FERMT1	7.06E-05	-0.2765	0.76	0.752	1	1.06E-08	-0.2735	0.678	0.708	0.0003567
PTTG1	0.0001561	-0.3548	0.327	0.402	1	2.52E-19	-0.5268	0.308	0.46	8.46E-15
ONECUT2	3.25E-09	-0.3993	0.348	0.497	0.000109	0.0001772	-0.2747	0.434	0.53	1
XIST	6.98E-07	-1.0131	0.569	0.667	0.02342	0.0057223	-0.6096	0.619	0.669	1
KPNA2	0.0101757	-0.2513	0.435	0.487	1	2.89E-12	-0.4025	0.405	0.507	9.69E-08
HIST1H4C	0.0279904	-0.4383	0.707	0.703	1	1.62E-09	-0.6083	0.763	0.756	5.43E-05
TFF2	0.4192927	0.34919	0.258	0.252	1	0.0076641	0.61681	0.232	0.201	1
MALAT1	0.0481608	-1.3572	0.988	0.976	1	0.8506252	-0.9156	0.992	0.986	1
NEAT1	0.9835795	-0.6117	0.871	0.871	1	0.1857934	-0.4472	0.885	0.876	1

Table S4. List of “Conserved Markers” in single cell RNA sequence analysis of Sph18-16. (D)
INT2 cluster.

pct.1, The percentage of cells where the feature is detected in the INT2 cluster.

pct.2 : The percentage of cells where the feature is detected in the other clusters.

D1, D1-inhibited sample; Ctrl, DMSO-used sample.

	D1_p_val	D1_avg logFC	D1_pct.1	D1_pct.2	D1_p_val_ adj	Ctrl_p_val	Ctrl_avg logFC	Ctrl_pct.1	Ctrl_pct.2	Ctrl_p_val_ adj
IGFBP2	1.10E-137	0.49285	0.491	0.045	3.70E-133	7.82E-188	0.52657	0.489	0.039	2.62E-183
KRT13	2.21E-110	0.78593	0.526	0.065	7.41E-106	1.06E-102	0.84202	0.395	0.049	3.56E-98
FCGBP	2.49E-112	1.01052	0.469	0.051	8.35E-108	4.56E-101	1.15947	0.556	0.104	1.53E-96
SPINK4	3.25E-80	1.45293	0.531	0.096	1.09E-75	7.40E-71	1.18969	0.57	0.153	2.48E-66
REG4	7.90E-65	1.66018	0.714	0.224	2.65E-60	1.06E-61	1.38412	0.659	0.235	3.55E-57
TRERF1	5.04E-58	0.27187	0.337	0.05	1.69E-53	7.52E-83	0.34906	0.377	0.055	2.52E-78
PLAC8	1.25E-56	0.50621	0.514	0.119	4.20E-52	1.82E-58	0.55808	0.498	0.135	6.11E-54
MRPS10	2.55E-53	1.23399	0.966	0.774	8.55E-49	4.75E-64	1.22495	0.946	0.778	1.59E-59
RNASE1	1.88E-49	0.3413	0.206	0.021	6.30E-45	3.17E-107	0.44403	0.332	0.032	1.06E-102
CSTB	9.96E-48	0.84934	0.994	0.883	3.34E-43	2.41E-65	0.8084	1	0.893	8.09E-61
CEACAM5	4.19E-45	1.01898	0.84	0.415	1.40E-40	2.68E-85	1.14293	0.87	0.35	8.99E-81
C6orf132	1.12E-43	0.89825	0.8	0.439	3.76E-39	1.74E-71	0.93656	0.848	0.422	5.83E-67
LGALS3	2.34E-43	0.57555	1	0.948	7.84E-39	2.95E-51	0.57401	1	0.957	9.89E-47
MSN	1.15E-41	0.30592	0.4	0.092	3.86E-37	2.21E-50	0.34066	0.359	0.079	7.42E-46
TAF8	2.31E-36	0.60408	0.743	0.389	7.76E-32	7.62E-42	0.5876	0.726	0.403	2.55E-37
AL512274.1	1.12E-35	0.35997	0.417	0.113	3.76E-31	1.55E-42	0.31959	0.377	0.098	5.20E-38
OARD1	4.82E-35	0.78188	0.931	0.749	1.62E-30	1.33E-43	0.7742	0.924	0.777	4.47E-39
VCAN	4.31E-33	0.49594	0.497	0.163	1.45E-28	1.16E-47	0.526	0.466	0.134	3.88E-43
CLDN2	2.44E-32	0.79227	0.937	0.736	8.19E-28	4.45E-43	0.74468	0.964	0.78	1.49E-38
UNC5CL	7.78E-41	0.36978	0.486	0.134	2.61E-36	6.72E-32	0.397	0.457	0.171	2.25E-27
FOXP4	1.73E-29	0.4204	0.571	0.242	5.81E-25	5.46E-36	0.44806	0.556	0.246	1.83E-31
TFF3	5.53E-29	0.6775	0.371	0.105	1.85E-24	2.97E-36	0.9773	0.381	0.11	9.97E-32
C12orf75	1.04E-28	-0.4981	0.943	0.924	3.48E-24	2.55E-47	-0.5764	0.946	0.941	8.56E-43
ECM1	4.44E-33	0.48024	0.617	0.254	1.49E-28	7.07E-28	0.44723	0.484	0.211	2.37E-23
ADH1C	3.28E-27	0.57044	0.457	0.165	1.10E-22	2.68E-38	0.64541	0.552	0.216	9.00E-34
MED20	9.01E-42	0.41595	0.554	0.182	3.02E-37	3.96E-27	0.37436	0.475	0.214	1.33E-22
CALD1	1.64E-26	-0.6768	0.537	0.826	5.48E-22	3.03E-52	-0.8763	0.457	0.851	1.02E-47
BYSL	2.83E-26	0.60459	0.669	0.374	9.48E-22	2.55E-37	0.62846	0.659	0.356	8.54E-33
CYSTM1	3.86E-26	0.49752	0.994	0.917	1.29E-21	1.41E-29	0.46685	1	0.926	4.74E-25
PPARG	4.47E-26	0.35356	0.686	0.341	1.50E-21	8.49E-35	0.36676	0.655	0.314	2.85E-30
RGS5	5.28E-36	0.52382	0.474	0.144	1.77E-31	1.32E-25	0.49989	0.453	0.193	4.41E-21
ITGA6	2.24E-25	0.46116	0.926	0.716	7.52E-21	6.22E-27	0.41864	0.879	0.693	2.09E-22
ALDH1A3	3.32E-25	0.34707	0.537	0.229	1.11E-20	1.70E-33	0.37023	0.525	0.214	5.70E-29
TXN	3.32E-25	0.34996	1	0.953	1.12E-20	3.44E-33	0.37202	1	0.963	1.15E-28
CST3	3.56E-25	0.45835	1	0.917	1.19E-20	1.04E-34	0.50817	1	0.932	3.48E-30
TSPAN8	4.83E-25	0.53287	0.989	0.92	1.62E-20	4.29E-30	0.52916	0.991	0.94	1.44E-25
HSD17B2	3.20E-27	0.38995	0.6	0.271	1.07E-22	2.81E-24	0.34914	0.596	0.31	9.41E-20
ACSM3	1.57E-25	0.25812	0.44	0.153	5.26E-21	2.50E-23	0.27984	0.493	0.226	8.39E-19
CALB1	1.13E-22	-1.0088	0.12	0.493	3.78E-18	4.35E-24	-0.8307	0.13	0.462	1.46E-19
MDFI	1.33E-29	0.37399	0.726	0.354	4.47E-25	4.90E-22	0.32208	0.587	0.34	1.64E-17
CPM	1.85E-20	0.4074	0.623	0.321	6.21E-16	1.26E-25	0.49967	0.655	0.368	4.23E-21
ARPC1B	2.67E-20	-0.4302	0.463	0.723	8.97E-16	6.85E-26	-0.4372	0.336	0.666	2.30E-21
FIS1	3.08E-20	-0.4101	0.891	0.891	1.03E-15	2.08E-28	-0.451	0.852	0.889	6.99E-24
IQGAP2	4.45E-30	0.4059	0.846	0.461	1.49E-25	3.60E-20	0.35382	0.767	0.529	1.21E-15
S100A4	2.12E-19	0.61034	0.731	0.468	7.12E-15	2.02E-28	0.7885	0.749	0.456	6.77E-24
BRI3	2.94E-19	-0.4233	0.886	0.905	9.86E-15	1.07E-20	-0.3799	0.879	0.914	3.60E-16
TMEM141	1.13E-18	0.41239	0.989	0.88	3.79E-14	2.37E-35	0.51397	0.978	0.89	7.96E-31
HSP90AB1	3.57E-18	-0.4502	1	0.979	1.20E-13	7.10E-30	-0.5368	1	0.979	2.38E-25
PHGR1	4.11E-18	0.26059	0.229	0.063	1.38E-13	1.48E-30	0.3865	0.291	0.08	4.95E-26
FAM3C	1.70E-17	-0.4842	0.76	0.854	5.71E-13	1.39E-27	-0.5596	0.677	0.851	4.66E-23
PLAT	2.49E-17	0.37258	1	0.93	8.37E-13	1.63E-23	0.47859	0.987	0.91	5.45E-19

RHEB	3.54E-16	-0.3934	0.657	0.784	1.19E-11	1.47E-19	-0.4108	0.601	0.774	4.93E-15
SEM1	9.20E-16	-0.3508	0.863	0.871	3.09E-11	2.06E-18	-0.3462	0.852	0.893	6.91E-14
MALL	1.02E-15	0.38698	0.863	0.696	3.42E-11	2.28E-22	0.43679	0.848	0.636	7.64E-18
CYBA	1.12E-15	-0.4079	0.331	0.607	3.75E-11	1.22E-25	-0.4721	0.296	0.657	4.10E-21
ITGB1	1.42E-15	-0.4752	0.891	0.901	4.75E-11	2.67E-19	-0.5049	0.87	0.893	8.95E-15
MTHFS	1.45E-15	0.29365	0.52	0.289	4.86E-11	9.98E-24	0.34983	0.493	0.25	3.35E-19
SLC40A1	1.60E-15	0.26076	0.829	0.543	5.38E-11	7.10E-17	0.25688	0.843	0.574	2.38E-12
CLDN4	1.93E-15	-0.4952	0.817	0.879	6.47E-11	4.12E-23	-0.5463	0.825	0.876	1.38E-18
DEPDC1B	2.01E-15	-0.4266	0.377	0.629	6.74E-11	9.88E-21	-0.4155	0.354	0.645	3.32E-16
ATP6V1F	6.22E-15	-0.36	0.777	0.83	2.09E-10	1.54E-18	-0.351	0.677	0.818	5.16E-14
LGALS4	7.04E-15	0.51803	0.971	0.883	2.36E-10	4.13E-18	0.41038	0.987	0.905	1.39E-13
MT-CYB	8.46E-15	0.43045	1	0.968	2.84E-10	4.08E-16	0.38694	0.996	0.98	1.37E-11
CAV1	2.10E-16	-0.6247	0.743	0.835	7.04E-12	8.86E-15	-0.4563	0.65	0.802	2.97E-10
GNB2	8.94E-15	-0.3558	0.749	0.81	3.00E-10	5.26E-20	-0.3637	0.623	0.792	1.76E-15
TFF2	1.26E-18	0.76045	0.52	0.243	4.23E-14	9.49E-15	0.44879	0.404	0.197	3.18E-10
ARPC1A	1.02E-14	-0.3415	0.817	0.847	3.43E-10	6.72E-16	-0.3091	0.704	0.835	2.25E-11
MDH2	1.43E-14	-0.3529	0.857	0.882	4.79E-10	2.89E-17	-0.3262	0.883	0.883	9.71E-13
SSBP1	1.91E-14	-0.3236	0.943	0.892	6.41E-10	3.23E-22	-0.3676	0.942	0.911	1.08E-17
LIMA1	2.01E-14	0.27633	0.886	0.667	6.75E-10	3.56E-24	0.35548	0.897	0.689	1.20E-19
LAMTOR4	2.06E-14	-0.3448	0.731	0.801	6.92E-10	8.83E-15	-0.3381	0.7	0.805	2.96E-10
LGMN	2.25E-14	0.28003	0.834	0.657	7.55E-10	5.99E-15	0.30744	0.825	0.682	2.01E-10
CD163L1	2.29E-14	0.28517	0.646	0.402	7.69E-10	1.19E-16	0.26667	0.583	0.361	3.98E-12
BUD31	2.70E-14	-0.3653	0.709	0.808	9.06E-10	3.00E-26	-0.4441	0.628	0.815	1.01E-21
NDUFC2	1.55E-14	0.2897	0.994	0.902	5.21E-10	4.14E-14	0.28598	0.996	0.904	1.39E-09
FHL2	4.47E-14	0.33958	0.914	0.73	1.50E-09	3.21E-20	0.32576	0.919	0.706	1.08E-15
FXYD3	4.84E-14	0.34581	0.994	0.881	1.62E-09	4.37E-17	0.35189	0.973	0.895	1.47E-12
PDAP1	7.80E-14	-0.3405	0.749	0.797	2.61E-09	7.42E-16	-0.305	0.686	0.791	2.49E-11
ATP5MF	8.89E-14	-0.3378	0.834	0.847	2.98E-09	8.51E-17	-0.3386	0.821	0.868	2.85E-12
COPS6	1.31E-13	-0.3625	0.726	0.779	4.40E-09	7.24E-20	-0.3856	0.632	0.777	2.43E-15
NDUFB2	1.59E-13	-0.3312	0.897	0.88	5.34E-09	2.60E-22	-0.3893	0.888	0.894	8.73E-18
ZNHIT1	1.66E-13	-0.3241	0.8	0.841	5.58E-09	5.80E-16	-0.3406	0.762	0.829	1.94E-11
CAV2	3.32E-15	-0.4261	0.674	0.82	1.11E-10	3.42E-13	-0.3788	0.713	0.805	1.15E-08
MMP1	4.18E-13	0.41559	1	0.957	1.40E-08	1.08E-19	0.51207	0.987	0.955	3.62E-15
MRPS33	4.33E-13	-0.3276	0.64	0.752	1.45E-08	3.52E-13	-0.2971	0.664	0.78	1.18E-08
POLR2J	4.44E-13	-0.3185	0.76	0.795	1.49E-08	1.70E-14	-0.3015	0.65	0.776	5.69E-10
HMGA1	6.16E-13	-0.4009	0.954	0.922	2.07E-08	7.10E-15	-0.3713	0.96	0.92	2.38E-10
KRTCAP3	1.30E-12	-0.3333	0.474	0.666	4.37E-08	3.91E-16	-0.329	0.413	0.647	1.31E-11
SQSTM1	3.42E-16	0.37219	0.966	0.857	1.15E-11	1.54E-12	0.26536	0.946	0.881	5.18E-08
SPATS2L	1.71E-16	0.30518	0.903	0.71	5.73E-12	3.29E-12	0.26771	0.834	0.708	1.10E-07
SLPI	2.74E-13	0.33808	0.977	0.81	9.21E-09	3.30E-12	0.26795	0.96	0.787	1.11E-07
ANXA1	5.82E-12	0.27166	0.857	0.613	1.95E-07	1.46E-21	0.38878	0.843	0.579	4.90E-17
ANXA5	1.52E-11	0.28814	0.971	0.902	5.11E-07	7.22E-16	0.30438	0.996	0.901	2.42E-11
GSTK1	1.54E-11	-0.3338	0.497	0.69	5.15E-07	5.81E-15	-0.327	0.511	0.694	1.95E-10
CAPZA2	2.28E-11	-0.32	0.663	0.797	7.66E-07	1.16E-13	-0.3016	0.709	0.82	3.88E-09
AGR2	2.73E-11	0.45162	1	0.949	9.15E-07	2.11E-13	0.33146	0.991	0.961	7.07E-09
CCND3	3.11E-19	0.41054	0.6	0.34	1.04E-14	3.26E-11	0.35993	0.511	0.343	1.09E-06
YWHAG	3.29E-11	-0.36	0.726	0.784	1.10E-06	2.73E-17	-0.3696	0.596	0.775	9.15E-13
ARF5	4.57E-11	-0.2888	0.623	0.749	1.53E-06	7.03E-20	-0.3591	0.664	0.798	2.36E-15
HSPB1	4.82E-11	-0.39	0.4	0.594	1.62E-06	8.80E-12	-0.3593	0.453	0.657	2.95E-07
EIF4H	3.62E-11	-0.3091	0.549	0.715	1.21E-06	1.43E-10	-0.2695	0.556	0.696	4.80E-06
CEACAM6	1.62E-10	0.27007	1	0.942	5.44E-06	8.13E-22	0.39385	1	0.946	2.73E-17
C6orf223	4.38E-10	-0.3347	0.423	0.592	1.47E-05	2.90E-16	-0.3807	0.336	0.592	9.73E-12
BUD23	5.35E-10	-0.2652	0.646	0.742	1.80E-05	1.27E-10	-0.2762	0.673	0.751	4.25E-06
SYPL1	5.87E-10	-0.276	0.863	0.867	1.97E-05	3.39E-17	-0.326	0.852	0.888	1.14E-12
CD47	1.21E-09	-0.3793	0.714	0.759	4.07E-05	8.45E-14	-0.3863	0.655	0.78	2.84E-09
SRI	1.33E-09	-0.3084	0.857	0.87	4.47E-05	4.61E-13	-0.3294	0.87	0.869	1.54E-08
PLAU	5.80E-12	-0.5662	0.189	0.424	1.94E-07	1.45E-09	-0.4862	0.184	0.368	4.86E-05
GABRP	5.99E-09	-0.5542	0.823	0.863	0.000201	1.54E-10	-0.4772	0.803	0.853	5.15E-06
TIMP1	3.79E-10	0.33885	0.989	0.901	1.27E-05	7.70E-09	0.30007	0.996	0.909	0.0002582
IL32	8.37E-09	-0.4524	0.703	0.79	0.000281	4.98E-12	-0.4274	0.682	0.8	1.67E-07
CLDN10	1.16E-08	-0.2549	0.137	0.339	0.000388	1.55E-12	-0.291	0.193	0.425	5.21E-08
SBDS	1.75E-08	-0.2957	0.554	0.666	0.000585	3.31E-11	-0.2913	0.48	0.653	1.11E-06

DYNLT3	3.51E-08	-0.2756	0.714	0.772	0.001179	1.71E-12	-0.3186	0.686	0.79	5.72E-08
HPGD	5.08E-13	0.29166	0.491	0.261	1.70E-08	3.86E-08	0.29363	0.43	0.283	0.001296
WASL	4.16E-08	-0.3027	0.497	0.629	0.001395	7.17E-13	-0.2718	0.413	0.635	2.40E-08
MRPL14	6.25E-08	-0.2753	0.909	0.88	0.002097	3.64E-14	-0.3583	0.924	0.897	1.22E-09
SERPINE2	1.78E-12	0.27189	0.617	0.376	5.97E-08	1.32E-07	0.26237	0.493	0.367	0.0044291
SPP1	1.57E-07	-0.3791	0.549	0.728	0.005259	1.32E-25	-0.901	0.556	0.817	4.43E-21
TM4SF4	2.04E-07	-0.3693	0.914	0.89	0.006857	5.62E-08	-0.3984	0.861	0.895	0.0018861
CLDN3	7.01E-08	-0.2937	0.411	0.563	0.002352	2.31E-07	-0.2947	0.453	0.593	0.0077521
SPRR3	3.58E-09	0.38842	0.743	0.566	0.00012	3.58E-07	0.47355	0.605	0.5	0.0120095
TFF1	1.20E-13	0.74761	0.829	0.597	4.02E-09	3.76E-07	0.41339	0.709	0.591	0.0125989
PLP2	3.76E-07	-0.252	0.874	0.838	0.012613	1.69E-08	-0.2673	0.812	0.819	0.0005672
LYZ	6.78E-07	0.28222	0.994	0.94	0.022744	3.57E-18	0.34823	1	0.96	1.20E-13
CDC5L	7.70E-07	-0.3195	0.617	0.697	0.02583	1.16E-08	-0.3204	0.646	0.732	0.0003879
TES	8.12E-07	-0.2516	0.594	0.693	0.027244	1.11E-07	-0.2577	0.547	0.669	0.0037171
BAIAP2L1	1.55E-07	-0.2739	0.537	0.662	0.005186	8.34E-07	-0.2504	0.52	0.641	0.0279624
INSIG1	1.16E-06	-0.3102	0.531	0.653	0.038778	2.10E-13	-0.3908	0.462	0.659	7.04E-09
HLA-A	1.24E-06	-0.3212	0.72	0.809	0.041645	1.15E-07	-0.3325	0.753	0.818	0.0038697
CST1	1.36E-06	0.7449	0.131	0.05	0.04555	2.66E-12	0.55027	0.296	0.137	8.93E-08
VEGFA	1.38E-06	-0.5028	0.589	0.691	0.046301	3.45E-12	-0.5191	0.547	0.7	1.16E-07
CYB5B	1.77E-06	-0.2713	0.857	0.89	0.059306	4.62E-08	-0.2839	0.879	0.904	0.0015479
SLC44A4	3.97E-06	-0.2549	0.303	0.451	0.133279	1.98E-11	-0.3083	0.26	0.466	6.65E-07
SLC14A1	1.59E-06	-0.3213	0.429	0.605	0.053304	4.71E-06	-0.2986	0.395	0.531	0.1580679
MKI67	5.24E-06	-0.3855	0.143	0.281	0.175617	9.27E-12	-0.4426	0.117	0.322	3.11E-07
BIRC5	9.94E-06	-0.3821	0.171	0.3	0.333322	4.99E-11	-0.4572	0.157	0.351	1.67E-06
GTF2I	1.09E-05	-0.2699	0.674	0.755	0.366102	2.39E-09	-0.2985	0.65	0.76	8.02E-05
COL17A1	1.52E-05	-0.3047	0.617	0.702	0.508949	2.64E-11	-0.3133	0.444	0.657	8.87E-07
RRM2	1.55E-05	-0.4558	0.166	0.304	0.51861	7.34E-09	-0.497	0.157	0.328	0.0002463
SPINK1	6.25E-05	-0.3208	0.103	0.23	1	1.11E-08	-0.5064	0.085	0.248	0.0003709
NUSAP1	7.29E-05	-0.2772	0.154	0.275	1	4.84E-09	-0.3187	0.135	0.304	0.0001622
CENPX	7.44E-05	-0.3128	0.84	0.821	1	5.00E-10	-0.385	0.852	0.82	1.68E-05
HMMR	8.12E-05	-0.258	0.177	0.295	1	5.50E-13	-0.4034	0.117	0.336	1.84E-08
TGM2	0.0002447	-0.4574	0.703	0.738	1	2.62E-05	-0.4322	0.673	0.734	0.8801525
MCM7	0.0002707	-0.3048	0.463	0.536	1	5.10E-07	-0.3287	0.43	0.533	0.0171062
TM4SF20	0.000306	-0.3921	0.063	0.161	1	3.01E-05	-0.4751	0.099	0.21	1
TUBB	0.0003359	-0.3148	0.8	0.797	1	0.0002997	-0.3138	0.812	0.775	1
ANKRD11	0.000485	-0.28	0.84	0.801	1	4.06E-06	-0.2544	0.735	0.806	0.1361973
UBE2C	0.0004899	-0.498	0.2	0.295	1	2.11E-11	-0.6581	0.135	0.324	7.07E-07
TOP2A	0.0005448	-0.2998	0.166	0.261	1	5.30E-09	-0.4045	0.152	0.316	0.0001776
UBE2T	0.0005744	-0.3007	0.417	0.487	1	2.23E-06	-0.3154	0.39	0.493	0.0749202
ONECUT1	0.0006083	-0.3509	0.337	0.452	1	5.28E-13	-0.4135	0.256	0.494	1.77E-08
DDIT4	9.43E-05	-0.3318	0.8	0.808	1	0.0010305	-0.2673	0.767	0.777	1
UBE2S	0.0031535	-0.4275	0.509	0.523	1	1.34E-08	-0.5136	0.413	0.533	0.0004508
STMN1	0.0032501	-0.3943	0.463	0.51	1	2.15E-09	-0.5361	0.422	0.556	7.21E-05
KPNA2	0.0051068	-0.3212	0.434	0.484	1	2.16E-06	-0.4289	0.386	0.499	0.0725562
TPX2	0.0056642	-0.2711	0.246	0.311	1	5.74E-07	-0.322	0.202	0.343	0.0192366
CDK1	0.0081737	-0.2724	0.217	0.275	1	3.77E-07	-0.2965	0.161	0.31	0.0126598
TK1	0.0096609	-0.3416	0.44	0.474	1	1.53E-08	-0.3923	0.309	0.483	0.0005126
PCLAF	0.0104294	-0.2862	0.371	0.446	1	0.0010217	-0.3002	0.417	0.485	1
CCNB1	0.0125609	-0.2742	0.16	0.228	1	9.24E-06	-0.3799	0.161	0.289	0.3099513
AKAP9	0.0166599	-0.2541	0.531	0.563	1	4.50E-08	-0.3153	0.453	0.622	0.0015102
HIST1H1A	0.0177785	-0.3468	0.2	0.259	1	0.0007161	-0.4386	0.202	0.284	1
TUBA1B	0.0989668	-0.2739	0.971	0.889	1	9.61E-05	-0.4249	0.964	0.88	1
PTTG1	0.2058383	-0.4084	0.411	0.395	1	3.72E-06	-0.5507	0.336	0.445	0.1248471
MALAT1	0.394811	-0.8292	0.989	0.976	1	0.4498097	-0.7232	0.996	0.986	1
XIST	0.6220141	-0.8991	0.68	0.658	1	0.4419799	-0.5933	0.668	0.663	1
HIST1H4C	0.7896524	-0.3392	0.76	0.702	1	0.0535514	-0.4168	0.812	0.755	1
ANKRD36C	0.9170109	-0.5124	0.589	0.575	1	0.0723648	-0.4979	0.525	0.57	1

Table S4. List of “Conserved Markers” in single cell RNA sequence analysis of Sph18-16. (E) H cluster.

pct.1, The percentage of cells where the feature is detected in the H cluster.

pct.2 : The percentage of cells where the feature is detected in the other clusters.

D1, D1-inhibited sample; Ctrl, DMSO-used sample.

	D1_p_val	D1_avg logFC	D1_pct.1	D1_pct.2	D1_p_val_ adj	Ctrl_p_val	Ctrl_avg logFC	Ctrl_pct.1	Ctrl_pct.2	Ctrl_p_val_ adj
RPS24	2.14E-186	0.51195	1	0.985	7.17E-182	8.38E-195	0.45334	1	0.991	2.81E-190
CALB1	1.29E-163	-1.2107	0.066	0.571	4.34E-159	5.32E-170	-1.0044	0.068	0.537	1.78E-165
TM4SF20	4.84E-162	1.06199	0.437	0.097	1.62E-157	4.10E-253	1.33255	0.549	0.128	1.38E-248
FXYD3	1.40E-158	0.59176	0.986	0.862	4.68E-154	8.17E-190	0.57775	0.988	0.878	2.74E-185
SLC40A1	9.24E-171	0.66939	0.851	0.487	3.10E-166	2.53E-158	0.62207	0.825	0.529	8.50E-154
ANXA1	8.13E-154	-0.9223	0.252	0.702	2.73E-149	8.40E-187	-0.8659	0.196	0.678	2.82E-182
RPL13	1.73E-138	0.29041	1	0.987	5.81E-134	4.49E-167	0.29372	1	0.988	1.51E-162
CYSTM1	2.43E-137	0.5581	0.992	0.903	8.14E-133	3.44E-182	0.58163	0.995	0.913	1.16E-177
CD24	1.23E-130	0.43304	1	0.941	4.13E-126	7.90E-162	0.4397	0.999	0.953	2.65E-157
RPL28	8.20E-130	0.321	1	0.956	2.75E-125	7.83E-185	0.36168	1	0.969	2.63E-180
DUOX2	1.45E-164	0.57415	0.451	0.099	4.86E-160	1.98E-126	0.45113	0.366	0.097	6.64E-122
ADD3	4.74E-122	0.44963	0.816	0.536	1.59E-117	3.39E-125	0.44586	0.821	0.58	1.14E-120
MACROD2	5.17E-122	0.78891	0.681	0.345	1.73E-117	1.61E-151	0.79403	0.724	0.395	5.39E-147
GOLM1	4.41E-121	0.54847	0.801	0.519	1.48E-116	2.55E-170	0.63493	0.799	0.498	8.57E-166
RPS16	1.57E-123	0.29628	1	0.961	5.28E-119	1.92E-120	0.27154	1	0.97	6.43E-116
FTL	1.80E-119	0.4583	0.999	0.939	6.02E-115	5.50E-182	0.50099	1	0.953	1.85E-177
DUOXA2	2.83E-153	0.75688	0.394	0.078	9.49E-149	9.32E-113	0.62757	0.324	0.084	3.13E-108
ANXA11	2.45E-110	0.38831	0.997	0.923	8.20E-106	1.74E-153	0.42381	0.994	0.929	5.83E-149
OCIAD2	3.04E-109	-0.5829	0.972	0.925	1.02E-104	5.31E-137	-0.5808	0.972	0.935	1.78E-132
TM4SF4	5.37E-109	0.53598	0.981	0.871	1.80E-104	1.90E-186	0.70523	0.983	0.874	6.36E-182
RPL13A	5.89E-108	0.32302	1	0.965	1.98E-103	7.88E-140	0.33962	1	0.975	2.64E-135
ARL6IP1	1.15E-116	0.46107	0.977	0.826	3.86E-112	2.37E-107	0.39132	0.966	0.829	7.96E-103
RPS27	4.46E-104	0.33155	0.999	0.95	1.50E-99	9.67E-150	0.35565	0.999	0.961	3.24E-145
RPL18	5.64E-104	0.29523	1	0.954	1.89E-99	8.95E-150	0.31143	1	0.968	3.00E-145
RPS5	1.04E-103	0.31365	1	0.953	3.48E-99	9.05E-141	0.33833	0.999	0.965	3.04E-136
LEMD1	2.20E-130	0.53965	0.505	0.17	7.39E-126	3.42E-103	0.38859	0.377	0.128	1.15E-98
RPS2	1.83E-99	0.27806	1	0.987	6.12E-95	7.77E-105	0.26778	1	0.99	2.61E-100
RPS9	3.72E-99	0.26632	0.999	0.951	1.25E-94	1.63E-138	0.2812	1	0.957	5.46E-134
TMC5	7.80E-98	0.32187	0.931	0.784	2.62E-93	7.23E-132	0.44577	0.918	0.766	2.43E-127
GSKIP	2.36E-97	0.40772	0.702	0.427	7.92E-93	2.28E-121	0.43922	0.718	0.454	7.64E-117
TK1	5.10E-97	-0.7631	0.189	0.535	1.71E-92	2.13E-134	-0.8277	0.166	0.548	7.14E-130
RPL31	2.19E-94	0.33518	0.994	0.93	7.36E-90	2.27E-118	0.33811	0.995	0.941	7.60E-114
SMIM22	5.24E-94	0.39925	0.846	0.642	1.76E-89	9.89E-114	0.44362	0.851	0.667	3.32E-109
CENPX	4.10E-93	-0.6714	0.76	0.835	1.38E-88	1.07E-103	-0.6605	0.749	0.837	3.59E-99
TM9SF3	4.63E-93	0.38658	0.933	0.805	1.55E-88	1.02E-94	0.34531	0.926	0.828	3.42E-90
B2M	1.48E-90	0.49161	0.997	0.944	4.98E-86	3.70E-105	0.47551	0.999	0.957	1.24E-100
LGALS3	6.28E-88	0.34513	0.998	0.939	2.11E-83	1.78E-103	0.33989	0.998	0.949	5.98E-99
LGALS4	1.13E-85	0.46566	0.988	0.864	3.80E-81	1.68E-131	0.55078	0.995	0.888	5.65E-127
PROX1	1.18E-82	0.41411	0.456	0.192	3.94E-78	1.81E-102	0.42984	0.444	0.183	6.09E-98
VDAC2	7.33E-80	0.30693	0.996	0.932	2.46E-75	3.54E-107	0.32795	0.994	0.938	1.19E-102
RRM2	4.45E-79	-0.7677	0.046	0.355	1.49E-74	2.95E-121	-0.837	0.025	0.389	9.90E-117
STMN1	2.80E-78	-0.735	0.263	0.562	9.41E-74	1.01E-121	-0.8577	0.279	0.613	3.38E-117
ORC6	1.49E-76	-0.4585	0.106	0.426	4.99E-72	4.25E-115	-0.4628	0.087	0.457	1.43E-110
TUBA1B	7.17E-76	-0.8203	0.935	0.882	2.40E-71	2.59E-125	-0.9838	0.871	0.885	8.70E-121
MAD2L1	9.43E-76	-0.3655	0.079	0.391	3.16E-71	7.85E-106	-0.4221	0.083	0.432	2.63E-101
SPINK1	2.62E-75	0.70973	0.431	0.181	8.79E-71	7.94E-95	0.78597	0.454	0.193	2.66E-90
RPS11	1.94E-76	0.28321	0.999	0.956	6.52E-72	1.93E-74	0.26802	0.998	0.964	6.47E-70
UBE2C	3.90E-74	-0.7193	0.048	0.345	1.31E-69	5.21E-103	-0.804	0.049	0.379	1.75E-98
TACSTD2	8.26E-74	-0.4708	0.24	0.569	2.77E-69	2.70E-94	-0.4564	0.227	0.579	9.06E-90
MDK	1.14E-73	0.49394	0.921	0.788	3.82E-69	1.49E-132	0.57936	0.955	0.808	5.00E-128
ASF1B	1.58E-73	-0.3283	0.03	0.326	5.29E-69	9.84E-94	-0.3341	0.031	0.34	3.30E-89

BIRC5	9.55E-73	-0.5225	0.052	0.349	3.20E-68	1.90E-106	-0.6284	0.064	0.407	6.36E-102
MKI67	9.91E-73	-0.5313	0.036	0.329	3.32E-68	2.24E-107	-0.6088	0.038	0.377	7.50E-103
MYBL2	8.25E-72	-0.3597	0.028	0.316	2.77E-67	1.61E-97	-0.3747	0.024	0.337	5.40E-93
CDK1	8.70E-72	-0.4643	0.036	0.325	2.92E-67	1.89E-98	-0.5045	0.044	0.364	6.33E-94
FEN1	9.04E-72	-0.3936	0.148	0.46	3.03E-67	2.75E-95	-0.3999	0.127	0.46	9.22E-91
PCLAF	1.21E-71	-0.743	0.206	0.495	4.06E-67	1.17E-103	-0.7947	0.222	0.542	3.92E-99
TYMS	1.74E-71	-0.5069	0.093	0.392	5.83E-67	2.67E-103	-0.564	0.104	0.442	8.96E-99
PNRC1	4.35E-71	0.32689	0.824	0.637	1.46E-66	7.97E-77	0.32396	0.816	0.662	2.67E-72
LCN2	4.83E-71	-0.7816	0.835	0.891	1.62E-66	1.99E-99	-0.8563	0.888	0.928	6.66E-95
GINS2	8.60E-70	-0.4331	0.123	0.428	2.88E-65	7.66E-91	-0.456	0.134	0.454	2.57E-86
MCM7	4.11E-69	-0.5059	0.301	0.584	1.38E-64	5.80E-89	-0.5026	0.281	0.586	1.95E-84
TUBB4B	5.22E-68	-0.6006	0.912	0.886	1.75E-63	7.88E-103	-0.7475	0.868	0.879	2.64E-98
FAM111B	1.94E-67	-0.4818	0.057	0.343	6.51E-63	1.90E-83	-0.5118	0.063	0.354	6.38E-79
CENPW	5.94E-67	-0.3347	0.109	0.414	1.99E-62	5.26E-108	-0.4419	0.108	0.468	1.77E-103
TCN1	2.70E-66	-0.5556	0.051	0.333	9.07E-62	1.86E-94	-0.7332	0.086	0.412	6.24E-90
ANLN	1.73E-65	-0.3506	0.053	0.336	5.81E-61	1.41E-98	-0.4302	0.041	0.363	4.72E-94
TPM1	7.34E-65	0.39997	0.997	0.945	2.46E-60	6.99E-90	0.44166	0.994	0.953	2.34E-85
BPIFB1	8.26E-65	0.44506	0.65	0.387	2.77E-60	2.77E-91	0.51425	0.691	0.412	9.30E-87
DTYMK	1.15E-64	-0.4017	0.284	0.571	3.86E-60	2.72E-89	-0.4517	0.268	0.573	9.12E-85
H2AFZ	1.99E-64	-0.6295	0.908	0.878	6.68E-60	3.40E-105	-0.7403	0.87	0.883	1.14E-100
AUP1	2.67E-64	-0.3871	0.56	0.773	8.94E-60	7.09E-66	-0.3456	0.562	0.766	2.38E-61
TOP2A	2.92E-64	-0.4237	0.036	0.306	9.79E-60	4.03E-97	-0.5382	0.048	0.369	1.35E-92
CSTB	5.02E-64	-0.4307	0.872	0.89	1.68E-59	4.77E-83	-0.4319	0.866	0.904	1.60E-78
TUBB	1.09E-63	-0.6076	0.76	0.805	3.66E-59	9.04E-105	-0.7422	0.692	0.796	3.03E-100
RANBP1	7.08E-63	-0.5013	0.825	0.853	2.38E-58	2.35E-93	-0.5564	0.812	0.855	7.89E-89
ZWINT	3.18E-62	-0.3352	0.131	0.417	1.07E-57	2.74E-81	-0.357	0.13	0.434	9.19E-77
SCD	1.25E-74	0.52738	0.941	0.822	4.18E-70	6.64E-62	0.44426	0.894	0.82	2.23E-57
GCNT3	9.82E-61	0.32904	0.806	0.614	3.29E-56	2.55E-95	0.40253	0.807	0.592	8.57E-91
CENPK	3.96E-60	-0.2978	0.081	0.355	1.33E-55	1.84E-84	-0.3157	0.08	0.386	6.17E-80
DHFR	4.07E-60	-0.4533	0.222	0.495	1.36E-55	3.36E-88	-0.5126	0.214	0.518	1.13E-83
AQP5	1.00E-59	-0.3745	0.045	0.308	3.37E-55	3.40E-59	-0.3127	0.055	0.288	1.14E-54
CLSPN	1.97E-58	-0.306	0.048	0.305	6.60E-54	3.00E-81	-0.3374	0.04	0.319	1.01E-76
SAT1	5.61E-74	0.55533	0.994	0.945	1.88E-69	3.30E-58	0.39327	0.993	0.952	1.11E-53
MCM4	5.93E-58	-0.3837	0.187	0.467	1.99E-53	1.58E-68	-0.3676	0.196	0.478	5.30E-64
NUSAP1	1.30E-57	-0.3875	0.059	0.317	4.35E-53	1.02E-97	-0.4665	0.04	0.357	3.43E-93
IQGAP2	1.18E-56	0.28807	0.664	0.433	3.95E-52	2.40E-82	0.34073	0.73	0.494	8.04E-78
PARK7	2.74E-56	-0.2527	0.992	0.923	9.19E-52	1.53E-82	-0.2708	0.988	0.936	5.12E-78
WWTR1	3.97E-56	-0.3292	0.164	0.446	1.33E-51	1.84E-63	-0.3008	0.174	0.454	6.16E-59
H2AFX	7.25E-56	-0.3985	0.155	0.417	2.43E-51	4.17E-75	-0.4168	0.14	0.428	1.40E-70
MVP	9.51E-55	0.27203	0.904	0.768	3.19E-50	1.33E-60	0.28089	0.856	0.754	4.46E-56
ACOT7	9.79E-55	-0.2817	0.263	0.542	3.28E-50	1.70E-70	-0.2836	0.195	0.498	5.69E-66
ATAD2	1.24E-54	-0.3373	0.069	0.322	4.15E-50	1.20E-70	-0.3571	0.082	0.351	4.04E-66
PCNA	1.70E-54	-0.5465	0.399	0.618	5.70E-50	3.41E-81	-0.6214	0.386	0.638	1.14E-76
CENPH	2.49E-54	-0.2938	0.16	0.434	8.36E-50	6.10E-70	-0.288	0.162	0.454	2.04E-65
CDKN3	8.16E-54	-0.3899	0.12	0.376	2.74E-49	1.93E-97	-0.5334	0.095	0.421	6.47E-93
HMGB2	1.93E-53	-0.2746	0.051	0.295	6.46E-49	1.20E-74	-0.3115	0.064	0.34	4.02E-70
TUBG1	2.10E-53	-0.3296	0.23	0.5	7.03E-49	1.21E-67	-0.3183	0.209	0.487	4.07E-63
TRIM29	2.48E-53	-0.316	0.138	0.412	8.30E-49	8.77E-61	-0.2659	0.12	0.384	2.94E-56
S100P	3.94E-53	0.35604	0.966	0.873	1.32E-48	5.39E-71	0.36717	0.948	0.874	1.81E-66
FANCI	9.43E-53	-0.2562	0.066	0.315	3.16E-48	7.37E-68	-0.2681	0.068	0.331	2.47E-63
CAMK2N1	6.00E-58	0.29378	0.947	0.84	2.01E-53	8.49E-52	0.27586	0.916	0.836	2.85E-47
LMO4	1.01E-51	0.29099	0.757	0.603	3.39E-47	1.96E-55	0.29511	0.755	0.631	6.58E-51
CENPM	1.15E-51	-0.3833	0.252	0.505	3.86E-47	2.63E-98	-0.4678	0.204	0.531	8.81E-94
MUC3A	3.39E-51	0.27934	0.309	0.127	1.14E-46	3.26E-106	0.41891	0.364	0.118	1.09E-101
ESCO2	3.81E-51	-0.2505	0.008	0.219	1.28E-46	4.40E-68	-0.2595	0.022	0.262	1.48E-63
WDR34	5.35E-51	-0.3428	0.374	0.611	1.80E-46	9.58E-53	-0.3212	0.396	0.613	3.21E-48
COX5B	1.06E-50	0.25332	0.991	0.921	3.55E-46	7.96E-77	0.27139	0.993	0.933	2.67E-72
LINC00326	1.97E-50	-0.402	0.016	0.229	6.60E-46	1.16E-79	-0.5009	0.022	0.291	3.90E-75
ALYREF	2.14E-50	-0.3734	0.598	0.747	7.19E-46	8.45E-95	-0.4669	0.529	0.756	2.83E-90
ANXA2	2.41E-50	-0.322	0.999	0.959	8.10E-46	3.26E-72	-0.3404	0.998	0.967	1.09E-67
TMEM106C	5.87E-50	-0.3935	0.453	0.657	1.97E-45	2.85E-73	-0.4359	0.43	0.665	9.57E-69
MCU	5.65E-50	0.28783	0.825	0.704	1.90E-45	7.69E-50	0.27407	0.793	0.69	2.58E-45

CCNB2	1.14E-49	-0.3068	0.035	0.258	3.82E-45	8.25E-74	-0.4106	0.055	0.322	2.77E-69
CENPN	1.45E-49	-0.2904	0.141	0.394	4.85E-45	6.19E-73	-0.324	0.137	0.43	2.08E-68
DNMT1	7.59E-49	-0.3556	0.33	0.571	2.54E-44	5.06E-57	-0.3431	0.322	0.569	1.70E-52
UBE2T	1.00E-48	-0.4507	0.298	0.526	3.35E-44	1.18E-76	-0.4856	0.266	0.54	3.96E-72
TPX2	4.02E-48	-0.3916	0.115	0.351	1.35E-43	5.20E-83	-0.4688	0.096	0.392	1.74E-78
HMGA1	4.35E-48	-0.3555	0.968	0.913	1.46E-43	3.81E-62	-0.3837	0.951	0.915	1.28E-57
PLAU	2.86E-47	-0.61	0.213	0.461	9.59E-43	2.97E-48	-0.5014	0.178	0.403	9.95E-44
ITGB1	9.92E-47	-0.4112	0.88	0.905	3.33E-42	4.58E-47	-0.393	0.86	0.9	1.54E-42
P4HB	1.20E-46	-0.3257	0.885	0.892	4.01E-42	1.97E-54	-0.3144	0.875	0.894	6.62E-50
RAN	8.56E-46	-0.2773	0.973	0.912	2.87E-41	2.72E-94	-0.3693	0.968	0.924	9.13E-90
GHITM	1.41E-45	0.29612	0.878	0.786	4.73E-41	4.57E-55	0.27909	0.879	0.791	1.53E-50
NUDT1	1.82E-45	-0.3022	0.368	0.597	6.10E-41	1.54E-61	-0.2992	0.34	0.603	5.17E-57
DKK1	4.14E-45	-0.3468	0.198	0.45	1.39E-40	1.46E-93	-0.538	0.147	0.482	4.91E-89
GNAS	4.25E-45	-0.2605	0.965	0.922	1.42E-40	1.43E-77	-0.3209	0.953	0.935	4.78E-73
HMGB1	8.38E-45	-0.3521	0.983	0.931	2.81E-40	9.00E-97	-0.4809	0.988	0.941	3.02E-92
CENPF	2.08E-44	-0.306	0.036	0.241	6.96E-40	1.12E-67	-0.402	0.05	0.3	3.75E-63
TM4SF5	6.42E-44	0.34111	0.702	0.544	2.15E-39	3.41E-82	0.43564	0.732	0.534	1.14E-77
GABRP	2.67E-43	-0.5898	0.836	0.867	8.96E-39	6.72E-69	-0.6246	0.789	0.866	2.25E-64
UBE2S	8.54E-43	-0.6084	0.362	0.557	2.86E-38	8.54E-67	-0.6701	0.35	0.57	2.87E-62
FAM213A	2.18E-45	0.30731	0.915	0.83	7.30E-41	9.28E-43	0.25697	0.897	0.827	3.11E-38
PFN1	1.60E-42	-0.3118	0.984	0.914	5.36E-38	6.66E-60	-0.3405	0.988	0.921	2.23E-55
SMC4	1.67E-42	-0.3107	0.208	0.444	5.59E-38	8.34E-68	-0.3942	0.214	0.492	2.80E-63
BRCA1	2.23E-42	-0.3163	0.155	0.387	7.47E-38	1.08E-71	-0.3708	0.134	0.419	3.61E-67
HIST1H1A	5.37E-42	-0.541	0.086	0.295	1.80E-37	1.10E-55	-0.6325	0.099	0.322	3.70E-51
KPNA2	3.45E-41	-0.4609	0.299	0.523	1.16E-36	2.72E-82	-0.6151	0.252	0.55	9.14E-78
HSP90AA1	4.36E-41	-0.3222	0.996	0.962	1.46E-36	2.19E-99	-0.454	0.994	0.968	7.33E-95
IFITM2	1.79E-62	0.52608	0.514	0.286	6.02E-58	6.85E-41	0.31665	0.433	0.273	2.30E-36
HELLS	7.91E-41	-0.3818	0.168	0.396	2.65E-36	2.06E-48	-0.3632	0.181	0.415	6.90E-44
HMGN1	1.55E-40	-0.2759	0.896	0.89	5.19E-36	1.28E-79	-0.3705	0.867	0.906	4.31E-75
DDIT4	2.79E-40	0.25942	0.893	0.79	9.35E-36	3.32E-61	0.25061	0.859	0.758	1.11E-56
TRNP1	7.66E-40	0.26878	0.776	0.661	2.57E-35	4.57E-63	0.3697	0.755	0.627	1.53E-58
CHEK1	9.19E-40	-0.2614	0.185	0.417	3.08E-35	8.43E-59	-0.2836	0.194	0.464	2.83E-54
LITAF	1.26E-39	0.3775	0.75	0.655	4.23E-35	6.80E-58	0.40391	0.754	0.637	2.28E-53
AGR2	3.01E-39	0.26484	0.997	0.94	1.01E-34	1.25E-63	0.32236	0.997	0.954	4.19E-59
HNRNPAB	3.47E-39	-0.3637	0.718	0.794	1.16E-34	6.27E-66	-0.4077	0.686	0.81	2.10E-61
RFC2	1.09E-38	-0.2732	0.216	0.44	3.64E-34	4.41E-55	-0.284	0.188	0.442	1.48E-50
CXCL5	1.23E-38	-0.4899	0.631	0.771	4.13E-34	1.10E-50	-0.4746	0.675	0.822	3.70E-46
HMMR	2.08E-38	-0.3144	0.118	0.329	6.96E-34	3.12E-73	-0.445	0.1	0.379	1.05E-68
SIVA1	2.47E-38	-0.3682	0.738	0.794	8.29E-34	8.83E-67	-0.4258	0.722	0.805	2.96E-62
PA2G4	2.58E-38	-0.3088	0.827	0.839	8.64E-34	1.22E-49	-0.3103	0.817	0.853	4.09E-45
SMC2	3.01E-38	-0.2717	0.222	0.461	1.01E-33	1.43E-71	-0.3582	0.205	0.503	4.80E-67
PTTG1	3.12E-38	-0.542	0.218	0.434	1.05E-33	3.11E-78	-0.7123	0.204	0.495	1.04E-73
CCT7	3.49E-38	-0.2684	0.864	0.86	1.17E-33	6.07E-53	-0.2955	0.825	0.864	2.04E-48
EIF5A	3.84E-39	-0.2936	0.878	0.876	1.29E-34	4.72E-38	-0.2631	0.855	0.859	1.58E-33
PSMA7	7.10E-38	-0.2629	0.985	0.936	2.38E-33	9.48E-63	-0.291	0.981	0.949	3.18E-58
KIF5B	7.28E-38	-0.3359	0.554	0.724	2.44E-33	2.92E-45	-0.3053	0.54	0.742	9.78E-41
SMC1A	9.20E-38	-0.3236	0.441	0.649	3.09E-33	6.83E-46	-0.3275	0.447	0.647	2.29E-41
RPL23	1.52E-37	0.45719	0.995	0.98	5.08E-33	7.12E-48	0.44719	0.998	0.978	2.39E-43
EIF4EBP1	1.87E-37	-0.2985	0.667	0.789	6.26E-33	5.92E-50	-0.3026	0.589	0.763	1.99E-45
DUT	1.22E-36	-0.4357	0.586	0.702	4.10E-32	2.59E-78	-0.5645	0.516	0.71	8.70E-74
DNAJC9	1.45E-36	-0.3424	0.427	0.61	4.86E-32	3.64E-66	-0.396	0.372	0.622	1.22E-61
POLE4	6.94E-35	-0.2657	0.584	0.728	2.33E-30	1.26E-49	-0.2871	0.515	0.725	4.24E-45
CLDN18	1.06E-34	0.31091	0.97	0.88	3.54E-30	4.67E-73	0.41884	0.978	0.904	1.57E-68
SUCLG1	1.29E-34	-0.2642	0.629	0.772	4.33E-30	1.05E-41	-0.2604	0.644	0.797	3.52E-37
TFF1	2.64E-34	0.39595	0.739	0.576	8.86E-30	1.19E-68	0.54904	0.764	0.557	3.99E-64
PDXK	2.97E-34	-0.2568	0.48	0.679	9.96E-30	6.41E-40	-0.2618	0.438	0.668	2.15E-35
LRRC8A	3.36E-34	-0.3349	0.382	0.582	1.13E-29	9.23E-37	-0.2502	0.267	0.489	3.10E-32
H2AFV	7.52E-34	-0.3445	0.768	0.814	2.52E-29	3.57E-67	-0.4161	0.747	0.826	1.20E-62
HMGB3	1.12E-33	-0.2543	0.304	0.519	3.76E-29	1.66E-58	-0.3175	0.287	0.554	5.56E-54
SLBP	1.50E-33	-0.3477	0.464	0.631	5.02E-29	1.25E-49	-0.3798	0.418	0.62	4.18E-45
PPM1G	1.73E-33	-0.2953	0.691	0.787	5.81E-29	1.46E-40	-0.2849	0.694	0.794	4.90E-36
CD44	2.24E-33	-0.348	0.694	0.829	7.50E-29	1.02E-35	-0.3113	0.713	0.834	3.44E-31

LSM4	2.48E-33	-0.2623	0.771	0.816	8.32E-29	1.35E-56	-0.3226	0.692	0.809	4.52E-52
LINC02300	2.59E-33	-0.3454	0.234	0.455	8.70E-29	3.99E-60	-0.3634	0.172	0.442	1.34E-55
CCNB1	2.71E-33	-0.388	0.079	0.257	9.08E-29	1.33E-58	-0.5024	0.091	0.328	4.46E-54
CALD1	4.30E-33	0.29131	0.877	0.803	1.44E-28	1.78E-41	0.28974	0.89	0.824	5.96E-37
CA9	8.10E-53	0.38523	0.497	0.276	2.72E-48	4.98E-33	0.2922	0.404	0.259	1.67E-28
LASP1	3.36E-32	0.29191	0.764	0.679	1.13E-27	1.38E-60	0.40368	0.794	0.684	4.64E-56
MUC13	3.55E-32	0.26602	0.251	0.115	1.19E-27	3.49E-53	0.35191	0.311	0.14	1.17E-48
CCT2	4.31E-32	-0.2821	0.879	0.87	1.44E-27	4.73E-54	-0.3196	0.865	0.879	1.59E-49
ATP5MC1	2.56E-31	-0.2883	0.783	0.834	8.57E-27	1.64E-58	-0.3576	0.775	0.854	5.49E-54
HIST1H4C	3.97E-31	-0.6912	0.645	0.716	1.33E-26	1.03E-46	-0.8009	0.7	0.77	3.47E-42
YWHAQ	5.92E-31	-0.2513	0.798	0.835	1.99E-26	4.53E-47	-0.2721	0.78	0.853	1.52E-42
C15orf48	1.91E-48	0.74517	0.675	0.5	6.39E-44	8.64E-31	0.61301	0.621	0.517	2.90E-26
RDX	9.05E-31	-0.2771	0.468	0.666	3.04E-26	5.10E-50	-0.2921	0.391	0.641	1.71E-45
CKLF	1.36E-30	-0.2765	0.56	0.723	4.55E-26	1.49E-42	-0.2717	0.541	0.715	5.00E-38
APOA2	1.23E-29	0.52778	0.123	0.035	4.14E-25	7.22E-35	0.45776	0.132	0.04	2.42E-30
S100A4	1.25E-29	-0.2606	0.304	0.515	4.18E-25	1.53E-47	-0.3153	0.26	0.514	5.13E-43
IER3	1.71E-29	-0.2768	0.413	0.619	5.74E-25	3.62E-59	-0.4129	0.343	0.614	1.21E-54
SPRR3	1.62E-30	-0.4165	0.414	0.607	5.42E-26	3.18E-29	-0.3792	0.356	0.538	1.07E-24
NME1	5.43E-29	-0.2895	0.804	0.817	1.82E-24	1.36E-49	-0.3371	0.739	0.819	4.57E-45
AREG	1.47E-31	-0.4317	0.741	0.85	4.92E-27	2.10E-28	-0.397	0.721	0.819	7.05E-24
RPA3	3.31E-28	-0.3783	0.826	0.804	1.11E-23	1.84E-52	-0.4346	0.821	0.828	6.18E-48
DEK	3.69E-28	-0.2975	0.766	0.819	1.24E-23	3.25E-37	-0.2986	0.787	0.836	1.09E-32
GGCT	4.89E-28	-0.2842	0.582	0.711	1.64E-23	4.15E-45	-0.3134	0.601	0.736	1.39E-40
ODC1	8.51E-28	-0.3403	0.453	0.631	2.85E-23	6.18E-43	-0.3308	0.419	0.621	2.07E-38
DCXR	2.58E-27	-0.2561	0.809	0.825	8.64E-23	3.42E-39	-0.2677	0.766	0.815	1.15E-34
TUBA1C	9.92E-26	-0.3533	0.906	0.866	3.33E-21	1.11E-45	-0.4258	0.907	0.872	3.72E-41
CKS1B	1.02E-25	-0.3128	0.577	0.672	3.41E-21	5.74E-43	-0.3367	0.512	0.683	1.92E-38
NASP	1.50E-25	-0.3034	0.572	0.697	5.02E-21	5.64E-35	-0.3038	0.581	0.714	1.89E-30
EGLN3	5.88E-32	0.39022	0.625	0.484	1.97E-27	2.00E-24	0.30603	0.548	0.439	6.71E-20
CXCL8	9.84E-24	-0.3782	0.139	0.305	3.30E-19	1.96E-53	-0.4303	0.123	0.366	6.57E-49
PRKDC	3.42E-23	-0.3136	0.711	0.793	1.15E-18	1.01E-32	-0.3145	0.686	0.796	3.40E-28
EHF	4.99E-24	-0.3091	0.544	0.71	1.67E-19	8.68E-23	-0.2678	0.595	0.737	2.91E-18
KRT7	4.26E-24	-0.2518	0.977	0.928	1.43E-19	1.45E-22	-0.2594	0.975	0.93	4.86E-18
MRPS10	1.08E-24	-0.3852	0.714	0.795	3.61E-20	3.00E-22	-0.3397	0.728	0.796	1.01E-17
PMEP1A1	7.30E-22	-0.4127	0.685	0.761	2.45E-17	8.73E-68	-0.6035	0.54	0.739	2.93E-63
HNRNP1	9.23E-22	-0.3851	0.695	0.794	3.10E-17	7.70E-28	-0.3155	0.729	0.821	2.58E-23
F3	2.11E-25	-0.416	0.392	0.566	7.08E-21	7.11E-21	-0.2926	0.332	0.492	2.38E-16
TMPO	1.08E-20	-0.2654	0.417	0.576	3.61E-16	2.54E-41	-0.3059	0.412	0.617	8.51E-37
LINC02404	7.40E-20	-0.411	0.259	0.414	2.48E-15	6.98E-53	-0.5323	0.212	0.459	2.34E-48
DCBLD2	1.02E-19	-0.2526	0.915	0.909	3.44E-15	6.38E-63	-0.4028	0.847	0.908	2.14E-58
SAV1	3.55E-19	-0.2878	0.536	0.681	1.19E-14	9.25E-22	-0.2574	0.509	0.668	3.10E-17
MMP7	2.15E-37	0.39821	0.988	0.896	7.22E-33	7.83E-19	0.28497	0.992	0.927	2.63E-14
IFITM3	3.31E-36	0.43112	0.574	0.424	1.11E-31	6.69E-18	0.28972	0.536	0.469	2.24E-13
HMG2	1.12E-17	-0.2902	0.699	0.743	3.74E-13	8.25E-43	-0.3887	0.649	0.766	2.77E-38
FAM3C	9.14E-17	-0.2603	0.814	0.859	3.06E-12	1.73E-33	-0.3181	0.785	0.858	5.79E-29
TMPRSS4	1.74E-16	-0.2691	0.766	0.832	5.85E-12	5.21E-25	-0.2715	0.745	0.845	1.75E-20
PGP	2.82E-16	-0.2564	0.592	0.696	9.46E-12	2.05E-36	-0.297	0.522	0.683	6.86E-32
PRSS1	2.74E-15	0.33054	0.431	0.314	9.19E-11	1.39E-20	0.28132	0.385	0.264	4.67E-16
PI3	4.47E-15	0.28087	0.224	0.132	1.50E-10	8.72E-41	0.45229	0.309	0.157	2.93E-36
CAV1	5.89E-13	-0.2521	0.812	0.836	1.97E-08	2.78E-39	-0.3927	0.71	0.816	9.33E-35
FUS	2.45E-12	-0.3195	0.707	0.775	8.20E-08	4.78E-24	-0.3407	0.66	0.773	1.60E-19
PNN	2.80E-08	-0.3414	0.628	0.718	0.00094	4.70E-10	-0.2554	0.612	0.719	1.58E-05
CKS2	3.82E-07	-0.3136	0.665	0.686	0.012796	3.81E-28	-0.5012	0.636	0.717	1.28E-23
MALAT1	1.04E-06	-0.7768	0.984	0.975	0.034912	7.91E-10	-0.4276	0.994	0.985	2.65E-05
RNF43	0.0001167	-0.3453	0.632	0.722	1	2.45E-08	-0.3184	0.637	0.73	0.0008211
ANKRD36C	0.0004486	-0.6524	0.509	0.589	1	3.62E-05	-0.5016	0.485	0.587	1

Table S5. Enriched gene sets for highly expressed genes in D1-inhibitor-treated cells.

ID	GeneR		pvalue	p.adjust	qvalue	geneID	Count
	atio	BgRatio					
EGFR1_IQB_EGFR1	24/189	390/25683	1.72174E-15	4.56491E-12	3.56898E-12	RPS10/ITGB4/KRT18/S100A14/GPRC5A/FLNB/CD59/RPS2/RPLP0/AHNAK/	24
EGFR1_NETPATH_EGFR1	24/189	398/25683	2.70593E-15	4.56491E-12	3.56898E-12	RPS10/ITGB4/KRT18/S100A14/GPRC5A/FLNB/CD59/RPS2/RPLP0/AHNAK/	24
WOUND HEALING_GOBP_GO:0042060	19/189	227/25683	6.87832E-15	7.382E-12	5.77147E-12	ACTB/PLAT/CD59/ACTG1/WNT7A/F3/SPRR3/MYOF/PLAUR/PLEC/DYSF/C	19
EUKARYOTIC TRANSLATION ELONGATION_REACTOME_R-HSA-14/189	94/25683	94/25683	8.75163E-15	7.382E-12	5.77147E-12	RPS10/RPL26/EEF2/RPS2/RPLP0/RPL8/RPS21/RPL7A/RPS4X/RPS16/RPSA/	14
RESPONSE TO WOUNDING_GOBP_GO:0009611	20/189	273/25683	1.6645E-14	1.12321E-11	8.78156E-12	ITGB4/ACTB/PLAT/CD59/ACTG1/WNT7A/F3/SPRR3/MYOF/PLAUR/PLEC/	20
CYTOPLASMIC RIBOSOMAL PROTEINS_WIKIPATHWAYS_20211213/189	87/25683	87/25683	7.78604E-14	4.37835E-11	3.42313E-11	RPS10/RPL26/RPL9/RPS2/RPLP0/RPL8/RPS21/RPL7A/RPS4X/RPS16/RPSA/	13
PEPTIDE CHAIN ELONGATION_REACTOME DATABASE ID RELEA13/189	89/25683	89/25683	1.05625E-13	5.09112E-11	3.98039E-11	RPS10/RPL26/EEF2/RPS2/RPLP0/RPL8/RPS21/RPL7A/RPS4X/RPS16/RPSA/	13
CAP-DEPENDENT TRANSLATION INITIATION_REACTOME_R-HSA14/189	119/25683	119/25683	2.53115E-13	9.489E-11	7.41879E-11	RPS10/RPL26/RPS2/RPLP0/RPL8/EIF4EBP1/RPS21/RPL7A/RPS4X/RPS16/EI	14
EUKARYOTIC TRANSLATION INITIATION_REACTOME_R-HSA-72614/189	119/25683	119/25683	2.53115E-13	9.489E-11	7.41879E-11	RPS10/RPL26/RPS2/RPLP0/RPL8/EIF4EBP1/RPS21/RPL7A/RPS4X/RPS16/EI	14
L13A-MEDIATED TRANSLATIONAL SILENCING OF CERULOPLASMA13/189	111/25683	111/25683	1.96036E-12	6.61425E-10	5.17122E-10	RPS10/RPL26/RPS2/RPLP0/RPL8/RPS21/RPL7A/RPS4X/RPS16/EIF4A2/RPS	13
GTP HYDROLYSIS AND JOINING OF THE 60S RIBOSOMAL SUBUN13/189	112/25683	112/25683	2.20366E-12	6.75921E-10	5.28456E-10	RPS10/RPL26/RPS2/RPLP0/RPL8/RPS21/RPL7A/RPS4X/RPS16/EIF4A2/RPS	13
CYTOPLASMIC TRANSLATION_GOBP_GO:0002181	13/189	113/25683	2.47427E-12	6.95684E-10	5.43906E-10	RPS10/RPL26/RPS2/RPLP0/RPL8/RPS21/RPL7A/RPS4X/RPS16/EIF4A2/RPS	13
EUKARYOTIC TRANSLATION TERMINATION_REACTOME DATAB12/189	93/25683	93/25683	4.39739E-12	1.05977E-09	8.28561E-10	RPS10/RPL26/RPS2/RPLP0/RPL8/RPS21/RPL7A/RPS4X/RPS16/RPSA/RPL41	12
SELENOCYSTEINE SYNTHESIS_REACTOME DATABASE ID RELEA12/189	93/25683	93/25683	4.39739E-12	1.05977E-09	8.28561E-10	RPS10/RPL26/RPS2/RPLP0/RPL8/RPS21/RPL7A/RPS4X/RPS16/RPSA/RPL41	12
NONSENSE MEDIATED DECAY (NMD) INDEPENDENT OF THE EX12/189	95/25683	95/25683	5.69653E-12	1.28134E-09	1.00179E-09	RPS10/RPL26/RPS2/RPLP0/RPL8/RPS21/RPL7A/RPS4X/RPS16/RPSA/RPL41	12
VIRAL MRNA TRANSLATION_REACTOME DATABASE ID RELEAS12/189	97/25683	97/25683	7.33518E-12	1.54681E-09	1.20934E-09	RPS10/RPL26/RPS2/RPLP0/RPL8/RPS21/RPL7A/RPS4X/RPS16/RPSA/RPL41	12
NEUTROPHIL DEGRANULATION_REACTOME DATABASE ID RELI22/189	479/25683	479/25683	9.53601E-12	1.89262E-09	1.47971E-09	TUBB4B/PRSS3/EEF2/CD59/PSMA2/FTH1/ANXA2/NDUFC2/RHOF/TIMP2/	22
FORMATION OF A POOL OF FREE 40S SUBUNITS_REACTOME DA12/189	101/25683	101/25683	1.19568E-11	2.12327E-09	1.66004E-09	RPS10/RPL26/RPS2/RPLP0/RPL8/RPS21/RPL7A/RPS4X/RPS16/RPSA/RPL41	12
RESPONSE OF EIF2AK4 (GCN2) TO AMINO ACID DEFICIENCY_RE12/189	101/25683	101/25683	1.19568E-11	2.12327E-09	1.66004E-09	RPS10/RPL26/RPS2/RPLP0/RPL8/RPS21/RPL7A/RPS4X/RPS16/RPSA/RPL41	12
SRP-DEPENDENT COTRANSLATIONAL PROTEIN TARGETING TO112/189	112/25683	112/25683	4.12996E-11	6.84427E-09	5.35106E-09	RPS10/RPL26/RPS2/RPLP0/RPL8/RPS21/RPL7A/RPS4X/RPS16/RPSA/RPL41	12
INFLUENZA VIRAL RNA TRANSCRIPTION AND REPLICATION_RE13/189	141/25683	141/25683	4.25992E-11	6.84427E-09	5.35106E-09	RPS10/RPL26/RPS2/RPLP0/RPL8/RPS21/RPL7A/RPS4X/RPS16/RPSA/RPL41	13
NONSENSE-MEDIATED DECAY (NMD)_REACTOME_R-HSA-9278012/189	115/25683	115/25683	5.65657E-11	8.29794E-09	6.48758E-09	RPS10/RPL26/RPS2/RPLP0/RPL8/RPS21/RPL7A/RPS4X/RPS16/RPSA/RPL41	12
NONSENSE MEDIATED DECAY (NMD) ENHANCED BY THE EXON12/189	115/25683	115/25683	5.65657E-11	8.29794E-09	6.48758E-09	RPS10/RPL26/RPS2/RPLP0/RPL8/RPS21/RPL7A/RPS4X/RPS16/RPSA/RPL41	12
SELENOAMINO ACID METABOLISM_REACTOME DATABASE ID R12/189	116/25683	116/25683	6.26911E-11	8.81332E-09	6.89052E-09	RPS10/RPL26/RPS2/RPLP0/RPL8/RPS21/RPL7A/RPS4X/RPS16/RPSA/RPL41	12
HALLMARK_ESTROGEN_RESPONSE_EARLY_MSIGDB_C2_HALLM14/189	179/25683	179/25683	6.88652E-11	9.29405E-09	7.26637E-09	KRT18/KRT19/FLNB/MYOF/ZNF185/CANT1/CALB2/SEMA3B/CLK10/RHO	14
INFLUENZA INFECTION_REACTOME DATABASE ID RELEASE78_13/189	161/25683	161/25683	2.26158E-10	2.93484E-08	2.29454E-08	RPS10/RPL26/RPS2/RPLP0/RPL8/RPS21/RPL7A/RPS4X/RPS16/RPSA/RPL41	13
REGULATION OF EXPRESSION OF SLITS AND ROBOS_REACTOME13/189	170/25683	170/25683	4.44915E-10	5.55979E-08	4.34681E-08	RPS10/RPL26/RPS2/PSMA2/RPLP0/RPL8/RPS21/RPL7A/RPS4X/RPS16/RPS	13
TRANSLATION_REACTOME DATABASE ID RELEASE78_72766_16/189	293/25683	293/25683	6.14748E-10	7.40771E-08	5.79157E-08	RPS10/RPL26/EEF2/RPS2/RPLP0/RPL8/EIF4EBP1/RPS21/RPL7A/RPS4X/RP	16
POSITIVE REGULATION OF CELL MIGRATION_GOBP_GO:0030335_19/189	438/25683	438/25683	6.97284E-10	8.11254E-08	6.34263E-08	S100A14/CAV1/ACTG1/F3/ANXA1/CLDN4/FERMT1/CEACAM6/EPHA2/SE	19
SIGNALING BY ROBO RECEPTORS_REACTOME DATABASE ID RE14/189	216/25683	216/25683	8.26768E-10	9.29839E-08	7.26976E-08	RPS10/RPL26/RPS2/PSMA2/RPLP0/RPL8/RPS21/RPL7A/RPS4X/RPS16/CAP	14
POSITIVE REGULATION OF CELL MOTILITY_GOBP_GO:2000147_19/189	458/25683	458/25683	1.45943E-09	1.58842E-07	1.24188E-07	S100A14/CAV1/ACTG1/F3/ANXA1/CLDN4/FERMT1/CEACAM6/EPHA2/SE	19
CELL JUNCTION ORGANIZATION_GOBP_GO:0034330_17/189	359/25683	359/25683	1.54536E-09	1.62939E-07	1.27391E-07	ITGB4/ACTB/WNT7B/ACTG1/WNT7A/WDR1/CLDN4/PLEC/CD9/VCL/RHO	17
POSITIVE REGULATION OF CELLULAR COMPONENT MOVEMENT19/189	466/25683	466/25683	1.94006E-09	1.91288E-07	1.49555E-07	S100A14/CAV1/ACTG1/F3/ANXA1/CLDN4/FERMT1/CEACAM6/EPHA2/SE	19
POSITIVE REGULATION OF LOCOMOTION_GOBP_GO:0040017_19/189	466/25683	466/25683	1.94006E-09	1.91288E-07	1.49555E-07	S100A14/CAV1/ACTG1/F3/ANXA1/CLDN4/FERMT1/CEACAM6/EPHA2/SE	19
CELLULAR RESPONSE TO STARVATION_REACTOME_R-HSA-971112/189	156/25683	156/25683	1.98432E-09	1.91288E-07	1.49555E-07	RPS10/RPL26/RPS2/RPLP0/RPL8/RPS21/RPL7A/RPS4X/RPS16/RPSA/RPL41	12
TRANSLATION_GOBP_GO:0006412_15/189	277/25683	277/25683	2.41593E-09	2.26426E-07	1.77027E-07	RPS10/RPL26/EEF2/RPS2/RPLP0/RPL8/RPS21/RPL7A/RPS4X/RPS16/EIF4A2	15
REGULATION OF BODY FLUID LEVELS_GOBP_GO:0050878_14/189	245/25683	245/25683	4.221E-09	3.83094E-07	2.99514E-07	ACTB/PLAT/CD59/CAV1/ACTG1/F3/CLDN4/PLAUR/CD9/VCL/FLNA/PLAU	14
HALLMARK_APICAL_JUNCTION_MSIGDB_C2_HALLMARK_APICAL12/189	167/25683	167/25683	4.31463E-09	3.83094E-07	2.99514E-07	ITGB4/ACTG1/RHOF/CLDN4/CALB2/CNN2/RRAS/COL17A1/CAP1/LAMB3	12
REGULATION OF WOUND HEALING_GOBP_GO:0061041_10/189	105/25683	105/25683	5.77773E-09	4.99847E-07	3.90796E-07	PLAT/TNFRSF12A/CAV1/ACTG1/F3/ANXA1/CLDN4/FERMT1/CD9/PLAU	10
PEPTIDE BIOSYNTHETIC PROCESS_GOBP_GO:0043043_15/189	300/25683	300/25683	7.11104E-09	5.99816E-07	4.68954E-07	RPS10/RPL26/EEF2/RPS2/RPLP0/RPL8/RPS21/RPL7A/RPS4X/RPS16/EIF4A2	15
CELL JUNCTION ASSEMBLY_GOBP_GO:0034329_13/189	220/25683	220/25683	1.0294E-08	8.47124E-07	6.62307E-07	ITGB4/ACTB/ACTG1/WNT7A/WDR1/CLDN4/PLEC/CD9/VCL/RHOD/RHOC	13
MAJOR PATHWAY OF RRNA PROCESSING IN THE NUCLEOLUS A112/189	182/25683	182/25683	1.13879E-08	9.14828E-07	7.1524E-07	RPS10/RPL26/RPS2/RPLP0/RPL8/RPS21/RPL7A/RPS4X/RPS16/RPSA/RPL41	12
ACTIVATION OF THE MRNA UPON BINDING OF THE CAP-BINDIN8/189	60/25683	60/25683	1.36774E-08	1.0732E-06	8.3906E-07	RPS10/RPS2/EIF4EBP1/RPS21/RPS4X/RPS16/EIF4A2/RPSA	8

ALPHA6BETA4INTEGRIN_NETPATH_ALPHA6BETA4INTEGRIN	8/189	61/25683	1.56435E-08	1.19957E-06	9.37862E-07	ITGB4/EIF4EBP1/PLEC/EIF6/COL17A1/RPSA/LAMB3/FOS	8
RRNA PROCESSING IN THE NUCLEUS AND CYTOSOL_REACTOME	12/189	192/25683	2.0704E-08	1.55234E-06	1.21366E-06	RPS10/RPL26/RPS2/RPLP0/RPL8/RPS21/RPL7A/RPS4X/RPS16/RPSA/RPL41	12
BLOOD COAGULATION_GOBP_GO:0007596	10/189	121/25683	2.28938E-08	1.67921E-06	1.31286E-06	ACTB/PLAT/CD59/ACTG1/F3/PLAUR/CD9/VCL/FLNA/VKORC1	10
EPH-EPHRIN SIGNALING_REACTOME_R-HSA-2682334.1	9/189	91/25683	2.43787E-08	1.74184E-06	1.36182E-06	ACTB/MYL6/ACTG1/EPHB6/CFL1/EPHA2/EFNB1/ARPC1B/ARPC1A	9
REGULATION OF RESPONSE TO WOUNDING_GOBP_GO:1903034	10/189	122/25683	2.47802E-08	1.74184E-06	1.36182E-06	PLAT/TNFRSF12A/CAV1/ACTG1/F3/ANXA1/CLDN4/FERMT1/CD9/PLAU	10
COAGULATION_GOBP_GO:0050817	10/189	123/25683	2.68026E-08	1.84555E-06	1.44291E-06	ACTB/PLAT/CD59/ACTG1/F3/PLAUR/CD9/VCL/FLNA/VKORC1	10
HEMOSTASIS_GOBP_GO:0007599	10/189	126/25683	3.37717E-08	2.27891E-06	1.78172E-06	ACTB/PLAT/CD59/ACTG1/F3/PLAUR/CD9/VCL/FLNA/VKORC1	10
RRNA PROCESSING_REACTOME_R-HSA-72312.3	12/189	202/25683	3.63618E-08	2.40558E-06	1.88076E-06	RPS10/RPL26/RPS2/RPLP0/RPL8/RPS21/RPL7A/RPS4X/RPS16/RPSA/RPL41	12
PATHOGENIC ESCHERICHIA COLI INFECTION_WIKIPATHWAYS_27	7/189	47/25683	5.12744E-08	3.32692E-06	2.60109E-06	KRT18/TUBB4B/ACTG1/TUBA1B/TUBB/ARPC1B/TUBA1C	7
ESTABLISHMENT OR MAINTENANCE OF CELL POLARITY_GOBP_	10/189	149/25683	1.65379E-07	1.05281E-05	8.23118E-06	ACTB/WNT7B/RHOF/WDR1/FERMT1/LMNA/RHOD/RHOC/MISP/CAP1	10
ALPHA6BETA4INTEGRIN_I0B_ALPHA6BETA4INTEGRIN	7/189	56/25683	1.78812E-07	1.09693E-05	8.57613E-06	ITGB4/EIF4EBP1/PLEC/EIF6/COL17A1/RPSA/LAMB3	7
RHO PROTEIN SIGNAL TRANSDUCTION_GOBP_GO:0007266	7/189	56/25683	1.78812E-07	1.09693E-05	8.57613E-06	TAX1BP3/EPS8L1/CFL1/ARHGDIARHOD/CDC42EP2/CTNNA1	7
REGULATION OF CELL MORPHOGENESIS_GOBP_GO:0022604	12/189	240/25683	2.38236E-07	1.43537E-05	1.12222E-05	ANXA1/RHOF/CLDN4/CFL1/FLNA/RHOD/CIB1/RHOC/MYADM/BCL9L/CI	12
RIBOSOMAL SCANNING AND START CODON RECOGNITION_REA	7/189	59/25683	2.58184E-07	1.50192E-05	1.17424E-05	RPS10/RPS2/RPS21/RPS4X/RPS16/EIF4A2/RPSA	7
TRANSLATION INITIATION COMPLEX FORMATION_REACTOME_17	7/189	59/25683	2.58184E-07	1.50192E-05	1.17424E-05	RPS10/RPS2/RPS21/RPS4X/RPS16/EIF4A2/RPSA	7
AMIDE BIOSYNTHETIC PROCESS_GOBP_GO:0043604	15/189	401/25683	3.17165E-07	1.81375E-05	1.41805E-05	RPS10/RPL26/EEF2/RPS2/RPLP0/RPL8/RPS21/RPL7A/RPS4X/RPS16/EIF4A2	15
PLATELET DEGRANULATION_REACTOME_R-HSA-114608.3	9/189	127/25683	4.39237E-07	2.46998E-05	1.9311E-05	WDR1/CFL1/APLP2/CD9/VCL/FLNA/CAP1/QSOX1/ACTN4	9
PEPTIDE METABOLIC PROCESS_GOBP_GO:0006518	15/189	415/25683	4.89663E-07	2.7084E-05	2.11751E-05	RPS10/RPL26/EEF2/RPS2/RPLP0/RPL8/RPS21/RPL7A/RPS4X/RPS16/EIF4A2	15
HALLMARK_KRAS_SIGNALING_UP_MSIGDB_C2_HALLMARK_KR	10/189	170/25683	5.62579E-07	3.06152E-05	2.39359E-05	AKAP12/PLAT/WNT7A/PLAUR/MALL/SEMA3B/TSPAN1/DCBLD2/EMP1/A	10
RESPONSE TO ELEVATED PLATELET CYTOSOLIC CA2+_REACTO	9/189	132/25683	6.09282E-07	3.26304E-05	2.55115E-05	WDR1/CFL1/APLP2/CD9/VCL/FLNA/CAP1/QSOX1/ACTN4	9
AMINO ACID AND DERIVATIVE METABOLISM_REACTOME DATA	14/189	368/25683	6.50415E-07	3.42891E-05	2.68082E-05	RPS10/RPL26/OAZ1/RPS2/PSMA2/RPLP0/RPL8/RPS21/RPL7A/RPS4X/RPS1	14
HALLMARK_APOPTOSIS_MSIGDB_C2_HALLMARK_APOPTOSIS	9/189	134/25683	6.91779E-07	3.59087E-05	2.80745E-05	KRT18/BCL2L1/PLAT/TNFRSF12A/IGFBP6/ANXA1/LMNA/EMP1/BIK	9
CELL-CELL JUNCTION ORGANIZATION_GOBP_GO:0045216	9/189	143/25683	1.19419E-06	6.08604E-05	4.75825E-05	ACTB/ACTG1/WDR1/CLDN4/CD9/VCL/RHOC/MYADM/CLDN7	9
SKIN DEVELOPMENT_GOBP_GO:0043588	8/189	106/25683	1.20855E-06	6.08604E-05	4.75825E-05	ITGB4/SPRR3/ANXA1/CLDN4/EPHA2/SPRR1B/ITGA3/SCEL	8
TISSUE MORPHOGENESIS_GOBP_GO:0048729	12/189	286/25683	1.52518E-06	7.5676E-05	5.91658E-05	ITGB4/ACTB/WNT7B/ACTG1/WNT7A/FKBP1A/EPHA2/VCL/FLNA/RHOC/I	12
CELL-CELL JUNCTION ASSEMBLY_GOBP_GO:0007043	8/189	110/25683	1.60128E-06	7.83002E-05	6.12175E-05	ACTB/ACTG1/WDR1/CLDN4/CD9/VCL/RHOC/CLDN7	8
ACTIN CYTOSKELETON ORGANIZATION_GOBP_GO:0030036	15/189	461/25683	1.81205E-06	8.73407E-05	6.82856E-05	ACTB/KRT19/ANXA1/RHOF/WDR1/CFL1/FLNA/RHOD/RHOC/ARPC1B/AR	15
DISSOLUTION OF FIBRIN CLOT_REACTOME DATABASE ID RELEA	4/189	13/25683	1.92852E-06	9.16457E-05	7.16513E-05	PLAT/ANXA2/PLAUR/PLAU	4
EPIDERMIS DEVELOPMENT_GOBP_GO:0008544	9/189	153/25683	2.09577E-06	9.821E-05	7.67835E-05	PTHLH/SPRR3/ANXA1/EPHA2/SPRR1B/COL17A1/EMP1/LAMB3/SCEL	9
FORMATION OF THE TERNARY COMPLEX, AND SUBSEQUENTLY	6/189	52/25683	2.25394E-06	0.000104175	8.14472E-05	RPS10/RPS2/RPS21/RPS4X/RPS16/RPSA	6
CELL-CELL COMMUNICATION_REACTOME_R-HSA-1500931.4	8/189	118/25683	2.71954E-06	0.000123996	9.6944E-05	ITGB4/CLDN4/PLEC/FLNA/COL17A1/LAMB3/CLDN7/ACTN4	8
REGULATION OF CELL-SUBSTRATE ADHESION_GOBP_GO:001081	9/189	160/25683	3.03175E-06	0.000136388	0.000106633	ACTG1/CEACAM6/VCL/FLNA/PLAU/CIB1/RRAS/MYADM/ACTN4	9
CELL JUNCTION ORGANIZATION_REACTOME_R-HSA-446728.2	7/189	86/25683	3.44024E-06	0.000152729	0.000119408	ITGB4/CLDN4/PLEC/FLNA/COL17A1/LAMB3/CLDN7	7
EPHB-MEDIATED FORWARD SIGNALING_REACTOME_R-HSA-3925	189	33/25683	4.1092E-06	0.000180058	0.000140774	ACTB/ACTG1/CFL1/ARPC1B/ARPC1A	5
SMOOTH MUSCLE CONTRACTION_REACTOME_R-HSA-445355.5	5/189	39/25683	9.6182E-06	0.000416049	0.000325279	MYL6/ANXA2/ANXA1/DYSF/VCL	5
REGULATION OF TRANSFORMING GROWTH FACTOR BETA RECE	7/189	101/25683	1.00367E-05	0.000428654	0.000335135	CAV1/FKBP1A/ITGA3/GIPC1/PMEP1/BCL9L/LTBP1	7
REGULATION OF CELLULAR RESPONSE TO TRANSFORMING GR	7/189	103/25683	1.14199E-05	0.000481636	0.000376557	CAV1/FKBP1A/ITGA3/GIPC1/PMEP1/BCL9L/LTBP1	7
RAS PROTEIN SIGNAL TRANSDUCTION_GOBP_GO:0007265	8/189	144/25683	1.18891E-05	0.000494185	0.000386369	TAX1BP3/EPS8L1/CFL1/ARHGDIARHOD/RRAS/CDC42EP2/CTNNA1	8
EXTRACELLULAR MATRIX ORGANIZATION_REACTOME DATA	11/189	293/25683	1.20104E-05	0.000494185	0.000386369	ITGB4/TIMP2/CEACAM6/PLEC/CAPN1/LTBP3/COL17A1/ITGA3/LAMB3/L	11
LONG-TERM MEMORY_GOBP_GO:0007616	4/189	20/25683	1.25512E-05	0.000510214	0.000398901	CALB1/LDLR/PRNP/CAMK2N1	4
VEGFA-VEGFR2 SIGNALING PATHWAY_WIKIPATHWAYS_2021121	12/189	364/25683	1.76367E-05	0.000708409	0.000553856	RPL26/SH3BGR13/BCL2L1/FLNB/ACTG1/F3/ANXA1/PLAUR/EPHA2/TMSE	12
LAMININ INTERACTIONS_REACTOME_R-HSA-3000157.2	4/189	23/25683	2.25464E-05	0.000894958	0.000699705	ITGB4/ITGA3/LAMB3/HSPG2	4
SUPRAMOLECULAR FIBER ORGANIZATION_GOBP_GO:0097435	13/189	437/25683	2.31472E-05	0.000908123	0.000709998	KRT19/FKBP1A/RHOF/WDR1/CFL1/FLNA/RHOD/CIB1/LTBP3/RHOC/ARPC	13
POSITIVE REGULATION OF WOUND HEALING_GOBP_GO:0090303	5/189	47/25683	2.44324E-05	0.000936759	0.000732386	ACTG1/F3/ANXA1/CLDN4/FERMT1	5
TRANSLATION FACTORS_WIKIPATHWAYS_20211210_WP107_HOM	5/189	47/25683	2.44324E-05	0.000936759	0.000732386	EIF4EBP1/EIF6/EIF5A/EIF4A2/EEF1D	5
REGULATION OF ACTIN FILAMENT-BASED PROCESS_GOBP_GO:0	11/189	320/25683	2.71202E-05	0.001028131	0.000803824	CAV1/ACTG1/RHOF/WDR1/CNN2/ARHGDIARHOD/RHOC/MYADM/TMS	11
HALLMARK_HYPOXIA_MSIGDB_C2_HALLMARK_HYPOXIA	8/189	163/25683	2.91367E-05	0.001092303	0.000853996	AKAP12/ANXA2/F3/PLAUR/ANGPTL4/IGFBP1/SULT2B1/FOS	8
KERATINOCYTE DIFFERENTIATION_GOBP_GO:0030216	5/189	49/25683	3.00131E-05	0.001108416	0.000866593	SPRR3/ANXA1/EPHA2/SPRR1B/SCEL	5
MORPHOGENESIS OF AN EPITHELIUM_GOBP_GO:0002009	9/189	213/25683	3.02235E-05	0.001108416	0.000866593	ACTB/WNT7B/ACTG1/WNT7A/EPHA2/VCL/FLNA/RHOC/KRT6A	9

CELL ACTIVATION_GOBP_GO:0001775	13/189	449/25683	3.06423E-05	0.001111691	0.000869153	ACTB/LRRC8A/PLAT/ACTG1/ANXA1/FKBP1A/DYSF/CD9/VCL/FLNA/ANX	13
RHO GTPASE EFFECTORS_REACTOME_R-HSA-195258.4	10/189	269/25683	3.27216E-05	0.001174497	0.000918257	ACTB/MYL6/TAX1BP3/ACTG1/CFL1/FLNA/RHOD/RHOC/ARPC1B/ARPC1	10
KERATINIZATION_REACTOME DATABASE ID RELEASE 78_680556	9/189	216/25683	3.3719E-05	0.001197557	0.000936286	KRT18/KRT19/KRT8/KRT7/SPRR3/CAPN1/SPRR1B/KRT6A/PPL	9
REGULATION OF TRANSMEMBRANE TRANSPORTER ACTIVITY_C9	189	220/25683	3.89076E-05	0.001367441	0.001069107	ACTB/AHNAK/CAV1/FKBP1A/PRNP/CAPN1/CALM2/VAMP2/ACTN4	9
POSITIVE REGULATION OF RESPONSE TO WOUNDING_GOBP_GO	5/189	52/25683	4.01822E-05	0.001397677	0.001092746	ACTG1/F3/ANXA1/CLDN4/FERMT1	5
HALLMARK_TNFA_SIGNALING_VIA_NFKB_MSIGDB_C2_HALLMA	8/189	174/25683	4.63889E-05	0.001597102	0.001248662	PHLDA2/F3/PLAUR/LDLR/AREG/LAMB3/KLF2/FOS	8
APICAL JUNCTION ASSEMBLY_GOBP_GO:0043297	5/189	54/25683	4.83169E-05	0.001630213	0.001274549	WDR1/CLDN4/VCL/RHOC/CLDN7	5
REGULATION OF BLOOD COAGULATION_GOBP_GO:0030193	5/189	54/25683	4.83169E-05	0.001630213	0.001274549	PLAT/CAV1/F3/CD9/PLAU	5
CELL-SUBSTRATE JUNCTION ASSEMBLY_GOBP_GO:0007044	4/189	28/25683	5.06544E-05	0.001687814	0.001319584	ITGB4/PLEC/RHOD/COL17A1	4
CELLULAR COMPONENT MORPHOGENESIS_GOBP_GO:0032989	12/189	406/25683	5.10246E-05	0.001687814	0.001319584	ACTB/KRT19/WNT7A/EPHB6/WDR1/EPHA2/SEMA3B/CD9/EFNB1/CCK/SI	12
REGULATION OF HEMOSTASIS_GOBP_GO:1900046	5/189	55/25683	5.28335E-05	0.001730681	0.001353099	PLAT/CAV1/F3/CD9/PLAU	5
NEGATIVE REGULATION OF PHOSPHATE METABOLIC PROCESS_11	189	346/25683	5.50305E-05	0.001757649	0.001374183	GPRC5A/CAV1/FKBP1A/MIDN/PRNP/CIB1/MYADM/CALM2/IGFBP3/PME	11
NEGATIVE REGULATION OF PHOSPHORUS METABOLIC PROCESS_11	189	347/25683	5.6473E-05	0.001757649	0.001374183	GPRC5A/CAV1/FKBP1A/MIDN/PRNP/CIB1/MYADM/CALM2/IGFBP3/PME	11
POSITIVE REGULATION OF CELL ADHESION_GOBP_GO:0045785_11	189	347/25683	5.6473E-05	0.001757649	0.001374183	CAV1/ANXA1/PLAUR/CEACAM6/CD55/FLNA/RHOD/CIB1/RRAS/MYADM	11
HALLMARK_ESTROGEN_RESPONSE_LATE_MSIGDB_C2_HALLMA	8/189	179/25683	5.6666E-05	0.001757649	0.001374183	KRT19/FLNB/MYOF/SEMA3B/KLK10/AREG/SULT2B1/FOS	8
SMALL GTPASE MEDIATED SIGNAL TRANSDUCTION_GOBP_GO:0008	189	179/25683	5.6666E-05	0.001757649	0.001374183	TAX1BP3/EP8L1/CFL1/ARHGDIARHOD/RRAS/CDC42EP2/CTNNA1	8
ACTIN FILAMENT ORGANIZATION_GOBP_GO:0007015	9/189	231/25683	5.67824E-05	0.001757649	0.001374183	RHOF/WDR1/CFL1/FLNA/RHOD/RHOC/ARPC1B/ARPC1A/CDC42EP2	9
REGULATION OF COAGULATION_GOBP_GO:0050818	5/189	56/25683	5.76693E-05	0.001768875	0.00138296	PLAT/CAV1/F3/CD9/PLAU	5
CELL-SUBSTRATE JUNCTION ORGANIZATION_GOBP_GO:0150115	4/189	29/25683	5.84221E-05	0.001775822	0.001388391	ITGB4/PLEC/RHOD/COL17A1	4
CELL MORPHOGENESIS INVOLVED IN DIFFERENTIATION_GOBP_11	189	350/25683	6.0997E-05	0.001837533	0.001436639	ACTB/WNT7A/EPHB6/EPHA2/SEMA3B/CIB1/EFNB1/CCK/LAMB3/SEMA4	11
REGULATION OF LOW-DENSITY LIPOPROTEIN PARTICLE CLEAR_3	189	11/25683	6.19663E-05	0.001850216	0.001446555	ANXA2/LDLR/CNPY2	3
REGULATION OF TRANSPORTER ACTIVITY_GOBP_GO:0032409_9	189	235/25683	6.48028E-05	0.001917934	0.001499499	ACTB/AHNAK/CAV1/FKBP1A/PRNP/CAPN1/CALM2/VAMP2/ACTN4	9
AXONOGENESIS_GOBP_GO:0007409	9/189	236/25683	6.69505E-05	0.00196427	0.001535725	ACTB/WNT7A/EPHB6/EPHA2/SEMA3B/EFNB1/CCK/SEMA4B/UNC5B	9
PROTEIN LOCALIZATION TO CELL PERIPHERY_GOBP_GO:1990778	189	188/25683	7.99394E-05	0.002325134	0.00181786	KRT18/CAV1/EPHA2/FLNA/TSPAN5/MYADM/RAB3B/VAMP2	8
REGULATION OF TRANSMEMBRANE TRANSPORT_GOBP_GO:003_11	189	364/25683	8.64609E-05	0.002492955	0.001949067	ACTB/AHNAK/CAV1/FKBP1A/FLNA/PRNP/CAPN1/CALM2/FGF19/VAMP2	11
NEGATIVE REGULATION OF TRANSFORMING GROWTH FACTOR_5	189	61/25683	8.71869E-05	0.002492955	0.001949067	CAV1/FKBP1A/PMEPA1/BCL9L/LTBP1	5
NEGATIVE REGULATION OF PHOSPHORYLATION_GOBP_GO:0042_10	189	303/25683	8.84827E-05	0.002508745	0.001961412	GPRC5A/CAV1/MIDN/PRNP/CIB1/MYADM/CALM2/IGFBP3/PMEPA1/CAM	10
REGULATION OF CELL-MATRIX ADHESION_GOBP_GO:0001952_6	189	99/25683	9.31986E-05	0.002620433	0.002048733	ACTG1/CEACAM6/VCL/PLAU/CIB1/RRAS	6
COOPERATION OF PREFOLDIN AND TRIC CCT IN ACTIN AND TUF_4	189	33/25683	9.83664E-05	0.002725403	0.002130802	ACTB/TUBB4B/TUBA1B/TUBA1C	4
CELL-MATRIX ADHESION_GOBP_GO:0007160	6/189	100/25683	9.85475E-05	0.002725403	0.002130802	ITGB4/FERMT1/VCL/RHOD/COL17A1/ITGA3	6
CANONICAL WNT SIGNALING PATHWAY_GOBP_GO:0060070	5/189	63/25683	0.000101794	0.002792294	0.0021831	CAV1/WNT7B/WNT7A/BCL9L/PORCN	5
CELL-SUBSTRATE ADHESION_GOBP_GO:0031589	7/189	146/25683	0.000107182	0.002916391	0.002280122	ITGB4/FERMT1/VCL/RHOD/COL17A1/ITGA3/LAMB3	7
EPITHELIAL CELL DIFFERENTIATION_GOBP_GO:0030855	10/189	313/25683	0.000115501	0.003092851	0.002418084	WNT7B/WNT7A/SPRR3/ANXA1/EPHA2/TUBB/DHRS9/SPRR1B/MYADM/S	10
REGULATION OF ANATOMICAL STRUCTURE SIZE_GOBP_GO:009_10	189	313/25683	0.000115501	0.003092851	0.002418084	LRRC8A/CAV1/WDR1/SEMA3B/MYADM/TMSB10/KLF2/SEMA4B/RAB3B	10
HALLMARK_CHOLESTEROL_HOMEOSTASIS_MSIGDB_C2_HALLM	5/189	65/25683	0.00011821	0.00314047	0.002455314	TNFRSF12A/ACTG1/PLAUR/SEMA3B/LDLR	5
REGULATION OF CELL DEVELOPMENT_GOBP_GO:0060284	10/189	315/25683	0.000121667	0.003202284	0.002503642	PTHLH/WNT7A/SEMA3B/LDLR/VCL/FLNA/CIB1/MYADM/SEMA4B/ACTN	10
REGULATION OF PROTEIN LOCALIZATION TO CELL PERIPHERY_6	189	104/25683	0.000122435	0.003202284	0.002503642	ACTB/BCL2L1/EPHA2/CIB1/ITGA3/MISP	6
RHO GTPASES ACTIVATE WASPS AND WAVES_REACTOME_R-HS	4/189	35/25683	0.000124429	0.003229416	0.002524854	ACTB/ACTG1/ARPC1B/ARPC1A	4
AXON DEVELOPMENT_GOBP_GO:0061564	9/189	257/25683	0.00012802	0.003297238	0.00257788	ACTB/WNT7A/EPHB6/EPHA2/SEMA3B/EFNB1/CCK/SEMA4B/UNC5B	9
SIGNALING BY INTERLEUKINS_REACTOME DATABASE ID RELE	12/189	448/25683	0.000129298	0.00330494	0.002583902	BCL2L1/PSMA2/RPLP0/ANXA2/ANXA1/CFL1/CNN2/IL1RL1/LIFR/MAOA/	12
PLATELET ACTIVATION, SIGNALING AND AGGREGATION_REAC	19/189	258/25683	0.000131818	0.00334401	0.002614447	WDR1/CFL1/APLP2/CD9/VCL/FLNA/CAP1/QSOX1/ACTN4	9
GENE AND PROTEIN EXPRESSION BY JAK-STAT SIGNALING AFT	14/189	36/25683	0.000139181	0.003478504	0.002719599	RPLP0/ANXA2/CFL1/CNN2	4
PLATELET AGGREGATION_GOBP_GO:0070527	4/189	36/25683	0.000139181	0.003478504	0.002719599	ACTB/ACTG1/VCL/FLNA	4
NEGATIVE REGULATION OF CELL DEVELOPMENT_GOBP_GO:001_6	189	108/25683	0.0001507	0.003738702	0.002923029	PTHLH/WNT7A/SEMA3B/LDLR/SEMA4B/ACTN4	6
CELL MORPHOGENESIS_GOBP_GO:0000902	12/189	456/25683	0.000152371	0.003752551	0.002933858	ACTB/WNT7A/EPHB6/EPHA2/SEMA3B/CIB1/CAP1/EFNB1/CCK/LAMB3/S	12
SEMAPHORIN-PLEXIN SIGNALING PATHWAY_GOBP_GO:0071526	4/189	37/25683	0.000155159	0.003776903	0.002952896	SEMA3B/FLNA/ARHGDIAR/SEMA4B	4
ALZHEIMER'S DISEASE_WIKIPATHWAYS_20211210_WP5124_HOM	8/189	207/25683	0.000155599	0.003776903	0.002952896	TUBB4B/PSMA2/WNT7B/WNT7A/TUBA1B/TUBB/CALM2/TUBA1C	8
REGULATION OF CATION TRANSMEMBRANE TRANSPORT_GOBP	9/189	266/25683	0.000165736	0.003994241	0.003122818	AHNAK/CAV1/FKBP1A/FLNA/PRNP/CAPN1/CALM2/VAMP2/ACTN4	9
LENS FIBER CELL DIFFERENTIATION_GOBP_GO:0070306	3/189	15/25683	0.000167206	0.004001078	0.003128163	WNT7B/WNT7A/EPHA2	3

NEGATIVE REGULATION OF PROTEIN PHOSPHORYLATION_GOB19/189	267/25683	0.000170446	0.004039902	0.003158517	GPRC5A/CAV1/PRNP/CIB1/MYADM/CALM2/IGFBP3/PMEP1/CAMK2N1	9
ALZHEIMER'S DISEASE AND MIRNA EFFECTS_WIKIPATHWAYS_28/189	210/25683	0.000171694	0.004039902	0.003158517	TUBB4B/PSMA2/WNT7B/WNT7A/TUBA1B/TUBB/CALM2/TUBA1C	8
MYELOID CELL ACTIVATION INVOLVED IN IMMUNE RESPONSE_4/189	38/25683	0.00017242	0.004039902	0.003158517	DYSF/ANXA3/S100A13/VAMP2	4
REGULATION OF ION TRANSMEMBRANE TRANSPORTER ACTIVI 8/189	213/25683	0.000189135	0.004400987	0.003440824	AHNAK/CAV1/FKBP1A/PRNP/CAPN1/CALM2/VAMP2/ACTN4	8
MUSCLE STRUCTURE DEVELOPMENT_GOBP_GO:0061061 9/189	273/25683	0.000201112	0.004647617	0.003633647	KRT19/MYL6/CAV1/FKBP1A/WDR1/MYOF/DYSF/CD9/ACTN4	9
CELL MORPHOGENESIS INVOLVED IN NEURON DIFFERENTIATIC 9/189	276/25683	0.000218087	0.005005624	0.003913547	ACTB/WNT7A/EPHB6/EPHA2/SEMA3B/EFNB1/CCK/SEMA4B/UNC5B	9
REGULATION OF LIPOPROTEIN PARTICLE CLEARANCE_GOBP_G 3/189	17/25683	0.000247194	0.005635346	0.004405883	ANXA2/LDLR/CNPY2	3
RHOF GTPASE CYCLE_REACTOME DATABASE ID RELEASE 78_904/189	42/25683	0.000255521	0.005786082	0.004523733	ACTB/AKAP12/CAV1/RHOF	4
EPIDERMAL CELL DIFFERENTIATION_GOBP_GO:0009913 5/189	77/25683	0.000263332	0.00586056	0.004581963	SPRR3/ANXA1/EPHA2/SPRR1B/SCEL	5
PLATELET ACTIVATION_GOBP_GO:0030168 5/189	77/25683	0.000263332	0.00586056	0.004581963	ACTB/ACTG1/CD9/VCL/FLNA	5
POSITIVE REGULATION OF I-KAPPAB KINASE/NF-KAPPAB SIGNA 7/189	169/25683	0.000264333	0.00586056	0.004581963	FKBP1A/CANT1/FLNA/RHOC/S100A13/CARD11/EEF1D	7
REGULATION OF ANGIOGENESIS_GOBP_GO:0045765 8/189	224/25683	0.000266013	0.00586056	0.004581963	F3/EPHA2/RRAS/ANXA3/PKM/ANGPTL4/KLF2/HSPG2	8
POSITIVE REGULATION OF TRANSLATION_GOBP_GO:0045727 6/189	120/25683	0.000267494	0.00586056	0.004581963	RPL26/EEF2/EIF6/RPS4X/EIF5A/PKM	6
REGULATION OF VASCULATURE DEVELOPMENT_GOBP_GO:19018/189	226/25683	0.000282412	0.006147463	0.004806272	F3/EPHA2/RRAS/ANXA3/PKM/ANGPTL4/KLF2/HSPG2	8
REGULATION OF ACTIN CYTOSKELETON ORGANIZATION_GOBP_9/189	287/25683	0.000290863	0.006260542	0.004894681	ACTG1/RHOF/WDR1/ARHGDI1A/RHOD/RHOC/MYADM/TMSB10/CDC42EI	9
AMEBOIDAL-TYPE CELL MIGRATION_GOBP_GO:0001667 6/189	122/25683	0.000292446	0.006260542	0.004894681	PRSS3/ID1/FERMT1/SEMA3B/GIPC1/SEMA4B	6
REGULATION OF APOPTOSIS BY PARATHYROID HORMONE-REL 3/189	18/25683	0.000295029	0.006260542	0.004894681	ITGB4/PTHLH/BCL2L1	3
REGULATION OF INSULIN-LIKE GROWTH FACTOR RECEPTOR SIC 3/189	18/25683	0.000295029	0.006260542	0.004894681	IGFBP6/IGFBP1/IGFBP3	3
PROTEIN LOCALIZATION TO PLASMA MEMBRANE_GOBP_GO:0077/189	173/25683	0.0003047	0.006425357	0.005023538	KRT18/EPHA2/FLNA/TSPAN5/MYADM/RAB3B/VAMP2	7
REGULATION OF IGF ACTIVITY BY IGFBP_REACTOME DATABAS 6/189	124/25683	0.000319188	0.006689072	0.005229717	IGFBP6/APLP2/IGFBP1/IGFBP3/LTBP1/QSOX1	6
MYOMETRIAL RELAXATION AND CONTRACTION PATHWAYS_W 6/189	125/25683	0.000333259	0.006836673	0.005345117	IGFBP6/ACTG1/CNN2/CALM2/IGFBP1/FOS	6
A6B1 AND A6B4 INTEGRIN SIGNALING_PATHWAY INTERACTION 4/189	45/25683	0.000334336	0.006836673	0.005345117	ITGB4/CD9/COL17A1/LAMB3	4
FGF SIGNALING PATHWAY_PATHWAY INTERACTION DATABASE 4/189	45/25683	0.000334336	0.006836673	0.005345117	PLAUR/PLAU/FGF19/FOS	4
INTERLEUKIN-12 SIGNALING_REACTOME_R-HSA-9020591.1 4/189	45/25683	0.000334336	0.006836673	0.005345117	RPLP0/ANXA2/CFL1/CNN2	4
GALANIN RECEPTOR PATHWAY_WIKIPATHWAYS_20211210_WP4 3/189	19/25683	0.000348453	0.007039999	0.005504083	KRT19/VAMP2/FOS	3
RHO GTPASES ACTIVATE ROCKS_REACTOME_R-HSA-5627117.3 3/189	19/25683	0.000348453	0.007039999	0.005504083	MYL6/CFL1/RHOC	3
HALLMARK_IL2_STAT5_SIGNALING_MSIGDB_C2_HALLMARK_IL 7/189	178/25683	0.000361968	0.007269514	0.005683525	BCL2L1/AHNAK/PLEC/PRNP/EMP1/IL1RL1/CDCP1	7
LEUKOCYTE DEGRANULATION_GOBP_GO:0043299 3/189	20/25683	0.00040773	0.008140116	0.006364187	ANXA3/S100A13/VAMP2	3
POSITIVE REGULATION OF CELL-SUBSTRATE ADHESION_GOBP_5/189	85/25683	0.000416948	0.0082752	0.0064698	CEACAM6/FLNA/CIB1/RRAS/MYADM	5
REGULATION OF CELLULAR AMIDE METABOLIC PROCESS_GOB 10/189	368/25683	0.000421356	0.008313771	0.006499956	RPL26/EEF2/EIF4EBP1/EIF6/RPS4X/EIF5A/PRNP/EIF4A2/PKM/RPL13A	10
ZYMOGEN ACTIVATION_GOBP_GO:0031638 4/189	48/25683	0.000429188	0.008419078	0.006582288	PRSS3/PLAT/ASPH/PLAU	4
REGULATION OF ION TRANSMEMBRANE TRANSPORT_GOBP_GO 9/189	303/25683	0.000431706	0.008419514	0.006582629	AHNAK/CAV1/FKBP1A/FLNA/PRNP/CAPN1/CALM2/VAMP2/ACTN4	9
REGULATION OF CELLULAR COMPONENT SIZE_GOBP_GO:0032538/189	244/25683	0.000470615	0.009121662	0.00713159	LRRC8A/WDR1/SEMA3B/MYADM/TMSB10/SEMA4B/RAB3B/CDC42EP2	8
MEMBRANE RAFT ORGANIZATION_GOBP_GO:0031579 3/189	21/25683	0.000473115	0.009121662	0.00713159	CAV1/ANXA2/MYADM	3
REGULATION OF PROTEIN LOCALIZATION TO PLASMA MEMBRA 5/189	88/25683	0.000489211	0.009378397	0.007332313	ACTB/BCL2L1/EPHA2/CIB1/ITGA3	5
CHEMOTAXIS_GOBP_GO:0006935 10/189	376/25683	0.000498126	0.009442008	0.007382046	ANXA1/EPHB6/PLAUR/EPHA2/SEMA3B/PLAU/PLP2/EFNB1/SEMA4B/UNC5B	10
TAXIS_GOBP_GO:0042330 10/189	376/25683	0.000498126	0.009442008	0.007382046	ANXA1/EPHB6/PLAUR/EPHA2/SEMA3B/PLAU/PLP2/EFNB1/SEMA4B/UNC5B	10
HOMOTYPIC CELL-CELL ADHESION_GOBP_GO:0034109 4/189	50/25683	0.000502194	0.009465938	0.007400755	ACTB/ACTG1/VCL/FLNA	4
RHO GTPASE CYCLE_REACTOME DATABASE ID RELEASE 78_901 11/189	448/25683	0.000513364	0.009622728	0.007523339	ACTB/AKAP12/CAV1/ACTG1/RHOF/TUBA1B/EPHA2/ARHGDI1A/RHOD/RI	11
REGULATION OF SUBSTRATE ADHESION-DEPENDENT CELL SPR 4/189	51/25683	0.000541825	0.01010009	0.007896554	FLNA/CIB1/MYADM/ACTN4	4
POSTSYNAPSE ORGANIZATION_GOBP_GO:0099173 4/189	52/25683	0.000583628	0.010807859	0.008449909	ACTB/WNT7A/PRNP/ITGA3	4
REGULATION OF CATION CHANNEL ACTIVITY_GOBP_GO:200125' 6/189	139/25683	0.0005862	0.010807859	0.008449909	AHNAK/CAV1/FKBP1A/CAPN1/CALM2/VAMP2	6
REGULATION OF TRANSLATION_GOBP_GO:0006417 9/189	317/25683	0.000597098	0.010948956	0.008560223	RPL26/EEF2/EIF4EBP1/EIF6/RPS4X/EIF5A/EIF4A2/PKM/RPL13A	9
POST-CHAPERONIN TUBULIN FOLDING PATHWAY_REACTOME I 3/189	23/25683	0.000623207	0.011365946	0.008886239	TUBB4B/TUBA1B/TUBA1C	3
NEURON PROJECTION MORPHOGENESIS_GOBP_GO:0048812 9/189	321/25683	0.000652871	0.011842942	0.009259169	ACTB/WNT7A/EPHB6/EPHA2/SEMA3B/EFNB1/CCK/SEMA4B/UNC5B	9
COMPLEMENT AND COAGULATION CASCADES_WIKIPATHWAYS 4/189	54/25683	0.000674019	0.012148134	0.009497777	PLAT/F3/PLAUR/CD55	4
POSITIVE REGULATION OF CELLULAR AMIDE METABOLIC PROC 6/189	143/25683	0.000680497	0.012148134	0.009497777	RPL26/EEF2/EIF6/RPS4X/EIF5A/PKM	6
REGULATION OF PROTEIN LOCALIZATION TO MEMBRANE_GOB 6/189	143/25683	0.000680497	0.012148134	0.009497777	ACTB/BCL2L1/EPHA2/PRNP/CIB1/ITGA3	6
MYELOID LEUKOCYTE ACTIVATION_GOBP_GO:0002274 5/189	95/25683	0.000694203	0.012194489	0.009534018	ANXA1/DYSF/ANXA3/S100A13/VAMP2	5

PLASMA MEMBRANE BOUNDED CELL PROJECTION MORPHOGENESIS	19/189	324/25683	0.000697439	0.012194489	0.009534018	ACTB/WNT7A/EPHB6/EPHA2/SEMA3B/EFNB1/CCK/SEMA4B/UNC5B	9
EPIBOLY INVOLVED IN WOUND HEALING_GOBP_GO:0090505	3/189	24/25683	0.000708394	0.012194489	0.009534018	WNT7A/FLNA/RHOC	3
EXTRACELLULAR MATRIX ASSEMBLY_GOBP_GO:0085029	3/189	24/25683	0.000708394	0.012194489	0.009534018	LTBP3/LAMB3/QSOX1	3
NATURAL KILLER CELL MEDIATED CYTOTOXICITY_GOBP_GO:003189	3/189	24/25683	0.000708394	0.012194489	0.009534018	TUBB4B/TUBB/VAMP2	3
SEMA4D IN SEMAPHORIN SIGNALING_REACTOME_R-HSA-4006853	3/189	24/25683	0.000708394	0.012194489	0.009534018	MYL6/RHOC/RRAS	3
WOUND HEALING, SPREADING OF CELLS_GOBP_GO:0044319	3/189	24/25683	0.000708394	0.012194489	0.009534018	WNT7A/FLNA/RHOC	3
INTERLEUKIN-12 FAMILY SIGNALING_REACTOME_R-HSA-4471154	4/189	55/25683	0.00072274	0.012378292	0.009677721	RPLP0/ANXA2/CFL1/CNN2	4
CELL PROJECTION MORPHOGENESIS_GOBP_GO:0048858	9/189	327/25683	0.000744462	0.01268594	0.009918249	ACTB/WNT7A/EPHB6/EPHA2/SEMA3B/EFNB1/CCK/SEMA4B/UNC5B	9
NEGATIVE REGULATION OF TRANSMEMBRANE RECEPTOR PROTEIN SIGNALING	15/189	98/25683	0.000799368	0.013373246	0.010455606	CAV1/FKBP1A/PMEP1A/BCL9L/LTBP1	5
BASIGIN INTERACTIONS_REACTOME_R-HSA-210991.1	3/189	25/25683	0.000800651	0.013373246	0.010455606	CAV1/ITGA3/SLC16A3	3
EPIBOLY_GOBP_GO:0090504	3/189	25/25683	0.000800651	0.013373246	0.010455606	WNT7A/FLNA/RHOC	3
NEUTROPHIL ACTIVATION_GOBP_GO:0042119	3/189	25/25683	0.000800651	0.013373246	0.010455606	ANXA1/ANXA3/VAMP2	3
REGULATION OF TRANSMEMBRANE RECEPTOR PROTEIN SERININTEGRIN INTERACTIONS	17/189	204/25683	0.000813882	0.013527276	0.010576032	CAV1/FKBP1A/ITGA3/GIPC1/PMEP1A/BCL9L/LTBP1	7
PARKIN-UBIQUITIN PROTEASOMAL SYSTEM PATHWAY_WIKIPATHWAYS_20211210_WP4	4/189	57/25683	0.000827564	0.013687255	0.010701108	TUBB4B/TUBA1B/TUBB/TUBA1C	4
WNT SIGNALING PATHWAY_GOBP_GO:0016055	5/189	100/25683	0.000875792	0.014414254	0.011269498	CAV1/WNT7B/WNT7A/BCL9L/PORCN	5
MEMORY_GOBP_GO:0007613	4/189	58/25683	0.000883801	0.014463269	0.011307819	CALB1/LDLR/PRNP/CAMK2N1	4
ALK1 SIGNALING EVENTS_PATHWAY INTERACTION DATABASE	3/189	26/25683	0.000900203	0.014463269	0.011307819	CAV1/ID1/FKBP1A	3
FORMATION OF TUBULIN FOLDING INTERMEDIATES BY CCT TRIPLEX	3/189	26/25683	0.000900203	0.014463269	0.011307819	TUBB4B/TUBA1B/TUBA1C	3
NATURAL KILLER CELL MEDIATED IMMUNITY_GOBP_GO:0002223	3/189	26/25683	0.000900203	0.014463269	0.011307819	TUBB4B/TUBB/VAMP2	3
WNT LIGAND BIOGENESIS AND TRAFFICKING_REACTOME_R-HSA-373755.1	3/189	26/25683	0.000900203	0.014463269	0.011307819	WNT7B/WNT7A/PORCN	3
MUSCLE CELL DEVELOPMENT_GOBP_GO:0055001	5/189	101/25683	0.000915982	0.01464589	0.011450598	KRT19/WDR1/MYOF/DYSF/ACTN4	5
CELL PART MORPHOGENESIS_GOBP_GO:0032990	9/189	337/25683	0.000920252	0.01464589	0.011450598	ACTB/WNT7A/EPHB6/EPHA2/SEMA3B/EFNB1/CCK/SEMA4B/UNC5B	9
CELL-CELL SIGNALING BY WNT_GOBP_GO:0198738	5/189	102/25683	0.000957529	0.015167619	0.011858501	CAV1/WNT7B/WNT7A/BCL9L/PORCN	5
GASTRIN SIGNALING PATHWAY_WIKIPATHWAYS_20211210_WP4	5/189	103/25683	0.00100046	0.015773614	0.012332286	BCL2L1/ANXA2/EIF4EBP1/RHOD/FOS	5
DENDRITIC SPINE ORGANIZATION_GOBP_GO:0097061	3/189	27/25683	0.00100727	0.015807116	0.012358479	WNT7A/PRNP/ITGA3	3
NEGATIVE REGULATION OF PROTEIN MODIFICATION PROCESSING	10/189	413/25683	0.001020221	0.015936228	0.012459423	GPRC5A/CAV1/FKBP1A/PRNP/CIB1/MYADM/CALM2/IGFBP3/PMEP1A/C	10
HALLMARK_COMPLEMENT_MSI_GDB_C2_HALLMARK_COMPLEMENT	6/189	156/25683	0.001069999	0.016636757	0.013007117	PLAT/CD59/F3/PLAUR/CD55/S100A13	6
DISEASES OF SIGNAL TRANSDUCTION BY GROWTH FACTOR RECEPTOR	10/189	417/25683	0.001096747	0.016974427	0.013271118	BCL2L1/PSMA2/FKBP1A/VCL/LMNA/LMO7/AREG/FGF19/POLR2J/PORCN	10
ALPHA 6 BETA 4 SIGNALING PATHWAY_WIKIPATHWAYS_20211210_WP4	3/189	28/25683	0.001122064	0.017130519	0.013393155	ITGB4/EIF4EBP1/LAMB3	3
GRANULOCYTE ACTIVATION_GOBP_GO:0036230	3/189	28/25683	0.001122064	0.017130519	0.013393155	ANXA1/ANXA3/VAMP2	3
PREFOLDIN MEDIATED TRANSFER OF SUBSTRATE TO CCT TRIPLEX	3/189	28/25683	0.001122064	0.017130519	0.013393155	ACTB/TUBB4B/TUBA1C	3
ENZYME LINKED RECEPTOR PROTEIN SIGNALING PATHWAY_GOBP_GO:0042692	11/189	494/25683	0.001138294	0.017300011	0.013525669	PLAT/ID1/FKBP1A/EPHB6/EPHA2/EFNB1/LIFR/AREG/FAM83A/FGF19/FO	11
POST-TRANSLATIONAL PROTEIN PHOSPHORYLATION_REACTOME_R-HSA-373755.1	5/189	107/25683	0.001186607	0.01795342	0.014036524	APLP2/IGFBP1/IGFBP3/LTBP1/QSOX1	5
ARRHYTHMOGENIC RIGHT VENTRICULAR CARDIOMYOPATHY_GOBP_GO:0097485	4/189	63/25683	0.001205916	0.018164104	0.014201243	ITGB4/ACTG1/LMNA/ACTN4	4
ANATOMICAL STRUCTURE FORMATION INVOLVED IN MORPHOGENESIS	11/189	498/25683	0.00121399	0.018204453	0.014232789	ITGB4/KRT19/ANXA2/ID1/ACTG1/FKBP1A/WDR1/CD9/CIB1/ITGA3/LAME	11
BETA2 INTEGRIN CELL SURFACE INTERACTIONS_PATHWAY INTERACTION DATABASE	3/189	29/25683	0.001244792	0.018583756	0.014529339	PLAT/PLAUR/PLAU	3
FOCAL ADHESION_WIKIPATHWAYS_20211210_WP306_HOMO SAFETY	6/189	161/25683	0.001258435	0.018704662	0.014623868	ITGB4/FLNB/ACTG1/FLNA/LAMB3/ACTN4	6
SEMAPHORIN INTERACTIONS_REACTOME_R-HSA-373755.1	4/189	64/25683	0.001278992	0.018891286	0.014769776	MYL6/CFL1/RHOC/RRAS	4
PROTEIN MATURATION_GOBP_GO:0051604	7/189	221/25683	0.001294823	0.018891286	0.014769776	PRSS3/PLAT/ASPH/F3/FKBP1A/PLAU/TSPAN5	7
AXON GUIDANCE_GOBP_GO:0007411	6/189	162/25683	0.001298986	0.018891286	0.014769776	EPHB6/EPHA2/SEMA3B/EFNB1/SEMA4B/UNC5B	6
MUSCLE CELL DIFFERENTIATION_GOBP_GO:0042692	6/189	162/25683	0.001298986	0.018891286	0.014769776	KRT19/WDR1/MYOF/DYSF/CD9/ACTN4	6
NEURON PROJECTION GUIDANCE_GOBP_GO:0097485	6/189	162/25683	0.001298986	0.018891286	0.014769776	EPHB6/EPHA2/SEMA3B/EFNB1/SEMA4B/UNC5B	6
REGULATION OF I-KAPPA B KINASE/NF-KAPPA B SIGNALING_GOBP_GO:0042692	7/189	222/25683	0.001328827	0.019242327	0.015044231	FKBP1A/CANT1/FLNA/RHOC/S100A13/CARD11/EEF1D	7
HALLMARK_MITOTIC_SPINDLE_MSI_GDB_C2_HALLMARK_MITOTIC	6/189	163/25683	0.001340529	0.019328818	0.015111852	FLNB/RHOF/FLNA/SEPT9/CDC42EP2/ACTN4	6
POSITIVE REGULATION OF PROTEIN LOCALIZATION_GOBP_GO:0042692	19/189	356/25683	0.00134686	0.019337468	0.015118614	LRRC8A/OAZ1/WNT7A/EPHA2/FLNA/PRNP/CIB1/ITGA3/VAMP2	9
REGULATION OF CELLULAR RESPONSE TO GROWTH FACTOR STIMULATION	7/189	223/25683	0.001363526	0.019493801	0.015240841	CAV1/FKBP1A/ITGA3/GIPC1/PMEP1A/BCL9L/LTBP1	7
PLASMINOGEN ACTIVATING CASCADE_PANTHER PATHWAY_P000000000	3/189	30/25683	0.001375655	0.019584224	0.015311536	PLAT/PLAUR/PLAU	3
VITAMIN D RECEPTOR PATHWAY_WIKIPATHWAYS_20211210_WP4	16/189	164/25683	0.001383079	0.019607173	0.015329478	PTH1L/ID1/SEMA3B/SPRR1B/IL1RL1/IGFBP1	6
DEGRADATION OF THE EXTRACELLULAR MATRIX_REACTOME_R-HSA-373755.1	5/189	111/25683	0.001397222	0.019724805	0.015421446	TIMP2/CAPN1/COL17A1/LAMB3/HSPG2	5

REGULATION OF METAL ION TRANSPORT_GOBP_GO:0010959	8/189	289/25683	0.00140476	0.019748581	0.015440035	AHNAK/CAV1/FKBP1A/FLNA/PRNP/CALM2/VAMP2/ACTN4	8
HALLMARK_EPITHELIAL_MESENCHYMAL_TRANSITION_MSIGDB	6/189	165/25683	0.001426652	0.019915387	0.015570449	PTHLH/CD59/TNFRSF12A/PLAUR/FLNA/AREG	6
BETA1 INTEGRIN CELL SURFACE INTERACTIONS_PATHWAY INT	4/189	66/25683	0.001434333	0.019915387	0.015570449	PLAUR/PLAU/ITGA3/LAMB3	4
HIF-1-ALPHA TRANSCRIPTION FACTOR NETWORK_PATHWAY IN	4/189	66/25683	0.001434333	0.019915387	0.015570449	SLC2A1/PKM/IGFBP1/FOS	4
MYELOID LEUKOCYTE MEDIATED IMMUNITY_GOBP_GO:000244	3/189	31/25683	0.001514849	0.020887534	0.016330503	ANXA3/S100A13/VAMP2	3
REGULATION OF PROTEIN TYROSINE KINASE ACTIVITY_GOBP_C	4/189	67/25683	0.00151673	0.020887534	0.016330503	GPRC5A/CAV1/PRNP/AREG	4
REGULATION OF CELL-CELL ADHESION_GOBP_GO:0022407	9/189	364/25683	0.001568579	0.021513756	0.016820102	CAV1/ANXA1/PLAUR/CEACAM6/CD55/CD9/PRNP/MYADM/CARD11	9
REGULATION OF ION TRANSPORT_GOBP_GO:0043269	10/189	438/25683	0.001579543	0.021576434	0.016869105	AHNAK/CAV1/FKBP1A/FLNA/PRNP/CAPN1/CALM2/RAB3B/VAMP2/ACT	10
REGULATION OF CELL SHAPE_GOBP_GO:0008360	5/189	115/25683	0.001634192	0.022232925	0.01738237	ANXA1/RHOF/RHOD/RHOC/CDC42EP2	5
REGULATION OF CYTOSKELETON ORGANIZATION_GOBP_GO:00	10/189	441/25683	0.001660781	0.022259883	0.017403446	ACTG1/RHOF/WDR1/ARHGDI1A/RHOD/CIB1/RHOC/MYADM/TMSB10/CDC	10
AMB2 INTEGRIN SIGNALING_PATHWAY INTERACTION DATABASE	3/189	32/25683	0.001662564	0.022259883	0.017403446	PLAT/PLAUR/PLAU	3
MAINTENANCE OF BLOOD-BRAIN BARRIER_GOBP_GO:0035633	3/189	32/25683	0.001662564	0.022259883	0.017403446	ACTB/ACTG1/VCL	3
SEALING OF THE NUCLEAR ENVELOPE (NE) BY ESCRT-III_REACT	3/189	32/25683	0.001662564	0.022259883	0.017403446	TUBB4B/TUBA1B/TUBA1C	3
RIBOSOMAL LARGE SUBUNIT BIOGENESIS_GOBP_GO:0042273	4/189	69/25683	0.001691308	0.022555224	0.017634353	RPL26/RPLP0/RPL7A/EIF6	4
POSITIVE REGULATION OF INTRACELLULAR TRANSPORT_GOBP	6/189	171/25683	0.001710489	0.022721225	0.017764138	OAZ1/ANXA2/FLNA/PRNP/CIB1/VAMP2	6
REGULATION OF SUPRAMOLECULAR FIBER ORGANIZATION_GO	8/189	299/25683	0.001739315	0.023013524	0.017992666	ACTG1/WDR1/LDLR/CIB1/RHOC/MYADM/TMSB10/CDC42EP2	8
POSITIVE REGULATION OF ANGIOGENESIS_GOBP_GO:0045766	5/189	117/25683	0.001763158	0.023147452	0.018097375	F3/RRAS/ANXA3/PKM/ANGPTL4	5
POSITIVE REGULATION OF VASCULATURE DEVELOPMENT_GOB	5/189	117/25683	0.001763158	0.023147452	0.018097375	F3/RRAS/ANXA3/PKM/ANGPTL4	5
MALIGNANT PLEURAL MESOTHELIOMA_WIKIPATHWAYS_20211	9/189	371/25683	0.001785825	0.023354164	0.018258989	ITGB4/WNT7B/ACTG1/WNT7A/EIF4EBP1/EPHA2/AREG/LAMB3/PORCN	9
RIBOSOME BIOGENESIS_GOBP_GO:0042254	7/189	235/25683	0.001837724	0.023940079	0.018717074	RPL26/RPLP0/RPS21/RPL7A/EIF6/RPS16/RPSA	7
HALLMARK_UV_RESPONSE_DN_MSIGDB_C2_HALLMARK_UV_R	5/189	120/25683	0.001970386	0.02548042	0.01992136	ANXA2/ID1/F3/LDLR/LTBP1	5
EPITHELIAL CELL MIGRATION_GOBP_GO:0010631	4/189	72/25683	0.001978622	0.02548042	0.01992136	PRSS3/ID1/FERMT1/GIPC1	4
REGULATION OF CELL MORPHOGENESIS INVOLVED IN DIFFERE	4/189	72/25683	0.001978622	0.02548042	0.01992136	FLNA/CIB1/MYADM/ACTN4	4
SIGNALING MEDIATED BY P38-ALPHA AND P38-BETA_PATHWAY	3/189	35/25683	0.002158649	0.027693089	0.02165129	KRT19/KRT8/EIF4EBP1	3
EPITHELIUM MIGRATION_GOBP_GO:0090132	4/189	74/25683	0.002187892	0.027961919	0.02186147	PRSS3/ID1/FERMT1/GIPC1	4
ANATOMICAL STRUCTURE HOMEOSTASIS_GOBP_GO:0060249	6/189	180/25683	0.002214197	0.028191327	0.022040828	ACTB/ACTG1/CALB1/CALB2/VCL/SLC2A1	6
NEGATIVE REGULATION OF CATALYTIC ACTIVITY_GOBP_GO:00	10/189	461/25683	0.002293179	0.028737121	0.022467546	GPRC5A/CAV1/ANXA1/FKBP1A/MIDN/TIMP2/PLAUR/EIF4A2/ANGPTL4/C	10
FORMATION OF THE CORNIFIED ENVELOPE_REACTOME_R-HSA-	4/189	75/25683	0.002298039	0.028737121	0.022467546	SPRR3/CAPN1/SPRR1B/PPL	4
ACTIN FILAMENT DEPOLYMERIZATION_GOBP_GO:0030042	2/189	10/25683	0.002331766	0.028737121	0.022467546	WDR1/CFL1	2
ADHERENS JUNCTION ASSEMBLY_GOBP_GO:0034333	2/189	10/25683	0.002331766	0.028737121	0.022467546	ACTB/VCL	2
MEMBRANE RAFT ASSEMBLY_GOBP_GO:0001765	2/189	10/25683	0.002331766	0.028737121	0.022467546	CAV1/ANXA2	2
PID_INTEGRIN4_PATHWAY_MSIGDB_C2_PID_INTEGRIN4_PATHW	2/189	10/25683	0.002331766	0.028737121	0.022467546	ITGB4/LAMB3	2
MORPHOGENESIS OF AN EPITHELIAL SHEET_GOBP_GO:0002011	3/189	36/25683	0.002342237	0.028737121	0.022467546	WNT7A/FLNA/RHOC	3
NEGATIVE REGULATION OF CATION CHANNEL ACTIVITY_GOBP	3/189	36/25683	0.002342237	0.028737121	0.022467546	CAV1/FKBP1A/CALM2	3
PID_A6B1_A6B4_INTEGRIN_PATHWAY_MSIGDB_C2_PID_A6B1_A	3/189	36/25683	0.002342237	0.028737121	0.022467546	ITGB4/COL17A1/LAMB3	3
POSITIVE REGULATION OF SUBSTRATE ADHESION-DEPENDENT	3/189	36/25683	0.002342237	0.028737121	0.022467546	FLNA/CIB1/MYADM	3
REGULATION OF CALCIUM ION TRANSPORT INTO CYTOSOL_GO	4/189	76/25683	0.002411947	0.029485178	0.0230524	CAV1/FKBP1A/PRNP/CALM2	4
APOPTOSIS MODULATION AND SIGNALING_WIKIPATHWAYS_20	4/189	77/25683	0.002529679	0.030370896	0.023744881	BCL2L1/BIK/TNFRSF10D/FOS	4
INTERMEDIATE FILAMENT CYTOSKELETON ORGANIZATION_GO	3/189	37/25683	0.002535215	0.030370896	0.023744881	KRT18/PLEC/PPL	3
NEURON PROJECTION ORGANIZATION_GOBP_GO:0106027	3/189	37/25683	0.002535215	0.030370896	0.023744881	WNT7A/PRNP/ITGA3	3
RHOH GTPASE CYCLE_REACTOME_R-HSA-9013407.2	3/189	37/25683	0.002535215	0.030370896	0.023744881	CAV1/TUBA1B/ARHGDI1A	3
VALIDATED TRANSCRIPTIONAL TARGETS OF AP1 FAMILY MEME	3/189	37/25683	0.002535215	0.030370896	0.023744881	ITGB4/PLAUR/PLAU	3
LEUKOCYTE MEDIATED IMMUNITY_GOBP_GO:0002443	6/189	185/25683	0.002538409	0.030370896	0.023744881	TUBB4B/CD55/TUBB/ANXA3/S100A13/VAMP2	6
CELL SURFACE RECEPTOR SIGNALING PATHWAY INVOLVED IN	5/189	128/25683	0.002609648	0.030894565	0.024154301	CAV1/WNT7B/WNT7A/BCL9L/PORCN	5
OREXIN RECEPTOR PATHWAY_WIKIPATHWAYS_20211210_WP	5/189	128/25683	0.002609648	0.030894565	0.024154301	HMGA1/ID1/CLDN4/LDLR/FOS	5
REGULATION OF INTRINSIC APOPTOTIC SIGNALING PATHWAY_C	5/189	128/25683	0.002609648	0.030894565	0.024154301	RPL26/BCL2L1/CAV1/PLAUR/EIF5A	5
NEGATIVE REGULATION OF NEUROGENESIS_GOBP_GO:0050768	4/189	78/25683	0.002651299	0.031168935	0.024368811	WNT7A/SEMA3B/LDLR/SEMA4B	4
TISSUE MIGRATION_GOBP_GO:0090130	4/189	78/25683	0.002651299	0.031168935	0.024368811	PRSS3/ID1/FERMT1/GIPC1	4
REGULATION OF PROTEIN-CONTAINING COMPLEX ASSEMBLY_C	8/189	321/25683	0.002697136	0.031526056	0.02464802	FERMT1/RHOC/MYADM/TMSB10/PMEP1/BIK/CDC42EP2/RPL13A	8

INTERMEDIATE FILAMENT-BASED PROCESS_GOBP_GO:0045103	3/189	38/25683	0.00273774	0.031526056	0.02464802	KRT18/PLEC/PPL	3
LENS DEVELOPMENT IN CAMERA-TYPE EYE_GOBP_GO:0002088	3/189	38/25683	0.00273774	0.031526056	0.02464802	WNT7B/WNT7A/EPHA2	3
LEUKOCYTE MEDIATED CYTOTOXICITY_GOBP_GO:0001909	3/189	38/25683	0.00273774	0.031526056	0.02464802	TUBB4B/TUBB/VAMP2	3
MAMMARY GLAND DEVELOPMENT_GOBP_GO:0030879	3/189	38/25683	0.00273774	0.031526056	0.02464802	CAV1/WNT7B/EPHA2	3
NEPHROTIC SYNDROME_WIKIPATHWAYS_20211210_WP4758_HO	3/189	38/25683	0.00273774	0.031526056	0.02464802	ITGB4/LMNA/ACTN4	3
POSITIVE REGULATION OF APOPTOTIC SIGNALING PATHWAY_G	4/189	79/25683	0.002776871	0.031867895	0.02491528	RPL26/TNFRSF12A/CAV1/EIF5A	4
ALPHA6 BETA4 INTEGRIN-LIGAND INTERACTIONS_PATHWAY IN	2/189	11/25683	0.002836166	0.032366348	0.025304985	ITGB4/LAMB3	2
REGULATION OF APOPTOTIC SIGNALING PATHWAY_GOBP_GO:2	7/189	254/25683	0.00283949	0.032366348	0.025304985	RPL26/BCL2L1/TNFRSF12A/CAV1/PLAUR/EIF5A/UNC5B	7
POSITIVE REGULATION OF INTRACELLULAR PROTEIN TRANSPO	5/189	131/25683	0.002884227	0.032765598	0.02561713	OAZ1/FLNA/PRNP/CIB1/VAMP2	5
CELLULAR COMPONENT MAINTENANCE_GOBP_GO:0043954	3/189	39/25683	0.002949966	0.033067062	0.025852824	PRNP/ITGA3/MYADM	3
NEGATIVE REGULATION OF BLOOD COAGULATION_GOBP_GO:0	3/189	39/25683	0.002949966	0.033067062	0.025852824	PLAT/CD9/PLAU	3
NEGATIVE REGULATION OF HEMOSTASIS_GOBP_GO:1900047	3/189	39/25683	0.002949966	0.033067062	0.025852824	PLAT/CD9/PLAU	3
NGF-STIMULATED TRANSCRIPTION_REACTOME DATABASE ID R	3/189	39/25683	0.002949966	0.033067062	0.025852824	ID1/F3/FOS	3
SECRETION BY CELL_GOBP_GO:0032940	7/189	257/25683	0.003029845	0.033741287	0.026379953	ANXA1/GIPC1/ANXA3/S100A13/RAB3B/VAMP2/PORCN	7
BLOOD COAGULATION_PANTHER PATHWAY_P00011	4/189	81/25683	0.003040116	0.033741287	0.026379953	PLAT/F3/PLAUR/PLAU	4
PROTEIN LOCALIZATION TO EXTRACELLULAR REGION_GOBP_G	4/189	81/25683	0.003040116	0.033741287	0.026379953	ANXA1/RAB3B/LTBP1/PORCN	4
MUSCLE CONTRACTION_REACTOME DATABASE ID RELEASE 78	6/189	192/25683	0.003050666	0.033747369	0.026384709	MYL6/ASPH/ANXA2/ANXA1/DYSF/VCL	6
POSTTRANSCRIPTIONAL REGULATION OF GENE EXPRESSION_G	9/189	404/25683	0.00315652	0.034699946	0.027129462	RPL26/EEF2/EIF4EBP1/EIF6/RPS4X/EIF5A/EIF4A2/PKM/RPL13A	9
PROSTAGLANDIN SYNTHESIS AND REGULATION_WIKIPATHWAY	3/189	40/25683	0.003172041	0.034699946	0.027129462	ANXA2/ANXA1/ANXA3	3
UPTAKE AND ACTIONS OF BACTERIAL TOXINS_REACTOME DAT	3/189	40/25683	0.003172041	0.034699946	0.027129462	EEF2/CD9/VAMP2	3
MAINTENANCE OF PROTEIN LOCATION_GOBP_GO:0045185	4/189	82/25683	0.003177914	0.034699946	0.027129462	CAV1/FLNA/TMSB10/LTBP1	4
TSLP_NETPATH_TSLP	5/189	135/25683	0.003282064	0.034804439	0.027211158	EIF4EBP1/PLEC/LMNA/CALM2/SEMA4B	5
COMPLEMENT SYSTEM_WIKIPATHWAYS_20211210_WP2806_HOM	4/189	83/25683	0.003319912	0.034804439	0.027211158	CD59/PLAUR/CD55/PRNP	4
EPITHELIAL CELL DEVELOPMENT_GOBP_GO:0002064	4/189	83/25683	0.003319912	0.034804439	0.027211158	WNT7B/WNT7A/EPHA2/MYADM	4
NEGATIVE REGULATION OF NERVOUS SYSTEM DEVELOPMENT	4/189	83/25683	0.003319912	0.034804439	0.027211158	WNT7A/SEMA3B/LDLR/SEMA4B	4
BIOCARTA_GCR_PATHWAY_MSIGDB_C2_BIOCARTA_GCR_PATH	2/189	12/25683	0.003386965	0.034804439	0.027211158	ANXA1/CALM2	2
BIOCARTA_GHRELIN_PATHWAY_MSIGDB_C2_BIOCARTA_GHREI	2/189	12/25683	0.003386965	0.034804439	0.027211158	IGFBP6/IGFBP1	2
BIOCARTA_PRION_PATHWAY_MSIGDB_C2_BIOCARTA_PRION_P	2/189	12/25683	0.003386965	0.034804439	0.027211158	PRNP/RPSA	2
NEGATIVE REGULATION OF COMPLEMENT ACTIVATION_GOBP	2/189	12/25683	0.003386965	0.034804439	0.027211158	CD59/CD55	2
NEGATIVE REGULATION OF RELEASE OF SEQUESTERED CALCIU	2/189	12/25683	0.003386965	0.034804439	0.027211158	FKBP1A/CALM2	2
NEGATIVE REGULATION OF RYANODINE-SENSITIVE CALCIUM-R	2/189	12/25683	0.003386965	0.034804439	0.027211158	FKBP1A/CALM2	2
NEUTROPHIL ACTIVATION INVOLVED IN IMMUNE RESPONSE_G	2/189	12/25683	0.003386965	0.034804439	0.027211158	ANXA3/VAMP2	2
REGULATION OF CELL COMMUNICATION BY ELECTRICAL COUP	2/189	12/25683	0.003386965	0.034804439	0.027211158	CAV1/CALM2	2
REGULATION OF VESICLE FUSION_GOBP_GO:0031338	2/189	12/25683	0.003386965	0.034804439	0.027211158	ANXA2/ANXA1	2
TP53 REGULATES TRANSCRIPTION OF DEATH RECEPTORS AND	12/189	12/25683	0.003386965	0.034804439	0.027211158	IGFBP3/TNFRSF10D	2
CELL DIVISION_GOBP_GO:0051301	5/189	136/25683	0.003387395	0.034804439	0.027211158	TUBA1B/TUBB/RHOC/ANXA11/TUBA1C	5
EPITHELIAL TO MESENCHYMAL TRANSITION IN COLORECTAL C	5/189	136/25683	0.003387395	0.034804439	0.027211158	WNT7B/ID1/WNT7A/CLDN4/CLDN7	5
MAINTENANCE OF LOCATION_GOBP_GO:0051235	5/189	136/25683	0.003387395	0.034804439	0.027211158	FTH1/CAV1/FLNA/TMSB10/LTBP1	5
NEGATIVE REGULATION OF COAGULATION_GOBP_GO:0050819	3/189	41/25683	0.003404109	0.034804439	0.027211158	PLAT/CD9/PLAU	3
POSITIVE REGULATION OF INTRINSIC APOPTOTIC SIGNALING	PA3/189	41/25683	0.003404109	0.034804439	0.027211158	RPL26/CAV1/EIF5A	3
REGULATION OF CELL ADHESION MEDIATED BY INTEGRIN_GOE	3/189	41/25683	0.003404109	0.034804439	0.027211158	EPHA2/PLAU/CIB1	3
REGULATION OF RELEASE OF CYTOCHROME C FROM MITOCHO	3/189	41/25683	0.003404109	0.034804439	0.027211158	BCL2L1/PLAUR/BIK	3
NEGATIVE REGULATION OF CELL DIFFERENTIATION_GOBP_GO:	9/189	410/25683	0.003477036	0.035442657	0.027710136	PTHLH/CAV1/WNT7A/ANXA1/SEMA3B/LDLR/CIB1/SEMA4B/ACTN4	9
REGULATION OF CELL JUNCTION ASSEMBLY_GOBP_GO:1901888	5/189	137/25683	0.003495136	0.035519843	0.027770482	CAV1/ACTG1/WNT7A/EPHA2/VCL	5
SIGNALING BY RECEPTOR TYROSINE KINASES_REACTOME DAT	10/189	491/25683	0.003591722	0.036391805	0.028452209	PLAT/CAV1/ID1/F3/ITGA3/AREG/FGF19/LAMB3/POLR2J/FOS	10
DIRECT P53 EFFECTORS_PATHWAY INTERACTION DATABASE N	5/189	138/25683	0.003605318	0.036420185	0.028474397	BCL2L1/CAV1/EPHA2/IGFBP3/TNFRSF10D	5
CARBOXYTERMINAL POST-TRANSLATIONAL MODIFICATIONS O	3/189	42/25683	0.003646308	0.036506364	0.028541774	TUBB4B/TUBA1B/TUBA1C	3
NON-INTEGRIN MEMBRANE-ECM INTERACTIONS_REACTOME_R	3/189	42/25683	0.003646308	0.036506364	0.028541774	ITGB4/LAMB3/HSPG2	3
UROKINASE-TYPE PLASMINOGEN ACTIVATOR (UPA) AND UPAR	3/189	42/25683	0.003646308	0.036506364	0.028541774	PLAUR/PLAU/ITGA3	3

NEGATIVE REGULATION OF CELL POPULATION PROLIFERATION	10/189	493/25683	0.003695622	0.036781793	0.028757113	HMGA1/PTHLH/IGFBP6/FTH1/CAV1/LMNA/PRNP/CIB1/IGFBP3/SULT2B1	10
RESPONSE TO CYTOKINE_GOBP_GO:0034097	10/189	493/25683	0.003695622	0.036781793	0.028757113	BCL2L1/F3/ANXA1/TIMP2/EIF5A/CIB1/PLP2/LIFR/RPL13A/ACTN4	10
NETWORK MAP OF SARS-COV-2 SIGNALING PATHWAY_WIKIPAT	6/189	200/25683	0.003726577	0.036980795	0.028912698	ACTG1/EIF4EBP1/RRAS/EIF4A2/FAM83A/FOS	6
FIBRINOLYSIS_GOBP_GO:0042730	2/189	13/25683	0.003983459	0.039184224	0.030635406	PLAT/PLAU	2
METABOLIC PATHWAY OF LDL, HDL AND TG, INCLUDING DISEA	2/189	13/25683	0.003983459	0.039184224	0.030635406	ANXA2/LDLR	2
REGULATION OF METALLOPEPTIDASE ACTIVITY_GOBP_GO:19052/189	13/25683	13/25683	0.003983459	0.039184224	0.030635406	CLDN4/TIMP2	2
POSITIVE REGULATION OF CELL DEATH_GOBP_GO:0010942	9/189	419/25683	0.004005246	0.039284012	0.030713423	RPL26/TNFRSF12A/CAV1/ANXA1/EIF5A/PRNP/CALM2/IGFBP3/FOS	9
POSITIVE REGULATION OF PROTEIN LOCALIZATION TO MEMBR.	4/189	88/25683	0.004095009	0.040048001	0.031310732	EPHA2/PRNP/CIB1/ITGA3	4
APOPTOTIC MITOCHONDRIAL CHANGES_GOBP_GO:0008637	3/189	44/25683	0.004161632	0.040464972	0.031636733	BCL2L1/VDAC2/BIK	3
POSITIVE REGULATION OF CELL-MATRIX ADHESION_GOBP_GO:13/189	44/25683	44/25683	0.004161632	0.040464972	0.031636733	CEACAM6/CIB1/RRAS	3
COLLAGEN FORMATION_REACTOME_R-HSA-1474290.3	4/189	89/25683	0.004263467	0.041336029	0.032317751	ITGB4/PLEC/COL17A1/LAMB3	4
REGULATION OF ACTIN FILAMENT ORGANIZATION_GOBP_GO:016/189	207/25683	207/25683	0.004404097	0.042577143	0.033288092	ACTG1/WDR1/RHOC/MYADM/TMSB10/CDC42EP2	6
OVERLAP BETWEEN SIGNAL TRANSDUCTION PATHWAYS CONT	3/189	45/25683	0.00443501	0.04263169	0.033330738	WNT7B/LMNA/MAOA	3
RHOA SIGNALING PATHWAY_PATHWAY INTERACTION DATABA	3/189	45/25683	0.00443501	0.04263169	0.033330738	CFL1/VCL/FOS	3
CHAPERONIN-MEDIATED PROTEIN FOLDING_REACTOME DATAI	4/189	91/25683	0.00461429	0.043466827	0.033983673	ACTB/TUBB4B/TUBA1B/TUBA1C	4
BIOCARTA_EIF_PATHWAY_MSIGDB_C2_BIOCARTA_EIF_PATHW	2/189	14/25683	0.004624953	0.043466827	0.033983673	EIF6/EIF4A2	2
CAMP METABOLIC PROCESS_GOBP_GO:0046058	2/189	14/25683	0.004624953	0.043466827	0.033983673	PTHLH/EPHA2	2
CELLULAR RESPONSE TO LOW-DENSITY LIPOPROTEIN PARTICLE	2/189	14/25683	0.004624953	0.043466827	0.033983673	CD9/LDLR	2
FAMILIAL HYPERLIPIDEMIA TYPE 1_WIKIPATHWAYS_20211210	2/189	14/25683	0.004624953	0.043466827	0.033983673	LDLR/ANGPTL4	2
NEGATIVE REGULATION OF HUMORAL IMMUNE RESPONSE_GOI	2/189	14/25683	0.004624953	0.043466827	0.033983673	CD59/CD55	2
POSITIVE REGULATION OF SEQUESTERING OF CALCIUM ION_GC	2/189	14/25683	0.004624953	0.043466827	0.033983673	FKBP1A/CALM2	2
SKELETAL MUSCLE TISSUE REGENERATION_GOBP_GO:0043403	2/189	14/25683	0.004624953	0.043466827	0.033983673	ANXA1/CD9	2
GASTRIN_CCK2R_240212_PANTHER PATHWAY_P06959	5/189	147/25683	0.004711854	0.044105263	0.034482822	BCL2L1/EIF4EBP1/PLAU/CCK/FOS	5
CORTICAL CYTOSKELETON ORGANIZATION_GOBP_GO:0030865	3/189	46/25683	0.004719028	0.044105263	0.034482822	RHOF/RHOD/RHOC	3
DNA DAMAGE RESPONSE (ONLY ATM DEPENDENT)_WIKIPATHV	4/189	92/25683	0.004796769	0.044708008	0.034954066	WNT7B/WNT7A/LDLR/BIK	4
REGULATION OF ACTIN DYNAMICS FOR PHAGOCYTOTIC CUP FORM	5/189	148/25683	0.004848127	0.045062209	0.035230991	ACTB/ACTG1/CFL1/ARPC1B/ARPC1A	5
CLASS B 2 (SECRETIN FAMILY RECEPTORS)_REACTOME DATAB	4/189	93/25683	0.004984036	0.046198176	0.036119125	PTHLH/WNT7B/WNT7A/CD55	4
METABOLISM OF FAT-SOLUBLE VITAMINS_REACTOME DATABA	3/189	47/25683	0.005013801	0.046220125	0.036136285	LDLR/VKORC1/HSPG2	3
REGULATION OF INTERLEUKIN-2 PRODUCTION_GOBP_GO:0032613/189	47/25683	47/25683	0.005013801	0.046220125	0.036136285	ANXA1/PRNP/CARD11	3
NEURON PROJECTION DEVELOPMENT_GOBP_GO:0031175	9/189	436/25683	0.005172858	0.047556462	0.037181073	ACTB/WNT7A/EPHB6/EPHA2/SEMA3B/EFNB1/CCK/SEMA4B/UNC5B	9
POSITIVE REGULATION OF APOPTOTIC PROCESS_GOBP_GO:004318/189	359/25683	359/25683	0.005273065	0.047988765	0.037519061	RPL26/TNFRSF12A/CAV1/ANXA1/EIF5A/PRNP/CALM2/IGFBP3	8
MESODERMAL CELL DIFFERENTIATION_GOBP_GO:0048333	2/189	15/25683	0.00531076	0.047988765	0.037519061	ITGB4/ITGA3	2
MUSCLE CELL MIGRATION_GOBP_GO:0014812	2/189	15/25683	0.00531076	0.047988765	0.037519061	PLAT/ANXA1	2
NEGATIVE REGULATION OF CALCIUM ION TRANSPORT INTO CY	2/189	15/25683	0.00531076	0.047988765	0.037519061	FKBP1A/CALM2	2
NEGATIVE REGULATION OF LIPASE ACTIVITY_GOBP_GO:0060192/189	15/25683	15/25683	0.00531076	0.047988765	0.037519061	ANXA1/ANGPTL4	2
REGULATION OF CELL COMMUNICATION BY ELECTRICAL COUP	2/189	15/25683	0.00531076	0.047988765	0.037519061	CAV1/CALM2	2
EPH-EPHRIN MEDIATED REPULSION OF CELLS_REACTOME_R-HS	3/189	48/25683	0.005319442	0.047988765	0.037519061	EPHB6/EPHA2/EFNB1	3

Table S6. Details of used gene sets.

Fig.	Name in Fig.	Original name	Collection	Source
Fig.3B	BILE DUCT CELLS 1	AIZARANI LIVER C4 EPCAM POS BILE DUCT CELLS 1	MSigDB: C8	Aizarani N, et al. Nature. 2019 Aug;572(7768):199-204.
	BILE DUCT CELLS 2	AIZARANI LIVER C7 EPCAM POS BILE DUCT CELLS 2	MSigDB: C8	Aizarani N, et al. Nature. 2019 Aug;572(7768):199-204.
	BILE DUCT CELLS 3	AIZARANI LIVER C24 EPCAM POS BILE DUCT CELLS 3	MSigDB: C8	Aizarani N, et al. Nature. 2019 Aug;572(7768):199-204.
	BILE DUCT CELLS 4	AIZARANI LIVER C39 EPCAM POS BILE DUCT CELLS 4	MSigDB: C8	Aizarani N, et al. Nature. 2019 Aug;572(7768):199-204.
	HEPATOCYTES 1	AIZARANI LIVER C11 HEPATOCYTES 1	MSigDB: C8	Aizarani N, et al. Nature. 2019 Aug;572(7768):199-204.
	HEPATOCYTES 2	AIZARANI LIVER C14 HEPATOCYTES 2	MSigDB: C8	Aizarani N, et al. Nature. 2019 Aug;572(7768):199-204.
	HEPATOCYTES 3	AIZARANI LIVER C17 HEPATOCYTES 3	MSigDB: C8	Aizarani N, et al. Nature. 2019 Aug;572(7768):199-204.
	LGR5POS STEM CELL	GAO LARGE INTESTINE 24W C5 LGR5POS STEM CELL	MSigDB: C8	Gao S, et al. Nat Cell Biol. 2018 Jun;20(6):721-734.
	DUODENAL DIFFERENTIATING STEM CELLS	BUSSLINGER DUODENAL DIFFERENTIATING STEM CELLS	MSigDB: C8	Busslinger GA, et al. Cell Rep. 2021 Mar 9;34(10):108819
	DUODENAL STEM CELLS	BUSSLINGER DUODENAL STEM CELLS	MSigDB: C8	Busslinger GA, et al. Cell Rep. 2021 Mar 9;34(10):108819
Fig3.CD	Bile Duct	AIZARANI LIVER C7 EPCAM POS BILE DUCT CELLS 2	MSigDB: C8	Aizarani N, et al. Nature. 2019 Aug;572(7768):199-204.
	Hepatocyte	AIZARANI LIVER C11 HEPATOCYTES 1	MSigDB: C8	Aizarani N, et al. Nature. 2019 Aug;572(7768):199-204.
	Duodenul Stem	BUSSLINGER DUODENAL STEM CELLS	MSigDB: C8	Busslinger GA, et al. Cell Rep. 2021 Mar 9;34(10):108819
	Adenylate Cyclase Inhibiting Dopamine Receptor	GO_ADENYLATE_CYCLASE_INHIBITING_DOPAMINE_RECEPTOR_SIGNALING_PATHWAY	GO:0007195	
	Adenylate Cyclase Activating Dopamine Receptor	GO_ADENYLATE_CYCLASE_ACTIVATING_DOPAMINE_RECEPTOR_SIGNALING_PATHWAY	GO:0007191	
	Dopamine Biosynthesis	GOBP_DOPAMINE_BIOSYNTHETIC_PROCESS	GO:0042416	
	WNT Biosynthesis	REACTOME_WNT_LIGAND_BIOGENESIS_AND_TRAFFICKING	MSigDB: C2	

Table S7. List of the antibodies.

IHC and Immunofluorescent Staining					
Antibody	Species	Dilution	Company	Cat#	RRID
Anti-Dopamine Receptor D1	Rabbit	1:600	Abcam	ab20066	AB_445306
Anti-WNT7B	Rabbit	1:500	Sigma	SAB2108321	
Anti-PROX1	Rabbit	1:500	Abcam	ab199359	AB_2868427
Anti-Cytokeratin 19	Rabbit	1:6400	ProteinTech Group	10712-1-AP	AB_2133325
Anti-TACSTD2 (TROP2)	Mouse	1:200	Biolegend	363802	AB_2564376
Anti-TH	Mouse	1:100	Millipore	MAB318	AB_2313764
Anti-MAOB	Rabbit	1:100	ProteinTech Group	12602-1-AP	AB_2137273
Alexa Fluor 488-conjugated anti-rabbit IgG	Goat	1:400	Abcam	ab150081	AB_2734747
Alexa Fluor 594-conjugated anti-mouse IgG	Goat	1:400	Abcam	ab150120	AB_2631447
Immunoblotting					
Antibody	Species	Dilution	Company	Cat#	RRID
Anti-Dopamine Receptor D1	Rabbit	1:1000	Abcam	ab20066	AB_445306
anti-beta Actin	Rabbit	1:50000	Abcam	ab49900	AB_867494
Flow cytometry					
Antibody	Species	Dilution	Company	Cat#	RRID
PE antihuman TACSTD2 (TROP2)	Mouse	1:100	BioLegend	363804	AB_2572022